INVESTIGATING CELLULAR ENERGY SENSING MECHANISMS FOR TREATING NON-ALCOHOLIC STEATOHEPATITS

INVESTIGATING CELLULAR ENERGY SENSING MECHANISMS FOR TREATING NON-ALCOHOLIC STEATOHEPATITS

by

Eric M. Desjardins, H.B.Sc. M.Sc

A Thesis Submitted to the School of Graduate Studies in Partial Fulfillment of the Requirements for the Degree Doctor of Philosophy

McMaster University DOCTOR OF PHILOSOPHY (2023) Hamilton, Ontario
(Medical Sciences – Nutrition & Metabolism)

TITLE: INVESTIGATING CELLULAR ENERGY SENSING MECHANISMS FOR TREATING NON-ALCOHOLIC STEATOHEPATITS

AUTHOR: Eric M. Desjardins, H.B.Sc., M.Sc.

SUPERVISOR: Professor Gregory R. Steinberg, Ph.D.

PAGE COUNT: xxi, 196

LAY ABSTRACT

Non-alcoholic fatty liver disease (NAFLD) is a growing epidemic and affects over 25% of the world's population. What can start with a fatty liver could progress to a liver that becomes inflamed and damaged, resulting in a loss in function to keep the body in balance – this is called non-alcoholic steatohepatitis (NASH). NASH can eventually lead to liver tissue scarring, cancer, and failure. There is currently no approved therapy to treat NASH. The rise in the prevalence of NAFLD and NASH is in parallel to rises in obesity, type 2 diabetes, and cardiovascular diseases, indicating that common metabolic mechanisms may be dysregulated in these diseases. In this thesis, we expand our understanding of the role of two major metabolic enzymes which control the metabolism of fat in our cells, AMP-activated protein kinase (AMPK) and ATP-citrate lyase (ACLY). We identify that, by controlling their activities using a particular type of activated fat molecule, they can promote the rejuvenation of liver cells by recycling damaged or unnecessary contents of the cell and can at least be partially responsible for improvements in NAFLD/NASH-related measures in our studies. Finally, using a drug that controls the activity of both enzymes, bempedoic acid, we demonstrate complementary effects to the common obesity and type 2 diabetes drug liraglutide when combining the two drugs, indicating a new potential combination therapy to treat NASH and linked metabolic diseases.

ABSTRACT

There is a large unmet medical need to establish therapies aimed at treating non-alcoholic steatohepatitis (NASH). NASH is a progressive form of non-alcoholic fatty liver disease (NAFLD) that is characterized by hepatic steatosis, hepatocellular ballooning, and lobular inflammation. The presence of NASH along with hepatic fibrosis significantly increases the risk for liver cirrhosis, hepatocellular carcinoma, and liver failure. Considered as the hepatic manifestation of metabolic syndrome, it has become critical to develop therapies that not only target the primary liver pathologies associated with NASH, but also the metabolic comorbidities that are typically coexistent with it, including obesity, hyperlipidemia, type 2 diabetes, and cardiovascular disease. Two known contributors to NASH are elevated *de novo* lipogenesis (DNL) and mitochondrial dysfunction, with the latter particularly related to reduced fatty acid oxidation, increased oxidative stress, and cell injury. AMP-activated protein kinase (AMPK) is a cellular energy sensor that integrates multiple physiological, hormonal, and nutritional cues to influence downstream metabolic pathways. In this thesis, we identified the physiological significance of AMPKβ1 Ser108 phosphorylation in increasing fatty acid oxidation, mitochondrial biogenesis, and autophagy in response to excess fatty acids in the liver by generating a targeted germline knock-in mutation Ser108Ala mouse model. We next determined that the AMPK activator and ATP-citrate lyase inhibitor bempedoic acid increased autophagic flux in cultured rat hepatocytes and caused changes in the expression of autophagy-related genes in a chemically induced

mouse model of NASH, potentially through reductions in the acetylation of proteins. These data expand our knowledge on how bempedoic acid has additional effects to reduce hepatocellular ballooning and fibrosis in NASH compared to DNL inhibition alone. Lastly, we tested the combination of bempedoic acid and the glucagon-like peptide-1 receptor (GLP-1R) agonist liraglutide and found favourable improvements in liver steatosis, inflammation, hepatocellular ballooning, and hepatic fibrosis compared to liraglutide alone. Importantly, these findings were without increases in serum triglyceride levels which has been shown with other compounds inhibiting DNL. Taken together, the data generated in this thesis provide further support to develop therapies which target and AMPK and ACLY for NAFLD and NASH, and warrant further consideration of the utility of bempedoic acid and GLP-1R agonists as a viable combinatorial therapy.

THESIS PUBLICATIONS

Desjardins EM, *et al*. (2022). The phosphorylation of AMPKβ1 is critical for increasing autophagy and maintaining mitochondrial homeostasis in response to fatty acids. *Proceedings of the National Academy of Sciences*, *119*(48).

Desjardins EM, *et al.* (2023). Pharmacological inhibition of ACLY in a mouse model of NASH promotes autophagy. *In preparation for submission 2023*.

Desjardins EM, *et al*. (2023). Combination of bempedoic acid with a GLP-1R agonist imparts additive benefits to treat metabolic-associated steatohepatitis and hepatic fibrosis in mice. *In submission 2023.*

OTHER PUBLICATIONS

Desjardins EM, Steinberg GR. (2023). Fine-tuning AMPK activity for the treatment of metabolic diseases. *Invited Review. In preparation for Nature Metabolism 2023*.

Desjardins EM, Day EA, Scott JW, Steinberg GR. (2023). Sensing of long chain fatty acyl-CoA esters by AMPK. In the press at *Methods in Molecular Biology*.

Tsakiridis EE, Morrow MR, **Desjardins EM**, Wang D, Llanos A, Wang B, Wade MG, Morrison KM, Holloway AC, Steinberg GR. (2023). Effects of the pesticide deltamethrin on high fat diet-induced obesity and insulin resistance in male mice. *Food and Chemical Toxicology, 176.*

Morrow MR, Batchuluun B, Wu J, Ahmadi E, Leroux JM, Mohammadi-Shemirani P, **Desjardins EM**, Wang Z, Tsakiridis EE, Lavoie DCT, Reihani A, Smith BK, Kwiecien JM, Lally JSV, Nero TL, Parker MW, Ask K, Scott JW, Jiang L, Paré G, Pinkosky SL, Steinberg GR. (2022). Inhibition of ATP-citrate lyase improves NASH, liver fibrosis, and dyslipidemia. *Cell Metabolism, 34*(6).

Ahmed BA, Ong FJ, Barra NG, Blondin DP, Gunn E, Oreskovich SM, Szamosi JC, Syed SA, Hutchings EK, Konyer NB, Singh NP, Yabut JM, **Desjardins EM**, Anhê FF, Foley KP, Holloway AC, Noseworthy MD, Haman F, Carpentier AC, Surette MG, Schertzer JD, Punthakee Z, Steinberg GR, Morrison KM. (2021). Lower brown adipose tissue activity is associated with non-alcoholic fatty liver disease but not changes in the gut microbiota. *Cell Reports Medicine, 2*(9).

Drake JC, Wilson RJ, Laker RC, Guan Y, Spaulding HR, Nichenko AS, Shen W, Shang H, Dorn MV, Huang K, Zhang M, Bandara AB, Brisendine MH, Kashatus JA, Sharma PR, Young A, Gautam J, Cao R, Wallrabe H, Chang PA, Wong M, **Desjardins EM**, Hawley SA, Christ GJ, Kashatus DF, Miller CL, Wolf MJ, Periasamy A, Steinberg GR, Hardie DG, Yan Z. (2021). Mitochondria-localized AMPK responds to local energetics and contributes to exercise and energetic stress-induced mitophagy. *Proceedings of the National Academy of Sciences, 118*(37).

Wang B, Tsakiridis EE, Zhang S, Llanos A, **Desjardins EM**, Yabut JM, Green AE, Day EA, Smith BK, Lally JSV, Wu J, Raphenya AR, Srinivasan KA, McArthur AG, Kajimura S, Patel JS, Wade MG, Morrison KM, Holloway AC, Steinberg GR. (2021). The pesticide chlorpyrifos promotes obesity by inhibiting diet-induced thermogenesis in brown adipose tissue. *Nature Communications, 12*(1).

Rhein P, **Desjardins EM**, Rong P, Ahwazi D, Bonhoure N, Stolte J, Santos MD, Ovens AJ, Ehrlich AM, Sanchez Garcia JL, Ouyang Q, Yabut JM, Kjolby M, Membrez M, Jessen N, Oakhill JS, Treebak JT, Maire P, Scott JW, Sanders MJ, Descombes P, Chen S, Steinberg GR, Sakamoto K. (2021). Compound- and fiber type-selective requirement of AMPKγ3 for insulin-independent glucose uptake in skeletal muscle. *Molecular Metabolism, 51.*
Desjardins EM, Smith BK, Steinberg GR, Brown RE. (2021). Sevoflurane-induced hyperglycemia is attenuated by salsalate in obese insulin-resistant mice. *Canadian Journal of Anesthesia, 68*(7)*.*

Pinkosky SL, Scott JW, **Desjardins EM**, Smith BK, Day EA, Ford RJ, Langendorf CG, Ling NXY, Nero TL, Loh K, Galic S, Hoque A, Smiles WJ, Ngoei KRW, Parker MW, Yan Y, Melcher K, Kemp BE, Oakhill JS, Steinberg GR. (2020). Long-chain fatty acyl-CoA esters regulate metabolism via allosteric control of AMPK β1 isoforms. *Nature Metabolism, 2*(9).

Day EA, Ford RJ, Lu JH, Lu R, Lundenberg L, **Desjardins EM**, Green AE, Lally JSV, Schertzer JD, Steinberg GR. (2020). The SGLT2 inhibitor canagliflozin suppresses lipid synthesis and interleukin-1 beta in ApoE deficient mice. *Biochemical Journal, 477*(12)*.*

Yabut JM, **Desjardins EM**, Chan EJ, Day EA, Leroux JM, Wang B, Crane ED, Wong W, Morrison KM, Crane JD, Khan WI, Steinberg GR. (2020). Genetic deletion of mast cell serotonin synthesis prevents the development of obesity and insulin resistance. *Nature Communications, 11*(1)*.*

Zhang D, Gava AL, Van Krieken R, Mehta N, Li R, Gao B, **Desjardins EM**, Steinberg GR, Hawke T, Krepinsky JC. (2019). The caveolin-1 regulated protein follistatin protects against diabetic kidney disease. *Kidney International, 96*(5)*.*

Desjardins EM, Steinberg GR. (2018). Emerging Role of AMPK in Brown and Beige Adipose Tissue (BAT): Implications for Obesity, Insulin Resistance, and Type 2 Diabetes. *Current Diabetes Reports, 18*(10)*.*

ACKNOWLEDGEMENTS

I would like to acknowledge several individuals without whom this work would not have been possible. It takes a village to raise a scientist.

I would like to thank my supervisor, Dr. Gregory Steinberg, for his guidance and mentorship over the many years I've been here. You have provided me with countless opportunities, the space and support to grow as a scientist and individually, and have always made yourself available to help me in any way. You have been an exemplar role model of passion, dedication and balance, and I am so fortunate to call you my mentor.

I would like to thank the members of my thesis committee, Drs. Jonathan Schertzer and Stuart Phillips, for their support and flexibility throughout the completion of this thesis work. You have provided me with the support I needed and alternate perspectives to the work I've collated in the lab over the years.

I would also like to express my gratitude to our coauthors and close collaborators. Specifically, Drs. Kei Sakamoto and Stephen Pinkosky, you have graciously shared your initial concepts and deep scientific understanding of the work that has led to the composition of this dissertation. Without your inputs, this work would not have been possible.

To all my fellow labmates in the Steinberg Lab, past and present, thank you for everything. You have truly enriched my time here. I have been here long enough to see multiple cohorts of people come and go, but what remained the same was everyone's willingness to share and help, and I am extremely grateful to be a part of this team. To go through a time machine: Emilio, Julian, Justin (BAT-pack), Brennan, Emily, Rebecca, Stephen, Adam, Katarina, Andrew, James, Vanessa, Linda, Rutu, Andreas, Lindsay, Alex G, Vito, Eulaine, Elizabeth, Alex A, Rohksana, Vivian, Ryan, Andrea, Russell, Bo, Shuman, Sonal, Robert, Eric, Jianhan, Evelyn, Marisa, Jaya, Dongdong, Logan, Elham, Tseegii, Declan, Lucie, Fiorella, Jenny, Therese, Zeel, Russta, Hannah, Danny, Junfeng, and Celina. That's 50 people and I'm sure there are more that I have not listed here.

Finally, thank you to my amazing family, Claude, Sylvie, and Christine. Your teachings and sacrifices have offered me the privilege of pursuing my passions. I am grateful to have had your continued presence in my life, your unwavering support, and patience as I worked through this degree.

TABLE OF CONTENTS

ABBREVIATIONS

3MA	3-methyladenine
AAV	Adeno-associated virus
ACC	Acetyl-CoA carbxoylase
ACC-DKI	ACC double knockin
ACCS2	Acetate-CoA synthetase 2
Acetyl-CoA	Acetyl-coenzyme-A
ACLY	ATP-citrate lyase
ACS	Acetyl-CoA synthetase
ADaM	Allosteric drug and metabolite
ADP	Adenosine diphosphate
AICAR	5-aminoimidazole-4-carboxamide ribonuceloside
AKT	protein kinase-b
ALT	Alanine aminotransferase
AMBRA1	Beclin1-regulated autophagy protein 1
AMP	Adenosine monophosphate
AMPK	AMP-activated protein kinase
ARG	Autophagy-related genes
ASCVL1	Very-long-chain acyl-CoA synthetase 1
ASH	N-terminal acyl-CoA csynthase homology
AST	Aspartate transaminase

ATG	Autophagy-related protein
ATGL	Adipose triglyceride lipase
ATP	Adenosine triphosphate
α-SMA	Alpha-smooth muscle actin
BemA	Bempedoic acid
BNIP3	BCL2 interacting protein 3
CAMKK	Calcium/calmodulin-dependent protein kinase kinase
cAMP	Cyclic AMP
CBM	Carbohydrate binding module
CBS3	Cystathionine-beta-synthase 3
ChREBP	Carbohydrate-responsive element binding protein
CISD1	CDGSH iron sulfur domain 1
CNS	Central nervous system
CPT1	Carnitine palmitoyltrasnferase 1
CPT2	Carnitine palmitoyltrasnferase 2
CQ	Chloroquine
CRP	C-reactive protein
CSH	C-terminal citrate synthase homology
CT	Computed tomography
CVD	Cardiovascular disease
CXCL10	Chemokine CXC motif ligand 10
DAMP	Danger-associated molecular pattern

DFCP1	Zinc-finger FYVE domain contain protein 1
DG	Diglyceride
DNA	Deoxyribonucleic acid
DNL	De novo lipogenesis
DRP1	Dynamin-related protein 1
EASD	European association for the study of diabetes
EASL	European association for the study of liver
EASO	European association for the study of obesity
ECM	Extracellular matrix
eIF2α	eukaryotic initiation factor 2 alpha
ELF	Enhanced liver fibrosis
ENPP1	Ectonucleotide pyrophosphatase/phosphodiesterase 1
ER	Endoplasmic reticulum
ETC	Electron transport chain
ETC-1002	Bempedoic acid
FA-CoA	Fatty acyl-CoA
FAD	Flavin adenine dinucleotide
FAO	Fatty acid oxidation
FAS	Fatty acid synthase
FDA	U.S. Food and Drug Administration
FFA	Free fatty acid
FIS1	Fission 1

FNDC5	Fibronectin type III domain containing 5
FOXO1	forkhead box protein O1
FUNDC1	FUN14 domain containing 1
G6P	Glucose 6-phosphate
GCKR	Glucokinase regulator
GCN5	General control non-depressible 5
GFP	Green fluorescent protein
GGT	Gamma-glutamyltransferase
GI	Gastrointestinal
GK	Glucokinase
GLP-1	Glucagon-like peptide-1
GLP-1R	Glucagon-like peptide-1 receptor
GLUT2	Glucose transporter 2
GP	Glycogen phosphorylase
GS	Glycogen synthase
GSK3β	Glycogen synthase kinase-3 beta
GTT	Glucose tolerance test
HCC	Hepatocellular carcinoma
HDAC	Histone deacetylase
HeHF	Heterzygous familial hypercholesterolemia
HFD	High-fat diet
HIF1	Hypoxia-inducible factor 1

HMGR	Hydroxy-3-methylglutarate-CoA reductase
HSC	Hepatic stellate cell
HSD17B13	Hydroxysteroid 17-beta dehydrogenase 13
IL-18	Interleukin-18
IL-1β	Interleukin-1 beta
IRE1α	Inositol-requiring enzyme 1 alpha
IRS1	Insulin receptor substrate-1
ITT	Insulin tolerance test
KHK	Ketohexokinase
KI	Knockin
KO	Knockout
LAMP2	Lysosomal associated membrane protein 2
LC3	Microtubule-associated protein light chain 3
LCAD	Long-chain acyl-CoA dehydrogenase
LCFA	Long chain fatty acyl
LDLR	Low-density lipoprotein receptor
LIR	LC3-interacting region
Lira	Liraglutide
LKB1	Liver kinase B1
LPL	Lipoprotein lipase
LRAT	Lecithin retinol acyltransferase
LRG	Lysosomal-related gene

LRP	LDLR-related protein
LSEC	Liver sinusoidal epithelial cell
LXR	Liver X receptor
LYPLAL1	Lysophospholipase like 1
MACE	Major adverse cardiovascular events
MBOAT7	Membrane bound O-acyltransferase 7
MCAD	Medium-chain acyl-CoA dehydrogenase
MERTK	Tyrosine-protein kinase MER
MFF	Mitochondrial fission factor
MiD	Mitochondrial division
MitoNEET	Mitochondrial protein containing NEET sequence
MR	Magnetic resonance
MRE	Magnetic resonance elestography
mTOR	Mammalian target of rapamycin
NADPH	Nicotinamide adenine dinucleotide phosphate
NAFL	Non-alcoholic fatty liver
NAFLD	Non-alcoholic fatty liver disease
NAS	NAFLD activity score
NASH	Non-alcoholic steatohepatitis
NBR1	Neighbor of BRCA1 gene 1
NDP52	Nuclear dot protein 52 kDa
NIT	Non-invasive test

NIX	BNIP3 like
NMR	Non-magnetic resonance
NRF	Nuclear respiratory factor
nTPM	Normalized transcript per million
NuGEMP	Nuclear genes encoding mitochondrial proteins
OPTN	Optineurin
P115	General vesicular transport factor
P300	Histone acetyltransferase p300
p38 MAPK	P38 mitogen-activated protein kinase
PAMP	Pathogen-associated molecular pattern
PAS	Phagophore assembly site
PDE3B	Phosphodiesterase 3B
PDFF	Proton density fat fraction
PDH	Pyruvate dehydrogenase
PE	Phosphatidylethanolamine
PERK	Protein kinase r-like ER kinase
PGC1α	PPAR co-activator 1-alpha
PI3K	Phosphoinositide 3-kinase
PI3KC3	Class III PI3K complex I
PI3P	Phosphatidylinositol-r-phosphate
PINK1	PTEN-induced kinase 1
PKA	Protein kinase A

PLIN2	Perilipin 2
PLIN3	Perilipin 3
PNPLA3	Patatin-like phospholipase domain-containing protein 3
PP2C	Protein phosphatase 2-C
PPAR	Peroxisome proliferator-activated receptor
PSR	Picrosirus red
PTT	Pyruvate tolerance test
RFP	Red fluorescent protein
RNA	Ribonucleic acid
ROS	Reactive oxygen species
SAA	Serum amyloid A
SCAD	Short-chain acyl-CoA dehydrogenase
SCD1	stearoyl-CoA desaturase 1
shRNA	Short hairpin RNA
SIRT1	Sirtuin 1
SNARE	Soluble n-ethylmaleimide-sensitive-factor attachment protein receptor
SNP	Single-nucleotide polymorphism
SOD2	Superoxide dismutase 2
sPLA2	Secretory phospholipase A2
SQSTM1	Sequestosome 1/P62
SREBP1c	Sterol regulatory element-binding protein 1c
sXBP1	spliced-form XBP1

T2D	Type 2 diabetes
TCA	Tricarboxylic acid
TE	Transient elastography
TEM	Tranmission electron microscopy
TFEB	Transcription factor EB
TG	Triglyceride
TGF-β	Transforming growth factor-beta
THRβ	Thyroid hormone receptor-beta
TM6SF2	Transmembrane 6 superfamily member 2
TNF-α	Tumor necrosis factor-alpha
TSC2	Tuberous sclerosis complex 2
TXNIP	Thioredoxin-interacting protein
UCP2	Uncoupling protein 2
ULK1	Unc-like kinase 1
UPR	Unfolded protein response
Veh	Vehicle
VLCAD	Very long-chain acyl-CoA dehydrogenase
VLDL	Very low-density lipoproteins
VPS34	Vacuolar protein sorting 34
WIPI2	WD repeat domain phosphoinositide-interacting protein 2
WT	Wildtype
XBP1	X-box binding protein 1

CHAPTER ONE

1 INTRODUCTION

1.1 THE LIVER AS AN INTEGRATIVE HUB FOR WHOLE BODY METABOLISM

1.1.1 FUNCTION AND ORGANIZATION

The liver is a critical organ that can regenerate itself in response to acute stressors such as mechanical or chemical injury (Michalopoulos and Bhushan 2021). This relatively unique ability can be affected by chronic diseases which trigger compensatory proliferation of damaged cells, leading to greater DNA damage and potentially neoplasia. The liver has several crucial functions including the filtration and storage of blood from the portal circulation, detoxification of toxins, breaking down red blood cells, formation of proteins and bile, and maintenance of energy homeostasis through the control of blood glucose and lipids (Trefts, Gannon, and Wasserman 2017).

The liver is composed of a vast array of cells including hepatocytes, cholangiocytes, stellate cells, Kupffer cells and liver sinusoidal endothelial cells (Cunningham and Porat-Shliom 2021). Hepatocytes make up ~60-80% of the liver and are specialized epithelial cells that perform many of the functions mentioned above. Cholangiocytes are specialized epithelial cells that line the bile ducts and lumen. Hepatic stellate cells (HSCs) represent a diverse range of cells that typically store Vitamin A in lipid droplets, but under activated states proliferate, then synthesize and secrete collagen in the injured liver. Kupffer cells are the specialized macrophage population of the liver and respond to pathogenic insults from the portal circulation. Lastly, liver sinusoidal epithelial cells line sinusoids

(LSECs) and are permeable to the diffusion of small particles due to the presence of fenestrae, allowing for the exchange of proteins and other particles between the plasma and liver cells listed above, while maintaining a barrier for immune protection (Ficht and Iannacone 2020).

Diverse physiological roles of the liver are permitted by the architectural assembly of its cells into functional units called hepatic lobules (Cunningham and Porat-Shliom 2021). Lobules consist of hepatocytes arranged in hexagonal divisions around a central vein at their core, while at their peripheral portion reside bile ducts, hepatic arteries, portal veins, and occasionally lymphatic vessels in a arrangement termed the “portal triad” (Ben-Moshe and Itzkovitz 2019). Therefore, the liver is supplied with low-pressure, low-flow from the portal circulation including the gut, pancreas, and spleen, through the sinusoids with blood flow from hepatic arteries, and drain through the central vein. While the basal portion of hepatocytes directly sample blood through the fenestrae of LSECs, their luminal side secretes bile to flow in parallel yet opposite directions. The gradients created by this assembly have led to the definition of zones, which encompass a spectrum of metabolic properties and functional heterogeneity of hepatocytes. Hepatocytes near the portal triad, or periportal hepatocytes, are identified as Zone 1 hepatocytes and are typically oxidative and glucose sparing, while pericentral hepatocytes (Zone 3) are typically glycolytic and lipogenic (Gebhardt 1992). The heterogeneity of hepatocytes in the liver highlights a strength in adapting to transient events, however, can be altered in chronic conditions and lead to detrimental effects.

1.1.2 HEPATIC METABOLISM OF CARBOHYDRATES AND FATS

One of the key roles of the liver is to act as the central distribution centre of glucose, lipids, and proteins to the rest of the body. Two key hormones that regulate these metabolic processes are insulin and glucagon. These hormones can rapidly shift glucose metabolism from storage to production, respectively.

1.1.2.1 FED STATE HEPATIC METABOLISM

In the fed state, food is digested in the gastrointestinal (GI) tract to liberate glucose, fatty acids, and amino acids, are then absorbed into the bloodstream, and transported to the liver through the portal vein. Concomitantly, an increased concentration of glucose, as well as other nutrients, in the bloodstream stimulate the synthesis and secretion of insulin from pancreatic β cells.

Glucose enters hepatocytes predominantly through the glucose transporter 2 (GLUT2) in an insulin-independent manner. This transporter is facilitative and bidirectional. Once in the cell, glucose is phosphorylated into glucose 6-phosphate (G6P) via glucokinase (GK), which can have multiple fates including being used to generate ATP via glycolysis, stored as glycogen, converted to NADPH via the pentose phosphate pathway, or utilized in the process of synthesizing lipids termed lipogenesis (Adeva-Andany et al. 2016; Samuel and Shulman 2016). Although insulin does not directly regulate glucose intake in hepatocytes, its signalling cues the storage of glucose through the activation of glycogen synthase (GS) to convert

G6P to glycogen. Briefly, but incompletely, insulin binding to its receptor results in a signalling cascade that converges on the phosphorylation and activation of protein kinase-b (AKT). The activation of AKT can inhibit glucose production by lowering the expression of gluconeogenic enzymes by suppressing the transcription factor forkhead box protein O1 (FOXO1), as well as promoting glucose storage through inhibiting glycogen synthase kinase-3 beta (GSK3ß), which relieves its inhibitory action on GS.

Fatty acids within the liver are derived either through dietary or endogenous sources. In the fed state, bile acids, which are synthesized by hepatocytes and localized to the intestinal lumen, emulsify triglycerides which can then be digested by pancreatic lipase to yield free fatty acids and glycerol. These components are then resynthesized into triglycerides by enterocytes to be packaged into chylomicrons. Chylomicrons can enter the lymphatic system and eventually reach the plasma, where they will mostly be taken up by skeletal muscle and adipose tissue due to the presence of lipoprotein lipase (LPL) at the luminal surface of capillary endothelial cells surrounding these tissues. The remnant chylomicrons, which must be a small enough size to be sieved through the fenestrae of the liver, can be taken up into hepatocytes directly via low-density lipoprotein receptors (LDLRs), LDLR-related protein (LRP), or sequestration (Cooper 1997). Finally, fatty acids are released via lysosomal processing to be processed within the cell. Under normal circumstances, the liver will process a large quantity of lipids and only store a small amount in the neutral form of lipid droplets via esterification into

triglycerides, phospholipids, and cholesterol esters. These lipids can also be incorporated into membrane structures or repackaged and exported back into the circulation. The fate of lipids is regulated through a variety of mechanisms that balance fatty acid uptake with fatty acid oxidation and secretion back into the plasma via triglyceride-enriched very low-density lipoproteins (VLDLs) (Alves-Bezerra and Cohen 2018).

Another source of fatty acids in the liver comes from the synthesis of excess glucose and fructose by a process called *de novo* lipogenesis (DNL). Briefly, (1) glucose and fructose are converted to pyruvate via glycolysis, (2) pyruvate is further processed by the pyruvate dehydrogenase complex in the mitochondria to be converted to acetyl-CoA, (3) acetyl-CoA goes through the TCA cycle, and due to high nutrient availability, ultimately leads to cytosolic citrate through the citrate/isocitrate transporter, (4) citrate, CoA, and ATP form into acetyl-CoA via the ATP-citrate lyase (ACLY), (5) acetyl-CoA carboxylase (ACC) catalyzes the carboxylation of acetyl-CoA into malonyl-CoA being the first committed step to fatty acid synthesis, (6) fatty acid synthase uses malonyl-CoA and acetyl-CoA to elongate fatty acid chains until a saturated 16-carbon palmitate is formed, (7) palmitate can then become unsaturated via the stearoyl-CoA desaturase 1 (SCD1) and further processed into a triglyceride by being esterified as three fatty acids to a glycerol backbone or be further modified (Batchuluun, Pinkosky, and Steinberg 2022).

AKT also promotes both transcriptional and post-transcriptional mechanisms important for promoting lipid synthesis. AKT activates ACLY through phosphorylation at Ser454. AKT increases the expression of DNL enzymes through phosphorylation of sterol regulatory element-binding protein 1c (SREBP1c) and carbohydrate-responsive element binding protein (ChREBP)(DeBose-Boyd and Ye 2018). The activity of these two transcription factors are also increased by acetylation by the histone acetyltransferase p300 (p300). Thus, there are multiple overlapping mechanisms by which insulin and the activation of AKT promote DNL (Y. Wang et al. 2015; Ponugoti et al. 2010; Bricambert et al. 2010).

1.1.2.2 FASTED STATE HEPATIC METABOLISM

In the fasted state, maintenance of blood glucose is a priority for the liver. Due to falling blood glucose levels during fasting, insulin secretion from the pancreatic beta cells is reduced, while glucagon secretion from pancreatic alpha cells is increased. This is concomitant with a rise in catecholamines from the CNS and plays a role in the regulation of hepatic metabolism. G6P can be dephosphorylated at the endoplasmic reticulum by G6Pase to release glucose, which can be facilitated to the circulation via GLUT2. Glycogenolysis is also activated by the change in these hormones - reduced insulin signalling results in GS being inhibited, while glycogen phosphorylase (GP) is activated by glucagon's effects (Rui 2017). And although the liver mainly produces glucose through

glycogenolysis in short-term fasting, during prolonged fasting, hepatocytes can synthesize glucose via gluconeogenesis using lactate, pyruvate, glycerol, and amino acids as precursors. Gluconeogenesis is a process that is specifically carried out by the liver and kidney. Increases in gluconeogenesis require that glycolysis is inhibited, shifting the liver's substrate oxidation towards fat oxidation to produce the ATP necessary to produce glucose. This allows for the liver to use the fatty acids liberated by adipose tissue, due to increases in catecholamines, as substrates for glucose production. Fat oxidation utilizes mitochondrial β oxidation to provide intermediates for the electron transport chain to generate ATP, but also generates ketone bodies such as β-hydroxybutyrate, acetoacetate, and acetone to be exported into the circulation and used as fuel by other organs during prolonged fasting (Rui 2017).

The liver depends on mitochondrial metabolic processes, including β-oxidation, the tricarboxylic acid (TCA or Kreb's) cycle and ketogenesis, to maintain homeostasis (Rui 2017). This occurs through the oxidation of substrates including amino acids, pyruvate, and fatty acids, which are tightly coupled to ATP synthesis through oxidative phosphorylation. Briefly, pyruvate which is provided by glycolysis is transported into the mitochondria and transformed into acetyl-coenzyme (acetyl-CoA) via pyruvate dehydrogenase (PDH). Furthermore, fatty acids of different carbon lengths are activated into fatty acyl-CoAs via acetyl-CoA synthetases (ACS), transported into the mitochondrion via carnitine palmitoyl transferase 1 (CPT1) and CPT2, then oxidized via β-oxidation with the involvement of the family

of acyl-CoA dehydrogenases (including very long-chain (VLCAD), long-chain (LCAD), medium (MCAD), and short-chain (SCAD)) and FAD as an electron acceptor to yield acetyl-CoA and acyl-CoA (Houten et al. 2016). Acetyl-CoA can then enter the TCA cycle to provide energy within the cell, or, in an extended fasted state, be processed to provide energy to extrahepatic tissues via ketogenesis. Mitochondrial fatty acid oxidation (FAO) is transcriptionally regulated via multiple transcription factors, including the peroxisome proliferator-activated receptor PPARα/γ/δ, forkhead box A2 and nuclear respiratory factors 1 and 2 (NRF-1/2), the transcriptional co-activator peroxisome proliferator-activated receptor coactivator 1-alpha (PGC1α), and the NAD-dependent deacetylase sirtuin 1 (SIRT1).

1.2 NON-ALCOHOLIC FATTY LIVER DISEASE AND STEATOHEPATITIS

Non-alcoholic fatty liver disease (NAFLD) is a common liver disorder with an estimated global prevalence of 25% and is characterized by the accumulation of fat in the liver in the absence of significant alcohol consumption. This growing epidemic poses an immense burden on health-related quality of life, healthcare costs, and economic losses, with upwards trending estimations beyond $100 billion in the United States and €35 billion in Germany, France, Italy, and the United Kingdom in 2016 (Z. M. Younossi, Blissett, et al. 2016). NAFLD is a spectrum of liver diseases that spans in severity from non-alcoholic fatty liver (NAFL) to non-alcoholic steatohepatitis (NASH) and hepatic fibrosis (Z. Younossi et al. 2018).

NAFL is defined as the presence of hepatic steatosis over 5% of liver volume without inflammation or hepatocellular injury (Z. M. Younossi, Koenig, et al. 2016). On the other hand, NASH is a more severe form of NAFLD that is characterized by hepatic steatosis, inflammation, and hepatocellular injury. NASH can progress to advanced fibrosis, cirrhosis, and hepatocellular carcinoma (HCC), and is becoming a leading indication for liver transplantation. In fact, advanced fibrosis is the most significant predictor of mortality in NAFLD (Dulai et al. 2017). It is estimated that approximately 20-30% of patients with NAFL will progress to NASH, and considering that the risk of progression may vary due to several factors including age, sex, ethnicity, menopausal status, obstructive sleep apnea, socioeconomic status, and other associated comorbidities, there has been considerable focus towards discovering a multitude of mechanisms by which NAFLD progression can be prevented or delayed (Harrison et al. 2023; Z. M. Younossi, Koenig, et al. 2016).

The growing prevalence of NAFLD closely matches that of other non-communicable diseases such as obesity, type 2 diabetes (T2D), dyslipidemia, and cardiovascular disease, leading many to consider it as the hepatic manifestation of metabolic syndrome (Z. M. Younossi 2019; Z. Younossi et al. 2019; Lobstein et al. 2023). In fact, T2D and NAFLD have a bidirectional causal relationship, meaning that not only does NAFLD increase the risk of developing T2D, but T2D also contributes to the progression and severity of NAFLD (Leite et al. 2009; Chalasani et al. 2018; Prashanth et al. 2009; Byrne and Targher 2015; Fan et al. 2016; Fruci et al. 2013). And although the exact mechanisms underlying this bidirectional

relationship are not fully understood, insulin resistance, dyslipidemia, and chronic low-grade inflammation are thought to play important roles in the pathogenesis of these multi-factorial diseases.

1.2.1 CLINICAL PRESENTATION, ASSESSMENT, AND DIAGNOSIS

Typically, NAFLD is a silent disease, meaning patients are asymptomatic and are incidentally discovered on routine imaging studies such as ultrasound or computed tomography (CT). If there are symptoms, they are generally nonspecific and include fatigue, abdominal discomfort, and a mild elevation in liver enzymes such as alanine aminotransferase (ALT), aspartate transaminase (AST), and/or gamma-glutamyltransferase (GGT). However, a large proportion of NAFLD patients have normal-range enzyme levels and do not have routine imaging, thus, many patients who are living with the disease can be overlooked (Dyson, Anstee, and McPherson 2014). This highlights a challenge in the field, where a large volume of patients which can prevent disease progression through diet and lifestyle modifications are going unnoticed. Symptoms do tend to arise when people develop NASH and fibrosis developing into cirrhosis, whereby clear symptoms involve intense itching, abdominal swelling, easy bruising or bleeding, jaundice, blood vessels appearing underneath the skin's surface, and some behaviour changes including confusion and slurred speech.

Formally, the diagnosis of NAFLD requires (1) the exclusion of significant alcohol consumption, (2) evidence of hepatic steatosis via imaging or histology, (3)

no competing etiology including hepatitis C, medications, parenteral nutrition, Wilson's disease, or malnutrition, and (4) no co-existing causes of chronic liver diseases including hemochromatosis, autoimmune liver disease, chronic viral hepatitis, or alpha-1 antitrypsin deficiency (Chalasani et al. 2018). Though the discussion of non-invasive tests (NITs) and methods to assess steatosis and fibrosis is beyond the scope of this literature review, magnetic resonance (MR) imaging by spectroscopy or proton density fat fraction (PDFF) are the most widely used tools in NAFLD clinical trials to quantify hepatic steatosis, while clinical decision aids (NAFLD fibrosis score and FIB-4 index), serum marker panels (Enhanced Liver Fibrosis (ELF), Fibrometer, FibroTest, and Hepascore), or imaging modalities including transient elastography (TE), MR elastography (MRE), acoustic radiation force impulse imaging, and supersonic shear wave elastography) are used to detect liver fibrosis (Kaswala, Lai, and Afdhal 2016; Chalasani et al. 2018). FibroScan, which is a specific type of ultrasound technology that is easier to access and can non-invasively measure liver steatosis and stiffness (fibrosis) was recently approved by the U.S. Food and Drug Administration (FDA) for use in both adults and children, and although it was inferior to MRE in identifying advanced fibrosis stages, it was superior in detecting moderate fibrosis (Vuppalanchi et al. 2018; X. Zhang, Wong, and Wong 2020). Collectively, there is great emphasis on the development of non-invasive biomarkers and tools to detect and/or predict the presence and severity of NAFLD, however, currently, each

measurement has its limitations (cost, reliability, access, breadth, time) and clinicians are awaiting consensus and standardization to incorporate into practice.

Based on the combination of clinical, laboratory, and imaging findings mentioned above, a clinician may decide to request a liver biopsy from a patient with suspected NAFLD. Although not required for diagnosis, this remains the gold standard in characterizing liver histological alterations as, irrespective of the underlying pathogenesis, the histopathological characteristics of adult NAFLD are relatively consistent. However, obtaining a liver biopsy is very expensive, requires time and expertise for interpretation, carries inherent morbidity risk, and very rarely mortality risk (Chalasani et al. 2018). Furthermore, there remains concern in sampling error, which has led to approaches in which larger needle sizes, multiple core biopsies, and repeated blinded assessments by pathologists are used to improve the reliability in diagnosing NASH (Vuppalanchi et al. 2009; Harrison et al. 2023). Nevertheless, liver biopsy is still the only means to definitively diagnose NASH and fibrosis.

One of the semiquantitative assessment scoring systems used to assess NAFL/NASH is the NAFLD Activity Score (NAS) (Kleiner et al. 2005). This system was developed to address the full spectrum of lesions in NAFLD for use in clinical trials and consists of 14 histological features: 4 of which are semiquantitative based on severity: including steatosis (0-3), lobular inflammation (0-2), hepatocellular ballooning (0-2), and fibrosis (0-4), while the remainder are binary as present or not present. The composite score, or the sum of the four measurements above can

be split into three categories, no NASH (0-2), borderline NASH (3-4) and definite NASH (5-8). Assessment of severity is specified for each category with general definitions and criteria. Of note is the classification of fibrosis severity, as early stage of fibrosis (F1), composed of either perisinusoidal or periportal, but not both, fibrosis is segmented into three categories to identify development from different microanatomical regions: (1A) consists of mild, zone 3, perisinusoidal fibrosis, (1B) consists of moderate, zone 3, perisinusoidal fibrosis, (1C) consists of portal/periportal fibrosis. F2 fibrosis is considered clinically significant and is characterized by both perisinusoidal and portal/periportal fibrosis. Advanced stage fibrosis consists of F3, which is bridging fibrosis between portal fields and central veins, while F4 constitutes cirrhosis.

1.2.2 PATHOGENESIS AND PROGRESSION OF NAFLD

The pathogenesis of NAFLD is complex and there are many molecular pathways that contribute to its development and progression. Each patient is likely to have a different combination of pathogenic drivers, making both the mechanisms and clinical manifestations highly heterogenous. Some patients can go decades with NAFL without progressing to NASH, while others progress in a relatively short period of time. In some cases, NASH may not even be preceded by NAFL, while fibrosis can occur in NAFL (yet at a slower rate than NASH) (S. Singh et al. 2015). This makes it difficult to understand the pathogenesis of NAFLD, however, a

conceptual framework can aid in tying the concepts of pathogenic drivers together (Friedman et al. 2018).

The substrate-overload liver injury model of NASH proposes that the liver's capacity to process, store, and export carbohydrates and lipids is overwhelmed, leading to the accumulation of toxic lipid species. These toxic lipid species lead to mitochondrial dysfunction, hepatocellular stress, injury, and death, leading to inflammation, and eventual fibrogenesis. Therefore, understanding the sources and fates of fatty acids, insulin resistance, the response of the liver cells to lipotoxic lipids, the inflammasome, fibrogenesis, and other key factors that influence these factors such as the microbiome and genetic polymorphisms is important to a wholistic understanding of NASH and fibrosis (Neuschwander-Tetri 2017).

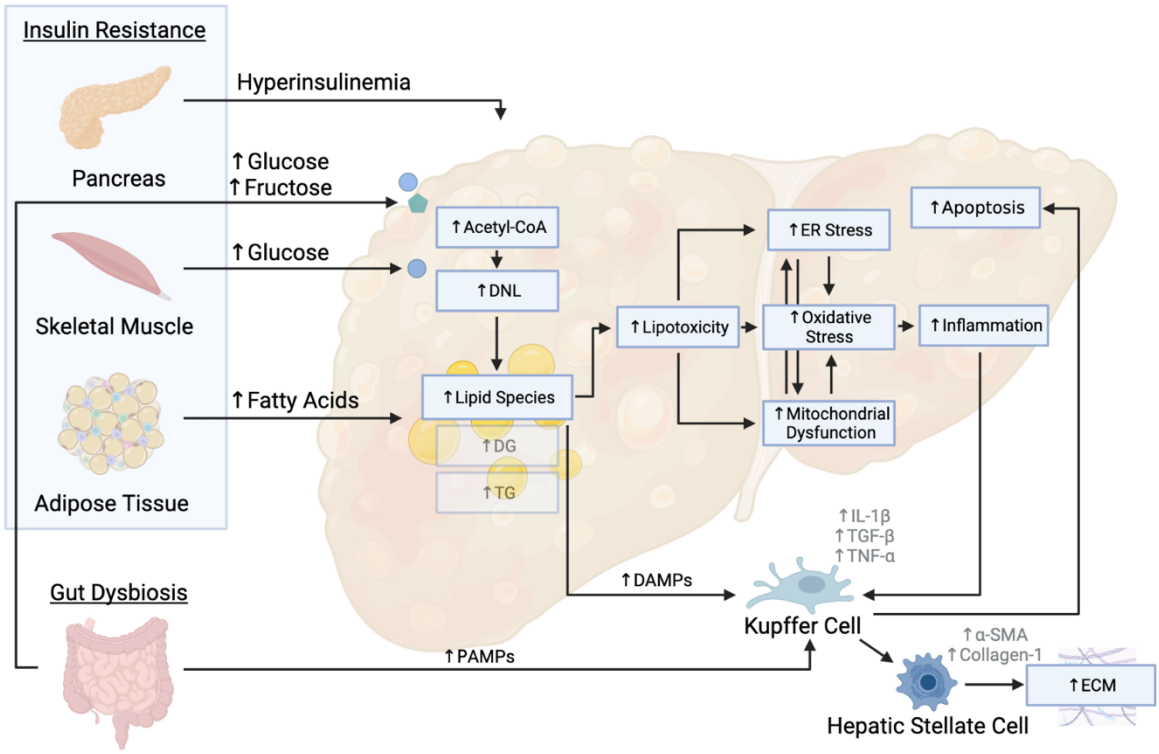

Figure 1.1. The substrate-overload liver injury model of NASH and hepatic fibrosis. This schematic summary of the pathogenesis of NAFL/NASH illustrates organ crosstalk leading to metabolic disturbances in the cells of the liver. Insulin resistance promotes hyperinsulinemia from the pancreas, reduced glucose uptake and storage in the skeletal muscle, and increased liberation of fatty acids from dysregulated adipose tissue lipolysis. Increases in these substrates contribute directly to the accumulation of lipid species including diglycerides and triglycerides; both from the direct synthesis of endogenous fatty acids and through the conversion of excess glucose and fructose through DNL. Increases in the accumulation of lipid species leads to a lipotoxic environment, which simultaneously and connectively activates the ER stress pathway, increases mitochondrial dysfunction, all ultimately leading to aberrant oxidative stress. This then promotes inflammation activates Kupffer cells to secrete IL-1β, TGF-β, and TNF-α. These cytokines lead to the activation of hepatic stellate cells to secrete extracellular matrix proteins such as α-SMA and Collagen-1 at a faster rate than they can be degraded.

1.2.2.1 INSULIN RESISTANCE AS A PRIMARY DRIVER OF NAFLD

Insulin resistance is a key driver in the pathogenesis of NAFLD and is characterized by reduced glucose disposal in non-hepatic tissues including muscle and adipose tissue (Loomba et al. 2012). Although a detailed description of the mechanisms of both tissue-specific and organismal responses to insulin are beyond the scope of this literature review, a brief overview of the concepts that coalesce to promote insulin resistance and NAFLD are provided (Petersen and Shulman 2018; Samuel and Shulman 2016).

Assuming that chronic overnutrition is the main cause of systemic insulin resistance, substrate spillover from dysfunctional adipose tissue and skeletal muscle result in lipid-induced hepatic insulin resistance. With chronic nutrient stress, the capacity of adipose tissue to uptake glucose and fatty acids is reduced due to adipocyte insulin resistance and apoptosis. Insulin signalling in adipocytes is not only a major driver of a lipogenic program through ChREBP activation but is extremely significant in the suppression of lipolysis through reductions in cAMP levels via phosphodiesterase 3B (PDE3B). With increases in lipolysis due to reduced insulin sensitivity, adipose tissue releases more free fatty acids into the circulation, which ultimately find their way to the skeletal muscle and the liver. This increase in fatty acid flux into the liver can serve as substrate for intrahepatic diglyceride and triglyceride synthesis, but also can have direct and indirect effects on gluconeogenesis via the conversion of glycerol into glucose (direct), and increases of hepatic acetyl-CoA concentrations which lead to increased pyruvate

carboxylase activity and increased conversion of pyruvate to glucose (indirect) (Perry et al. 2015). Diglycerides can promote the activation of protein kinase Cε (PKCε) which is a key inhibitor of the insulin signalling cascade (Samuel et al. 2007). Consequently, hepatic insulin resistance ensues, which impairs the ability for insulin to stimulate glycogen synthesis and collectively contributes to increases in hepatic glucose output. In parallel, increases in intramyocellular lipid content results in lipid-induced insulin resistance in skeletal muscle, which ultimately reduces the capacity for skeletal muscle to take up glucose and store it as glycogen, which further worsens hepatic insulin resistance (Petersen and Shulman 2018).

Collectively, the points above support the notion that substrate spillover from adipose tissue and skeletal muscle can result in the development of hepatic insulin resistance. However, there remains the paradox that hepatic insulin resistance results in a failure to suppress hepatic glucose production and subsequent hyperglycemia, while also increasing lipogenesis leading to hyperlipidemia and steatosis. And while this may mostly be explained by the increased flux of fatty acids from adipose tissue that can be reesterified into lipids, the ability for glucose and fructose to regulate hepatic lipogenesis independently from insulin in the liver has been demonstrated to play an important role (Samuel and Shulman 2016). This is evidenced by a study showing that obese individuals with high liver fat content had a 3-fold increase in DNL compared to obese individuals with low liver fat (Lambert et al. 2014). These increases are primarily mediated through glucose

and fructose activation of DNL and the promotion of transcription factors SREBP1c (via activation of mTORC1), ChREBP, PGC-1β, and liver X receptor (LXR) (Bindesbøll et al. 2015; Nagai et al. 2009; Uyeda and Repa 2006; Matsuzaka et al. 2004). Notably, although more glucose is shuttled to the liver with insulin resistance, fructose – which is consumed in relatively similar amounts as glucose – is considered more harmful than glucose as it causes changes in the gut barrier and microbiota community as well as is primarily funneled into the liver and induces the expression of its own metabolizing enzyme ketohexokinase (KHK) (S. Yu et al. 2021). To summarize, the substrate spillover model supports the interconnectivity between insulin resistance and NAFLD, and indicates that elevations in DNL are a key contributor to NAFLD.

1.2.2.2 LIPOTOXIC LIPIDS AND MITOCHONDRIAL DYSNFUNCTION IN NAFLD

Lipotoxic lipids such as diglycerides and ceramides can promote cell injury in the liver. Their accumulation can lead to responses such as endoplasmic reticulum (ER) stress, a dysfunctional unfolded protein response, inflammasome activation, activation of apoptotic pathways, inflammation and an enhanced wound response (Friedman et al. 2018). Whether increased levels of fatty acids and lipotoxic lipids are a cause or consequence for mitochondrial dysfunction remains unclear.

Initially, with early NAFL, there is a compensatory response to increase the number and oxidative capacity of mitochondria, leading to enhanced FAO, and the production of reactive oxygen species (ROS) in limited amounts (Garcia-Roves et al. 2007; Carabelli et al. 2011). And while this response can temporarily prevent the development of a lipotoxic environment, at some point, due to a chronic oversupply of substrate, the ETC is overloaded and produces enough ROS to stimulate stress responses within the cell (Boland et al. 2018). This generation of oxidative stress, which has been shown to stimulate the ER stress response and promote mitochondrial dysfunction through mitochondrial DNA damage, interruption of the ETC, the alteration of mitochondrial membrane permeability, and Ca^{2+} homeostasis, has been debated as a fulcrum point of NAFL progression to NASH. In 1998, Day and James hypothesized a “two hit” NASH model, whereby steatosis was the “first hit” and the “second hit” consisted of the generation of ROS (C. P. Day and James 1998). Over the years, the portrait of NASH pathogenesis has evolved and multiple parallel influences that lead to cell injury and inflammation have shed light on the complexity and disparateness of each case of NASH, highlighting the difficulty in finding a therapy that will aide a large proportion of patients living with the disease. However, promoting mitochondrial homeostasis through mechanisms which increase content and function, while decreasing dysfunctional and damaging sites, are a subject of intense investigation and could ameliorate several features of NASH.

1.2.2.3 HEPATIC INFLAMMASOME

The inflammasome is a multiprotein complex that responds to danger-associated molecular patterns (DAMPs) as well as pathogen-associated molecular proteins (PAMPs) and may be a crucial driver in the progression of hepatocyte stress responses and the stimulation of fibrogenesis in NASH (Csak et al. 2011). In the context of NASH, the inflammasome is activated in response to excess saturated fatty acids (DAMPs) and products of the gut microbiome that spill over into the portal circulation (PAMPs), and this results in the expression of proinflammatory cytokines such as interleukin (IL)-1β and IL-18 that can promote apoptosis through activation of caspase-1.

1.2.2.4 HEPATIC FIBROGENESIS

Fibrogenesis is driven by signalling from stressed or injured hepatocytes, activated macrophages and leads to the activation of hepatic stellate cells into myofibroblasts (Tsuchida and Friedman 2017). Myofibroblasts then produce and secrete matrix proteins, such as α-smooth muscle actin (α-SMA) and type 1 collagen, at a faster rate than can be degraded. Collagen deposition can be assessed by visualizing and quantifying the presence of picrosirius red. The accumulation of extracellular matrix in the liver can then lead to progressive fibrosis, cirrhosis, portal hypertension, and liver failure. Thus, fibrogenesis is the major cause of liver-related death in patients with NASH.

1.2.2.5 GENETIC PREDISPOSITION TO NAFLD

Evidence from human genetic analyses associating gene variants with histological severity have revealed some degree of heritability in NAFLD (Pafili and Roden 2021). Polymorphisms have been described in at least 12 genes, including PNPLA3, TM6SF2, GCKR, IRS1, ENPP1, MBOAT7, HSD17B13, SOD2, UCP2, MERTK, LYPLAL1, and FNDC5. Their functions involve processes for fatty acid and triglyceride composition and degradation, insulin signalling, oxidative stress, and hepatic stellate cell activation. These genetic predispositions coupled with obesity and insulin resistance may trigger the development and progression of NAFLD. And although there are still a lack of studies representing ethnic populations and all stages of NAFLD, certain studies have illustrated genetic links to autophagy and NAFLD (Mancina et al. 2016; Dongiovanni et al. 2010; Baselli et al. 2022; Schwerbel et al. 2020; Petta et al. 2014; Seitz et al. 2019).

1.3 NAFLD AND AUTOPHAGY

There are many different genetic and environmental factors that can trigger the progression of NAFL to NASH. A converging aspect is that many of these triggers result in the impairment of cellular function and organelles, which results in endoplasmic reticulum (ER) stress, lysosomal dysfunction, and mitochondrial dysfunction. In the liver, autophagy not only serves as a nutrient stress rescue pathway, but also responds to fasting and feeding cycles and plays a crucial role in overall organ metabolism. The role of autophagy is to degrade damaged

organelles and proteins through sequestration into vesicles and subsequent fusion with acidic lysosomes in order to liberate reusable building blocks such as glucose and amino acids for cellular homeostasis. There are three major categories of autophagy, including (1) macroautophagy – in which autophagosomes are formed to engulf and sequester cellular components to be degraded by the lysosome, (2) microautophagy - which encompasses small parts within the cytoplasm that are directly sequestered and degraded by endosome and lysosome, and (3) chaperone-mediated autophagy – which targets proteins with the common KFERQ motif to be directed for degradation by lysosomes (Dikic and Elazar 2018). In this thesis work, the focus is particular to macroautophagy as it is considered the main route for cytoplasmic components to be incorporated into the lysosome and will be referred to as autophagy from hereon.

The overall process of autophagy involves three main stages, including (1) initiation, (2) phagophore expansion and nucleation, and (3) autophagosome maturation, fusion, and degradation. The cellular mechanisms of each of these processes have been vigorously studied and summarized previously, however, this is beyond the scope of this thesis introduction and therefore only components that are necessary to understand the work will be covered (L. Yu, Chen, and Tooze 2018).

Unc-like kinase 1 (ULK1) is the primary initiator of autophagy and exists in a complex of proteins including ULK1, the focal adhesion kinase family interacting protein of 200 kDa (FIP200), autophagy-related protein 13 (ATG13), and ATG101.

When activated via alterations in phosphorylation, acetylation, or ubiquitination status, the phosphorylating components of the class III PI3K (PI3KC3) complex I (which includes PI3KC3, vacuolar protein sorting 34 (VPS34), Beclin1, ATG14, activated molecule in Beclin1-regulated autophagy protein 1 (AMBRA1), and general vesicular transport factor (p115)) triggers nucleation of the phagophore and activates phosphatidylinositol-r-phosphate (PI3P) production at an intracellular membrane called the phagophore assembly site (PAS; mostly studied at the site of the ER called omegasomes, but has been found at other membranes such as ER-mitochondria, ER-plasma membrane, recycling endosome sites). This leads to the recruitment of PI3P effector proteins, including WD repeat domain phosphoinositide-interacting protein 2 (WIPI2) and zinc-finger FYVE domain-containing protein 1 (DFCP1), which allow for recruitment of the ATG12~ATG5-ATG16L1 complex. This complex is necessary to conjugate ATG8 proteins that are required for the elongation and closure mechanisms of the phagophore and is also required for the maturation and lipidation of the microtubule-associated protein light chain 3 (LC3) proteins with membrane bound phosphatidylethanolamine (PE). This conjugation reaction of cytosolic LC3-I to membrane-bound LC3-II via PE is the characteristic signature of autophagic membranes and is a reliable measure of an activated autophagosome.

LC3-II is involved in the closure of the phagophore into an autophagosomal membrane, as well as the sequestration of components that contain an LC3-interacting region (LIR) in both non-selective and selective autophagy. Once cargo

is tagged for degradation via ubiquitin, autophagic adaptor proteins which bind to both ubiquitin and LC3 (e.g. p62/SQSTM1, NBR1, NDP52, OPTN, NIX, BNIP3, FUNDC1) allow for targeted sequestration, and with the help from other cell membranes to contribute to membrane elongation, results in autophagosomal membrane encapsulation and sealing into a double-membraned vesicle called the autophagosome. The autophagosome matures by shedding its ATG proteins and fusing with early endosomes and is eventually transported towards lysosomes via microtubules for degradation. Once fused with the lysosome (via soluble N-ethylmaleimide-sensitive-factor attachment protein receptor (SNARE)-dependent and lysosomal associated membrane protein 2 (LAMP2)-mediated processes), the autophagosome is called an autophagolysosome and its constituents are degraded by acid hydrolases so that nutrients can be salvaged and released back into the cytoplasm for reuse (Dikic and Elazar 2018; Yim and Mizushima 2020; Y. G. Zhao and Zhang 2019).

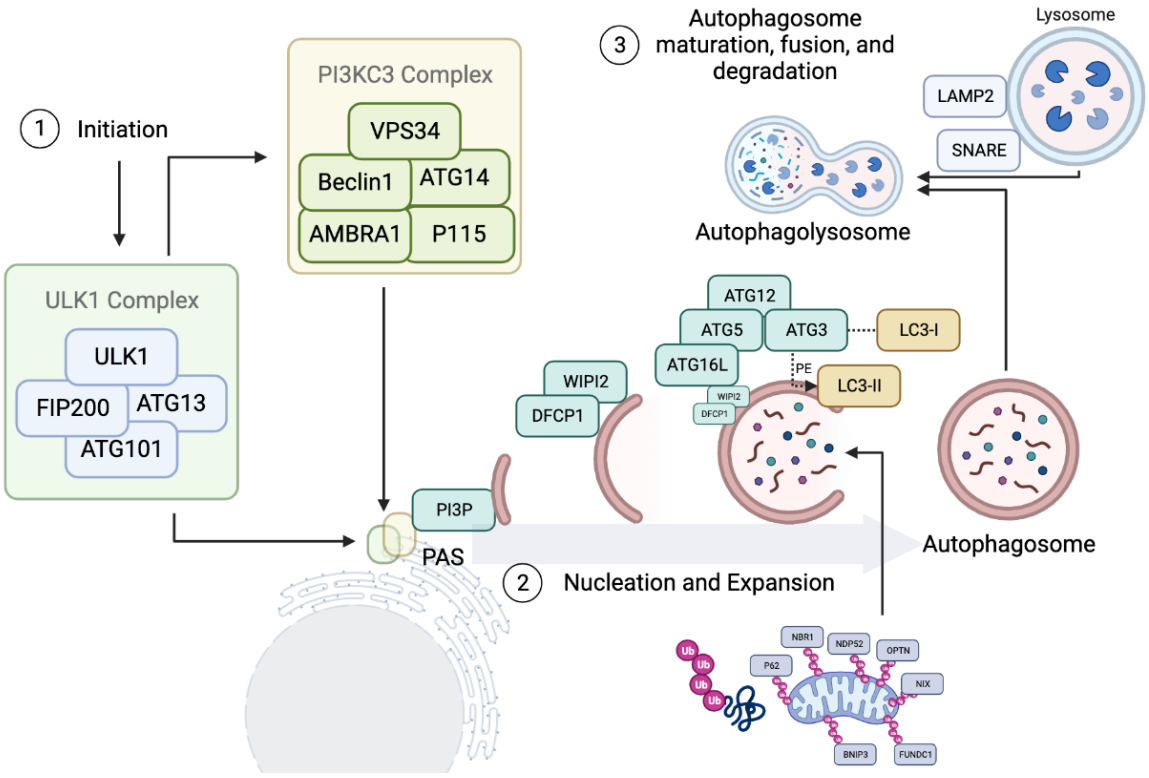

Figure 1.2 Autophagosome formation, maturation, fusion, and degradation. The formation and processing of an autophagosome requires several phases and can be broken down into (1) initiation, (2) nucleation and expansion, and (3) maturation, fusion, and degradation. Activation of the ULK1 complex (ULK1, FIP200, ATG13, ATG101) is the first step required which also activates the PI3KC3 complex (VPS34, Beclin1, ATG14, AMBRA1, P115). These complexes colocalize at the phagaphore assembly site (PAS) and stimulate the nucleation of the phagophore via PI3P production. PI3P recruits WIPI2 and DFCP1 which then allow for the recruitment of the ATG12-ATG5-ATG16L complex. This complex is necessary for ATG3 to conjugate ATG8 proteins, most notably LC3B. LC3-I is lipidated and incorporated into the phagophore membrane with PE to yield LC3-II. Once cargo is tagged for degradation via ubiquitination (Ub) and adaptor proteins (P62, NBR1, NDP52, OPTN, NIX, FUNDC1, BNIP3) they are sequestered, encapsulated, and sealed to yield an autophagosome. Autophagosome travel via microtubules towards the lysosome, where SNARE and LAMP2-dependent fusion yield an autophagolysosome. Acidic hydrolases are then able to degrade the cargo into reusable constituents for the cell.

Autophagy is an active process, making it difficult to assess its function within humans. This active process, which is commonly referred to as autophagic flux, involves several markers of autophagy (LC3, p62, etc.) which can be compared to determine whether there are alterations in their content. However, caution must be exercised in interpreting these results as it is difficult to interpret with certainty whether a change in content means a particular conclusion with directionality (e.g. if markers of the pathway are up, it is difficult to surmise whether there is an enhanced ability to respond to cues, or whether there is actually less clearance and more aggregation of the markers).

Certain studies involving liver samples from people with or without NAFL and NASH have made associations of altered autophagy markers with NAFLD severity. Carotti and colleagues have shown that p62 clusters and lipid droplet-loaded lysosomes were positively correlated with NAFLD activity score (NAS) and fibrosis severity (Carotti et al. 2020). These findings are in concert with some (Fukuo et al. 2014), but not all studies assessing autophagic markers and NAFLD, as some have seen reduced markers of LC3 (Kashima et al. 2014) and others have indicated that the defining point between NAFL and NASH is the cell's ability to match autophagy with demand for degradation and recycling (González-Rodríguez et al. 2014; Ding et al. 2020; Challa et al. 2019). The same can be found in preclinical rodent studies, as a recent structured review presented dissimilarities in findings that measured several autophagy markers in steatosis models (Ramos, Kowaltowski, and Kakimoto 2021).

Although reviewed extensively in the “Guidelines for the use and interpretation of assays for monitoring autophagy”, there are many ways to assess the activity of the autophagy pathway (Klionsky et al. 2021). One of the most common and easily accessible methods is to assess autophagic “carrier flux” by measuring LC3-II turnover in the presence and absence of lysosomal or vacuolar degradation via western blot. This can be done both in cultured cells and in rodent models with several compounds including protease inhibitors, compounds that neutralize the lysosomal pH, or agents that block the fusion of the autophagosome with the lysosome. Chloroquine (CQ) is commonly used to assess autophagic flux, as it inhibits the fusion of autophagosomes with lysosomes but also neutralizes the pH of the lysosome (Mauthe et al. 2018). Thus, to determine if a treatment or genetic model increases or decreases autophagic carrier flux, it is important to interpret results in the presence and absence of the inhibitor of lysosomal degradation. In the case of an agent that increases autophagic carrier flux, the use of the lysosomal inhibitor (e.g CQ) will result in a large increase in the accumulation of carrier proteins such as LC3 or p62 on its own, and with the addition of the agent an additive or supra-additive effect may be suggestive of increased autophagic flux. Even with this assay, caution should still be exercised as lysosomal function and fusion are not being assessed, and it is recommended to have multiple measures of autophagic activity using different methods.

Another method that is becoming more commonly utilized is the use of tandem monomeric RFP-GFP tagged LC3, whereby the GFP is sensitive to the

acidic and proteolytic environment within the lysosome, while the RFP is more stable (C. Zhou et al. 2012; Tanida, Ueno, and Uchiyama 2014). Therefore, using colocalization tools allows for the comparison of compartments of the fluorophore, where an overlap resulting in “yellow” indicates a phagophore, amphisome or autophagosome, while a red-only signal indicates an autophagolysosomal compartment. This method requires the ability to transfect cells, as well as high resolution confocal microscopes and therefore is much less accessible, however, does allow to detect a time-lapse of the process.

Ultimately, the process of assessing autophagy requires careful consideration when designing experiments and interpreting results. And while there is no consensus on “the gold-standard method” for monitoring autophagy, it is accepted that multiple assays be utilized in order to infer how the process can be altered.

1.3.1 ROLE OF AUTOPHAGY IN THE LIVER

Autophagy has traditionally been viewed as a process to maintain cellular energy homeostasis in times of fasting and to break down dysfunctional constituents into building blocks for cellular rejuvenation. However, since the discovery of autophagy in rodent liver tissue in the 1960s, many other functions of autophagy have been uncovered, particularly in the liver (de Duve 1963; Straus 1964a, 1964b). With regards to NAFLD, although it is not clear which occurs first – defective autophagy or development of hepatic steatosis – a self-perpetuating

cycle is likely to exist whereby impaired autophagy further worsens steatosis and insulin insensitivity, which in turn results in further dysregulation of autophagy signalling pathways.

Within the hepatocyte, autophagy mediates the metabolism of intracellular lipids through several mechanisms. Both regulatory and functional similarities exist between lipolysis and autophagy, and spurred explorations to investigate the degradation of hepatic lipids via a process termed “lipophagy”. In 2009, Singh and colleagues discovered that pharmacological blocking of autophagy using 3-methyladenine (3MA) or Atg5 gene silencing led to increased triglyceride accumulation with a reduction of triglyceride oxidation and decay in hepatocytes (R. Singh et al. 2009). The authors went on to identify lipid droplets being delivered to lysosomes in autophagosomal structures using electron microscopy and found that mice with a hepatocyte-specific knockout of the autophagy gene Atg7 had increased liver triglycerides and cholesterol on a high-fat diet. Similar findings have been shown in models of defective autophagy in the liver from different parts of the pathway including ATG14 (initiation) and TFEB (transcriptional and lysosomal) (Xiwen Xiong et al. 2012; Settembre et al. 2013).

In addition to the degradation of lipid droplets, several other studies have found that chaperone-mediated autophagy can regulate lipolysis through the degradation of proteins that coat the surface of lipid droplets. For example, chaperone-mediated autophagy degrades perilipin 2 (PLIN2) and perilipin 3 (PLIN3) in order to increase the association of adipose triglyceride lipase (ATGL)

and macroatuophagy proteins to the lipid droplet, while genetic knockout of LAMP2 in mice leads to hepatic steatosis (Schneider, Suh, and Cuervo 2014; Kaushik and Cuervo 2015). Thus, in the context of NAFLD, the degradation of lipids via lipophagy play an important role in reducing toxic levels of lipid species to promote metabolic homeostasis in hepatocytes (Grefhorst et al. 2021).

Aside from the degradation of lipid droplets, autophagy in the liver also serves a purpose to protect hepatocytes from cell injury and death via multiple mechanisms. There is clear crosstalk between the autophagy pathways and apoptotic cell death pathways. Investigations around this topic include the antiapoptotic protein Bcl-2 inhibiting Beclin 1-dependent autophagy, and calpain-mediated cleavage of Atg5 which triggers its mitochondrial translocation and association with Bcl-x_L to cause cytochrome *c* release and caspase activation to promote apoptotic cell death (Jung, Jeong, and Yu 2020; Yousefi et al. 2006; Pattingre et al. 2005). A central theme to impaired autophagy in NAFLD revolves around dysfunction in the later steps of the autophagic process such as decreased lysosomal function and autophagosome-lysosome fusion (Ramos, Kowaltowski, and Kakimoto 2021). These impairments may be due in part to a consequence of increased ER-stress in NAFLD models.

Autophagy has been shown to share regulatory pathways with the unfolded protein response (UPR) pathway, which is a network of adaptive responses that restore ER function in times of duress. The UPR is activated in response to alterations in ER homeostasis in three classical ways, including (1) the

serine/threonine-protein kinase/endoribonuclease inositol-requiring enzyme 1α (IRE1α) regulation of x-box binding protein 1 (XBP1) nuclear localization and mRNA degradation, (2) the protein kinase r-like ER kinase (PERK) phosphorylation of eukaryotic initiation factor 2α (eIF2α) resulting in the inhibition of translation and stimulation of the transcription of genes associated with degradative pathways, and (3) activating transcription factor 6 (ATF6) translocation to golgi for cleavage and nuclear localization (reviewed in (Bhattarai et al. 2021)). Ultimately, under acute conditions these three steps lead to adaptive responses which restore homeostasis within the cell, however, under chronic pathological conditions may become maladaptive, promote an accumulation of misfolded proteins, and result in the activation of apoptosis pathways.

For example, one study showed that palmitic acid treatment induced ER-stress in cultured hepatocytes and resulted in the induction of autophagy, however, the fusion of autophagosomes with lysosomes was impaired in chronic treatment conditions (Miyagawa et al. 2016). Interestingly, this study showed that lipid-induced ER stress interfered with the general macroautophagy process, but selective forms of autophagy including ubiquitin-positive aggregate proteins were not affected (Miyagawa et al. 2016). Another study demonstrated that ER-stress promoted increased levels of asparagine, which in turn reduced lysosomal acidification. This provides evidence that mechanisms exist to finely-tune and specify autophagic processes based on the needs of the cell (Xiaojuan Wang et al. 2018). In addition to this fine-tuning signalling, Zhang and colleagues showed that

the spliced form of XBP1 (sXBP1) – which is a transcription factor necessary for UPR activation – binds to the promoter region and activates the expression of the transcription factor EB (TFEB) to protect HFD-fed mice from obesity-associated metabolic dysfunction and liver steatosis (Z. Zhang et al. 2020). TFEB is known as the master regulator of lysosomal biogenesis, but it also increases the expression of several autophagy related genes. Thus, in the liver, its downregulation results in a reduction of lysosomal function, lipophagy, and fatty acid oxidation (Napolitano and Ballabio 2016).

Although the way in which these signalling pathways are dysregulated in NAFLD are not fully understood, the studies above indicate a clear connection between ER-stress and autophagy and suggest that autophagy is activated after ER-stress in order to promote cell survival.

1.3.2 MITOPHAGY

As discussed above, mitochondrial oxidative phosphorylation is important for liver homeostasis and may be impaired with NASH. Mitophagy is a specific type of macroautophagy used to describe the selective degradation of defective or redundant mitochondria. It is a set of pathways that occur in addition to regular autophagy, which will still non-selectively phagocytose mitochondria. Ultimately, by removing dysfunctional or unneeded mitochondria, mitophagy contributes to maintaining mitochondrial network homeostasis by preventing the production of ROS in excess. Thus, its dysfunction could lead to the progression of liver diseases

such as NAFLD (N. P. Zhang et al. 2019). In fact, a recent study using liver biopsies found that compromised hepatic fatty acid oxidation and mitochondrial turnover are intimately linked to increasing NAFLD severity in patients with obesity (Moore et al. 2022). In this study, they found that hepatic autophagy, mitophagy, and mitochondrial dynamics markers were downregulated with increasing fibrosis severity. And while mitophagy operates with much of the same machinery as autophagy, there are important distinctions and unique molecular mechanisms (Choubey, Zeb, and Kaasik 2022).

Mitophagy is often initiated when low membrane potential of mitochondria or irreversible mtDNA damage signalling leads to asymmetric apportioning of the mitochondrial network, a process called mitochondrial fission (Quintana-Cabrera and Scorrano 2023). This is typically controlled by the GTPase dynamin-related protein (Drp1), which constricts tubular membranes and oligomerizes actin to maintain membrane tension. Drp1 then recruits outer mitochondrial membrane adaptor proteins to fission sites in order to have the ER wrap around the site, further constricting mitochondria until they are split into two separate entities. These adaptor proteins include fission 1 (Fis1), mitochondrial fission factor (MFF), and mitochondrial division (MiD) 49 and 51.

Once mitochondria are ‘fissioned’ out of the network, they can be tagged for degradation via adaptor proteins containing LIRs which interact with LC3. Two of the major mitophagy pathways involve the PTEN-induced kinase 1 (PINK1)/Parkin pathway and the BNIP3/NIX pathway (Zhu, Wu, and Liao 2023). Briefly, PINK1 is

typically a protein that gets imported into the mitochondrion, however, when there is a loss of membrane potential, PINK1 accumulates on the outer surface, leading to the phosphorylation of the E3 ubiquitin ligase Parkin. Once Parkin is phosphorylated, it can catalyze further ubiquitination of mitochondrial proteins, including CISD1 and mitofusin 2, leading to the recruitment of the adaptor protein P62 and LC3 to sequester the cargo. Through an increase in ROS, hypoxia-inducible factor 1 (HIF1) can lead to the phosphorylation of BNIP3 and NIX, which then leads to the release of Beclin-1. BNIP3, NIX, and Beclin-1 have LIRs which localize LC3 and allows for subsequent autophagic processing. It is important to note that this is a simplified description of the primary mechanisms controlling mitophagy.

Hepatic mitochondria from NASH mouse models and patients have structural and molecular differences compared to their healthy counterparts (Einer et al. 2018). Structural changes are observed by transmission electron microscopy and characterized by large swollen mitochondria, aberrant structures, disorganized cristae, and altered distribution. Liver-specific Parkin knockout mice have increased steatosis, ballooning, inflammation, and composite NAS either on a HFD or Western-diet (Edmunds et al. 2020; Undamatla et al. 2023). Furthermore, loss of BNIP3 in the liver results in increased lipid synthesis, decreased fatty acid oxidation, increased ROS, and steatohepatitis (Glick et al. 2012; Springer et al. 2021; Xiaojing Wang et al. 2019). These findings illustrate the importance of mitophagy in regulating mitochondrial homeostasis in the context of NASH.

1.4 AMPK

An important regulator of autophagy and mitophagy is the AMP-activated protein kinase (AMPK). AMPK is a ubiquitously expressed serine-threonine kinase in nearly all eukaryotic cells that regulates cellular energy status by simultaneously integrating multiple physiological, hormonal, and nutritional cues to influence downstream metabolic pathways. When activated, AMPK hinders energy-consuming anabolic pathways, while stimulating pathways associated with efficient energy-producing catalytic pathways. Complexed as a heterotrimer, AMPK consists of a catalytic α subunit, a structural scaffolding and regulatory β subunit, and a regulatory γ subunit. In mammals, distinct genes encode two isoforms of α (α1/ α2) and β (β1/ β2) subunits, while there are three isoforms of the γ (γ1/ γ2/ γ3) subunit. This allows for the possibility of at least 12 distinct heterotrimeric combinations, when excluding variants, which are uniquely and differentially expressed within each tissue. Although the differences in structure and functions of these distinct heteromeric assemblies are still being unlocked, there is considerable interest in the alterations these subunits have both in allosteric and covalent modifications of the enzyme.

1.4.1 STRUCTURE AND ACTIVATION

A comprehensive description of the structure of AMPK is provided elsewhere, however, succinct, simplified, and relevant descriptions will be provided below (Steinberg and Hardie 2022). As its name implies, AMPK is canonically

activated by an increase in the cellular AMP/ADP:ATP ratio – which is indicative of energy demand – whereby AMP and ADP competitively bind over ATP to the third cystathionine-β-synthase (CBS3) repeat on the γ subunit (Gu et al. 2017). In comparing structures from different studies, this binding event causes a dramatic conformational shift and increases basal activity of the enzyme by protecting the activation loop from dephosphorylation by protein phosphatase 2-C (PP2C) (Yan et al. 2021; Xin et al. 2013; Davies et al. 1995). Phosphorylation of a conserved threonine residue (T172/T183) in the activation loop of the α subunit, primarily via the constitutively active liver kinase B1 (LKB1) or the calcium/calmodulin-dependent protein kinase kinase (CAMKK), covalently activates AMPK and increases its activity more than 100-fold compared to the non-phosphorylated state at T172 (Willows et al. 2017; Shaw et al. 2004; Woods et al. 2003; Simon A. Hawley et al. 2003, 2005; Woods et al. 2005). There are several other serine-threonine sites on the α subunit that can be phosphorylated to influence AMPK activity, such as AKT, protein kinase A (PKA), and mTORC1, some of which have been identified as isoform specific, and illustrates the complex and sensitive regulation of AMPK activity via multiple distinct inputs (Steinberg and Hardie 2022).

In addition to being the structural scaffold between the α and γ subunits, the β subunit of AMPK can also influence enzymatic activation through allosteric modulation by (auto)phosphorylation and myristoylation (Mitchelhill et al. 1997; Iseli et al. 2005; Yan et al. 2018; Dite et al. 2017; Oakhill et al. 2010; Neopane et al. 2022; Xiao et al. 2007, 2013a). Within the β subunit is the carbohydrate binding

module (CBM), also known as the glycogen binding domain, which is a region sharing sequence similarities to a number of proteins that metabolize glycogen or starch (Machovič and Janeček 2006). This site, along with the N-lobe of the α kinase domain, creates a deep cleft by which many pharmacological activators allosterically activate AMPK, including, but not limited to A-769662, MK-8722, PF-739, and salicylate (Cool et al. 2006; Myers et al. 2017; Cokorinos et al. 2017; S. A. Hawley et al. 2012; Xiao et al. 2013b; Steinberg and Carling 2019). This is called the allosteric drug and metabolite (ADaM) site of AMPK and is stabilized via phosphorylation of Ser108 on the β subunit. Interestingly, AMPK can autophosphorylate Ser108 in both β isoforms. In addition, linking AMPK with autophagy, studies in cell free assays have shown that ULK1 also phosphorylates β1-containing complexes and this effect may be enhanced by an AMP-myristoyl switch mechanism to promote colocalization with the lysosome (Scott et al. 2014; Dite et al. 2017). Importantly, Dite and colleagues clarified that phosphorylaton of AMPK β1 Ser108 can occur independently from αT172 phosphorylation. This is an important as it may explain inconsistencies in studies that have observed differences in phosphorylation of the catalytic AMPK αT172 phosphorylation versus phosphorylation of AMPK substrate downstream substrates such as ACC Ser79/212 or Raptor Ser792. Collectively, the findings from this work unveiled a complex positive feedback mechanism between ULK1 and AMPK and highlight an important role for AMPK in autophagy.

1.4.2 HEPATIC AMPK

AMPK plays several important roles in maintaining cellular energy homeostasis in the liver, including regulating fatty acid, carbohydrate, cholesterol, and amino acid metabolism (Steinberg and Carling 2019). It also influences mitochondrial health via biogenesis, fission, and autophagy/mitophagy. And though it is still being uncovered how particular heterotrimers may influence the cellular localization of AMPK, AMPK can influence the activity, localization, and activation status of transcriptional programs to fine-tune cellular energy status (Steinberg and Hardie 2022).

In rodents, hepatic AMPK is predominantly expressed as β1-containing heterotrimers (α1β1γ1 and α2β1γ1), which contrasts with human livers in which β2 heterotrimers predominate (Dzamko et al. 2010; Stephenne et al. 2011). Knockout of AMPK β1 reduces liver AMPK activity by 95%, while knockouts of α1, α2, and β2 have little to no effect on liver AMPK activity (Viollet, Andreelli, Jørgensen, Perrin, Flamez, et al. 2003; Viollet, Andreelli, Jørgensen, Perrin, Geloen, et al. 2003; Steinberg et al. 2010; Jørgensen et al. 2004; E. A. Day, Ford, and Steinberg 2017).

AMPK was originally identified as an enzyme that suppressed fatty acid and cholesterol synthesis, which was caused by inhibitory phosphorylation on ACC and HMGR, respectively (Carlson and Kim 1973; Munday 2002; Beg, Allmann, and Gibson 1973). AMPK activation also increases fatty acid oxidation through the inhibitory phosphorylation of ACC (H. M. O. O'Neill et al. 2014). This event causes

a reduction in the conversion of acetyl-CoA to malonyl-CoA, which is the rate-limiting step in fatty acid synthesis, but also has an inhibitory effect on the rate limiting step of fatty acid transport into the mitochondrion through the allosteric inhibition of carnitine palmitoyl transferase-1 (CPT-1). Thus, when ACC is inhibited by AMPK phosphorylation, less malonyl-CoA is produced, reducing the allosteric inhibition of CPT-1 and resulting in more fatty acid transport into the mitochondrion for β-oxidation.

AMPK also has the potential role to suppress hepatic gluconeogenesis and promote glucose uptake in the liver. Though studies have conflicting evidence as to whether the gluconeogenesis-suppressing effects of known AMPK activators (991, metformin) are specific to AMPK – likely due to high concentrations leading to non-specific effects –, studies by Cao and colleagues used primary hepatocytes which were acutely depleted of AMPK activity via shRNA and demonstrated a large role for AMPK in mediating the clinically relevant dose of metformin-induced suppression of hepatic gluconeogenesis (Johanns et al. 2022; Shaw et al. 2005; Miller et al. 2013; Foretz et al. 2010; G. Zhou et al. 2001; Cao et al. 2014; Hasenour et al. 2017). Furthermore, AMPK can promote glucose uptake in hepatocytes via the degradation of thioredoxin-interacting protein (TXNIP) and perhaps through the phosphorylation of other recently identified substrates of glucose uptake in a chemical genetic screen (N. Wu et al. 2013; Ducommun et al. 2019).

Liver AMPK activity is repressed in NASH mouse models (Viollet et al. 2010; Boudaba et al. 2018; P. Zhao et al. 2020). Though genetic loss of liver AMPK

activity studies have inconsistent results regarding liver steatosis– possibly due to differing compositions of diet which include supraphysiological levels of fat. However, numerous studies involving both pharmacological and genetic activation of liver AMPK indicates benefits to multiple aspects of NAFLD and NASH including steatosis, inflammation, ballooning, and fibrosis (P. Zhao et al. 2020; Garcia et al. 2019; Esquejo et al. 2018; B. K. Smith et al. 2016; Z. Liang et al. 2017; Boudaba et al. 2018). Importantly, these beneficial effects also extend to humans, as clinical trials have shown that activation of AMPK or inhibition of ACC reduces steatosis (Cusi et al. 2021; Loomba et al. 2018).

1.4.3 FATTY ACID SENSING AND OXIDATION BY AMPK

Early studies even before the name AMPK was adopted suggested that lipid moieties could activate the kinase (Carling, Zammit, and Hardie 1987). Considering fatty acids stored as triglycerides are the most dense and inert form of energy in most organisms and that their oxidation results in a high amount of ATP generation from the electron transport chain in times of need like starvation, it seems logical to suspect that there might be a direct sensing mechanism between cellular fatty acids and AMPK. Supporting the connection between AMPK and fatty acids, a collection of studies in the early 2000s showed that AMPK activity was increased with short-term treatment of fatty acids in the heart, cardiac myocytes, and myotubes (Clark, Carling, and Saggerson 2004; Hickson-Bick, Buja, and McMillin 2000; Watt et al. 2006).

Recent studies in purified enzyme preparations and cultured cells have since identified the molecular mechanisms mediating these effects. Specifically, CoA esters of fatty acids, that are 12 to 18 carbons in length, were found to activate AMPK β1 containing heterotrimers (Pinkosky et al. 2020). Using *in silico* modelling, this was shown to be mediated through FA-CoA flexibly docking into a hydrophobic channel that encompassed the ADaM site, making this the first metabolite that directly activates the kinase through this allosteric mechanism. Interestingly, while phosphorylated AMPKβ1 Ser108 makes no direct interaction with the acyl chain of palmitoyl-CoA, its importance in stabilizing the interaction between α2-β1-CBM was demonstrated in bacterial cell lines rendering the site phospho-deficient by mutating the serine to alanine.

These findings were extended *in vivo* by testing mice harboring mutations in the AMPK inhibitory phosphorylation sites on both ACC1 (S79A) and ACC2 (Ser212A) (ACC DKI). After a fast-refeed cycle, ACC DKI mice were unable to increase fatty acid oxidation in response to an exogenous administration of a lipid emulsion formula (Intralipid) (Pinkosky et al. 2020). These data suggest that fatty acid sensing by AMPK plays an important role in promoting fatty acid oxidation, however, whether this sensing axis plays a role in the pathogenesis of chronic diseases such as obesity, diabetes, and NAFLD remain unexplored.

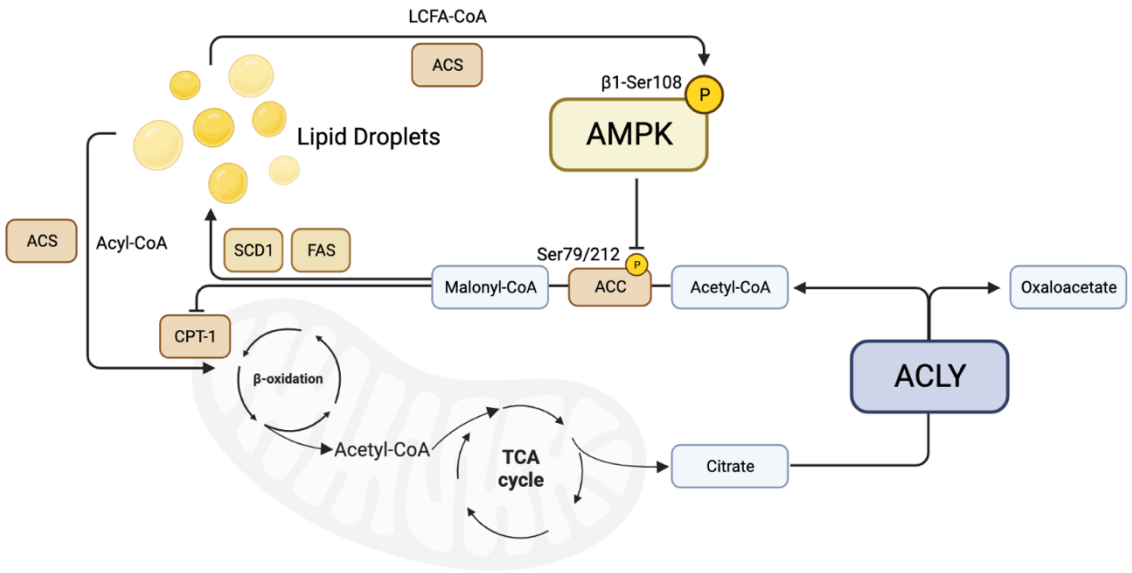

Figure 1.3. AMPK senses LCFA-CoA and increases fatty acid oxidation through the inhibitory phosphorylation of ACC. AMPK β1-containing complexes can sense LCFA-CoA through a mechanism dependent on the Ser108 residue. This results in increased activity of AMPK and the phosphorylation of ACC at Ser79 for ACC1 and Ser212 for ACC2. This is an inhibitory phosphorylation, which results in the inhibition of acetyl-CoA being converted to malonyl-CoA. Malonyl-CoA is the rate-limiting step for fatty acid synthesis, but also blocks fatty acid oxidation via the inhibition of CPT-1. Thus, when the inhibition of CPT-1 is removed, CPT-1 can increase the import of fatty acyl-CoA into the mitochondria for β-oxidation and subsequent processing through the TCA cycle. ACLY contributes to the generation of acetyl-CoA from mitochondria-derived citrate.

1.4.4 AMPK PROMOTES MITOCHONDRIAL HOMEOSTASIS

AMPK is an important regulator of mitochondrial homeostasis which includes fission, mitophagy, and biogenesis. Mitochondrial biogenesis occurs via the growth and division of pre-established mitochondria and increase their mass by adding new material to their existing network. Mitochondrial DNA encodes some of the mitochondrial proteins, however, many proteins are encoded within the nucleus. Thus, when parts of the mitochondrial network are not producing enough ATP, retrograde signals must exist to promote transcription factors to stimulate the expression of nuclear genes encoding mitochondrial proteins (NuGEMPs). When activated, AMPK can promote mitochondrial biogenesis through multiple mechanisms including increasing the expression and/or activity of PGC1α, SIRT1, p53, HDAC5, p38 MAPK, or TFEB (Hongbin Zhang et al. 2015; Jager et al. 2007; Than et al. 2015; Iwabu et al. 2010; Z. Wu et al. 1999; Houde et al. 2017; Czubryt et al. 2003; Mihaylova et al. 2011; McGee et al. 2008).

1.4.5 AMPK REGULATION OF AUTOPHAGY/MITOPHAGY

The role of AMPK in autophagy is rapidly expanding, however, there are three major categories to consider: (1) facilitation of initiation, (2) promotion of autophagosome biogenesis, and (3) autophagolysosomal fusion. Though the details of these mechanisms are beyond the scope of this review, we will review key points in the pathways (S. Wang et al. 2022).

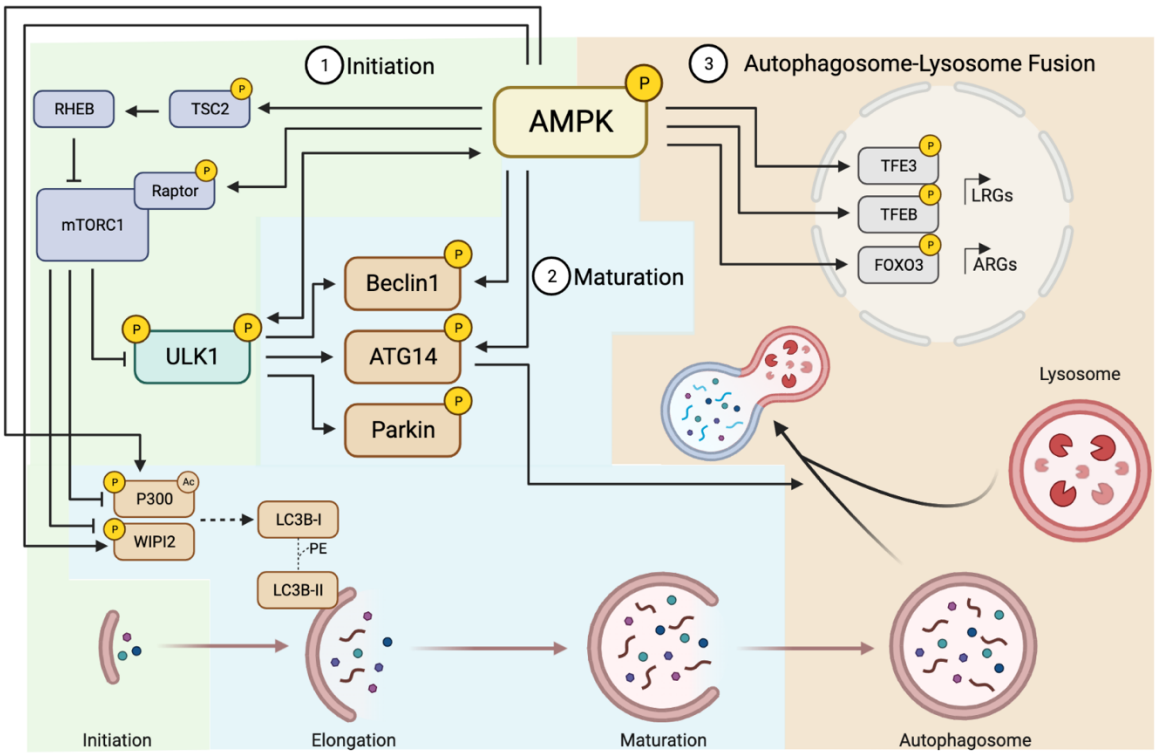

Figure 1.4. AMPK promotes autophagy via the facilitation of initiation, promotion of autophagosome biogenesis, and autophagolysosomal fusion. Starting from the top left and working around through the steps of (1) Initiation, (2) Maturation, and (3) Autophagome-Lysosome Fusion. AMPK phosphorylates TSC2 and Raptor to inhibit the mTORC1 complex. This will indirectly act to relieve the inhibition of ULK1 by mTORC1 phosphorylation. AMPK also directly phosphorylates ULK1. The mTORC1 complex phosphorylates and inhibits the ability for P300 and WIPI2 to promote VSP34 complex stability, the elongation of the phagophore, as well as the lipidation of LC3B (LC3BII) to tether to the phagophore membrane. AMPK can also directly phosphorylate WIPI2 to promote its activity. ULK1 phosphorylates multiple enzymes, including Beclin1, ATG14, and Parkin which aid in multiple mechanisms of autophagy initiation and maturation. Finally, AMPK promotes nuclear translocation of TFEB, TFE3, and FOXO1 to increase the transcription of lysosomal-related genes (LRGs) and autophagy-related genes (ARGs). This ultimately helps in autophagolysosomal fusion.

With respect to initiation, AMPK controls the fragmentation of the mitochondrial network through the phosphorylation of mitochondrial fission factor 1 (MFF) (Toyama et al. 2016; Ducommun et al. 2015).

It also phosphorylates the mTOR upstream regulator TSC2 and the mTORC1 subunit Raptor at two sites each, reducing mTORC1 activity therefore relieving the inhibitory phosphorylation of ULK1 (Inoki, Zhu, and Guan 2003; Gwinn et al. 2008). AMPK also phosphorylates ULK1 on at least four residues, with Ser555 being the most well characterized (Egan et al. 2011; J. Kim et al. 2011). This direct activation of ULK1 by AMPK is especially important for mitophagy, as mutant cell lines lacking the ability for AMPK to phosphorylate ULK1 accumulate defective mitochondria. The AMPK-ULK1 axis can also trigger the phosphorylation of Parkin at Ser108 to localize and trigger PINK1/Parkin-dependent mitophagy (Hung et al. 2021). AMPK also phosphorylates many other autophagy-initiating enzymes, including Beclin1, ATG14, and other proteins essential to form and stabilize VPS34-containing complexes (Herzig and Shaw 2018; S. Wang et al. 2022).

Phosphorylation of TSC2, mTOR1C, and ULK1 also contributes to the maturation of the autophagosome through the phagophore elongation phase. Specifically, mTORC1 phosphorylation of p300 and WIPI2 inhibits VSP34 activity and LC3 lipidation. Finally, AMPK can promote autophagosome-lysosome fusion via phosphorylation of ATG14, by promoting translocation of TFEB and FOXO3 into the nucleus (Paquette et al. 2021; Sanchez et al. 2012).

Overall, AMPK promotes biogenesis, fission, and mitophagy, and, therefore, is essential for maintaining mitochondrial homeostasis.

1.5 ACLY

1.5.1 REGULATION AND FUNCTION OF ACLY

ATP-citrate lyase (ACLY) is a ubiquitously expressed enzyme most well-known for its involvement in the *de novo* lipogenesis pathway, however, is also ideally positioned to influence nutrient catabolism and lipid biosynthesis through its control of nucleocytosolic acetyl-CoA levels (Pinkosky et al. 2017). ACLY converts TCA-derived citrate into acetyl-CoA and oxaloacetate within the cytosol. This is an essential step that catalyzes the fatty acid synthesis pathway via the conversion of acetyl-CoA to malonyl-CoA via ACC, the mevalonate pathway through a series of intermediate steps ultimately leading to the reduction to mevalonic acid through 3-hydroxy-3-methylglutarate-CoA reductase (HMGR), and gluconeogenesis through the transformation of oxaloacetate.

Although ACLY is ubiquitously expressed, it is most highly expressed in the lipogenic tissues adipose tissue and liver (Human Protein Atlas). It is a homotetramer, with four identical subunits comprising of an N-terminal acyl-CoA synthase homology (ASH) domain, a flexible linker connecting to a C-terminal citrate synthase homology (CSH) domain (Wei et al. 2020; Verschueren et al. 2019). In the liver, ACLY transcription increases with elevations in glucose and insulin levels via a coregulated response with other lipogenic genes controlled by

three transcription factors: SREBP-1c, ChREBP, and LXR (Horton, Goldstein, and Brown 2002; Ma, Robinson, and Towle 2006; Ishii et al. 2004). The activity and localization of ACLY can be influenced by allosteric activation via phosphorylation at Ser454 by cAMP-dependent protein kinase and protein kinaseB/Akt, Thr446 and Ser 450 by GSK3, and Ser454 by mTORC2.

1.5.2 ROLE FOR ACLY IN NAFLD

Mendelian randomization studies have supported that multiple independently inherited single-nucleotide polymorphisms (SNPs) are associated with serum markers of liver injury including, alanine transaminase (ALT), aspartate transaminase (AST), and gamma-glutamyl transferase (GGT) (Morrow et al. 2022). Furthermore, data from a meta-analysis of human gene expression data indicates that the expression of ACLY is higher in patients with NASH versus simple steatosis, alluding to the possibility that ACLY is an important driver of NAFLD progression (Ryaboshapkina and Hammar 2017).

A previous report from our lab demonstrated that genetically knocking out ACLY from hepatocytes using an adeno-associated virus (ACLY-LKO) resulted in improvements in liver steatosis and hepatocellular ballooning in a mouse model fed a high-fat, high-fructose diet housed at thermoneutrality (Morrow et al. 2022). Primary hepatocytes from ACLY-LKO mice had reductions in lactate-driven sterol and fatty acid synthesis, and an increase in palmitate-driven fatty acid oxidation.

These data suggest that the inhibition of DNL and activation of fatty acid oxidation by ACLY knockout can reduce the severity of NASH.

1.5.3 ACLY PROMOTES CELLULAR ACETYLATION

In addition to serving as a substrate for DNL, acetyl-CoA generated by ACLY can also be a substrate for acetyl-CoA transferases (Wellen et al. 2009). Posttranslational modification of proteins by acetylation can either increase or decrease their activity. The E1A binding protein (p300) and general control non-depressible 5 (GCN5) are lysine acetyltransferases that promote the acetylation of both histone and non-histone proteins. In 2009, Wellen and colleagues discovered that nuclear ACLY-derived acetyl-CoA was required for GCN5-dependent histone acetylation in response to growth factors and glucose (Wellen et al. 2009). GCN5 also acetylates and inhibits PGC-1α (Lerin et al. 2006; Jeninga, Schoonjans, and Auwerx 2010). PGC-1α has an established role in promoting autophagy in multiple tissues (D. Liang et al. 2020). In fact, there are several acetyltransferase and de-acetylases that modify autophagy-related proteins (Y. Xu and Wan 2022). For example, P300 has also been shown to inhibit autophagy in response to nutrient deprivation in HeLa cells (I. H. Lee and Finkel 2009).

These data support the concept that depleting ACLY-derived acetyl-CoA may mimic some of the effects of caloric restriction and promote the restoration of metabolic homeostasis in chronic conditions of energy surplus and mitochondrial dysfunction. Whether inhibiting ACLY results in the reduction of global acetylation

and the promotion of autophagy and mitochondrial biogenesis in the liver has not yet been investigated. This could potentially provide a new hepatoprotective effect in the context of NASH.

1.5.4 BEMPEDOIC ACID

Bempedoic acid (also known at ETC-1002) is an oral medication approved to reduce low-density lipoprotein-cholesterol (LDL-C) in adults with heterozygous familial hypercholesterolemia (HeHF) or established atherosclerotic cardiovascular disease. It is a small molecule prodrug that is converted to its active moiety, bempedoyl-CoA, by the very-long-chain acyl-CoA synthetase 1 (ASCVL1) (Pinkosky et al. 2013a, 2016). ASCVL1 is expressed almost exclusively in the liver and the kidney, and not in skeletal muscle or other tissues. This conversion is important to minimize the myotoxicity which is typically found with long-term use of statins (Bouitbir et al. 2020). Bempedoyl-CoA can inhibit ACLY via a CoA competitive, ATP and citrate non-competitive manner. Importantly, bempodyl-CoA, but not bempedoic acid, allosterically activates AMPK β1 but not AMPK β2 containing complexes. These data suggest that like fatty acyl-CoA molecules described previously, bempedoyl-CoA is likely allosterically activating AMPK through a mechanism involving AMPK β1 Ser108 phosphorylation (Pinkosky et al. 2013a, 2016).

In a recent study from our lab, using a NASH mouse model induced by housing male mice at thermoneutrality and feeding them a diet high in fat and

fructose, we found that bempedoic acid reduced liver steatosis, hepatocellular ballooning, lobular inflammation, and hepatic fibrosis (Morrow et al. 2022). In this study, it was discovered that bempedoic acid exerted actions on murine and human hepatic stellate cells to reduce TGFβ-induced proliferation and activation, in turn, reducing collagen secretion. Taking these data together with evidence from previous clinical studies showing that bempedoic acid (1) has a good safety and tolerability profile without increasing serum triglycerides, and (2) reduces the risk of major adverse cardiovascular events (MACE) in statin-intolerant patients, this could position bempedoic acid as an ideal adjuvant therapy with other NASH-treating agents, as many therapies do not directly target fibrosis and NASH-associated comorbidities such as hypercholesterolemia (Ballantyne et al. 2018; Bays et al. 2020; Ray et al. 2019; Nissen et al. 2023; Keaney 2023; Alexander 2023).

1.6 LIFESTYLE MODIFICATIONS TO MANAGE OR REVERSE NAFLD

The current management of NAFLD consists of treating liver disease as well underlying metabolic comorbidities including obesity, hyperlipidemia, insulin resistance, and T2D. For patients with no sign of steatohepatitis or fibrosis, pharmacological treatments should not be primarily aimed at improving liver disease (Chalasani et al. 2018). Lifestyle modification recommendations including diet, exercise, and weight loss are commonplace, and have shown a dose-response curve where the greater the weight loss the more significant

improvements in histopathology (Musso et al. 2012). Bariatric surgery is also accepted, however, only reserved for extreme cases. In fact, weight loss of over 10% of initial body weight in 52 weeks was associated with improvements in all features of NASH, including portal inflammation and fibrosis (Vilar-Gomez et al. 2015). A systematic literature review investigating whether moderate-intensity continuous training or high-intensity interval training reduce NASH and liver fibrosis revealed that high-intensity interval training resulted in greater improvements in liver stiffness, but the overall effect of aerobic exercise did not result in fibrosis improvements generally (Houttu et al. 2022). However, as Musso and colleagues highlighted in a systematic review and meta-analysis, less than 50% of patients can achieve a loss of body weight of 7%, even with structure, guidance, and coaching. Furthermore, maintenance of weight loss is also a challenge, however, the benefits of diet and exercise go beyond weight loss with regards to NAFLD (Ryan et al. 2013; Della Corte et al. 2017; Mardinoglu et al. 2018; Magkos et al. 2016). Recommendations from the European Association for the Study of Liver, Diabetes, and Obesity (EASL, EASD, EASO), supported by other studies, suggest that physical exercise, reductions in carbohydrate consumption, increases in protein and fibre ingestion, and predominant sources of fats coming from polyunsaturated fatty acids are beneficial to reducing liver fat content (European Association for the Study of the Liver (EASL) 2016; Romero-Gómez, Zelber-Sagi, and Trenell 2017). One interesting fact gathered from systematic reviews and meta-analyses is that consuming three cups of coffee (caffeinated or not) or more

per day is associated with reduced liver disease severity (Chen et al. 2019). Understanding the mechanisms by which foods and modalities of exercise reduce features of NAFLD, NASH, and hepatic fibrosis have and continue to inform the development of pharmacotherapies.

1.6.1 CURRENT PHARMACOLOGICAL LANDSCAPE OF NASH

There are currently no FDA-approved therapies for the treatment of NAFLD, NASH, and hepatic fibrosis. The revised guidelines for the diagnosis and management of NAFLD from the American Association for the Study of Liver Disease (AASLD) support the use of drugs that treat associated comorbidities with benefit in NAFLD (Rinella et al. 2023). Semaglutide can be considered for patients with T2D or obesity, as there is evidence of efficacy in resolving NASH and it is known that it confers cardiovascular benefit. Pioglitzaone can be considered for patients with T2D and biopsy-proven NASH, as there is evidence of efficacy in resolving NASH and confers cardiovascular benefit. Vitamin E can be considered in patients with NASH that do not have T2D. These treatments carry a statement that they do not demonstrate antifibrotic effects. Metformin, ursodeoxycholic acid, dipeptidyl peptidase-4, silymarin, and statins are well studied and should not be used as a treatment for NASH as they do not confer meaningful histological benefit.

This unmet clinical need and a market valuation projecting $27.2 billion by 2029 has spurred a “race” to become the first FDA-approved therapeutic option to treat NASH (Fraile et al. 2021). With over 100 compounds being tested in clinical trials as of 2021, and none of them being approved by the time of writing this thesis in

Q1 2023, this highlights the difficulty in targeting this complex metabolic condition (Fraile et al. 2021). In order to gain approval by the FDA, sponsors have been recommended to evaluate NASH and fibrosis separately and meet the criteria of (1) improvement of liver fibrosis by 1 stage without worsening of NASH, and (2) resolution of NASH with no worsening of fibrosis (Omokaro and Golden 2020). And although there is some pushback on the stringency of these demands, there are several compounds that hold promise.

Treatments can be generally classified as metabolic, anti-inflammatory, and anti-fibrotic drugs and effect distinct cellular pathways (Konerman, Jones, and Harrison 2018; X. Xu et al. 2022; Harrison et al. 2023). 7 separate compounds with distinct mechanisms of action are now in Phase 3 clinical trials for the treatment of NASH. These include, dapagliflozin, semaglutide, cenicriviroc, resmetirom, obeticholic acid, saroglitazar, and aramchol (Fraile et al. 2021). Sarogltiazar is a first-in-class dual PPAR alpha and gamma agonist that reduces serum triglyceride and glucose levels, and has been approved for the treatment of NASH in India, but has not been approved by other approving bodies (Gawrieh et al. 2021). Obeticholic acid acts as a farnesoid X receptor (FXR) agonist which has shown a reduction in liver fibrosis without worsening of NASH and recently applied for an accelerated approval based on their interim results from the REGENERATE trial with nearly 2500 patients with NASH and fibrosis involved (Z. M. Younossi et al. 2019). However, the FDA reported several active liver toxicity concerns, LDL as well as total cholesterol were increased, thus the drug was not supported for fast

track. Resmetirom is an oral thyroid hormone receptor-beta (THRβ) agonist that reduces hepatic fat and resolves NASH without worsening of fibrosis after 52 weeks of treatment by modulating lipid metabolism (Harrison et al. 2019). As demonstrated, each of these drug candidates act on separate pathways, however, they all have something in common in that they can only meet 1 of the 2 criteria set out by the FDA.

Therefore, although there have been many advancements made in the therapeutic landscape of NASH, no therapy has proven both safe and efficacious in both criteria set by the FDA. Thus, identifying new therapies which have a single target that can influence multiple pathways of NASH and fibrosis progression or finding complementary combinations of therapies are warranted.

1.6.1.1 GLP-1R AGONISTS FOR THE TREATMENT OF NASH

Multiple glucagon-like peptide-1 receptor agonists are being used in the clinic for the treatment of T2D. While short-acting peptides such as exendin-4 or lixisenatide are only used for the treatment of T2D, the long-acting molecules liraglutide and semaglutide are also approved for the treatment of obesity (Drucker 2022). GLP-1 is an incretin hormone whose secretion from gut enteroendocrine L cells and the CNS is increased in the postprandial state to regulate blood glucose, satiety, and gastrointestinal motility (Baggio and Drucker 2021). Its receptor GLP-1R is expressed in pancreatic β cells, some α and δ cells, the enteric and central nervous system, kidney, gut, lung, intestinal intraepithelial lymphocytes,

endothelial cells, vascular smooth muscle cells, and the heart (B. A. McLean, Wong, Campbell, et al. 2021). And while GLP-1R is not expressed on the cells of the liver including hepatocytes, Kupffer cells, or hepatic stellate cells, both preclinical and clinical studies have demonstrated the efficacy of GLP-1R agonists to reduce liver fat and NASH. This suggests that most of the effects are indirect and are likely mediated via appetite-regulated weight loss, insulin-sensitizing effects for glucose and fatty acid uptake, reduced chylomicron secretion due to reduced synthesis and gut motility, and a reduction in cytokine release from γδ T-cells and intraepithelial lymphocytes (Yabut and Drucker 2022).

Using MR to assess pre- and post- 6-month liver fat content in patients with uncontrolled T2D, Petit and colleagues found that liraglutide treatment reduced liver fat content by 31% (Petit et al. 2017). In a multicentre, randomized, placebo-controlled trial, liraglutide treatment for 48 weeks resulted in the histological resolution of definite NASH in 39% of patients versus 9% in the control arm (Armstrong et al. 2016). This was associated with greater histological improvements in steatosis and ballooning, but not lobular inflammation. Furthermore, there was not a significant difference in fibrosis stage improvement. 72 weeks of once-daily semaglutide treatment in biopsy-confirmed NASH and liver fibrosis stage F1-3 patients resulted in a significant difference in NASH resolution in 59% of patients vs 17% in the control arm, while no difference was found in fibrosis score improvement (Newsome et al. 2021). In NASH with compensated cirrhosis, once-weekly semaglutide for 48 weeks did not improve fibrosis score or

achieve NASH resolution to a greater extent than the control arm (Loomba et al. 2023). There were, however, improvements in liver fat content as assessed by MR-PDFF. Collectively, considering these results, the large improvements in cardiometabolic risk parameters, and the excellent safety and tolerability profile, GLP-1R agonists are ideally positioned to be combined with a therapeutic that reduces fibrosis and other associated comorbidities. Combination trials with semaglutide have already started, as a 24 week open-label study evaluating the efficacy of semaglutide combined with firsocostat (FXR agonist) and/or cilofexor (ACC inhibitor) in patients with NASH and mild-to-moderate fibrosis was associated with additional improvements in NITs measuring hepatic steatosis, liver stiffness, and serum measures when in combination versus semaglutide alone (Alkhouri et al. 2022). Given the heterogeneity of the patient population with NASH, combination approaches may offer greater benefits than monotherapies, providing an opportunity for personalized medicine to treat NASH, fibrosis, and particular associated comorbidities such as hypercholesterolemia.

1.7 MAIN OBJECTIVES

Characterize the molecular mechanisms by which AMPK and ACLY regulate autophagy in the liver of mice and their potential implications for the development of NAFLD. Using bempedoic acid as a tool compound that activates AMPK and inhibits ACLY, determine whether targeting these pathways exerts favorable effects in a preclinical mouse model of NASH when combined with a GLP1-R agonist.

1.8 THESIS AIMS

1) Identify the physiological significance of the AMPKβ1 Ser108 site in controlling fatty acid metabolism and autophagy in the liver.
2) Explore whether the AMPK activator and ACLY inhibitor bempedoic acid exerts hepatoprotective effects to reduce hepatocellular ballooning and fibrosis in NASH by affecting autophagy.
3) Establish whether pharmacological activation of AMPK and inhibition of ACLY using bempedoic acid exerts complimentary effects when combined with a GLP-1R agonist to reduce NASH and associated comorbidities.

CHAPTER TWO

THE PHOSPHORYLATION OF AMPKβ1 IS CRITICAL FOR INCREASING AUTOPHAGY AND MAINTAINING MITOCHONDRIAL HOMEOSTASIS IN RESPONSE TO FATTY ACIDS

Published in *The Proceedings of the National Academy of Sciences*. 2022.11.
DOI: https://doi.org/10.1073/pnas.2119824119

Eric M. Desjardins, Brennan K. Smith, Emily A. Day, Serge Ducommun, Matthew J. Sanders, Joshua P. Nederveen, Rebecca J. Ford, Stephen L. Pinkosky, Logan K. Townsend, Robert M. Gutgesell, Rachel Lu, Kei Sakamoto, and Gregory R. Steinberg

In this chapter, we extend upon our lab's discovery that AMPK directly senses fatty acids via long chain fatty acyl-CoAs and describe the physiological relevance of the Ser108 amino acid residue within the allosteric drug and metabolite (ADaM) site of the AMPKβ1 subunit. We developed a mouse model with a targeted germline knock-in mutation of AMPKβ1 Ser108 to Ala108 (S108A-KI), rendering a phosphorylation site predictively involved in palmitoyl-CoA binding AMPK to be phospho-deficient. We found a reduction of AMPK activity by 50-75% in the liver, but not skeletal muscle, without alterations in subunit content. We then determined that Ser108 was required for acute changes in fat oxidation in response to exogenous fatty acids both *in vivo* and *in vitro*. We explored the significance of this site in the pathophysiology of obesity and NAFLD and found that S108A-KI mice had exacerbated glucose intolerance and greater liver lipid deposition on a HFD. This was ascribed to reductions in mitochondrial content and function and related to alterations in autophagy initiation *in vivo*. In primary hepatocytes, we identified that, in response to palmitate, AMPKβ1 Ser108 was not only important in stimulating mitochondrial biogenesis as a compensatory response to increased lipid availability, but also to initiate autophagy through phosphorylation of ULK1 at the AMPK-site Ser555, and its loss led to reduced autophagic/mitophagic flux. These studies demonstrate that fatty acid sensing by AMPK is an important mediator of lipid metabolism in the hepatocyte and that AMPK phosphorylation can mediate acute increases in fatty acid flux in the liver via facilitating fatty acid oxidation through ACC phosphorylation, and chronically promoting mitochondrial homeostasis when lipids are in excess through mitochondrial biogenesis and autophagy.
EMD was involved in all experiments except the following: Figure 1A (SD), Figure 3A (BKS), Supplemental 1A-E (MJS), Supplemental 2 (KS), and Supplemental 3A (SD).

PNAS RESEARCH ARTICLE | PHYSIOLOGY OPEN ACCESS

The phosphorylation of AMPKβ1 is critical for increasing autophagy and maintaining mitochondrial homeostasis in response to fatty acids

Eric M. Desjardins[a,b], Brennan K. Smith[a,b], Emily A. Day[a,b,1], Serge Ducommun[c,2], Matthew J. Sanders[c], Joshua P. Nederveen[a,d], Rebecca J. Ford[a,b], Stephen L. Pinkosky[a,b], Logan K. Townsend[a,b], Robert M. Gutgesell[a,b], Rachel Lu[a,b], Kei Sakamoto[c,e,3], and Gregory R. Steinberg[a,b,f,3]

Edited by Gerald Shulman, Yale University, New Haven, CT; received October 29, 2021; accepted October 18, 2022

Fatty acids are vital for the survival of eukaryotes, but when present in excess can have deleterious consequences. The AMP-activated protein kinase (AMPK) is an important regulator of multiple branches of metabolism. Studies in purified enzyme preparations and cultured cells have shown that AMPK is allosterically activated by small molecules as well as fatty acyl-CoAs through a mechanism involving Ser108 within the regulatory AMPK β1 isoform. However, the in vivo physiological significance of this residue has not been evaluated. In the current study, we generated mice with a targeted germline knock-in (KI) mutation of AMPKβ1 Ser108 to Ala (S108A-KI), which renders the site phospho-deficient. S108A-KI mice had reduced AMPK activity (50 to 75%) in the liver but not in the skeletal muscle. On a chow diet, S108A-KI mice had impairments in exogenous lipid-induced fatty acid oxidation. Studies in mice fed a high-fat diet found that S108A-KI mice had a tendency for greater glucose intolerance and elevated liver triglycerides. Consistent with increased liver triglycerides, livers of S108A-KI mice had reductions in mitochondrial content and respiration that were accompanied by enlarged mitochondria, suggestive of impairments in mitophagy. Subsequent studies in primary hepatocytes found that S108A-KI mice had reductions in palmitate- stimulated Cpt1a and Ppargc1a mRNA, ULK1 phosphorylation and autophagic/mitophagic flux. These data demonstrate an important physiological role of AMPKβ1 Ser108 phosphorylation in promoting fatty acid oxidation, mitochondrial biogenesis and autophagy under conditions of high lipid availability. As both ketogenic diets and intermittent fasting increase circulating free fatty acid levels, AMPK activity, mitochondrial biogenesis, and mitophagy, these data suggest a potential unifying mechanism which may be important in mediating these effects.

AMPK | fat oxidation | mitochondria | NAFLD | autophagy

Significance

The data in this manuscript indicate a crucial role for a single phosphorylation site on the regulatory beta subunit of AMPK to stimulate mitochondrial biogenesis and autophagy/mitophagy in response to increases in fatty acids. This suggests a potential unifying mechanism which may be important for mediating the beneficial effects of dietary interventions that increase free-fatty acid availability such as intermittent fasting and ketogenic diets.

Fatty acids are a predominant substrate for most cell types and also act as critical building blocks for membranes and signaling molecules. However, high levels of fatty acids –common in obesity– promote the development of lipotoxicity in multiple organ systems, triggering inflammation, fibrosis, and eventually cell death (1). As such, multiple homeostatic mechanisms have evolved to closely match fatty acid availability with oxidation rates. This includes allosteric inhibition of key enzymes regulating fatty acid oxidation including acetyl-CoA carboxylase (ACC) (2). Fatty acids can also increase their own oxidation by enhancing mitochondrial function through the coordinated regulation of mitochondrial biogenesis and degradation (3–5). However, to date, the mechanisms coordinating the effects of fatty acids on mitochondrial homeostasis are incompletely understood.

The AMP-activated protein kinase (AMPK) is a central governor of cellular energy homeostasis that is influenced by multiple physiological, hormonal, and nutritional signals. AMPK is a heterotrimeric protein consisting of a catalytic α (α1/α2) subunit, a regulatory γ (γ1/γ2/γ3) subunit, and a β (β1/β2) subunit, which is critical for both maintaining the structure of the enzyme complex and regulating enzyme activity (6). Studies in knock-out mice have shown that AMPKβ1 is essential for maintaining AMPK activity in metabolic tissues such as the liver (7), while AMPKβ2 is important in the skeletal muscle and heart (8). In addition to acting as a structural scaffold, the β subunit is also (auto)phosphorylated and myristoylated to allosterically regulate enzymatic activity (9–13). Of these posttranslational modifications, phosphorylation of AMPKβ1 Ser108 has been shown to play a vital role in enhancing AMPK activity in response to many distinct, small-molecule, allosteric activators including A769662, salicylate, 991, MK-8722, PF-06409577, and lusianthridin (14–20) (reviewed in ref. 6). And, while the endogenous ligand(s) for β1 Ser108 remained elusive for many years, recent studies conducted in cultured cells and purified enzyme preparations identified that long-chain fatty acyl-CoAs increase AMPK

Author contributions: E.M.D., B.K.S., K.S., and G.R.S. designed research; E.M.D., B.K.S., E.A.D., S.D., M.J.S., J.P.N., R.J.F., S.L.P., L.K.T., R.M.G., and R.L. performed research; E.M.D., B.K.S., E.A.D., S.D., J.P.N., R.J.F., and S.L.P. analyzed data; and E.M.D., K.S., and G.R.S. wrote the paper.

Competing interest statement: The authors declare a competing interest. M.J.S. is a current, and K.S. and S.D. were former employees of Nestlé Research (Switzerland). S.L.P. is an employee of Esperion Therapeutics. G.R.S. has received consulting and/or speaking fees from Astra Zeneca, Boehringer-Ingelheim, Cambrian BioPharma, EchoR1, Eli-Lilly, Esperion Therapeutics, Fibrocor Therapeutics, Merck, Novo Nordisk, Pfizer and Poxel Pharmaceuticals, research funding from Esperion Therapeutics, Espervita Therpeutics, Nestle, Novo Nordisk and Poxel Pharmaceuticals and is co-founder and shareholder of Espervita Therapeutics.

This article is a PNAS Direct Submission.

[1]Present address: School of Biochemistry and Immunology, Trinity College Dublin, Trinity Biomedical Sciences Institute, Dublin D02 R590, Ireland.

[2]Present address: Department of Physiology and Pharmacology, Karolinska Institute, Solna 17165, Sweden.

[3]To whom correspondence may be addressed. Email: kei.sakamoto@sund.ku.dk or gsteinberg@mcmaster.ca.

This article contains supporting information online at https://www.pnas.org/lookup/suppl/doi:10.1073/pnas.2119824119/-/DCSupplemental.

Published November 21, 2022.

activity in part through this residue (2). Ser108 is also phosphorylated by the autophagy initiator Unc-51-like kinase 1 (ULK1) (12). Despite the growing appreciation of this posttranslational modification, little is known about the physiological importance of AMPKβ1 Ser108, information that is especially relevant given new small molecules that activate AMPK through this residue have entered clinical trials for nonalcoholic steatohepatitis (21, 22) and may be potentially utilized for other chronic diseases.

Results

We find that, consistent with previous studies in cell-free assays (12, 15–17), β1 S108A-containing AMPK trimeric complexes were not responsive to A769662-mediated activation but were sensitive to phosphorylation by Ca^{2+}/calmodulin-dependent protein kinase kinase-β (CaMKKβ) and allosteric activation by AMP (*SI Appendix*, Fig. S1). To investigate the physiological importance of AMPKβ1 Ser108 phosphorylation, we generated a mouse model with a targeted germline knock-in (KI) mutation in which this residue was rendered phospho-deficient by mutating the Ser to Ala (S108A-KI) (*SI Appendix*, Fig. S2).

In mice fed a control high-carbohydrate chow diet (CD), S108A-KI mice had lower AMPK activity in the liver but not in the skeletal muscle (Fig. 1*A*), a finding consistent with the predominant expression of the AMPKβ1 subunit in the liver but not in the skeletal muscle (*SI Appendix*, Fig. S3*A*). Importantly, this lower AMPK activity was independent of observable changes in the expression of AMPK α, β, or γ isoforms (*SI Appendix*, Fig. S3*A*). We subsequently examined body mass, energy expenditure, fasting blood glucose, caloric consumption, physical activity levels, the respiratory exchange ratio (RER), and glucose tolerance and found that there were no genotypic differences in these parameters (*SI Appendix*, Fig. S3 *B–H*). These data indicate that on a control chow diet S108A-KI mice have reductions in AMPK activity within the liver that are independent of changes in AMPK isoform expression profiles, but that this does not have a significant impact on whole-body glucose homeostasis or energy balance.

Given previous studies in purified enzyme preparations found that AMPKβ1 Ser108 was important for activating AMPK in response to increases in fatty acyl-CoA availability (2), we next challenged WT and S108A-KI mice fed a control chow diet with an oral bolus of the lipid emulsion intralipid (Fig. 1*B*). Food intake (*SI Appendix*, Fig. S4*A*) and activity levels (*SI Appendix*, Fig. S4*B*) were not different between genotypes or following intralipid gavage. Compared to vehicle control, there was a tendency for intralipid gavage to reduce the RER in WT (P = 0.2, *SI Appendix*, Fig. S4 *C* and *E*) but not S108A-KI (P = 0.9, *SI Appendix*, Fig. S4 *D* and *E*) mice, and when changes in fatty acid oxidation were calculated, this was increased by intralipid in WT but not in S108A-KI mice (Fig. 1*C*). In contrast, treatment of WT and S108A-KI mice with 5-aminoimidazole-4-carboxamide-1-β-D-ribofuranoside (AICAR)–which is metabolized into the AMP-mimetic (ZMP or AICAR monophosphate) and activates AMPK via the γ not the β1 isoform (23)–did not change food intake or activity (*SI Appendix*, Fig. S4 *F* and *G*), but reduced RER (*SI Appendix*, Fig. S4 *H–J*) and increased fatty acid oxidation in both genotypes (Fig. 1*D*).

AMPK phosphorylation of ACC is important for increasing fatty acid oxidation in response to intralipid (2). Consistent with these previous findings, treatment of primary hepatocytes with palmitate increased ACC1/2 S79/212 phosphorylation in WT mice but not in S108A-KI mice (Fig. 1*E*), while the effect of AICAR was maintained in both genotypes (Fig. 1*F*). Similar to palmitate, S108A-KI mice were also resistant to the effects of A769662 to increase ACC phosphorylation (Fig. 1*G*). These findings demonstrate that AMPKβ1 Ser108 is important for increasing

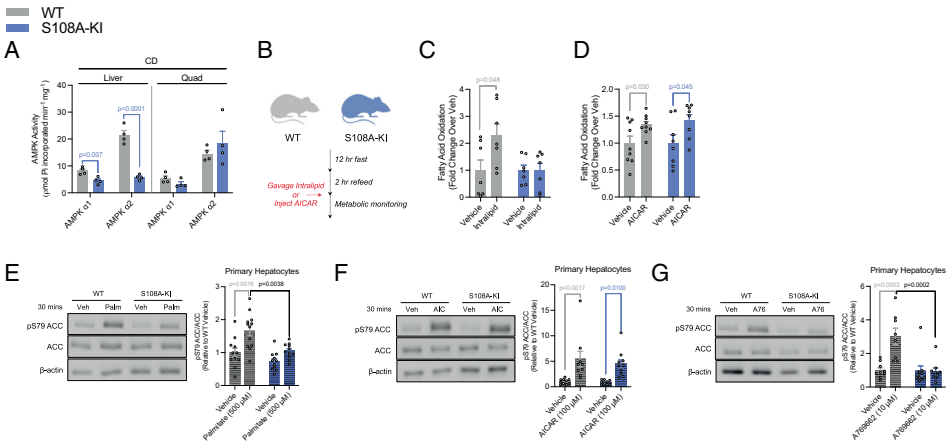

Fig. 1. AMPKβ1 Ser108 phosphorylation is important for acute fatty acid-induced increases in ACC phosphorylation and whole-body fatty acid oxidation. (*A*) AMPKα isoform-specific phosphotransferase activity assay from basal chow-fed (CD) WT and S108A-KI (KI) mice for liver and quadriceps muscle (Quad). (*B–D*) Schematic of fast-refeed experiments with or without intralipid or AICAR in metabolic monitoring units (*B*). Fatty acid oxidation (*C*) was calculated from VO_2 and VCO_2 over 4 h, starting 1 h postgavage of either saline or 20% intralipid (10 mL/kg) in WT and S108A-KI mice fed a chow diet. Following an i.p. injection of saline or AICAR (500 mg/kg), fatty acid oxidation (*D*) was calculated from VO_2 and VCO_2 over 1 h, starting 6 h postinjection. Representative ACC immunoblotting and densitometrical analysis assessing inhibitory phosphorylation of ACC by AMPK in response to palmitate (Palm: 500 μM) (*E*), AICAR (AIC: 100 μM) (*F*), and A-769662 (A76: 10 μM) (*G*) in primary hepatocytes from CD-fed WT and S108A-KI mice. Data are means ± SEM with *P*-values reported in the graphs. Gray bars equal WT differences, blue bars equal to S108A-KI differences, and black bars indicate differences between groups in same treatment condition. Statistical significance was accepted at $P < 0.05$ and determined via multiple *t* tests or two-way ANOVA with Tukey's posthoc analysis. White circles are individual mice or experimental replicates with three technical replicates per group.

the phosphorylation of ACC in response to acute increases in free fatty acids, but not AMP-mimetics such as AICAR.

To examine the chronic consequences of elevations in free fatty acids, WT and S108A-KI mice were fed a high-fat diet (HFD). Although we could not perform densitometrical analyses reliably due to a low-molecular-weight nonspecific band, compared to chow-fed controls, HFD feeding seemed to increase AMPKβ1 Ser108 phosphorylation in the liver of WT mice, while, as expected, this signal was undetectable in S108A-KI mice (Fig. 2*A*). However, we did not detect a significant reduction in ACC phosphorylation as total ACC protein content was markedly reduced in HFD compared to chow-fed controls (Fig. 2 *A*–*C*). Body mass, energy expenditure, fasting blood glucose, caloric intake, and physical activity levels were similar between WT and S108A-KI mice fed a HFD (*SI Appendix*, Fig. S3 *B*–*G*). In contrast to the acute increase in free fatty acid availability induced by intralipid gavage (Fig. 1), there was no difference in RER between WT and S108A-KI mice fed a HFD (*SI Appendix*, Fig. S3*G*). This finding is consistent with the comparably large reductions in ACC expression elicited by the HFD in both WT and S108A-KI mice and previous observations that ACC S79/S212A (ACC-DKI, (24)) mice have normal increases in fatty acid oxidation (i.e., reductions in RER) in response to a HFD. HFD-fed S108A-KI mice had a tendency for modest impairments in glucose tolerance (Fig. 2*D*). This tendency for reduced glucose tolerance was not associated with differences in insulin levels which were similar between HFD-fed WT and S108A-KI mice at 2- and 10-min post glucose injection (Fig. 2*E*), suggesting that S108A-KI mice had impaired insulin sensitivity. As hepatic steatosis contributes to insulin resistance, we examined liver lipids and found that S108A-KI mice had increased steatosis and an ~10% increase in liver triglycerides compared to WT controls fed a HFD (Fig. 2 *F* and *G*).

In addition to acutely stimulating fatty acid oxidation through phosphorylation of ACC (24), AMPK may chronically increase fatty acid oxidation by enhancing mitochondrial function through the coordinated regulation of mitochondrial biogenesis, mitophagy, and mitochondrial fission (25, 26). Under conditions of a HFD, S108A-KI mice had lower protein abundance of the electron transport chain complexes 2-5 in the liver (Fig. 2*H*), effects not observed in animals fed a chow diet (*SI Appendix*, Fig. S3*I*). HFD-fed S108A-KI mice also had reduced mRNA expression of *Ppargc1a* (Fig. 2*I*). Furthermore, when treated with palmitate for 6 h, primary hepatocytes from S108A-KI mice had an attenuated induction in the mRNA expression of both *Cpt1a* and *Ppargc1a* (Fig. 2 *J*–*L*). These data indicate that AMPKβ1 Ser108 is important for increasing mitochondrial biogenesis in response to chronic increases in fatty acid availability.

To examine whether there might be changes in mitochondrial function independently of reductions in mitochondrial content, we measured respiration in isolated liver mitochondria from chow- and HFD-fed mice. In mice fed a HFD, succinate-stimulated respiration was increased in WT mice but not in S108A-KI mitochondria (Fig. 3*A*). Reduced rates of respiration per mitochondrial mass led us to examine mitochondrial morphology by transmission electron microscopy (TEM), where it was observed that the average surface area of liver mitochondria from HFD-fed S108A-KI mice was increased (Fig. 3 *B* and *C*), while there was a reduced number of mitochondria (Fig. 3 *B* and *D*). Taking these two measurements into consideration, we calculated the average mitochondrial surface area per field and found that HFD-fed S108A-KI mice had a greater mitochondrial area per micrograph compared to WT mice (Fig. 3 *B* and *E*). Enlarged and dysfunctional mitochondria are hallmarks of impaired autophagy and have been observed in other models of AMPK deficiency as well as in people with NAFLD (25, 27). Therefore, we investigated

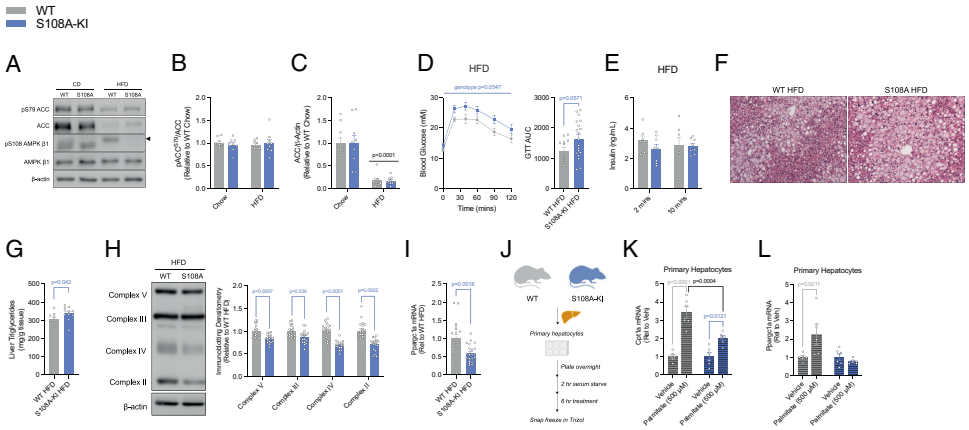

Fig. 2. AMPKβ1 Ser108 phosphorylation is important for increasing mitochondrial biogenesis in mice fed a HFD or hepatocytes treated with palmitate. (*A*) Representative immunoblots of ACC1/2 S79/S212 and AMPKβ1 S108 and densitometrical analysis of pACC/ACC (*B*) and total ACC (*C*) from the livers of chow-fed (CD) and HFD-fed (HFD) WT and S108A-KI mice. (*D*) Intraperitoneal glucose tolerance test (Intraperitoneal glucose tolerance tests (ipGTT), 0.8 g/kg) and area under the curve (GTT AUC) at 24 wk of age in HFD-fed WT and S108A-KI mice. (*E*) Serum insulin at 2- and 10-min post glucose injection from some of the mice in *D* in which blood samples could be collected. Representative H&E stains (10×, *F*) and liver triglycerides (*G*) of WT and S108A-KI mice fed a HFD for 20 wk. Representative immunoblots and densitometrical analysis of OXPHOS complexes 2-5 of WT and S108A-KI mice fed a HFD (*H*). mRNA expression of peroxisomeproliferator activated receptor gamma coactivator 1-alpha (*Ppargc1a*) in WT and S108A-KI mice fed a HFD (*I*). (*J*–*L*) Schematic representation of mRNA experiments in primary hepatocytes for mitochondrial biogenesis in response to elevated LCFAs (*J*). Carnitine-palmitoyl transferase 1-alpha (*Cpt1a*) (*K*) and *Ppargc1a* (*L*) mRNA expression from primary hepatocytes. Data are means ± SEM with *P*-values reported in the graphs. Gray bars equal WT differences, blue bars equal to S108A-KI differences, and black bars indicate differences between groups in same treatment condition. Significance was accepted at $P < 0.05$ and determined via *t* tests, ordinary two-way, or repeated-measures two-way ANOVA with Tukey's posthoc analysis, where appropriate. White circles are individual mice per group. Black arrow in *A* indicates area for specific band of AMPKβ1 S108.

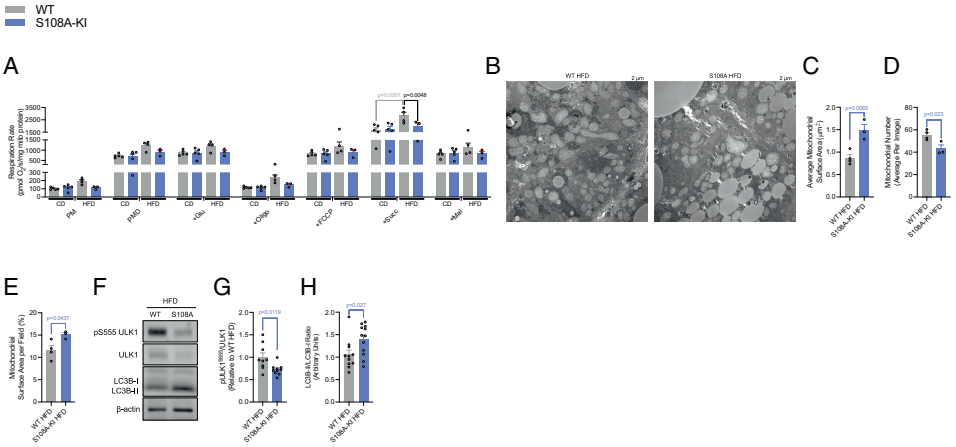

Fig. 3. AMPKβ1 Ser108 phosphorylation is important for increasing ULK1 phosphorylation and maintaining mitochondrial morphology and function in response to a HFD. Respiration rates (*A*) from isolated liver mitochondria from CD and HFD-fed WT and S108A-KI mice (PM; 0.5 mM malate, 5 mM pyruvate, PMD; + 1 mM ADP, +Glu; 5 mM glutamate, +Oligo; 1.25 μM oligomycin, +FCCP; titration of 0.5 μM FCCP until maximal uncoupled respiration reached, +Succ; 10 mM succinate, and +Mal; 5 mM malonate). Representative electron micrographs (*B*) with quantification of average mitochondrial surface area (*C*), mitochondrial number (*D*), and mitochondrial surface area per field (*E*) from WT and S108A-KI mice fed a HFD. Representative immunoblotting (*F*) and densitometrical analysis of pULK S555/ULK1 (*G*) and LC3BII (*H*) from the livers of WT and S108A-KI mice fed a HFD. Data are means ± SEM with *P*-values reported in the graphs. Gray bars equal WT differences and blue bars equal to S108A-KI differences. Statistical significance was accepted at $P < 0.05$ and determined via unpaired *t* test, two-way ANOVA with Tukey's posthoc analysis, or repeated-measures two-way ANOVA with Sidak's posthoc analysis, where appropriate. White circles are individual mice or technical replicates from three experimental replicates per group.

whether this process was also dysregulated in the liver of the HFD-fed S108A-KI mice. We found that ULK1 S555 phosphorylation was reduced (Fig. 3 *F* and *G*), while the ratio of LC3B-II/LC3B-I was increased (Fig. 3 *F* and *H*) in S108A-KI mice fed a HFD. These data indicate that AMPKβ1 Ser108 is critical for maintaining ULK1 phosphorylation, mitochondrial function, and morphology in the liver when mice are fed a HFD.

Considering autophagy as an active process, we used primary hepatocytes to investigate the initiation and flux through the pathway due to excess palmitate (Fig. 4*A*). After 30 min of treatment with palmitate, primary hepatocytes from WT mice had increases in the phosphorylation of ULK1 S555, but this effect was not observed in S108A-KI mice (Fig. 4 *B* and *C*). Furthermore, the downstream substrate of ULK1, ATG14, had unaltered S29 phosphorylation by palmitate treatment in either group but was modestly reduced in hepatocytes from S108A-KI mice (Fig. 4 *B* and *D*). We subsequently assessed autophagic flux using the lysosomal pH neutralizing agent chloroquine and detected reduced palmitate-induced autophagic flux (chloroquine treated vs. untreated) in S108A-KI-derived hepatocytes in comparison to WT counterparts by measurements of LC3B-II levels (Fig. 4*E*). Similarly, under a more chronic condition, palmitate-induced autophagic flux was attenuated in S108A-KI hepatocytes transfected with a tandem fluorescent protein construct including an acid-sensitive GFP and an acid-insensitive RFP (Fig. 4 *F*–*H*). Last, to determine whether mitophagy was sensitive to palmitate and if this response was altered in S108A-KI hepatocytes, we isolated mitochondrially enriched extracts and found that mitochondrial LC3B-II levels were significantly higher in response to palmitate in WT versus S108A-KI hepatocytes (Fig. 4 *I*–*K*). Other markers of mitophagy including p62, BNIP3, NIX, and CISD1 did not show any differences in response to palmitate between groups (*SI Appendix*, Fig. S5 *A*–*E*). Taken together, these findings describe a critical role for an AMPK-fatty acid sensing axis for acutely increasing fatty acid oxidation while chronically enhancing autophagy/mitophagy and mitochondrial biogenesis (Fig. 4*L*).

Discussion

Structural and cell-based studies have identified phosphorylation of Ser108 within the AMPKβ1 subunit as an important event for allosteric activation of AMPK in response to small molecules (15–17) and fatty acyl-CoA (2), but the in vivo physiological importance of this residue is unknown. In the current study, we find that in mice fed a control high-carbohydrate diet, there are reductions in liver AMPK activity in S108A-KI mice that occur independently of changes in AMPK subunit expression. This reduction in liver AMPK activity does not result in detectable changes in whole-body metabolic parameters or liver mitochondrial content and function. These findings are consistent with previous observations that phosphorylation of AMPKβ1 Ser108 is maintained at low levels in the basal state (28) and that small amounts of AMPK activity are sufficient to maintain metabolic homeostasis and mitochondrial function in the absence of a metabolic challenge. We find that acutely increasing free fatty acids through an oral gavage of intralipid and treating primary hepatocytes with palmitate promotes fatty acid oxidation and ACC phosphorylation, respectively, in WT mice but not in S108A-KI mice. This is in contrast to the effects of AICAR which stimulates fatty acid oxidation and ACC phosphorylation in both WT and S108A-KI mice to a comparable degree, highlighting the specificity of this response. These data, in combination with previous studies (2), support a model in which acute elevations in fatty acids promote fatty acid oxidation through: 1) interactions with Ser108 within the AMPKβ1 subunit; 2) allosteric activation of AMPK; 3) phosphorylation and inhibition of ACC; 4) reduced malonyl-CoA, relieving allosteric inhibition of carnitine palmitoyl-transferase 1 (CPT1); and 5) increased flux of fatty acyl-CoA

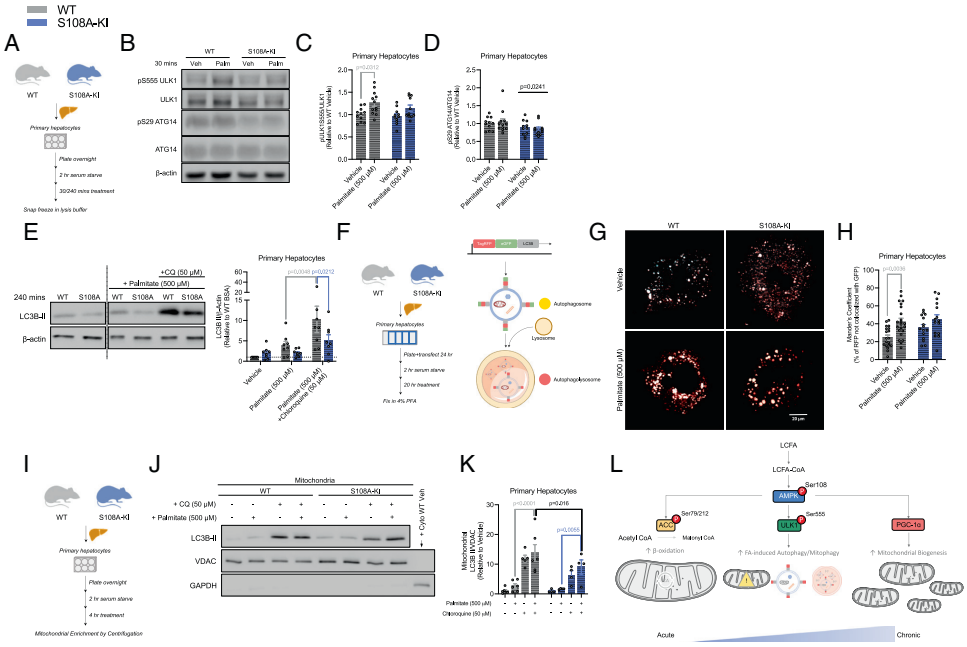

Fig. 4. AMPKβ1 Ser108 phosphorylation is important for increasing autophagy and mitophagy in response to increases in fatty acid availability. (*A–F*) Schematic of immunoblotting experiments for palmitate-induced autophagy and autophagic flux experiments in primary hepatocytes (*A*). Representative immunoblots (*B*) and densitometrical analysis of ULK1 (S555) (*C*) and ATG14 (S29) (*D*) assessing the induction of autophagy via AMPK activation in response to palmitate (500 μM) in primary hepatocytes from CD-fed WT and S108A-KI mice. Representative LC3B-II immunoblotting and densitometrical analysis (*E*) assessing autophagic flux in response to palmitate (500 μM) in primary hepatocytes from CD-fed WT and S108A-KI mice. (*F–H*) Schematic of palmitate-induced autophagic flux in primary hepatocyte experiments by tandem fluorescence and graphical illustrating result of using the LC3B protein with an acid-sensitive GFP and an acid-insensitive RFP (*F*). Representative colorblindness-friendly confocal micrographs with green being replaced with cyan (autophagosomes appear as white, while autophagolysosomes are red) (*G*), and quantification of percent red not overlapping green (*H*) in CD-fed WT and S108A-KI primary hepatocytes treated with vehicle or palmitate. (*I–K*) Schematic of immunoblotting experiments for palmitate-induced mitophagic flux experiments in primary hepatocytes (*I*). Representative immunoblotting (*J*) and densitometrical analysis of LC3B-II (*K*) assessing mitophagic flux in response to palmitate (500 μM) in primary hepatocytes from CD-fed WT and S108A-KI mice. Working model of the role of AMPKβ1 Ser108 phosphorylation in an AMPK-fatty acid-sensing axis to increase fatty acid oxidation, autophagy/mitophagy, and mitochondrial biogenesis (*L*). Data are means ± SEM with *P*-values reported in the graphs. Gray bars equal WT differences, blue bars equal to S108A-KI differences, and black bars indicate differences between groups in same treatment condition. A straight black line indicates a main effect of genotype in *D*. Statistical significance was accepted at $P < 0.05$ and determined via repeated-measures two-way ANOVA with Sidak's posthoc analysis, unpaired *t* tests, or two-way ANOVA with Tukey's posthoc analysis, where appropriate. White circles are individual mice or technical replicates from experiments with three experimental replicates per group. For confocal microscopy analysis, white circles represent individual micrographs from two experimental replicates per group.

into the mitochondria for β-oxidation. These data also suggest that allosteric inhibition of ACC is insufficient to enhance fatty acid oxidation in the absence of covalent regulation by AMPK.

We find that feeding mice a HFD increases AMPKβ1 Ser108 phosphorylation compared to chow-fed controls. This is not accompanied by reductions in ACC phosphorylation in S108A-KI mice fed a HFD and is consistent with studies in mice lacking inhibitory phosphorylation sites on ACC, which have comparable rates of fatty acid oxidation when fed a HFD (24). Furthermore, previous studies in obese mice with reductions in ACC expression have been linked to hyperleptinemia-induced activation of PPARα and subsequent reductions in SREBP1c (29). These data indicate that, in contrast to the acute increases in free fatty acid availability, chronic feeding of an obesity-promoting HFD enhances whole-body fatty acid oxidation independently of AMPKβ1 Ser108 phosphorylation.

In addition to modulating ACC, chronic exposure of fatty acids increases mitochondrial biogenesis (5, 30). Many genetic models of AMPK deficiency have a reduction in tissue mitochondrial content, while treatment of rodents with pharmacological activators of AMPK stimulates mitochondrial biogenesis (31–34). We found that S108A-KI mice were resistant to the stimulatory effects of a HFD to increase mitochondrial content in the liver and were also resistant to the acute stimulatory effects of palmitate to increase *Cpt1a* and *Ppargc1a* in hepatocytes. These findings highlight an important role of AMPKβ1 Ser108 phosphorylation in enhancing mitochondrial biogenesis–an effect which may involve increases in PGC1α (reviewed in refs. 25 and 26). Supporting this concept, mice heterozygous for liver PGC1α that were fed a HFD had a very similar metabolic phenotype to S108A-KI mice, with reductions in mitochondrial beta-oxidation genes, hepatic steatosis, and glucose intolerance (35). These data are also consistent with observations in clinical populations, which indicate that modest reductions in maximal mitochondrial respiration can, over time, promote steatosis and insulin resistance (36).

Mitochondria isolated from the livers of S108A-KI mice had reductions in respiration in the setting of a HFD, indicating that there were also impairments in mitochondrial function that were independent of reductions in mitochondrial content. Subsequent analysis of mitochondrial morphology revealed large and distended

mitochondria within the liver of S108A-KI mice, a hallmark of impaired mitophagy. Many previous studies have shown that fatty acids stimulate mitophagy (reviewed in 37); however, the mechanisms mediating these effects were not fully resolved. An important mechanism by which AMPK maintains mitophagy involves the phosphorylation and activation of ULK1 (38–42). We find that S108A-KI mice have reduced phosphorylation of ULK1 in the liver when fed a HFD and in hepatocytes treated acutely with palmitate. These data indicate that fatty acids stimulate mitophagy through AMPKβ1 Ser108 and that reductions in liver mitochondrial function in HFD-fed S108A-KI mice may be due to impaired mitophagy. As ULK1 can phosphorylate AMPKβ1 Ser108 (12), we measured a downstream substrate of ULK1, ATG14, and found no changes with palmitate treatment, suggesting that ULK1 is unlikely directly activated by free fatty acids. The role of AMPK in regulating mitophagy is extremely complex (43) with several new molecular mechanisms emerging, including an initiation cue of Parkin phosphorylation at Ser108 (42), mitoAMPK-mediated mitochondrial fission factor (MFF) phosphorylation (44), as well as several other signaling events which are beyond the scope of our work. Here, we show that LC3B-II flux is attenuated in mitochondrial enrichments from S108A-KI hepatocytes treated with palmitate, while no differences were found in the adaptor protein SQSTM1/P62 or other markers of mitophagy (BNIP3, NIX, and CISD1/MitoNEET). In addition to impairments in mitophagy, it is also possible that enlarged mitochondria may be a function of reduced mitochondrial fission induced through AMPK phosphorylation of MFF (45, 46) or dynamin-related protein 1 (47). These data highlight the importance of AMPKβ1 Ser108 in promoting ULK1 phosphorylation and autophagy/mitophagy in response to increased fatty acid availability while also highlighting the complexity of the mitophagy response that requires further study.

The sequence surrounding Ser108 is relatively well conserved between AMPKβ1 and β2, and while both β1 Ser108 and β2 Ser108 can be phosphorylated by CaMKKβ in vitro, only AMPKβ1 Ser108 phosphorylation is detectable in both basal and H_2O_2-stimulated HEK293 cells (12). However, it is unclear whether β2 Ser108 is phosphorylated in tissues. Currently, there is no high-resolution structural information for β2-containing AMPK trimeric complexes bound to an allosteric drug and metabolite site-binding activator; thus, the molecular basis for differential requirements of Ser108 phosphorylation between β-isoforms remains elusive. A potential limitation of our findings is that human liver is primarily composed of AMPKβ2-containing heterotrimers (48–50) which are insensitive to acute allosteric activation by free fatty acids (2). Despite the selectivity of this response toward the β1-isoform, it is important to note that AMPKβ1-specific activation in humans is sufficient to increase liver AMPK activity and impart physiological effects (19, 21, 22). These data suggest that fatty acyl-CoAs may also be important for regulating liver lipid metabolism and mitochondrial homeostasis in humans; however, this will require further study in primary human hepatocytes. Furthermore, since AMPKβ1 is the predominant β isoform in most other cell types besides cardiac and skeletal muscles, these findings may have implications for other metabolic processes outside of the liver, which will require further study. For example, ketogenic diets and intermittent fasting increase free fatty acids, an effect associated with activation of AMPK, mitochondrial biogenesis, mitophagy, and consequential improvements in mitochondrial function in multiple tissues and cell types. Future studies examining whether these effects may be mediated through AMPKβ1 Ser108 will be important. Additional understanding of the importance of the AMPK Ser108 residue will also be important to inform further refinement of compounds to control tissue specificity, duration, and magnitude of AMPK activation.

Materials and Methods

AMPK Activity Assay. AMPK was immunoprecipitated from 30–100 μg lysates with 1 μg antibodies against α1 or α2 subunit with protein G Sepharose. Phosphotransferase activity of AMPK toward the AMARA peptide (AMARAASAAALARRR) was assayed using [γ-^{32}P]ATP (51). Isoform-specific AMPKα subunit antibodies were custom made for immunoprecipitation as previously described (52).

Immunoblotting. For immunoblotting, tissue homogenates were prepared in lysis buffer (50 mM HEPES pH 7.4, 150 mM NaCl, 100 mM NaF, 10 mM Na-pyrophosphate, 5 mM EDTA, 250 mM sucrose, 1 mM DTT and 1 mM Na-orthovanadate, 1% Triton X-100, and complete protease inhibitor cocktail (Roche)), denatured in 4× SDS or Laemmli sample buffer, separated by SDS-PAGE, and transferred to nitrocellulose or PVDF membrane. Membranes were blocked for 1 h in 20 mM tris (pH 7.6), 137 mM NaCl, and 0.1% (v/v) Tween-20 (TBST) containing 5% (w/v) skim milk or BSA. The membranes were incubated in primary antibody prepared in TBST containing 1–5% (w/v) BSA overnight at 4°C. The following antibodies were used: pAMPKα1/α2 T172 (CST, 2535), AMPKα1 (Millipore, 07-350), AMPKα2 (Millipore, 07-363), pAMPKβ1 S108 (CST, 4181, CST, 23021*nonspecific band), AMPKβ1/β2 (CST, 4150), AMPKβ1 (CST, 12063), AMPKγ1 (OriGene, TA300519), pACC S79 (CST, 3661), ACC (CST, 3676), OXPHOS (Abcam, ab110413), β-actin (CST, 5125), pULK1 S555 (CST, 5869), ULK1 (CST, 8054), LC3B (CST, 2775), pATG14 S29 (CST, 92340), ATG14 (CST, 96752), p62 (CST, 5114), VDAC (CST,4661), GAPDH (CST, 2118), BNIP3 (CST, 3769), NIX (CST, 12396), and CISD1 (CST, 83775). Detection was performed using horseradish peroxidase-conjugated secondary antibodies and enhanced chemiluminescence reagent. OXPHOS samples were not boiled to avoid the degradation of complexes.

Animals. We generated a targeted germline KI mouse model (in collaboration with Taconic Biosciences GmbH) in which the codon in exon 2 for Ser108 of *Prkab1* was modified to encode nonphosphorylatable Ala (*SI Appendix*). All experiments were approved by the McMaster University Animal Ethics Committee (#16-12-41) and conducted under the Canadian guidelines for animal research or approved by the local Ethical Committee of the Canton of Vaud Switzerland and performed under license number 3247. All mice were maintained under controlled environmental conditions: 12/12-h light/dark cycle with lights on at 0700 h, group housing, enrichment provided, and at room temperature (22–23°C). Male mice were used for all in vivo experiments. For HFD-fed studies, mice were switched from a normal chow diet (Diet 8640, Harlan Teklad) to a HFD (60% calories from fat; D12492 Research Diets) at 8 wk of age, and tests were performed at indicated weeks.

Metabolic Measurements. Metabolic monitoring was performed in a Comprehensive Lab Animal Monitoring System (CLAMS; Columbus Instruments) at 12 wk of age for chow-fed mice and 18 wk of age for HFD-fed mice. For intralipid and AICAR challenges, mice were given 48 h to acclimatize to the system, were fasted overnight starting at 1900 h, and given access to food for 2 h at 0700 h before having food removed simultaneously with an oral gavage of saline vs. 10 ml/kg intralipid or intraperitoneal injection of saline vs. 500 mg/kg AICAR at 0900 h. The mean lipid oxidation rates were calculated using the formula (1.6946 * VO_2) – (1.7012 * VCO_2) over 4 h starting 1 h postgavage for intralipid and over 1 h starting 6 h postinjection for AICAR as previously described (2, 53). ipGTT were performed in 6 h-fasted (0700 h to 1300 h) mice at 24 wk of age (16 wk of HFD). Basal blood glucose values were measured via tail-nick using an Accu-Chek blood glucose monitor (Roche) prior to an i.p. injection of 2.0 g/kg and 0.8 g/kg dextrose for chow-fed and HFD-fed mice, respectively. Blood glucose values were then followed following the injection at indicated time points. Intraperitoneal insulin tolerance tests were performed similarly to ipGTT, with an administration of 1.2 U/kg insulin in place of dextrose in HFD-fed mice (17 wk of HFD). Intraperitoneal pyruvate tolerance tests were performed in 12-h fasted mice (1900 h to 0700 h) with 1.5 g/kg sodium pyruvate in HFD-fed mice (18 wk of HFD).

Primary Hepatocytes. Primary hepatocytes were isolated from 10 to 15 wk-old WT or S108A KI mice fed a normal chow diet. Once mice were anesthetized and at surgical plane, livers were perfused with a solution containing 500 μM EGTA followed by type IV collagenase (320 U/mL, Sigma, C5138). The livers were removed,

placed in warm William's Medium E, and gently teased apart with forceps. For plated experiments, cells were suspended in William's Medium E (10% FBS, 1% antibiotic-antimycotic, and 1% L-glutamine), plated to ~85% confluency, and left to adhere overnight. The following morning, the cells were washed with PBS and serum starved for 1–2 h prior to the start of the experiment.

For autophagic assessment by western blotting experiments, following serum starving, the cells were treated with media containing 1% BSA (fatty acid, endotoxin-free Sigma catalog: A8806) ± 500 μM sodium palmitate (freshly made) and 50 μM chloroquine as indicated for 0.5 or 4 h. The cells were washed with cold PBS and snap frozen in cell lysis buffer containing 50 mM HEPES, 150 mM NaCl, 100 mM NaF, 10 mM Na-pyrophosphate, 5 mM EDTA, 250 mM sucrose, 1 mM DTT, and 1 mM Na-orthovanadate, with 1% Triton X and 1 tablet/50 ml complete protease inhibitor cocktail (Roche) and stored at −80°C until future analysis for western blotting. For autophagic flux by tandem fluorescence experiments, the cells were suspended in William's Medium E (10% FBS, 1% antibiotic-antimycotic, and 1% L-glutamine), plated to ~70% confluency, and simultaneously transfected on culture slides for 24 h using the Premo™ Autophagy Tandem Sensor RFP-GFP-LC3B Kit (ThermoFisher Scientific, P36239) according to the manufacturer's instructions. The next day, the cells were washed with warm PBS and serum starved for 2 h prior to the start of the experiment. The cells were treated for 20 h. To end experiments, the cells were washed with room-temperature PBS and fixed for 10 min using 4% PFA before mounting with ProLong™ Gold Antifade with DAPI (ThermoFisher Scientific, P36931) and adding coverslips.

Tissue Processing and TEM. For TEM, liver tissue was fixed in 2% glutaraldehyde in 0.1 M sodium cacodylate buffer (pH 7.4) for at least 24 h. Thin sections were cut by a Leica UCT ultramicrotome and picked up on Cu grids. Sections were poststained with uranyl acetate and lead citrate. Preparation, fixing, and sectioning were performed by the electron microscopy group at McMaster University Medical Center. Electron micrographs were obtained at a direct magnification of 7500× in an AMT 4-megapixel CCD camera (Advanced Microscopy Techniques) mounted in a JEOL JEM 1200 EX TEMSCAN transmission electron microscope and operating at an accelerating voltage of 80 kV. For quantification purposes, the researcher was blinded and 20 images per sample were acquired by random sampling. The total mitochondrial number and surface area were analyzed by a blinded researcher using Image J (NIH) and tracing the outer membrane of each mitochondria using the freehand selection tool with a stylus (Wacom). Samples per animal were averaged to give the represented values.

Tissue Triglycerides. Liver lipids were extracted by an adapted Folch method to determine triglyceride levels (54). Tissues were chipped (30–50 mg), homogenized in 1 mL of 2:1 chloroform:methanol, and mixed end-over-end overnight at 4°C. Samples were spun at 4,500 g for 10 min at 4°C, 0.9% NaCl added, and vortexed before being spun down at the same settings above. 400 μL of the bottom fraction was freeze-dried and solubilized in 100% 2-propranol before being assayed using a colorimetric kit as per manufacturer's instructions (Cayman Chemicals, Triglyceride Kit).

RNA Isolation and Real-Time Quantitative PCR (RT-qPCR). Tissues were lysed in 1 mL TRIzol reagent (Invitrogen) using ceramic beads and a Precellys 24 homogenizer (Bertin Technologies). Samples were spun down for 10 min at 12,000 g at 4°C. 200 μL of chloroform was added and shaken vigorously before spinning samples again at same settings. Supernatant was placed in new tubes and an equal amount of 70% ethanol was added and then vortexed. Solutions were loaded onto RNeasy columns and manufacturer's instructions were followed (Qiagen). 2 ng/μL RNA was added to a first master mix with 0.5 mM dNTPs (Invitrogen) and 50 ng/μL random hexamers (Invitrogen). The solutions were heated to 65°C for 5 min and then cooled back to 4°C. A second master mix containing 50 units of SuperScript III, DTT, and 5x First-Strand Buffer (Invitrogen) was added and heated to 25°C for 5 min and then 50°C for 1 h. All Taqman primers were purchased from Invitrogen (*Ppargc1a*, Mm01208835_m1; *Cpt1a,* Mm01231183_m1; and *Actb*, Mm02619580_g1), and relative gene expression was calculated using ($2^{-\Delta\Delta Ct}$) method. Values were normalized and expressed as relative to the housekeeping gene *Actb*.

Mitochondrial Respiration. Mitochondrial respiration was measured by high-resolution respirometry (Oroboros Oxygraph-2 k, Innsbruck, Austria) at 37°C and room air-saturated oxygen tension. The mitochondrial isolation procedure was similar to that described previously (55). Isolated liver mitochondrial respiration was performed in MIRO5 buffer containing EGTA (0.5 mM), $MgCl_2 \cdot 6H_2O$ (3 mM), K-lactobionate (60 mM), KH_2PO_4 (10 mM), HEPES (20 mM), sucrose (110 mM), and fatty acid-free BSA (1 g/L). The order of substrate addition was malate (0.5 mM), pyruvate (5 mM), ADP (1 mM), glutamate (5 mM), oligomycin (1.25 μM), FCCP (titration of 0.5 μM until maximal uncoupled respiration reached), succinate (10 mM), and then malonate (5 mM).

Autophagic Flux Analyses by Confocal Microscopy. Images were obtained via Olympus FLUOVIEW FV1000 confocal laser scanning microscope (Olympus Corporation, Tokyo, Japan) equipped with a 60× (NA 1.42) oil immersion objective (Olympus) and Olympus FLUOVIEW software (ver4.2a) with appropriate filter conditions for the Premo™ Autophagy Tandem Sensor RFP-GFP-LC3B Kit. Image acquisitions were performed in at least five randomly selected fields of view, and experiments were performed in duplicate, per condition. Image analysis was performed using Fiji open-source software based on ImageJ, using the JACoP plugin. In brief, all colocalization analysis images were processed equally to remove background without altering signal, prior to the calculation of Mander's coefficient. Mander's coefficient values were expressed as the inverse of the percentage of pixels from one channel (i.e., RFP) overlapping with another (i.e., GFP), with independent RFP signal representing the degradation of acid-sensitive GFP.

Mitochondrial Enrichment. Primary hepatocytes were treated as above for autophagic assessment by western blotting experiments, with the following modifications. Cells were rinsed with ice-cold PBS twice before the application of lysis buffer supplemented with protease inhibitor solution supplied in the Qproteome mitochondria isolation kit (Qiagen, 37612). The cells were scraped on ice, and duplicates from 6-well dishes were combined to ensure sufficient protein content. Manufacturer's instructions were followed to yield standard preparations for enriched mitochondria, and 30 μL of cell lysis buffer (listed above) was added immediately to resuspend the pellet. Following kit instructions, 400 μL of cytosolic protein fraction was added to four volumes of ice-cold acetone to concentrate samples before resuspending in 50 μL of cell lysis buffer.

Statistics. Values were reported as mean ± SEM throughout the manuscript. White circles are individual mice per group or technical replicates from 3 to 5 separate experiments. Data were graphed and analyzed in GraphPad Prism 9 software using two-tailed Student's *t* tests, two-way ANOVA with Tukey's posthoc analysis, or repeated-measures two-way ANOVA with Sidak's posthoc analysis, where appropriate. Statistical significance was accepted at $P < 0.05$. Raw data is available in the *SI Appendix* section.

Data, Materials, and Software Availability. All study data are included in the article and/or *SI Appendix*.

ACKNOWLEDGMENTS. We would like to thank Fiorella Di Pastena for help with mitochondrial preps and Marcia Reid from the electron microscopy group at McMaster University Medical Center for her technical assistance and expertise in sample preparation. These studies were supported by grants from Diabetes Canada (G.R.S., DI-5-17-5302-GS), the Canadian Institutes of Health Research (G.R.S., 201709FDN-CEBA-116200) and Novo Nordisk Foundation (K.S., NNF21OC0070257). G.R.S. is supported by a Tier 1 Canada Research Chair and the J. Bruce Duncan Chair in Metabolic Diseases. E.M.D. is a Vanier Scholar. B.K.S. was supported by Canadian Institutes of Health Research and Michael DeGroote Postdoctoral fellowships. E.A.D. was a recipient of an Ontario Graduate Scholarship (Queen Elizabeth II Graduate Scholarship in Science and Technology) and a Douglas C. Russell Memorial Scholarship. J.P.N. is supported by a Canadian Institutes of Health Research Postdoctoral fellowship. K.S. is supported by the Novo Nordisk Foundation Center for Basic Metabolic Research as an independent Research Center based at the University of Copenhagen, Denmark, which is partially funded by an unconditional donation from the Novo Nordisk Foundation (www.cbmr.ku.dk) (grant number NNF18CC0034900).

Author affiliations: [a]Centre for Metabolism Obesity and Diabetes Research, McMaster University, Hamilton ON L8N 3Z5, Canada; [b]Division of Endocrinology and Metabolism, Department of Medicine, McMaster University, Hamilton ON L8N 3Z5, Canada; [c]Nestlé Institute of Health Sciences, Nestlé Research, Société des Produits Nestlé S.A., Lausanne 1015, Switzerland; [d]Department of Pediatrics, Faculty of Health Sciences, McMaster University, Hamilton ON L8N 3Z5, Canada; [e]Novo Nordisk Foundation Center for Basic Metabolic Research, University of Copenhagen, Copenhagen 2200, Denmark; and [f]Department of Biochemistry and Biomedical Sciences, McMaster University, Hamilton ON L8N 3Z5, Canada

1. R. H. Unger, P. E. Scherer, Gluttony, sloth and the metabolic syndrome: A roadmap to lipotoxicity. *Trends Endocrinol. Metab.* **21**, 345–352 (2010).
2. S. L. Pinkosky *et al.*, Long-chain fatty acyl-CoA esters regulate metabolism via allosteric control of AMPK β1 isoforms. *Nat. Metab.* **2**, 873-881 (2020), 10.1038/s42255-020-0245-2.
3. J. E. Song *et al.*, Mitochondrial fission governed by drp1 regulates exogenous fatty acid usage and storage in hela cells. *Metabolites* **11**, 322 (2021).
4. N. Turner *et al.*, Excess lipid availability increases mitochondrial fatty acid oxidative capacity in muscle: Evidence against a role for reduced fatty acid oxidation in lipid-induced insulin resistance in rodents. *Diabetes* **56**, 2085–2092 (2007).
5. P. Garcia-Roves *et al.*, Raising plasma fatty acid concentration induces increased biogenesis of mitochondria in skeletal muscle. *Proc. Natl. Acad. Sci. U S A.* **104**, 10709–10713 (2007).
6. G. R. Steinberg, D. Carling, AMP-activated protein kinase: The current landscape for drug development. *Nat. Rev. Drug Discov.* **18**, 527–551 (2019).
7. N. Dzamko *et al.*, AMPK β1 deletion reduces appetite, preventing obesity and hepatic insulin resistance. *J. Biol. Chem.* **285**, 115–122 (2010).
8. G. R. Steinberg *et al.*, Whole body deletion of AMP-activated protein kinase β2 reduces muscle AMPK activity and exercise capacity. *J. Biol. Chem.* **285**, 37198–37209 (2010).
9. K. I. Mitchelhill *et al.*, Posttranslational modifications of the 5′-AMP-activated protein kinase β1 subunit. *J. Biol. Chem.* **272**, 24475–24479 (1997).
10. T. J. Iseli *et al.*, AMP-activated protein kinase B subunit tethers a and y subunits via Its C-terminal sequence (186–270). *J. Biol. Chem.* **280**, 13395–13400 (2005).
11. Y. Yan, X. E. Zhou, H. E. Xu, K. Melcher, Structure and physiological regulation of AMPK. *Int. J. Mol. Sci.* **19**, 3534 (2018).
12. T. A. Dite *et al.*, The autophagy initiator ULK1 sensitizes AMPK to allosteric drugs. *Nat. Commun.* **8**, 1–13 (2017).
13. J. S. Oakhill *et al.*, Subunit myristoylation is the gatekeeper for initiating metabolic stress sensing by AMP-activated protein kinase (AMPK). *Proc. Natl. Acad. Sci.* **107**, 19237–19241 (2010).
14. B. Xiao *et al.*, Structure of mammalian AMPK and its regulation by ADP. *Nature* **472**, 230–233 (2011).
15. S. A.Hawley, The ancient drug salicylate directly activates amp-activated protein kinase. *Science* **336**, 918–922 (2012).
16. M. J. Sanders *et al.*, Defining the mechanism of activation of AMP-activated protein kinase by the small molecule A-769662, a member of the thienopyridone family. *J. Biol. Chem.* **282**, 32539–32548 (2007).
17. B. Xiao *et al.*, Structural basis of AMPK regulation by small molecule activators. *Nat. Commun.* **4**, 1–10 (2013).
18. R. W. Myers *et al.*, Systemic pan-AMPK activator MK-8722 improves glucose homeostasis but induces cardiac hypertrophy. *Science* **357**, 507–511 (2017).
19. R. M. Esquejo *et al.*, Activation of liver AMPK with PF-06409577 corrects NAFLD and lowers cholesterol in rodent and primate preclinical models. *EBioMedicine* **31**, 122–132 (2018).
20. M. J. Sanders *et al.*, Natural (dihydro)phenanthrene plant compounds are direct activators of AMPK through its allosteric drug and metabolite binding site. *J. Biol. Chem.* **298**, 101852 (2022).
21. K. Cusi *et al.*, Efficacy and safety of PXL770, a direct AMP kinase activator, for the treatment of non-alcoholic fatty liver disease (STAMP-NAFLD): A randomised, double-blind, placebo-controlled, phase 2a study. *Lancet Gastroenterol. Hepatol.* **6**, 889–902 (2021).
22. P. Gluais-Dagorn *et al.*, Direct AMPK activation corrects NASH in rodents through metabolic effects and direct action on inflammation and fibrogenesis. *Hepatol. Commun.* **6**, 101–119 (2021).
23. S. A. Hawley *et al.*, Use of cells expressing γ subunit variants to identify diverse mechanisms of AMPK activation. *Cell Metab.* **11**, 554–565 (2010).
24. M. D. Fullerton *et al.*, Single phosphorylation sites in Acc1 and Acc2 regulate lipid homeostasis and the insulin-sensitizing effects of metformin. *Nat. Med.* **19**, 1649–1654 (2013).
25. S. Herzig, R. J. Shaw, AMPK: Guardian of metabolism and mitochondrial homeostasis. *Nat. Rev. Mol. Cell Biol.* **19**, 121–135 (2018).
26. H. M. O'Neill, G. P. Holloway, G. R. Steinberg, AMPK regulation of fatty acid metabolism and mitochondrial biogenesis: Implications for obesity. *Mol. Cell. Endocrinol.* **366**, 135–151 (2013).
27. G. A. Baselli *et al.*, Rare ATG7 genetic variants predispose patients to severe fatty liver disease. *J. Hepatol.* **77**, 596–606 (2022).
28. J. W. Scott *et al.*, Small molecule drug A-769662 and AMP synergistically activate naive AMPK independent of upstream kinase signaling. *Chem. Biol.* **21**, 619–627 (2014).
29. Y. Lee *et al.*, PPARα is necessary for the lipopenic action of hyperleptinemia on white adipose and liver tissue. *Proc. Natl. Acad. Sci. U.S.A.* **99**, 11848–11853 (2002).
30. J. Carabelli *et al.*, High fat diet-induced liver steatosis promotes an increase in liver mitochondrial biogenesis in response to hypoxia. *J. Cell. Mol. Med.* **15**, 1329–1338 (2011).
31. E. P. Mottillo *et al.*, Lack of adipocyte AMPK exacerbates insulin resistance and hepatic steatosis through Brown and Beige adipose tissue function. *Cell Metab.* **24**, 118–129 (2016).
32. H. M. O'Neill *et al.*, AMP-activated protein kinase (AMPK) β1β2 muscle null mice reveal an essential role for AMPK in maintaining mitochondrial content and glucose uptake during exercise. *Proc. Natl. Acad. Sci. U.S.A.* **108**, 16092–16097 (2011).
33. S. Galic *et al.*, Hematopoietic AMPK β1 reduces mouse adipose tissue macrophage inflammation and insulin resistance in obesity. *J. Clin. Invest.* **121**, 4903–4915 (2011).
34. C. M. Hasenour *et al.*, 5-Aminoimidazole-4-carboxamide-1-β-D-ribofuranoside (AICAR) effect on glucose production, but not energy metabolism, is independent of hepatic AMPK in vivo. *J. Biol. Chem.* **289**, 5950–5959 (2014).
35. J. L. Estall *et al.*, Sensitivity of lipid metabolism and insulin signaling to genetic alterations in hepatic peroxisome proliferator-activated receptor-γ coactivator-1α expression. *Diabetes* **58**, 1499–1508 (2009).
36. Y. Kupriyanova *et al.*, Early changes in hepatic energy metabolism and lipid content in recent-onset type 1 and 2 diabetes mellitus. *J. Hepatol.* **74**, 1028–1037 (2021).
37. T. Zhang, Q. Liu, W. Gao, S. A. Sehgal, H. Wu, The multifaceted regulation of mitophagy by endogenous metabolites. *Autophagy* **00**, 1–24 (2021).
38. D. F. Egan *et al.*, Phosphorylation of ULK1 (hATG1) by AMP-activated protein kinase connects energy sensing to mitophagy. *Science* **331**, 456–462 (2011).
39. J. Kim, M. Kundu, B. Viollet, K. Guan, AMPK and mTOR regulate autophagy through direct phosphorylation of Ulk1. *Nat. Cell Biol.* **13**, 132–141 (2011).
40. J. W. Lee, S. Park, Y. Takahashi, H. G. Wang, The association of AMPK with ULK1 regulates autophagy. *PLoS One* **5**, 1–9 (2010).
41. W. J. Lee *et al.*, AMPK activation increases fatty acid oxidation in skeletal muscle by activating PPARα and PGC-1. *Biochem. Biophys. Res. Commun.* **340**, 291–295 (2006).
42. C. M. Hung *et al.*, AMPK/ULK1-mediated phosphorylation of Parkin ACT domain mediates an early step in mitophagy. *Sci. Adv.* **7**, 1–15 (2021).
43. R. Iorio, G. Celenza, S. Petricca, Mitophagy: Molecular mechanisms, new concepts on parkin activation and the emerging role of ampk/ulk1 axis. *Cells* **11**, 1–25 (2022).
44. J. C. Drake *et al.*, Mitochondria-localized AMPK responds to local energetics and contributes to exercise and energetic stress-induced mitophagy. *Proc. Natl. Acad. Sci. U.S.A.* **118**, 1–10 (2021).
45. S. Ducommun *et al.*, Motif affinity and mass spectrometry proteomic approach for the discovery of cellular AMPK targets: Identification of mitochondrial fission factor as a new AMPK substrate. *Cell. Signal.* **27**, 978–988 (2015).
46. E. Q. Toyama *et al.*, AMP-activated protein kinase mediates mitochondrial fission in response to energy stress. *Science* **351**, 275–281 (2016).
47. L. Xie *et al.*, Drp1-dependent remodeling of mitochondrial morphology triggered by EBV-LMP1 increases cisplatin resistance. *Signal Transduct. Target. Ther.* **5**, 1–12 (2020).
48. R. J. Ford *et al.*, Metformin and salicylate synergistically activate liver AMPK, inhibit lipogenesis and improve insulin sensitivity. *Biochem. J.* **468**, 125–132 (2015).
49. X. Stephenne *et al.*, Metformin activates AMP-activated protein kinase in primary human hepatocytes by decreasing cellular energy status. *Diabetologia* **54**, 3101–3110 (2011).
50. J. Wu *et al.*, Chemoproteomic analysis of intertissue and interspecies isoform diversity of AMP-activated protein kinase (AMPK). *J. Biol. Chem.* **288**, 35904–35912 (2013).
51. S. Ducommun *et al.*, Enhanced activation of cellular AMPK by dual-small molecule treatment: AICAR and A769662. *Am. J. Physiol. Endocrinol. Metab.* **306**, E688–96 (2014).
52. L. Bultot *et al.*, Benzimidazole derivative small-molecule 991 enhances AMPK activity and glucose uptake induced by AICAR or contraction in skeletal muscle. *Am. J. Physiol. Endocrinol. Metab.* **311**, E706–E719 (2016).
53. H. M. O. O'Neill *et al.*, AMPK phosphorylation of ACC2 is required for skeletal muscle fatty acid oxidation and insulin sensitivity in mice. *Diabetologia* **57**, 1693–1702 (2014).
54. J. Folch, M. Lees, G. H. Sloane Stanley, A simple method for the isolation and purification of total lipides from animal tissues. *J. Biol. Chem.* **226**, 497–509 (1957).
55. B. K. Smith *et al.*, Salsalate (salicylate) uncouples mitochondria, improves glucose homeostasis, and reduces liver lipids independent of ampk-β1. *Diabetes* **65**, 3352–3361 (2016).

PNAS

Supplementary Information for

The phosphorylation of AMPKβ1 is critical for increasing autophagy and maintaining mitochondrial homeostasis in response to fatty acids

Eric M. Desjardins[1,2], Brennan K. Smith[1,2], Emily A. Day[1,2,&], Serge Ducommun[3,#], Matthew J. Sanders[3], Joshua P. Nederveen[1,4], Rebecca J. Ford[1,2], Stephen L. Pinkosky[1,2], Logan K. Townsend[1,2] , Robert M. Gutgesell[1,2], Rachel Lu[1,2], Kei Sakamoto[3,5*] and Gregory R. Steinberg[1,2,6*]

[1]Centre for Metabolism Obesity and Diabetes Research, McMaster University, Hamilton, Canada
[2]Division of Endocrinology and Metabolism, Department of Medicine, McMaster University, Hamilton, Canada
[3]Nestlé Institute of Health Sciences, Nestlé Research, Société des Produits Nestlé S.A., Lausanne, Switzerland
[4]Department of Pediatrics, Faculty of Health Sciences, McMaster University, Hamilton, Canada
[5]Novo Nordisk Foundation Center for Basic Metabolic Research, University of Copenhagen, Copenhagen, Denmark
[6]Department of Biochemistry and Biomedical Sciences, McMaster University, Hamilton, Canada
[&]Current address: School of Biochemistry and Immunology, Trinity College Dublin, Trinity Biomedical Sciences Institute, Dublin, Ireland
[#]Current address: Department of Physiology and Pharmacology, Karolinska Institute, Solna, Sweden

*Correspondence to Gregory R. Steinberg or Kei Sakamoto

Centre for Metabolism, Obesity and Diabetes Research, McMaster University, 1280 Main St. West, Hamilton, Ontario, L8N 3Z5, Canada, Tel: 905.525.9140 ext. 21691
Email: gsteinberg@mcmaster.ca

Novo Nordisk Foundation Center for Basic Metabolic Research, University of Copenhagen, Copenhagen 2200, Denmark
Email: kei.sakamoto@sund.ku.dk

This PDF file includes:

Figures S1 to S5
SI References

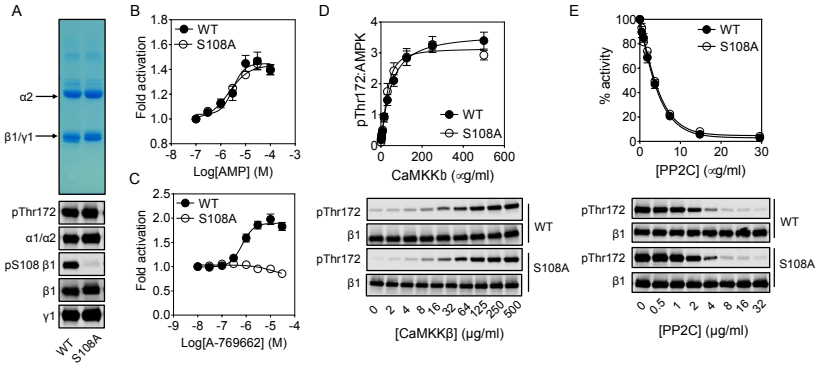

Supplemental Figure 1. **Regulation of recombinant AMPKα2β1γ1 WT and S108A mutant.** (A) Recombinant human AMPKα2β1γ1 wild-type (WT) and AMPKα2β1(S108A)γ1 mutant was expressed and purified as described previously (1), resolved by SDS-PAGE and stained with Coomassie blue (upper image) or subjected to immunoblot analysis (lower images) with the indicated antibodies. (B-C) AMPK activity of bacterially expressed recombinant α2β1γ1 WT or S108A mutant in the presence of increasing concentrations of AMP (B) or A769662 (C) was measured as described (1). Results are presented as fold activation compared to no activator control (average ± SEM of at least 3 independent experiments). (D) Unphosphorylated AMPKα2β1γ1 WT and S108A was incubated with varying concentrations of recombinant CaMKKβ and the phosphorylation of AMPKα Thr172 was determined by immunoblot analysis. The bands were quantified and normalized to AMPKβ1 expression and displayed in the graph above a representative blot (average ± SEM of at least 3 independent experiments). (E) Phosphorylated AMPKα2β1γ1 WT and S108A was incubated with varying concentrations of recombinant protein phosphatase 2Cα (PP2C) and phosphorylation of AMPKα Thr172 was determined by immunoblot analysis. The percentage of pThr172 was determined relative to phosphorylated AMPKα2β1γ1 WT or S108A in the absence of PP2Cα and a graph is displayed above a representative blot (average ± SEM of at least 3 independent experiments).

2

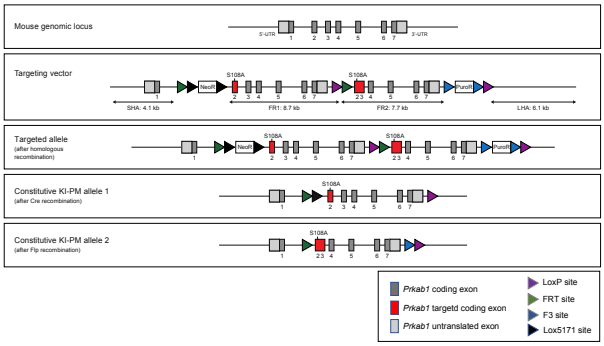

Supplemental Figure 2. S108A knock-in targeting strategy. A schematic illustrating the targeting strategy used to generate C57BL/6NTac Prkab1/AMPKβ1 S108A knock-in (KI) mouse model. The targeting strategy is based on NCBI transcript NM_031869.2. Exons and FRT recombination sites are represented by dark grey boxes and triangles, respectively. The amino acid to be exchanged (Ser108) is encoded by nucleotides located at the exon-intron boundary. There was a risk that changes in the nucleotide sequence might interfere with splicing of the transcript (leading to a hypomorphic effect). Therefore, we designed the targeting vector to achieve the S108A mutation with two options (KI-PM allele 1 or KI-PM allele 2). The constitutive KI-PM allele 1 is obtained after Cre-mediated removal of exons 2 to 7 (containing the joint exon 2 and 3) and of the NeoR selection marker. The KI-PM allele 1 strategy resulted in normal expression of the mutant (S108A) protein in tissues studied as demonstrated in Figure 1B and C.

3

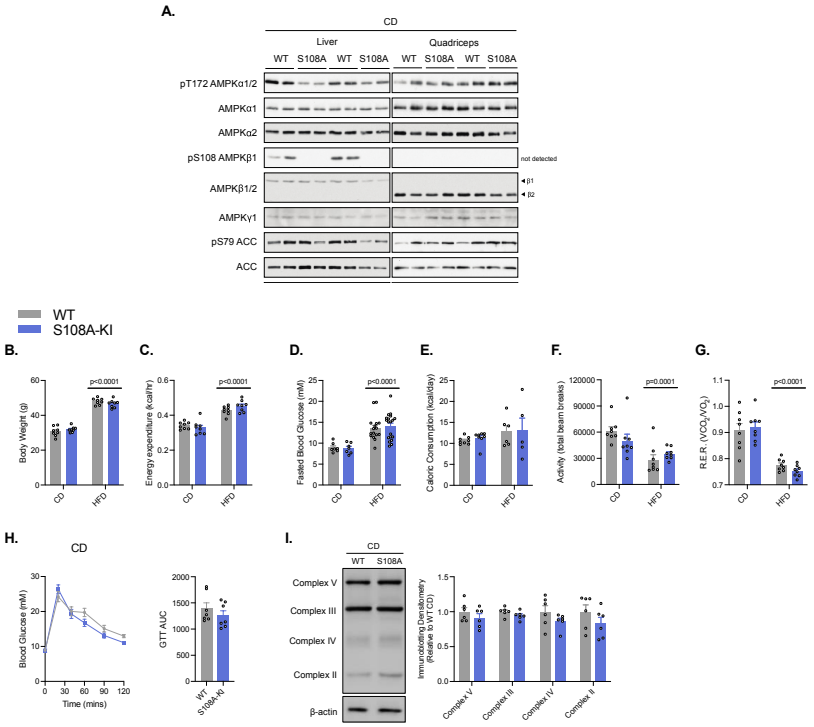

Supplemental Figure 3. S108A-KI mice have no alterations in basal metabolic parameters on a chow or high-fat diet. (A) Immunoblots of AMPK subunits, phosphorylation, and downstream markers of activation in the same liver and Quad samples from Figure 1A (CD: chow diet-fed). (B-G) Body weight (B), energy expenditure (C), 6 hr fasted blood glucose (D), caloric consumption (E), activity levels (F), and respiratory exchange ratio (R.E.R.) (G) in WT and S108A-KI mice fed a control chow diet (CD) or high-fat diet (HFD). (H) Intraperitoneal glucose tolerance test (2.0 g/kg) and calculated area under the curve (GTT AUC) in WT and S108A-KI mice fed a control chow diet. (I) Representative immunoblots and densitometrical analysis of OXPHOS complexes 2-5 of WT and S108A-KI mice fed a control chow diet. Data are means ± S.E.M. with p-values reported in the graphs. Black bars signify main effects for diet. Statistical significance was accepted at $p < 0.05$ and determined via two-way ANOVA. White circles are individual mice per group.

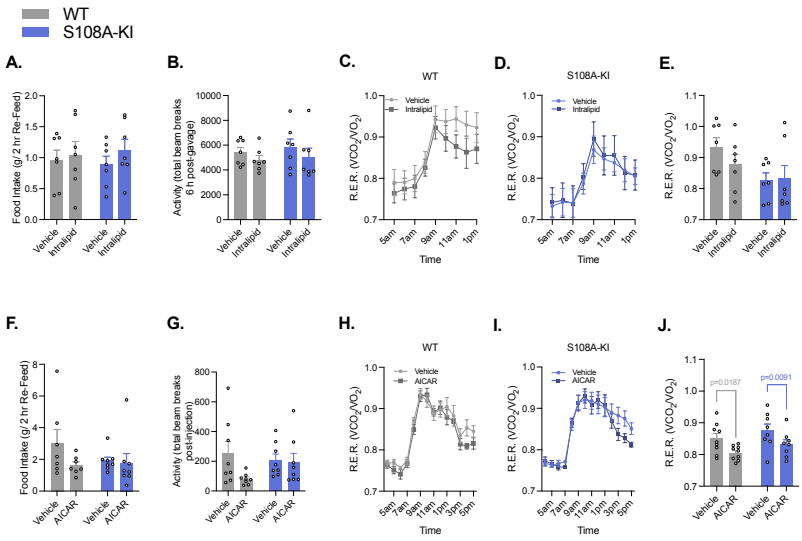

Supplemental Figure 4. S108A-KI mice have an attenuated response in lipid oxidation to exogenous lipids, but have a normal response to AICAR in vivo. Food intake during 2 hr refeed (A) prior to, and activity levels over 6 hrs (B) following, an oral gavage of saline or Intralipid (10 mL/kg) in chow diet-fed WT and S108A-KI mice. Respiratory exchange ratio (R.E.R.) time plots of chow-fed WT (C) and S108A-KI (D) treated with saline or Intralipid. Average RER (E) over 4 hrs, starting 1 hr post-gavage of saline or Intralipid (10 mL/kg). Food intake during 2 hr refeed (F) prior to, and activity levels over 1 hr,(G) starting 6 hours following, an injection of saline or AICAR (500 mg/kg). Respiratory exchange ratio (R.E.R.) time plots of chow-fed WT (H) and S108A-KI (I) treated with saline or AICAR. Average RER (J) over 1 hr, starting 6 hrs post-injection of saline or AICAR. Data are means ± S.E.M. White circles are individual mice per group.

5

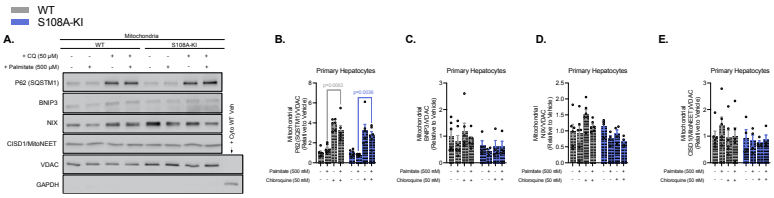

Supplemental Figure 5. Other markers of mitophagy are not altered with palmitate treatment or S108A-KI in primary hepatocytes from mice. Representative immunoblotting (A) and densitometrical analysis of P62 (B) BNIP3 (C), NIX (D), CISD1 (E) assessing mitophagy in response to palmitate (500 μM) in primary hepatocytes from CD-fed WT and S108A-KI mice. Data are means ± S.E.M. and white circles are technical replicates from experiments from 3 experimental replicates per group. Grey bar equals a WT difference and blue bar equals to a S108A-KI difference. Statistical significance was accepted at $p < 0.05$ and determined via repeated-measures two-way ANOVA with Tukey's posthoc analysis.

SI References

1. M. J. Sanders, *et al*., Defining the mechanism of activation of AMP-activated protein kinase by the small molecule A-769662, a member of the thienopyridone family. *J. Biol. Chem.* **282**, 32539–32548 (2007).

CHAPTER THREE

PHARMACOLOGICAL INHIBITION OF ACLY IN A MOUSE MODEL OF NASH PROMOTES AUTOPHAGY

Prepared for publication, 2023

Eric M. Desjardins, Emily A. Day, Stephen L. Pinkosky, Gregory R. Steinberg

In this chapter, we interrogated mechanisms beyond the inhibition of DNL by which bempedoic acid provides hepatoprotective effects in NAFL/NASH. In a previous study, we demonstrated that both genetic and pharmacological inhibition of ACLY by bempedoic acid improved liver steatosis and hepatocellular ballooning, while only bempedoic acid improved fibrosis in a mouse model fed a high-fat high-fructose diet. The protective effects of bempedoic acid against hepatocellular ballooning and fibrosis were recapitulated in the STAM mouse model, which is a streptozotosin-induced short-term HFD-fed diabetes mouse model not characterized by obesity, hyperinsulinemia, or elevated DNL. In the work outlined below, we find that bempedoic acid increases autophagic flux in cultured hepatocytes; findings which are further supported by assessing multiple markers of autophagy in liver samples collected from the STAM mice mentioned just above. We describe that these effects are mediated through increases in gene expression of genes related to the autophagy pathway and not via phosphorylation events which trigger initiation. The increases in expression of genes related to the autophagy pathway were further confirmed by data from a metabolic-associated NASH mouse model treated with bempedoic acid. Using proteomics to assess protein acetylation status in STAM mice, we identified that a key transcriptional regulator of autophagy that is sensitive to acetyl-CoA levels, P300, had reductions in multiple acetylation sites within its activation loop, reducing its activity and ability to suppress autophagy. Thus, this supports a model by which bempedoic acid reduces acetyl-CoA availability, in turn leading to changes in the acetylation of proteins and reducing the activity of enzymes which suppress autophagic flux. These data identify additional mechanisms by which bempedoic acid treatment confers hepatoprotective effects and further supports the development of this therapy for the treatment of NASH and fibrosis.

EMD was involved in all experiments illustrated except for Figures 2C and 3E.

Pharmacological inhibition of ACLY in a mouse model of NASH promotes autophagy

Eric M. Desjardins[1,2], Emily A. Day[1,2], Stephen L. Pinkosky[3*], and Gregory R. Steinberg[1,2,4*]

Author Information
[1]Centre for Metabolism, Obesity and Diabetes Research, McMaster University, 1280 Main Street West, Hamilton, Ontario, Canada L8S 4K1.
[2]Division of Endocrinology and Metabolism, Department of Medicine, McMaster University, 1280 Main Street West, Hamilton, Ontario, Canada L8S 4K1.
[3]Esperion Therapeutics, Inc., 3891 Ranchero Drive, Suite 150, Ann Arbor, Michigan 48108, USA.
[4]Department of Biochemistry and Biomedical Sciences, McMaster University, 1280 Main Street West, Hamilton, Ontario, Canada L8S 4K1.

*Correspondence to:
Gregory R. Steinberg gsteinberg@mcmaster.ca, Phone (905) 525-9140 x21691

Abstract

A discordance between energy sensing mechanisms and substrate utilization can promote the progression of nonalcoholic fatty liver disease (NAFLD) to nonalcoholic steatohepatitis (NASH) and hepatic fibrosis. A key hallmark of NAFLD and NASH are increases in *de novo* lipogenesis and reductions in autophagy within the liver. Acetyl-CoA is a central intracellular metabolic intermediate linking nutrient availability and demand and is generated in the cytosol through ATP-citrate lyase (ACLY). The inhibition of ACLY in mouse models reduces liver cholesterol and fatty acid synthesis while increasing fatty acid oxidation and this is associated with reductions in steatosis and fibrosis in several preclinical models. In addition to being a key substrate for lipid synthesis, in cancer cells, reductions in acetyl-CoA will also trigger autophagy. However, whether this also occurs in the liver following inhibition of ACLY has not been evaluated. In the current study, we investigated the effects of the ACLY inhibitor bempedoic acid (BemA) in a preclinical mouse model of NASH and found increased markers of autophagy. Similarly, treatment of primary mouse hepatocytes with BemA enhanced autophagic flux. This data suggests that, in addition to lowering fatty acid and cholesterol synthesis, the inhibition of ACLY may exert positive effects in mouse models of NASH by promoting autophagy.

Introduction

Normal liver function is dependent on a number of homeostatic mechanisms that integrate nutrient availability and energy status signals with multiple cellular processes (Pinkosky et al. 2017). Chronic over nutrition can disrupt these mechanisms and promote insulin resistance, aberrant hepatic lipid metabolism, and liver injury, leading to nonalcoholic fatty liver disease (NAFLD) and nonalcoholic steatohepatitis (NASH) (Cohen, Horton, and Hobbs 2011). Intracellular acetyl-CoA levels are critical for linking cellular nutrient status to metabolism(Pietrocola et al. 2015; Galluzzi et al. 2015; Mariño et al. 2014). Acetyl-CoA is converted to malonyl-CoA – the first committed step in fatty acid synthesis and an allosteric inhibitor of carnitine palmitoyl-transferase 1 – through acetyl-CoA carboxylase (ACC). Cytosolic acetyl-CoA is also converted to cholesterol through the sterol synthesis pathway. Importantly, increases in fatty acid and cholesterol synthesis have been causally linked to the development of NAFLD and NASH in mice and humans, findings that have led to clinical evaluation of inhibitors targeting this pathway (Batchuluun, Pinkosky, and Steinberg 2022).

In addition to being a substrate for fatty acid and cholesterol synthesis, emerging evidence indicates that depletion of acetyl-CoA also enhances autophagy (Y. Xu and Wan 2022). Autophagy is a vital process for recycling dysfunctional or aggregated proteins, and organelles including mitochondria and peroxisomes (Fukuo et al. 2014; González-Rodríguez et al. 2014; Kashima et al. 2014). Although incompletely understood, reductions in acetyl-CoA are proposed

to promote autophagy through the acetyltransferase p300 while increases in acetyl-CoA reduce autophagy by enhancing mTORC1 which inactivates the autophagic initiating protein ULK1 through phosphorylation at Ser757 (I. H. Lee and Finkel 2009). Importantly, it is now well recognized that in both rodent models and people with NAFLD/NASH autophagy in the liver is reduced (Ramos, Kowaltowski, and Kakimoto 2021). These data suggest that in addition to lowering fatty acid and cholesterol synthesis reductions in acetyl-CoA availability may exert positive effects on reducing NASH by enhancing autophagy.

A key enzyme controlling cytosolic acetyl-CoA is ATP-citrate lyase (ACLY). ACLY is upregulated in the liver of people with NASH and using mendelian randomization analysis we have linked this to increases in markers of liver damage (Ahrens et al. 2013; Morrow et al. 2022). Consistent with these clinical observations, we and others have shown that inhibition of ACLY reduces fatty acid and sterol synthesis and increases fatty acid oxidation in hepatocytes and this is associated with reductions in steatosis (Morrow et al. 2022; Srere 1959; M. Singh et al. 1976; Sullivan et al. 1974; Q. Wang et al. 2009; Pinkosky et al. 2013b, 2016; Samsoondar et al. 2017). ACLY can be inhibited pharmacologically with bempedoic acid (BemA; ETC-1002) (Pinkosky et al. 2013b, 2016), with recent studies showing this not only reduces low-density lipoprotein cholesterol (Ray et al. 2019) but also cardiovascular events in statin-intolerant patients (Nissen et al. 2023). Bempedoic acid also reduces liver steatosis, hepatocellular ballooning, lobular inflammation, NAFLD activity composite scores and fibrosis in preclinical

mouse models; effects that were linked to reductions in fatty acid and cholesterol synthesis and increases in fatty acid oxidation in both hepatocytes and hepatic stellate cells (Morrow et al. 2022). And while the effects of bempedoic acid on steatosis could be explained by reductions in cholesterol and fatty acid synthesis as well as increases in fatty acid oxidation, the pronounced effects of bempedoic acid to reduce ballooning and fibrosis were not directly correlated with changes in steatosis. These data suggest that additional mechanisms might also be important for the beneficial effects of BemA on NASH.

It is known that autophagy is downregulated in people with NAFLD/NASH and that reductions in acetyl-CoA that may enhance autophagy, therefore, the purpose of this study was to investigate whether the ACLY inhibitor bempedoic acid might affect this pathway. We find that bempedoic acid increases autophagic flux in isolated hepatocytes and leads to increased markers of autophagy in the STAM mouse model of NASH. These data suggest that, in addition to regulating lipid metabolism, bempedoic acid may reduce hepatocellular ballooning and fibrosis in NASH by enhancing autophagy.

Results

Bempedoic acid increases autophagic flux in cultured rat hepatocytes

To directly evaluate the effects of bempedoic acid on autophagy independently of changes in substrate availability (i.e. glucose or free fatty acids) or hormonal regulators (i.e. insulin, glucagon) we conducted studies in cultured rat

hepatocytes (McCardle Cells) with or without chloroquine which inhibits lysosomal degradation of autophagosomes (Figure 1A). We utilized McCardle cells because they are known to express the acyl-CoA synthetase ACSVL1, the enzyme that converts bempedoic acid to its active component bempedoyl-CoA (Pinkosky et al. 2017). In the absence of chloroquine, BemA tended to increase LC3BII, however this was not significant (Figure 1B). As anticipated, the treatment of hepatocytes with chloroquine increased LC3BII levels, however, this effect was dramatically enhanced by the addition of BemA (Figure 1B). These data indicate that in an isolated controlled system, inhibition of ACLY using BemA increases autophagic flux.

Bempedoic acid increases markers of autophagy in the livers of STAM mice.

To examine whether these effects might also extend to mice with NASH, we assessed the LC3BII/LC3BI ratio in STAM mice treated with vehicle or BemA (Figure 2A). We found that chronic treatment with BemA increased the LC3BII/LC3BI ratio in the liver of STAM mice relative to vehicle controls suggesting that autophagy might be enhanced (Figure 2B). In mouse models, low rates of autophagy in NASH will lead to the accumulation of misfolded proteins including cytokeratin-18 (CK-18) (Bratoeva et al. 2018; Wieckowska et al. 2006). Consistent with enhanced recycling of mis-folded proteins we found that BemA reduced CK-18 fragment staining (Figure 2C). These data suggest that consistent with

observations in hepatocytes BemA may be enhancing autophagy in the livers of the STAM mouse model of NASH.

Bempedoic acid increases the expression but not phosphorylation of autophagic proteins in the liver of mice

To examine the potential mechanism contributing to the increase in autophagy we assessed the expression and phosphorylation of key components of the autophagic pathway from the livers of STAM mice (Figure 3A). Treatment of mice with BemA did not alter the phosphorylation of ULK1 at either the AMPK (S555) or mTOR (S757) phosphorylation sites (Figure 3B) but led to increased protein content of ULK1 ($p = 0.06$), Parkin, BNIP3 and p62 (Figure 3C). When assessing mRNA expression, no effects were observed on *Ulk1*, *Map1c3,* and *Tfeb*, however, BemA did increase the expression of *Park2, Bnip3, Sqstm1, Dnm1, Fis1, Tfe3,* and *Gaa* (Figure 3D). These data suggest that BemA increases autophagy through regulation of gene expression and not through posttranslational modifications.

Bempedoic acid reduces acetylation of the activation loop of p300.

Our findings indicating increased expression of autophagic proteins, in the absence of changes in phosphorylation of ULK1, suggested that BemA may be working through transcriptional mechanisms. A key transcriptional regulator of autophagy that is sensitive to changes in acetyl-CoA availability is the

acetyltransferase p300 (Mariño et al. 2014). Consistent with this hypothesis BemA reduced the acetylation of peptides within the activation loop of p300 (k1553, k1554, and k1557); an effect which is known to suppress the acetyltransferase activity of p300 (Figure 3E) (Karanam et al. 2006).

Pharmacological inhibition of liver ACLY increases expression of autophagy genes in a mouse model of metabolic-associated NASH

In addition to our findings that ETC treatment increased the gene expression of autophagy markers in STAM mice, we pulled autophagy-related data from a NanoString Fibrosis panel to determine whether markers of autophagy were also increased in a different mouse model of NASH driven by long-term high-fat high-fructose feeding and thermoneutral housing. BemA increased the expression of *Map1lc3, Pik3c3, Mtor, Hif1a, Lamtor2,* and *Vamp8*, indicating that the proposed mechanism remains physiologically relevant in a model where increased obesity, insulin resistance, and DNL contribute to the severity of disease.

Taken together these data suggest that lowering acetyl-CoA through ACLY inhibition with BemA, leads to reduced p300 activity, transcriptional upregulation of autophagic proteins and increases in autophagic flux. These data suggest that, in addition to regulating lipid metabolism, ACLY inhibition may exert favorable effects on hepatocellular ballooning and fibrosis by promoting autophagy (Figure 5).

Discussion

NAFLD has rapidly emerged as a leading cause of chronic liver disease that presents a global health challenge with no approved therapies. Owing to the complexity of NASH pathogenesis, several therapeutic strategies are in development that target different stages of disease progression. Recently, a new class of drugs targeting ACC, the rate-limiting step in de novo fatty acid synthesis, has emerged as a promising strategy to reduce hepatic steatosis and potentially improve liver-related morbidity and mortality (Lawitz et al. 2018; Stiede et al. 2017; Loomba et al. 2018). However, three studies using three different compounds have demonstrated that inhibition of ACC results in hypertriglyceridemia, an undesirable side effect associated with target engagement (C. W. Kim et al. 2017a; Goedeke et al. 2018; Loomba et al. 2018). ACLY is a cytosolic enzyme that is one step upstream of ACC and is strategically positioned at the intersection of nutrient catabolism, and cholesterol and fatty acid biosynthesis (Pinkosky et al. 2017). Based on this unique position, ACLY activity not only modulates cholesterol and fatty acid biosynthesis rates, but also cytosolic acetyl-CoA levels which is thought to function as a metabolic checkpoint used by cells to gauge nutrient availability via protein acetylation (Pietrocola et al. 2015; Jeninga, Schoonjans, and Auwerx 2010; Wellen et al. 2009; Wellen and Thompson 2012). Therefore, ACLY inhibition may mimic the beneficial effects of caloric restriction and could offer a therapeutic strategy to reduce hepatic steatosis and address the underlying metabolic derangements associated with NASH. This is supported by previous studies which

showed that the ACLY inhibitor, bempedoic acid, attenuated the development of hepatic steatosis, inflammation, and insulin resistance in rodent models of obesity-driven metabolic disease and NAFLD (Pinkosky et al. 2013b; Samsoondar et al. 2017; Morrow et al. 2022).

Further mechanistic investigation revealed that ETC-1002 reduced the acetylation of key sites within p300, an acetyltransferase known to regulate many cellular processes in response to changing nutritional status (Mariño et al. 2014; Dancy and Cole 2015; Pietrocola et al. 2018). When acetyl-CoA levels are high, p300 facilitates high nutrient availability signals by catalyzing the acetylation of several target proteins including those involved in autophagy (I. H. Lee and Finkel 2009). Autophagy in the liver is a critical hepatoprotective process that recycles dysfunctional or aggregated proteins and is known to be suppressed in NASH (Arab, Arrese, and Trauner 2018). Evidence to date suggests that the induction of autophagy through caloric restriction or through interventions that reduce acetyl-CoA may provide hepatoprotective effects and improve NASH (Madeo et al. 2014), however, pharmacological strategies that mimic these effects have not been described. In the present study, ETC-1002 reduced p300 acetylation, increased markers of autophagy, and this was associated with improved NAS and fibrosis. These findings support the concept that the suppression of ACLY can recapitulate some of the beneficial effects of caloric restriction and reverse molecular defects thought to be critical in NASH pathogenesis.

This study had several limitations. Most notable is that we did not assess acetyl-CoA levels to see whether they were changed with the treatments. We also used a chemically induced mouse model of NASH that produces pathology that may differ from disease in humans. Lastly, we did not conduct studies in hepatic stellate cells, the cell type in the liver which is vital for controlling fibrosis. Future studies investigating whether genetic inhibition of ACLY in hepatic stellate cells alters acetylation and whether this is important for inhibiting TGFβ-induced activation will be important.

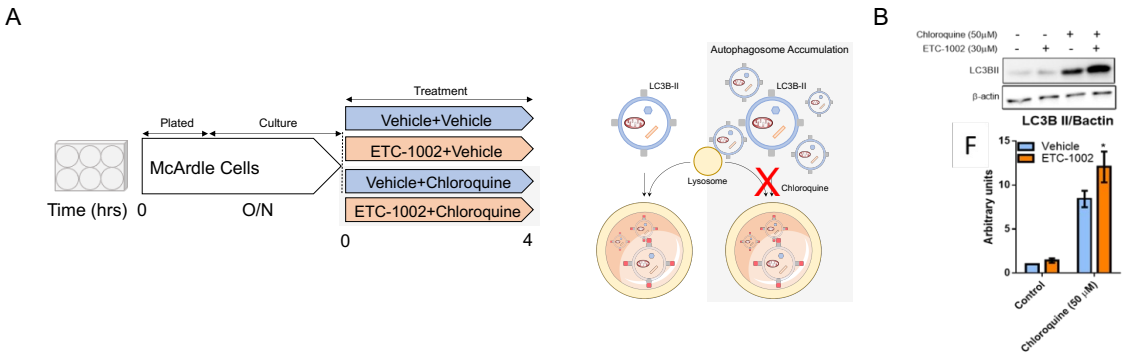

Figure 1. Bempedoic acid promotes autophagic flux in hepatocytes. (A) Schematic of immunoblotting experiments for bempedoic acid (ETC-1002)-induced autophagic flux in cultured McArdle hepatocytes with a graphical illustrating the use of chloroquine as a tool to halt autophagolysosomal fusion and degradation. Hepatocytes were treated with 30μM BemA or DMSO (0.1% v/v), with or without 50μM chloroquine, for 4 hours then rapidly lysed in cold cell lysis buffer. (B) Immunoblotting and densitometrical analysis assessing autophagic flux in response to ETC-1002. Statistical significance was determined was accepted at $P < 0.05$ and assessed by two-way ANOVA with Bonferroni multiple comparisons posthoc test. Data are expressed as mean ± SEM of 4 independent experiments.

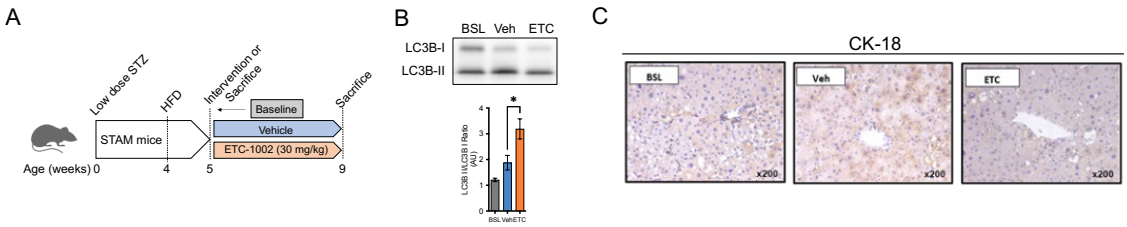

Figure 2. Bempedoic acid increases the LC3BII/I ratio and reduces CK-18 accumulation in STAM mice. (A) Schematic of experimental design. (B) Immunoblotting and densitometrical analysis assessing the LC3BII-to-I ratio in livers from STAM mice sacrificed at baseline or treated with Vehicle or ETC-1002 for another 4 weeks. (C) Representative photomicrographs of CK-18 fragment staining in livers from STAM mice sacrificed at baseline or treated with Vehicle or ETC-1002 for another 4 weeks. Statistical significance was determined was accepted at $P < 0.05$ and assessed by one-way ANOVA with Bonferroni multiple comparisons posthoc test. Data are expressed as mean ± SEM of N=7-8 per group.

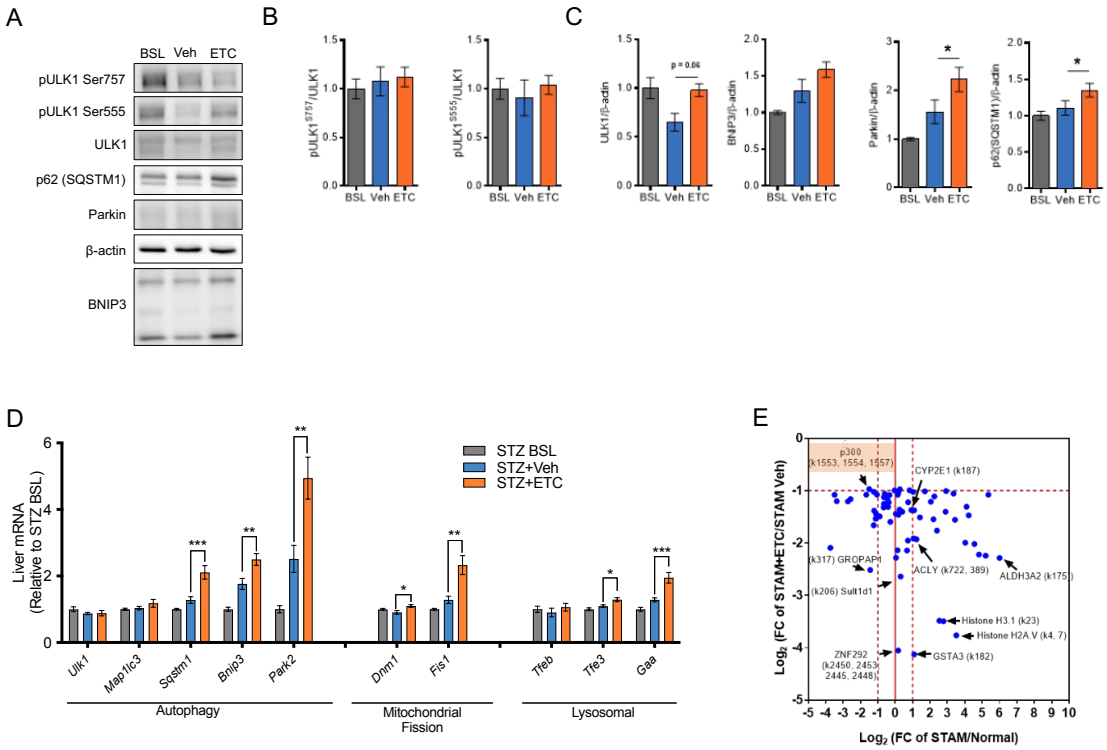

Figure 3. Bempedoic acid increases the expression of genes associated with autophagy and reduces acetylation of P300. (A-C) Immunoblotting and densitometrical analysis or (D) mRNA expression of autophagy/mitophagy markers in the livers from STAM mice sacrificed at baseline or treated with Vehicle or ETC-1002 for another 4 weeks. (E) Scatter plot of Log2 (FC STAM+ETC/STAM+Veh) versus Log2 (FC STAM /Normal) shown to have reduced acetylation by ETC-1002 treatment in the livers from STAM mice sacrificed at baseline or treated with Vehicle or ETC-1002 for another 2 weeks. Statistical significance was determined was accepted at $P < 0.05$ and assessed by one-way ANOVA with Bonferroni multiple comparisons posthoc test (A-D) or via Student's t-test (E). Data are expressed as mean ± SEM of N=7-8 per group, while proteomic analyses were performed on 2 samples each generated from 4 pooled mice.

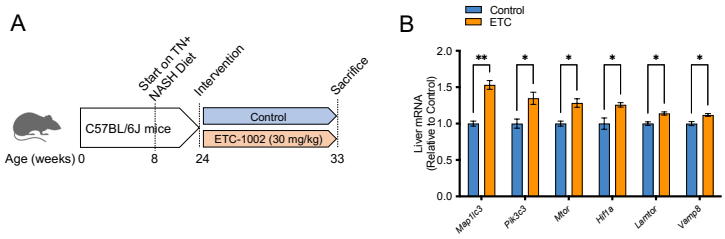

Figure 4. Bempedoic acid increases the expression of autophagy-related genes in a metabolic-associated NASH mouse model. (A) Schematic of experimental design. (B) Gene expression of autophagy-related markers from a NanoString Fibrosis panel in the livers of WT mice treated with or without ETC-1002 for 9 weeks. Statistical significance was determined was accepted at $P < 0.05$ and assessed by multiple t-tests with a Holm-Sidak adjustment posthoc test. Data are expressed as mean ± SEM of N=4-5 per group.

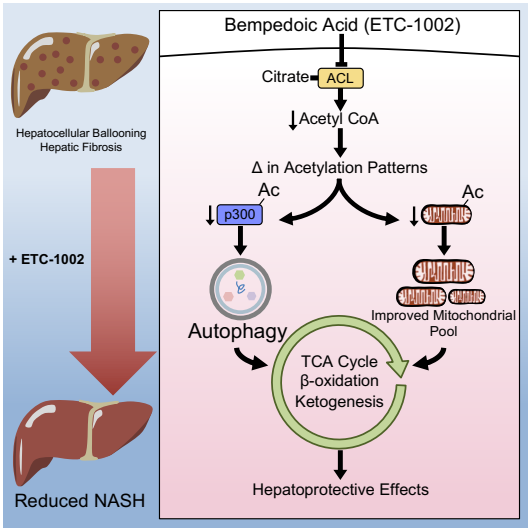

Figure 5: Bempedoic acid promotes autophagy in the liver of mice with NASH. Schematic illustrating the mechanism by which BemA promotes autophagy. Briefly, excess carbon is transported out of the mitochondria in the form of citrate. In the cytosol, citrate is cleaved by ACLY to form acetyl-CoA which promotes the acetylation and activation of p300, resulting in the suppression of autophagy. In the mitochondria, multiple enzymes required to maintain metabolic homeostasis are hyper-acetylated, resulting in altered cellular function. BemA inhibits ACLY which promotes the reversal of p300 acetylation, activation of autophagy, mitochondrial protein de-acetylation, and restoration of several metabolic processes that lead to hepatoprotection.

Materials and Methods

Autophagic flux

McArdle cells were maintained in DMEM supplemented with 10% FBS, 1% antibiotic-antimycotic. For experiments cells plated at a density of 2.5 x 105 cells per well in 6 well culture dishes. The following day, cells were washed with PBS and media was replaced. Cells were treated with 30μM ETC-1002 or DMSO (0.1% v/v), with or without 50μM chloroquine (BioShop), for 4 hours then rapidly lysed in cold cell lysis buffer (1M DTT, 200 mM Na3VO4, 20% triton-X, protease inhibitor cocktail tablet (Roche), 50 mM HEPES, 150 mM NaCl, 100 mM NaF, 10 mM Na pyrophosphate, 5 mM EDTA, 250 mM Sucrose) and snap frozen. Protein concentration was determined by BCA assay (Thermo Scientific). Proteins were resolved by molecular mass on SDS-PAGE gels and transferred to polyvinylidene difluoride membranes prior to blocking in 5% bovine serum albumin. Membranes were incubated overnight in primary antibodies β-actin (CST Cat # 5125, 1:1500) and LC3B (CST Cat # 2775 1:1000).

Lysate preparation and Immunobloting

Lysates were prepared in lysis buffer (50 mM HEPES pH 7.4, 150 mM NaCl, 100 mM NaF, 10 Na- pyrophosphate, 5 EDTA mM, 250 mM sucrose, and freshly added 1 mM DTT, and 1 mM Na-orthovanadate, 1% Triton X and Complete protease inhibitor cocktail (Roche)).

Immunoblotting was performed similarly to previously described[35]. 5 ug of protein for liver samples and 7.5 ug of protein for hepatocytes, made at 1 μg/μL and

determined via BCA assay, were prepared in 4x SDS sample buffer and boiled at 95 °C for 5 minutes with the exception of OXPHOS immunoblotting, which was kept at room temperature to avoid the degradation of complex IV (MTCO1). Antibodies used were from Cell Signaling Technology (listed below).

Antibodies

Provider	Protein	Product #
Cell Signaling Technology	β-actin	#4970
	LC3B	#2775
	SQSTM1/p62	#5114
	pULK1 Ser555	#5869
	pULK1 Ser757	#6888
	ULK1	#8054
	BNIP3	#3769
	Parkin	#2132
	anti-Rabbit IgG horseradish peroxidase (HRP)-linked	#7074

Briefly, membranes were blocked for 1 h in 10 mM Tris (pH 7.6), 137 mM NaCl, 0.1% (vol/vol) Tween 20 (TBST) containing 5% (wt/vol) BSA. Membranes were incubated in primary antibody (TBST containing 5% (wt/vol) BSA overnight at 4°C as recommended by the manufacturer. Detection was performed with HRP-conjugated secondary antibodies and enhanced chemiluminescence reagent (BioRad Clarity ECL solution). Phospho and total levels were determined

separately and were normalized first to loading control (β-actin or β-tubulin). Densitometry was then performed using Image J Software (NIH, MD, USA).

Animals

STAM mice: C57BL/6 mice (14-day-pregnant female) were obtained from Japan SLC, Inc. (Japan). All animals used in the study were housed and cared for in accordance with the Japanese Pharmacological Society Guidelines for Animal Use. The animals were maintained in a SPF facility under controlled conditions of temperature (23 ± 2°C), humidity (45 ± 10%), lighting (12-hour artificial light and dark cycles; light from 8:00 to 20:00) and air exchange. A high pressure was maintained in the experimental room to prevent contamination of the facility. The animals were housed in TPX cages (CLEA Japan) with a maximum of 4 mice per cage. Sterilized Paper-Clean (Japan SLC) was used for bedding and replaced once a week. Sterilized solid HFD was provided ad libitum, being placed in a metal lid on the top of the cage. Pure water was provided ad libitum from a water bottle equipped with a rubber stopper and a sipper tube. Water bottles were replaced once a week, cleaned, and sterilized in an autoclave and reused. Mice were identified by ear punch. Each cage was labeled with a specific identification code. The viability, clinical signs and behavior were monitored daily. Body weight was recorded before the treatment. Food consumption was measured twice weekly per cage during the treatment period. Mice were observed for significant clinical signs of toxicity, moribundity and mortality approximately 60 minutes after each administration. Mice in Group 2-5 were sacrificed 24 ± 2 hours after the last dose

at 9 weeks of age by exsanguination through direct cardiac puncture under ether isoflurane anesthesia (Pfizer Inc.). Each 3 mice in Group 6-9 were sacrificed at 1, 2, 6, 12 and 24 ± 2 hours after the last dose at 9 weeks of age to prepare the serum sample for shipment by exsanguination through direct cardiac puncture under ether isoflurane anesthesia.

ETC-1002 was administered orally in a volume of 10 mL/kg at 3 dose levels of 3, 10 and 30 mg/kg once daily. The individual dosage was calculated by body weight of the morning on the day. The test substances were administered from 9 to 11 am.

Mice were randomized and separated into five treatments groups (1 to 5), n =16/group. NASH baseline was determined at the initiation of ETC-1002 treatment in mice fed with HFD ad libitum without any treatment and sacrificed at 5 weeks of age. For groups 2 to 5, mice were orally administered vehicle [0.5% CMC (pH7-8)], or ETC-1002 (3, 10, or 30 mg kg in a volume of 10 mL/kg once daily from 5 to 9 weeks of age. Satellite groups were (n =15) were treated in parallel and used for ITT, OGTT and PK analyses.

Induction of NASH

NASH was induced in 120 male mice by a single subcutaneous injection of 200 µg streptozotocin (STZ, Sigma-Aldrich, USA) solution 2 days after birth and feeding with high fat diet (HFD, 57 kcal% fat, Cat# HFD32, CLEA Japan, Inc., Japan) after 4 weeks of age.

Plasma collection and biochemistry

For plasma biochemistry, blood was collected in polypropylene tubes with anticoagulant (Novo-Heparin, Mochida Pharmaceutical Co. Ltd., Japan) and centrifuged at 1,000 xg for 15 minutes at 4°C. The supernatant was collected and stored at -80°C until use. Plasma ALT were measured by FUJI DRI-CHEM 7000 (Fujifilm, Japan).

Test articles

ETC-1002 (bempedoic acid) was weighed and dissolved in vehicle [0.5% CMC (pH7-8)] according to the formulation instructions. This formulation was prepared every two weeks

Statistical Management and Control

At the end of study individual and group results were provided to Esperion with an accompanying summary table describing dates of individual procedures. Group means and standard deviations or standard errors were calculated for all measured outcomes. Comparisons of variables were determined by analysis of variance and post-hoc analysis. A probability level of 0.95 was used as the criterion of significance.

rt-qPCR

Briefly, RNA was diluted to a concentration of 2 µg/13.5 µL using RNase-free water, was mixed with DNTPs and random hexamers, incubated at 65 °C for 5 mins and cooled to 4 °C. SuperScript III, First Strand Buffer, and DTT were then mixed and incubated for 5 mins at 25 °C, 60 mins at 50 °C, 15 mins at 70 °C, and cooled to 4

°C (Invitrogen, CA, USA). cDNA was then diluted 1:20 using RNase-free water. Using an optimized mastermix including 1.7 µL RNase-free water, 1 µL 10X Buffer, 1 µL MgCl2 (25 mM), 1 µL dNTPs (2 mM), 0.05 µL Ampli-Taq Gold, and 0.25 µL TaqMan probe per reaction. RT-qPCR was performed with a 10 µL reaction (5 µL diluted cDNA, 5 µL mastermix) in a qPCR thermocycler (Corbett Rotor Gene 6000, MBI, QC, Canada). Within the thermocycler, the samples were incubated at 95 °C for 10 mins to activate the Ampli-Taq Gold, and were amplified with 40 cycles of 10 secs at 95 °C and 45 secs at 60 °C. Slopes were corrected for and thresholds were set at 0.05 using the Corbett Rotorgene software (Corbett Research, Australia). All PCR products and TaqMan probes were purchased from Invitrogen (CA, USA) and are listed below. Relative gene expression was calculated using the comparative Ct method, where values were normalized to a 5 housekeeping genes average, and expressed as relative to baseline (BSL) samples.

Primers

Provider	TaqMan Gene Expression	Product #
Invitrogen	Actb	Mm02619580_g1
	Ppia	Mm02342430_g1
	B2m	Mm00437762_m1
	Tbp	Mm00446971_m1
	Gapdh	Mm99999915_g1
	Map1lc3b	Mm00782868_sH
	P62 (Sqstm1)	Mm00448091_m1
	Bnip3	Mm01275600_g1
	Park2	Mm00450187_m1
	Ulk1	Mm00437238_m1
	Tfeb	Mm00448968_m1
	Tfe3	Mm01341186_m1
	Gaa	Mm00484581_m1
	Dnm1	Mm01342903_m1
	Fis1	Mm00481580_m1

Proteomics

Samples were analyzed using the PTMScan method as previously described (Rush, Stokes) Cellular extracts were prepared in urea lysis buffer, sonicated, centrifuged, reduced with DTT, and alkylated with iodoacetamide. 15mg total protein for each sample was digested with trypsin and purified over C18 columns for enrichment with the Acetyl-Lysine Motif Antibody (#13416). Enriched peptides were purified over C18 STAGE tips (Rappsilber). Enriched peptides were subjected to secondary digest with trypsin and second STAGE tip prior to LC-MS/MS analysis.

Replicate injections of each sample were run non-sequentially for each enrichment. Peptides were eluted using a 90-minute linear gradient of acetonitrile in 0.125% formic acid delivered at 280 nL/min. Tandem mass spectra were collected in a data-dependent manner with a Thermo Orbitrap Fusion™ Lumos™ Tribrid™ mass spectrometer using a top-twenty MS/MS method, a dynamic repeat count of one, and a repeat duration of 30 sec. Real time recalibration of mass error was performed using lock mass (Olsen) with a singly charged polysiloxane ion m/z = 371.101237.

MS/MS spectra were evaluated using SEQUEST and the Core platform from Harvard University (Eng, Huttlin, Villen). Files were searched against the SwissProt mus musculus FASTA database. A mass accuracy of +/-5 ppm was used for precursor ions and 0.02 Da for product ions. Enzyme specificity was limited to trypsin, with at least one tryptic (K- or R-containing) terminus required per peptide

and up to four mis-cleavages allowed. Cysteine carboxamidomethylation was specified as a static modification, oxidation of methionine and acetylation on lysine residues were allowed as variable modifications. Reverse decoy databases were included for all searches to estimate false discovery rates, and filtered using a 5% FDR in the Linear Discriminant module of Core. Peptides were also manually filtered using a -/+ 5ppm mass error range and presence of an acetylated lysine residue. All quantitative results were generated using Skyline (MacLean) to extract the integrated peak area of the corresponding peptide assignments. Accuracy of quantitative data was ensured by manual review in Skyline or in the ion chromatogram files.

Metabolic-associated NASH mouse model

In vivo experiments were approved by the McMaster University Animal Ethics Committee (#21-01-4) and conducted under the Canadian guidelines for animal research. Male mice with a C57BL/6J background were purchased from Jackson Laboratories at 6-7 weeks of age. Mice were housed 3-5 per cage in a controlled environment; 12-hour light/dark cycle, given food and water *ad libitum*, and enrichment provided. At 8 weeks of age, mice were moved into specific-pathogen free (SPF) microisolators in a room maintained at ~29 ºC and fed a high-fat, high-fructose diet (NASH Diet; ND; 40% fat from mostly palm, 20% fructose, 0.02% cholesterol). Due to fructose being supplemented in the diet, diet was changed every few weeks. 16 weeks later, mice were grouped by matching body weight and adiposity randomly and placed on respective interventional arms. Adiposity

was assessed based on time-domain NMR using a Bruker Minispec LF90II. Bempedoic acid-treated mice had the drug supplemented in the diet at a dose of 30 mg/kg. After 9 weeks of treatment, all mice were sacrificed in the fed state between 0900 and 1100 hrs, using a ketamine/xylazine mixture to sedate mice before collecting blood via cardiac puncture. Mice were presumed dead by exsanguination and cervical dislocation was performed as a secondary measure.

NanoString Gene Expression Analysis

For NanoString analysis, 4-5 RNA samples per group were inspected by a BioAnalyzer quality control test. The McMaster Genomics Facility ran an nCounter Fibrosis v2 Panel (NanoString Technologies) containing 760 target genes. Gene expression data was normalized using NanoString Technologies' nSolver 4.0 software (version 4.0.70) and the embedded PLAGE algorithm. Linear expression data was taken for genes associated with the autophagy pathway on the software and were normalized to Control. Multiple t-tests were performed with an adjusted p value of <0.05 with the Bonferroni adjustment being deemed significant.

CHAPTER FOUR

COMBINATION OF BEMPEDOIC ACID WITH A GLP-1R AGONIST IMPARTS ADDITIVE BENEFITS TO TREAT METABOLIC-ASSOCIATED STEATOHEPATITIS AND HEPATIC FIBROSIS IN MICE

Prepared for publication, 2023

Eric M. Desjardins, Jianhan Wu, Declan C.T. Lavoie, Elham Ahmadi, Marisa R. Morrow, Logan K. Townsend, Dongdong Wang, Evangelia E. Tsakiridis, Battsetseg Batchuluun, Russta Fayyazi, Jacek M. Kwiecien, Theodoros Tsakiridis, James S.V. Lally, Guillaume Paré, Stephen L. Pinkosky, and Gregory R. Steinberg

NASH and associated fibrosis are multifaceted pathologies that currently have no approved pharmacotherapies. To date, monotherapies have struggled to reach primary endpoint goals or cannot demonstrate enough benefit to outweigh their risks. Considering most people with NASH have an associated metabolic comorbidity, with the highest percentages being 69% hyperlipidemia and 51% obesity, it is likely that combinatorial therapies will be needed to target diverse contributors to the disease. In this chapter, we explored the combination of two approved treatments that have distinct molecular targets to not only treat NASH, but associated comorbidities with NAFLD. The GLP-1R agonist liraglutide is approved for the treatment of obesity and type 2 diabetes, and has shown positive results with regards to NASH resolution within the clinic, however, has not been able to simultaneously improve fibrosis stage. Bempedoic acid, which is known as an ACLY inhibitor, is approved to reduce LDL-cholesterol in patients with hypercholesterolemia or established atherosclerosis and has recently been shown to reduce NASH and fibrosis in mice. We showed that combining bempedoic acid with the GLP-1R agonist liraglutide resulted in favourable improvements in liver steatosis, inflammation, hepatocellular ballooning, and hepatic fibrosis without increasing serum triglycerides. We also show improvements in some serum inflammatory markers. With directed transcriptomic analysis, we found that combination therapy resulted in an additive downregulation in pathways associated with NASH, had reductions in genes that have been identified as prognostically significant in human NASH, and a predictive gene signature towards improving fibrosis stage. Overall, these findings provide proof of concept data suggesting the combination of bempedoic acid and a GLP-1R agonist could have complementary actions which would result in achieving NASH resolution with improvement in fibrosis stage.

E.M.D. was involved in all experiments. J.W. and R.F. performed bioinformatic analyses, and E.A. scored liver histopathology.

Combination of bempedoic acid with a GLP-1R agonist imparts additive benefits to treat metabolic-associated steatohepatitis and hepatic fibrosis in mice.

Eric M. Desjardins[1,2], Jianhan Wu[1,2], Declan C.T. Lavoie[1,2], Elham Ahmadi[1,2], Marisa R. Morrow[1,2], Logan K. Townsend[1,2], Dongdong Wang[1,2], Evangelia E. Tsakiridis[1,2], Battsetseg Batchuluun[1,2], Russta Fayyazi[1,2], Jacek M. Kwiecien[3], Theodoros Tsakiridis[1,4], James S.V. Lally[1,2], Guillaume Paré[1,5,6], Stephen L. Pinkosky[7], and Gregory R. Steinberg[1,2,8*]

[1]Centre for Metabolism Obesity and Diabetes Research, McMaster University, Hamilton, ON L8S 4L8, Canada
[2]Division of Endocrinology and Metabolism, Department of Medicine, McMaster University, Hamilton, ON L8S 4L8, Canada
[3]Department of Pathology, McMaster University, Hamilton, ON L8S 4L8, Canada
[4]Department of Oncology, McMaster University, Hamilton, ON L8S 4L8, Canada
[5]Population Health Research Institute, McMaster University, Hamilton, ON L8L 2X2, Canada
[6]Thrombosis and Atherosclerosis Research Institute, McMaster University, Hamilton, ON L8L 2X2, Canada
[7]Esperion Therapeutics, Inc., Ann Arbor, USA
[8]Department of Biochemistry and Biomedical Sciences, McMaster University, Hamilton, Canada

*Correspondence to Gregory R. Steinberg
Centre for Metabolism, Obesity and Diabetes Research, McMaster University, 1280 Main St. West, Hamilton, Ontario, L8N 3Z5, Canada, Tel: 905.525.9140 ext. 21691
Email: gsteinberg@mcmaster.ca

Summary

Increased liver *de novo* lipogenesis is a hallmark of nonalcoholic fatty liver disease (NAFLD) that is characterized by increases in the activity of acetyl-CoA carboxylase (ACC) and ATP citrate lyase (ACLY). Glucagon like peptide-1 receptor (GLP-1R) agonists lower body mass, improve glucose homeostasis, and are being pursued for the treatment of nonalcoholic steatohepatitis (NASH). Recent clinical evidence demonstrates GLP-1R agonism resolves NASH without improving fibrosis stage, while preclinical evidence indicates pharmacological inhibition of ACLY reduces liver fibrosis in mice via direct effects on hepatic stellate cells. Here, we find that combining an inhibitor of liver ACLY, bempedoic acid, and the GLP-1R agonist liraglutide results in favorable improvements in liver steatosis, inflammation, hepatocellular ballooning, and hepatic fibrosis without increases in serum triglycerides in a mouse model of NASH. Liver RNA analyses revealed additive downregulation of pathways that are predictive of NASH resolution, reductions in the expression of prognostically significant genes compared to clinical NASH samples, and a predicted gene signature profile that supports fibrosis resolution. These findings support further investigation and development of this combinatorial therapy to treat obesity, insulin resistance, hypercholesterolemia, steatohepatitis, and fibrosis in people with NASH.

Keywords: NAFLD; NASH; Hepatic Fibrosis; ACLY; Bempedoic Acid; GLP-1R agonist; Liraglutide; Combination Treatment; Mouse Model

Introduction

The rising prevalence of both adult and childhood nonalcoholic fatty liver disease (NAFLD) poses immense burden on patients' health-related quality of life, healthcare costs, and economic losses (Lazarus et al. 2021). The progressive form of NAFLD – nonalcoholic steatohepatitis (NASH) – is typically characterized by liver steatosis, hepatocellular ballooning, and lobular inflammation with or without perisinusoidal fibrosis and can manifest itself to cirrhosis, liver failure, cancer, and death (Kleiner et al. 2005; Friedman et al. 2018). Currently, there are no approved therapies for the treatment of NASH. To date, monotherapy strategies in human trials have struggled to reach primary endpoint goals or have been called into question as to whether benefit outweighs risk (C. W. Kim et al. 2017b). Bearing in mind that almost half of the people with NAFLD also live with an associated metabolic comorbidity (69% hyperlipidemia, 51% obesity, 39% hypertension, 22% type 2 diabetes, and 42% metabolic syndrome) (Z. Younossi et al. 2018), it is reasonable to suspect that combinatorial therapies which target different aspects of the pathophysiology of NASH and associated comorbidities could lead not only to improved efficacy in treating NASH, but also secondary measures and tolerability which would sway the risk-benefit ratio (Dufour, Caussy, and Loomba 2020; Baggio and Drucker 2021).

Multiple glucagon-like peptide-1 receptor (GLP-1R) agonists have been and are currently being studied in the clinic for the treatment of NAFLD (Newsome et al. 2021; Petit et al. 2017; Armstrong et al. 2016) (NCT04166773). GLP-1 is an incretin hormone that is secreted in the postprandial phase by intestinal L cells to control blood glucose, satiety, and gastrointestinal motility (Baggio and Drucker 2021). Liraglutide is a long-acting GLP-1R agonist that is approved for the treatment of both type 2 diabetes and obesity (Drucker, Habener, and Holst 2017). In a multicentre, randomized, placebo-controlled trial, liraglutide treatment resulted in a statistically significant percentage of NASH resolution (39%) versus placebo (9%) (Armstrong et al. 2016). More recently, semaglutide, a long-acting GLP-1R agonist similar to liraglutide but with more pronounced metabolic effects, showed a higher percentage of NASH resolution (59% 0.4 mg dose) versus placebo (17%) in a 72-week double-blinded phase 2 trial with biopsy-confirmed NASH and liver fibrosis of stage F1-3 (Newsome et al. 2021). Although still not clear, liraglutide appears to elicit its effects on NAFLD/NASH primarily through reductions in appetite and improvements in glucose homeostasis and insulin resistance which indirectly lead to improvements in inflammation and steatosis. More recent evidence highlights that semaglutide may exert some of its anti-inflammatory effects on the liver through a subset of liver-localized γδ T cells and these cells are also important for the cardioprotective actions of liraglutide (B. McLean et al. 2021; B. A. McLean et al. 2022). Altogether, observations that the GLP-1R is not expressed in hepatocytes, Kupffer cells, or hepatic stellate cells suggests that the

effects of the GLP-1R agonists are likely largely mediated through indirect mechanisms (reviewed thoroughly in (Yabut and Drucker 2022)). However, even with some effect on NASH resolution, to date, GLP-1R agonists have not demonstrated efficacy at improving fibrosis severity in patients (Armstrong et al. 2016; Newsome et al. 2021), potentially because they do not act directly on the liver and the key cells driving fibrosis, hepatic stellate cells.

Increases in liver *de novo* lipogenesis (DNL) are a hallmark of patients with NAFLD (Lambert et al. 2014; Softic, Cohen, and Kahn 2016; G. I. Smith et al. 2020). Two critical enzymes controlling flux through the DNL pathway are acetyl-CoA carboxylase (ACC) and ATP citrate lyase (ACLY) (reviewed in (Batchuluun, Pinkosky, and Steinberg 2022)). Several ACC inhibitors have been developed and have been tested in clinical populations where they are found to dramatically reduce steatosis, while having modest effects on markers of fibrosis. However, an on-target effect of ACC inhibition is an increase in serum triglycerides which elevates the risk of pancreatitis and cardiovascular disease. This has led to combination trials with inhibitors of DGAT and GLP-1R agonists which have elicited encouraging results, however, to date, phase 3 studies have not been completed.

Bempedoic acid is a small molecule ATP citrate lyase (ACLY) inhibitor that reduces risk of major adverse cardiovascular events in statin-intolerant patients and has been approved by the U.S. Food and Drug Administration (FDA) and European Commission (EC) to reduce low-density lipoprotein cholesterol (LDL-C) in adults with heterozygous familial hypercholesterolemia (HeFH) or established

atherosclerotic cardiovascular disease (Nissen et al. 2023; Keaney 2023; Alexander 2023; Bays et al. 2020; Ray et al. 2019; Pinkosky et al. 2013a). Bempedoic acid is a prodrug that is converted to its active moiety, bempedoyl-CoA, in the liver by the very-long-chain acyl-CoA synthetase 1 (ASCVL1) (Pinkosky et al. 2016). This liver-targeted conversion is important to minimize myotoxicity which is common with the use of statins (Pinkosky et al. 2016). We have recently established a mouse model of NASH that has very similar metabolic (i.e. obesity, insulin resistance), histological, and transcriptional characteristics to people with advanced NASH. The model is induced by housing male mice at thermoneutrality (~29 ºC) and feeding a high-fat diet supplemented with fructose and physiological concentrations of cholesterol for 16 weeks before initiating treatment (Morrow et al. 2022). Using this model, we found that bempedoic acid dramatically reduced liver steatosis, hepatocellular ballooning, lobular inflammation and also fibrosis (Morrow et al. 2022). Additional experiments in hepatic stellate cells from mice and humans demonstrated that bempedoic acid suppressed lipogenesis and blocked TGFβ-induced proliferation and activation (Morrow et al. 2022). Importantly, bempedoic acid also exerted pronounced anti-fibrotic effects independently of reductions in steatosis in the STAM mouse model of NASH, which does not have obesity and insulin resistance (Morrow et al. 2022). Taken together, these data suggest that the beneficial effects of bempedoic acid on NASH and fibrosis are likely to be completely distinct from the primary pathways targeted by liraglutide; suggesting there may be additive effects combining the two therapeutics.

Considering the distinct mechanisms by which liraglutide and bempedoic acid reduce NAFLD, the purpose of this study was to evaluate whether the addition of bempedoic acid to liraglutide would elicit added benefits to treating NASH and hepatic fibrosis in a physiologically relevant mouse model that replicates many of the metabolic, histological, and transcriptional characteristics of advanced NASH patients.

Results

Combination of liraglutide and bempedoic acid reduces body weight, adiposity, glucose intolerance, insulin resistance, and serum cholesterol

As we have previously described, housing C57BL6J mice at thermoneutrality and feeding a diet high-in fat and fructose leads to metabolic, pathological and transcriptional characteristics similar to human NASH (Morrow et al. 2022). Using this diet and housing paradigm, after 16 weeks, mice were assigned to five interventional arms by matching body weight and adiposity so there were no differences at the start of the treatment period.

Consistent with our recent study (Morrow et al. 2022), bempedoic acid (BemA) was mixed with the diet at a concentration of 10 mg/kg and its effects on the mice were compared to mice that received the same diet minus BemA (Control). BemA did not alter body weight, adiposity, glucose tolerance, insulin sensitivity, pyruvate tolerance (a measure of hepatic gluconeogenesis), fasting serum insulin or triglyceride levels, but did reduce serum cholesterol (Supplementary Figure 1A-H). Despite similar adiposity and glucose homeostasis,

BemA reduced liver fat percentage, pathological scoring of liver steatosis, hepatocellular ballooning, and the NAFLD activity composite score (Supplementary Figure 2A-G). Importantly, BemA also reduced percent fibrosis area assessed using picrosirius red (PSR) (Supplementary Figure 2H). These data indicate that, consistent with our previous study (Morrow et al. 2022) using thermoneutral housing but a shorter duration of dietary intervention before initiating treatment (10 vs. 16 wks in the current study), BemA reduces liver steatosis, ballooning and fibrosis independently of changes in body mass or adiposity.

Modest reductions in body mass can completely resolve NASH in mouse models (Xuelian Xiong et al. 2019). Treatment of mice with GLP-1R agonists such as liraglutide (Lira) dose-dependently suppress appetite and body mass and can, at higher doses, reduce body mass by greater than 25% over just 14 days of treatment after 8 weeks of a high-fat diet (Park, Oh, and Kim 2022). Human clinical trials with Lira in people with NASH elicit 5-10% weight loss (Armstrong et al. 2016). Therefore, to enhance the potential translatability of Lira treatment in mice to humans with NASH, we utilized a submaximal dose of Lira with the aim to elicit similar reductions in body mass/adiposity to that observed in participants within clinical trials. Consistent with this aim, treatment of mice with Lira compared to mice injected at the same frequency with vehicle control, reduced body mass by 6% at 9 weeks of treatment and this effect on body mass was not altered by the addition of BemA (Lira+BemA) (Figure 1A and B). Compared to vehicle control mice, Lira and Lira+BemA improved glucose tolerance (Figure 1C) and insulin

sensitivity (Figure 1D) but did not alter pyruvate tolerance (Figure 1E). Lira lowered fasting serum insulin (Figure 1F) and cholesterol levels (Figure 1G), and these effects were also observed in mice treated with Lira+BemA. Serum triglycerides (Figure 1H) were unchanged in either Lira or Lira+BemA combination groups.

Combination of liraglutide and bempedoic acid results in additive benefits in liver steatosis, ballooning, and fibrosis

In comparison to the vehicle group, Lira and Lira+BemA reduced percent liver fat by 36 and 47%, respectively (Figure 2A), and triglycerides by 69 and 81%, respectively (Figure 2B). Consistent with these observations, steatosis scores from H&E sections were reduced with Lira (63%) and Lira+BemA treatments (74%) (Figure 2C&D). Hepatocellular ballooning scores were reduced with Lira by 56% and Lira+BemA by 94% (Figure 2C&E). Lira and Lira+BemA reduced lobular inflammation score to a similar degree (~50%) (Figure 2C&F). In sum, the NAFLD activity score (NAS) was reduced by 56% by Lira and by 75% by Lira+BemA (NAS: Figure 2G). Importantly, Lira and Lira+BemA treatment groups reduced fibrosis area assessed using PSR (40 and 44%, respectively) (Figure 2C & H) and had fewer (Lira 1 of 9) or no (Lira+BemA 0 of 9) moderate zone 3, perisinusoidal fibrosis (1C) compared to vehicle-treated mice (4 of 8) (Figure 2C&I).

Serum markers of liver inflammation/damage including alanine transaminase (ALT), aspartate aminotransferase (AST), serum amyloid A (SAA), the C-X-C motif chemokine ligand 10 (CXCL10), c-reactive protein (CRP) and secreted phospholipase A2 (sPLA2) were measured. BemA reduced ALT, AST,

SAA, CXCL10, CRP (Ridker et al. 2023), and sPLA2 compared to Control, while Lira significantly reduced SAA and sPLA2 versus Vehicle. Combination of Lira+BemA reduced SAA similarly to Lira alone, while it resulted in a significant reduction in CRP in comparison to Vehicle. Finally, Lira+BemA significantly reduced sPLA2 in comparison to both Vehicle and Lira groups (Table 1).

Collectively, Lira+BemA led to greater percent reductions and lower p-values for steatosis, ballooning, NAS, PSR and sPLA2 compared to Lira monotherapy. And although not statistically different compared to Lira monotherapy, these data suggest BemA may have additive effects towards improving liver pathology.

Targeted gene expression profiling identifies additive downregulation of fibrosis-related molecular pathways that are predictive of NASH resolution

To determine the transcriptional differences between our treatment cohorts, we examined the expression of 760 genes implicated in 49 fibrosis related pathways using the nCounter Fibrosis v2 Panel. Differential expression analysis comparing liraglutide, bempedoic acid and combination treatment to diseased control yielded 249, 132, and 263 genes respectively (Supplemental Figure 3A, Supplemental Table 3). Combination treatment resulted in the greatest number of downregulated genes, significantly reducing the expression of 172 genes compared to 97 and 86 by Lira and BemA alone. Of these, 56 genes were uniquely altered by combination treatment,113 genes overlapped between all treatment cohorts and 3 genes were upregulated by Lira but downregulated in the

combination cohort (Supplemental Figure 3B, Supplemental Table 4). Conversely, 8 genes were uniquely upregulated by combination treatment (Supplemental Figure 3C). Over-representation analysis of the uniquely downregulated and overlapping genes, which we defined as additive if the effect size was largest in the combination treatment cohort, identified seven disease processes of interest related to inflammation, fibrosis, and wound healing (Supplemental Figure 3D, Supplementary Table 5). Next, we utilized a more comprehensive approach to identify gene sets altered by combination treatment by using all genes in the nCounter panel (Supplemental Figure 4A) (Tomfohr, Lu, and Kepler 2005). Combination treatment led to reductions across 17 pathways with hierarchical clustering identifying reductions in overarching disease processes related to fibrosis (e.g., collagen biosynthesis & modification, myofibroblast regulation), inflammation (e.g., chemokine signaling, cytokine signaling) and wound healing (e.g., phagocytic cell function, angiogenesis) which was consistent with pathway annotation analysis (Figure 3A).

To assess gene set association with phenotype observations, we regressed disease outcome measurements on the first principal component (PC1) of the 17 gene sets (Figure 3B) most affected by combination treatment relative to monotherapy. This demonstrated a significant predictive relationship between PC1 increment and hepatic steatosis, inflammation, fibrosis, adiposity, and NAS resolution (Figure 3C).

Hepatic stellate cells are critical for driving liver fibrosis and therefore we explored the expression of key markers implicated in NASH progression (Payen et al. 2021). Consistently, markers of activated stellate cells (*Col1a1, Col1a2, Col3a1, Lox, Timp1)* were significantly reduced in the Lira+BemA treatment groups to a greater extent than monotherapies of Lira or BemA (Figure 3D). Interestingly, BemA appeared to counteract Lira-induced upregulation of TGFβ effectors, including *Smad3,* a transcription factor critical for upregulating fibrotic pathways in NASH (Supplementary Figure 4B). Moreover, combination therapy generally reduced the expression of several chemokines implicated in NASH progression greater than Lira or BemA treatment alone (Figure 3E). Collectively, these data indicate that combination therapy with Lira+BemA induces an anti-fibrotic and anti-inflammatory gene-expression profile that is predictive of reduced liver pathology (steatosis, ballooning, and fibrosis).

Combination treatment induces a prognostically favorable gene expression profile that most closely resembles those from healthy human liver biopsies

In humans a 25-gene signature has been established to be predictive of NASH severity (Govaere et al. 2020). Therefore, to contextualize the clinical significance of our experimental therapies, we performed an integrative analysis combining the expression data of 22 orthologous genes derived from our treatment cohorts with the expression data derived from 216 NAFLD/NASH patients. Combination treatment significantly downregulated the expression of 13 genes in this prognostic signature. Hierarchical clustering using Pearson correlation reveals

four clusters with differential compositions of healthy individuals, patients with pre-fibrotic (NAFLD, F0-F1) or fibrotic (F2-F4) disease and our experimental cohorts (Figure 4A). Cluster II exhibits the most clinically benign phenotype. 80% of healthy individuals in the patient derived dataset are represented in this cluster compared to 7.55%, 1.85% and 0% of patients with F2, F3 and F4 stages of disease (Figure 4B). We find 4 out of 6 of our combination treatment samples colocalized in this cluster while monotherapy treatment samples are mostly grouped in clusters I and II which exhibit more advanced disease. Using PCA, we show the progressive resolution of NASH in human patients on PC1 (Figure 4C). Mapping our control, monotherapy, and combination treatment cohorts with human NASH disease stages further supports the increased transcriptional similarity between healthy individuals and combination treatment samples beyond what can be achieved using Lira and BemA alone.

Classification of patients into disease subtypes based on their expression of pre-defined gene signatures can inform risk stratification and elucidate molecular characteristics between disease subtypes. Recent studies have similarly utilized treatment specific gene signatures to classify patients exhibiting similar or dissimilar gene expression profiles into treatment responsive or non-responsive subtypes (Torrens et al. 2021; Geeleher, Cox, and Huang 2014). This analysis may provide preliminary evidence informing clinical translation and elucidate molecular differences driving therapeutic response in patients. As such, we derived a combination treatment specific gene signature by filtering for genes that were

differentially regulated by combination treatment both when compared to control and monotherapy (Supplemental Figure 5A).

To determine the prognostic significance of this gene signature, we first compared its predictive performance using multivariate logistic regression to the reference gene signature derived by Govaere et al in the human NAFLD/NASH cohort. For the prediction of fibrosis stage > 2, the treatment signature achieved an area under receiver operating curve (AUROC) score of 0.899 which approximates the score of 0.922 achieved by the reference signature (Figure 4D). Further variable selection using elastic net regularization did not improve prediction accuracy (AUROC = 0.893). Among the signature genes, *AXL, SLC2A2, CYBB, DOCK2, C3AR1, CYFIP1* and *LEPR* were significantly associated with advanced fibrosis in the multivariate model. Subsequently, we utilized Nearest Template Prediction to classify patients based on their expression similarity to our treatment signature (Hoshida 2010). Patients classified as similar predominantly exhibited pre-fibrotic stages of disease (NAFLD and F0-F1) whereas those classified as dissimilar were enriched for fibrotic stages (F2 – F4) (Supplemental Figure 5C). Single sample GSEA (ssGSEA) of hallmark gene sets and liver cell types reveal a favorable transcriptional profile for NASH resolution. Patients in the similar class exhibit significant downregulation of fibrosis, inflammation, and cellular damage related gene sets while pathways related to fatty acid metabolism, oxidative phosphorylation and DNA repair are significantly upregulated (Supplemental Figure 5D). Correspondingly, liver cell type analysis based on markers derived

from the human liver cell atlas (Aizarani et al. 2019) reveals significant downregulation of all non-parenchymal liver cell types including hepatic stellate cells, liver sinusoidal endothelial cells and, conversely, upregulation of hepatocytes (Supplemental Figure 5B). Overall, the gene expression pattern identified in patients who exhibit a similar gene signature profile as combination treatment supports fibrosis, steatosis, and inflammation resolution among NAFLD/NASH patients.

Discussion

In this study, we combined two approved treatments that have distinct molecular targets, have excellent safety profiles, and treat separate comorbidities associated with NAFLD. Lira caused reductions in adiposity, glucose intolerance, and insulin resistance, while BemA treatment resulted in reductions in total cholesterol consistent with both drugs' primary approved indication; type 2 diabetes/obesity and cardiovascular disease, respectively. With respect to liver pathology, both BemA and Lira monotherapies lowered steatosis, ballooning and fibrosis to a similar degree and we found that when combined there were greater percent reductions in hepatocellular ballooning and fibrosis.

As *de novo* lipogenesis (DNL) is a major player in the accumulation of intrahepatic triglycerides in NAFLD (Loomba, Friedman, and Shulman 2021; Donnelly et al. 2005), targeting ACLY – an enzyme upstream from acetyl-CoA carboxylase (ACC) – with the inhibitor BemA presents an opportunity to reduce fatty acid and cholesterol synthesis within the liver (Morrow et al. 2022). In the

current study, we found significant reductions in liver fat percentage, triglycerides and steatosis scores with both BemA and Lira treatments on their own. With their combination, more profound reductions in liver fat percentage and triglycerides were found. Importantly, these changes did not result in elevated serum triglycerides.

As distinguishable by its suffix, the prominent feature differentiating steatohepatitis from simple liver steatosis is the development of inflammation. Our transcriptome analysis indicates a unique cluster with which the combination of both BemA and Lira reduced markers of inflammation as characterized by cytokine and chemokine signalling, the adenosine pathway, TLR and NF-κB signalling, phagocytic cell function, neutrophil degranulation, and interferon signalling. Furthermore, the reductions in inflammatory markers within the liver were more broadly apparent in the measurements of systemic markers of inflammation in serum as shown by large reductions in CRP and SAA.

Perhaps most importantly, in this study, we found that combining BemA with Lira resulted in reductions in fibrosis. These pathological findings were supported by transcriptome data indicating combination therapy reduced extracellular matrix synthesis, epithelial-to-mesenchymal transition, myofibroblast regulation, focal adhesion kinase, and collagen biosynthesis and modification. This is of great importance as, to date, neither Lira or semaglutide have shown efficacy at reducing fibrosis stage in patients with NASH – although results from the ESSENCE Phase III trial (NCT04822181) are to follow (Newsome et al. 2021; Armstrong et al. 2016).

Furthermore, our analyses revealed that a potentially unique effect of BemA may be due to its effects on countering Lira-induced increases in the TGF-β activated transcription factor *Smad3,* which is a critical driver of fibrosis (Schwabe, Tabas, and Pajvani 2020). As the GLP-1R is not expressed on hepatic stellate cells (Yabut and Drucker 2022), and BemA treatment attenuates TGF-β-mediated activation of both murine and human hepatic stellate cells *in vitro* (Morrow et al. 2022)*,* this direct effect on hepatic stellate cells may be important for reducing fibrosis. However, further studies evaluating the effects of genetically inhibiting ACLY in hepatic stellate cells will be required to fully interrogate this hypothesis.

Given the complexity of NASH pathophysiology, targeting multiple distinct pathways may be required to confer clinical improvements not only in liver steatosis, inflammation, and fibrosis, but also associated comorbidities which are more likely to cause death to patients living with the disease (Z. Younossi et al. 2018). There are several other rationales for the use of combination therapies to treat NASH, as combining two or more drugs could increase response rates, maximize response to treatment, reduce side effects, and address loss of effects over time (Dufour, Caussy, and Loomba 2020). And although combinatorial therapies may increase the difficulty of designing trials and present more challenges in patient recruitment/retainment, these efforts may improve the benefit:risk ratio compared to monotherapies.

Our data demonstrate a benefit of combining the ACLY inhibitor BemA and the GLP-1R agonist Lira, however, this study has several limitations. Our

experimental design and analyses were not able to detect statistically significant differences in pathological scoring between Lira and Lira+BemA, although, the percent reduction in most parameters was consistently greater with the combination treatment regime. This finding is similar to other preclinical studies that have also tested combination therapies with GLP-1R agonists in mice (Boland et al. 2020). The dramatic effects of Lira to reduce liver steatosis make it difficult to observe further improvements given that liver steatosis is comparable to that observed in control chow-fed mice (Morrow et al. 2022). Lastly, we utilized a highly sensitive and direct method to assess mRNA signatures related to fibrosis using NanoString technology, however, there may be additional mechanistic insights to uncover utilizing non-biased high-throughput -omics technologies such as single cell RNA-seq and metabolomics.

In summary, the current study demonstrates that combining BemA with Lira leads to greater percent reductions in liver pathology compared to monotherapy in a mouse model of metabolic-associated NASH and fibrosis. These findings support further investigation and potential development of this combinatorial therapy to treat obesity, insulin resistance, hypercholesterolemia, steatohepatitis, and fibrosis in people with NASH.

Acknowledgements

This research was supported by grants awarded to G.R.S. from the Canadian Institutes of Health Research (201709FDN-CEBA-116200), Diabetes Canada (DI-5-17-5302), Esperion Therapeutics, a Tier 1 Canada Research Chair and a J. Bruce Duncan Endowed Chair in Metabolic Diseases. E.M.D. and J.W. are Canada Vanier scholars. L.K.T. and B.B. are funded by Canadian Institutes of Health Research postdoctoral fellowships. The authors would like to thank Dr. Thomas J. Hawke for access to the upright microscope and Dr. Jonathan D. Schertzer for access to and Dr. Nicole G. Barra for calibration of the Bio-Plex instrument.

Author Contributions

G.R.S. and S.L.P. developed the original concept of the study. E.M.D., D.C.T.L., M.R.M., E.E.T., D.W., L.K.T., and B.B. performed the experiments. E.A. and J.M.K. completed blinded assessment of liver pathology scoring. J.W. performed transcriptome analysis. J.S.V.L. provided intellectual contributions. E.M.D. and J.W. analyzed data. E.M.D. and G.R.S. wrote the manuscript. All authors provided comments and approved of the final manuscript.

Competing Interests

G.R.S. has received research funding from Esperion Therapeutics, Novo Nordisk, Poxel Pharmaceuticals and Espervita Therapeutics; honoraria and/or consulting fees from Astra Zeneca, Eli-Lilly, Esperion Therapeutics, Poxel Therapeutics, and Merck; is a founder and shareholder of Espervita Therapeutics. S.L.P. is employed by Esperion Therapeutics.

STAR Methods

Animals

All *in vivo* experiments were approved by the McMaster University Animal Ethics Committee (#21-01-4) and conducted under the Canadian guidelines for animal research. Male mice with a C57BL/6J background were purchased from Jackson Laboratories at 6-7 weeks of age. Mice were housed 3-5 per cage in a controlled environment; 12-hour light/dark cycle, given food and water *ad libitum*, and enrichment provided. At 8 weeks of age, mice were moved into specific-pathogen free (SPF) microisolators in a room maintained at ~29 ºC and fed a high-fat, high-fructose diet (NASH Diet; ND; 40% fat from mostly palm, 20% fructose, 0.02% cholesterol). Due to fructose being supplemented in the diet, diet was changed every few weeks. 16 weeks later, mice were grouped by matching body weight and adiposity randomly and placed on respective interventional arms. Adiposity was assessed based on time-domain NMR using a Bruker Minispec LF90II. Control mice were continued on diet alone, vehicle-treated mice (Vehicle) were given subcutaneous saline injections every second day 1-2 hrs before the dark cycle, bempedoic acid-treated mice (BemA) had the drug supplemented in the diet at a dose of 10 mg/kg, liraglutide-treated mice (Lira) were given subcutaneous injections of Victoza diluted in saline to a dose of 70 µg/kg every second day 1-2 hrs before the dark cycle, and combination-treated mice (Lira+BemA) were given subcutaneous injections of Victoza diluted in saline to a dose of 70 µg/kg every second day 1-2 hrs before the dark cycle with bempedoic acid supplemented in the

diet at a dose of 10 mg/kg. After 9 weeks of treatment, all mice were sacrificed in the fed state between 0900 and 1100 hrs, using a ketamine/xylazine mixture to sedate mice before collecting blood via cardiac puncture. Mice were presumed dead by exsanguination and cervical dislocation was performed as a secondary measure.

Metabolic Testing

Metabolic tests were performed between 4 and 9 weeks of intervention, in respective order below. Intraperitoneal glucose (ipGTT; 1.25 g/kg) and insulin (ipITT; 1.3 U/kg) tolerance tests were performed in 6-hour fasted mice, with fasting starting at 0700 hrs and basal values being tested at 1300 hrs. Intraperitoneal pyruvate tolerance tests (ipPTT; 1.5 g/kg) were performed in 15-hour fasted mice, with fasting occurring overnight and basal values being evaluated at 0900hrs. Fasting blood glucose and serums were collected in 6-hour fasted mice, mimicking ipGTT and ipITT times. Blood collection for these tests were obtained via tail-knick.

Liver lipid analysis

Liver fat percentage was assessed based on time-domain NMR using a Bruker Minispec LF90II. Briefly, ~30-50 mg tissue chips were obtained on dry ice, given 10 minutes to thaw on ice and given 10 minutes to equilibrate at room temperature before being placed in biopsy tubes purchased from Bruker. Liver triglycerides were assessed using the Cayman Chemicals Triglyceride Colorometric Assay kit

(Item no. 10010303). Briefly, 10-20 mg of frozen liver was immediately homogenized in 400 µL of diluted NP40 substitute assay reagent. The manufacturer's instructions were followed for all other aspects of the assay.

Histology

Tissues were fixed in 10% neutral buffered formalin for 48 hrs before being stored in 70% ethanol. The medial lobe of the liver was processed, paraffin embedded, serially sectioned, and stained with haemotoxylin and eosin (H&E), Masson's Trichrome, and picrosirius red (PSR) by the McMaster Immunology Research Centre's core histology facility. Images were acquired by a Nikon 90i Eclipse upright microscope. Liver histology scores were obtained by a blinded pathologist who utilized descriptions as documented by Kleiner and colleagues as their basis (Kleiner et al. 2005). NAFLD activity scores were compiled by the sum of scores: liver steatosis, lobular inflammation, and hepatocellular ballooning, as assessed using H&E-stained slides. Fibrosis scores were obtained by the assessment of both Masson's Trichrome and PSR-stained slides.

RNA isolation and analysis

Liver tissue (~15 mg) was lysed in 1 mL TRIzol reagent (Invitrogen) using ceramic beads and a Precellys 24 homogenizer (Bertin Technologies). Samples were spun down for 10 mins at 12 000 g at 4 ºC. 200 µL of chloroform was added and shaken vigorously before spinning samples again at same settings. Supernatant was

placed in new tubes and an equal amount of 70% ethanol was added then vortexed. Solutions were loaded onto RNeasy columns and manufacturer's instructions were followed (Qiagen).

NanoString Gene Expression Analysis

For NanoString analysis, 4-5 RNA samples per group were inspected by a BioAnalyzer quality control test. The McMaster Genomics Facility ran an nCounter Fibrosis v2 Panel (NanoString Technologies) containing 760 target genes as well as a CustomSet Panel consisting of 22 orthologous mus musculus genes that correspond to the 25-gene NASH severity signature described by Govaere and colleagues (Govaere et al. 2020). Gene expression data was normalized and log-transformed prior to differential gene expression analysis and pathway signature score computation using NanoString Technologies' nSolver 4.0 software (version 4.0.70) and the embedded PLAGE algorithm.

Uniquely regulated genes were defined as differentially expressed genes (FDR < 0.05) between control and combination treatment but not monotherapy. Additively regulated genes were defined as differentially expressed genes (FDR < 0.05) exhibiting the largest fold change between control and combination treatment compared to monotherapy. Combination specific signature was derived based on the overlap between uniquely and additively regulated genes and differential expression (p-value < 0.05) between combination treatment and monotherapy. An elastic net regularization model with 10-fold cross validation was used to further

identify a subset of genes associated with fibrosis stages > 2 in a cohort of 216 human NAFLD/NASH patients using methods implemented in caret v6.0.93 and glmnet v4.1.6.Pathway over-representation was determined by tabulating the pathway annotations associated with genes in the unique and additive gene sets. Statistical significance was computed using Chi-square test.

RNA-Seq Analysis

Patient derived RNA-Seq data was obtained from GEO repository GSE135251 and processed for quality control, alignment, and count as described previously (Govaere et al. 2020). Variance stabilizing transformation was applied to compute relative mRNA abundance using DESeq2 v1.36.0..

Integrated Human and Mouse Gene Expression Analysis

Gene expression data derived from NanoString and DESeq2 analyses underwent log-scale and z-score transformation prior to integration with human data. PCA and hierarchical clustering using Pearson correlation, as implemented in stats v4.2.2, were applied to integrated gene expression data to assess sample similarity between treatment cohorts and human NASH/NAFLD disease stages.

Multivariate logistic regression, as implemented in the caret v6.0.93, using the combination treatment specific gene signatures and the 25-gene signature reported by Govaere et al. were used to predict advanced fibrosis stages in

patients. AUROC scores were computed to assess the predictive performance of each gene signature using methods implemented in pROC v1.18.0.

Classification of patients based on similarity to the combination specific gene signature was computed using Nearest Template Prediction as implemented in GenePattern (Hoshida 2010). The gene set associated with the similar class is defined as upregulated genes within the combination specific gene signature. The gene set associated with the dissimilar class is defined as downregulated genes within the combination specific gene signature. Only patients with statistically significant classification (p-value < 0.05) were included in downstream analyses.

ssGSEA was performed as implemented in GenePattern. Log-transformed gene expression along with hallmark gene sets and Aizarani liver cell type gene sets derived from MSIgDB were used as the respective inputs for ssGSEA. Differential ssGSEA scores were computed using T-test followed by FDR adjustment and significance was defined as FDR < 0.05.

Serum measurements

Serum insulin was assessed in 6-hour fasted samples using the manufacturer's instructions for the Ultra-Sensitive Mouse Insulin ELISA kit (Crystal Chem, Catalog # 90080). Fed serum samples were assessed using the manufacturer's instructions for: cholesterol E (Fujifilm, No. 999-02601) triglycerides (Cayman Chemicals, Item no. 10010303), non-esterified fatty acids (Fujifilm, NEFA-HR (2), 999-34691, 991-34891, 993-35191), ALT (Cohesion, #CAK1002), AST (Cohesion #CAK1004),

Serum Amyloid A (R&D Systems, MSAA00), and sPLA2 (Cayman Chemical, Item No. 765001-96). ProCartaPlex Mouse kits from ThermoFisher were used to measure CRP and CXCL10 on a Bio-Rad Bio-Plex Reader.

Statistics

All other statistical analyses not previously specified using R packages or GenePattern softwares were performed using GraphPad Prism 9. Values throughout the illustrations are shown as means ± S.E.M. with p-values reported in the graphs. Colored bars signify comparisons between groups (with respective colors) and control groups (both ND and ND+Veh). Significance was accepted at $p < 0.05$ and determined via unpaired t-tests, one-way or repeated-measures two-way ANOVA with Tukey or Sidak's posthoc, where appropriate. For histological score analysis, a Kruskal-Wallis test or Mann-Whitney tests were used – these are nonparametric tests, with the Kruskal-Wallis test comparing the rank of each column with every other column, and correcting for multiple comparisons using Dunn's posthoc test. White circles are individual mice per group (n=8-9 mice/group).

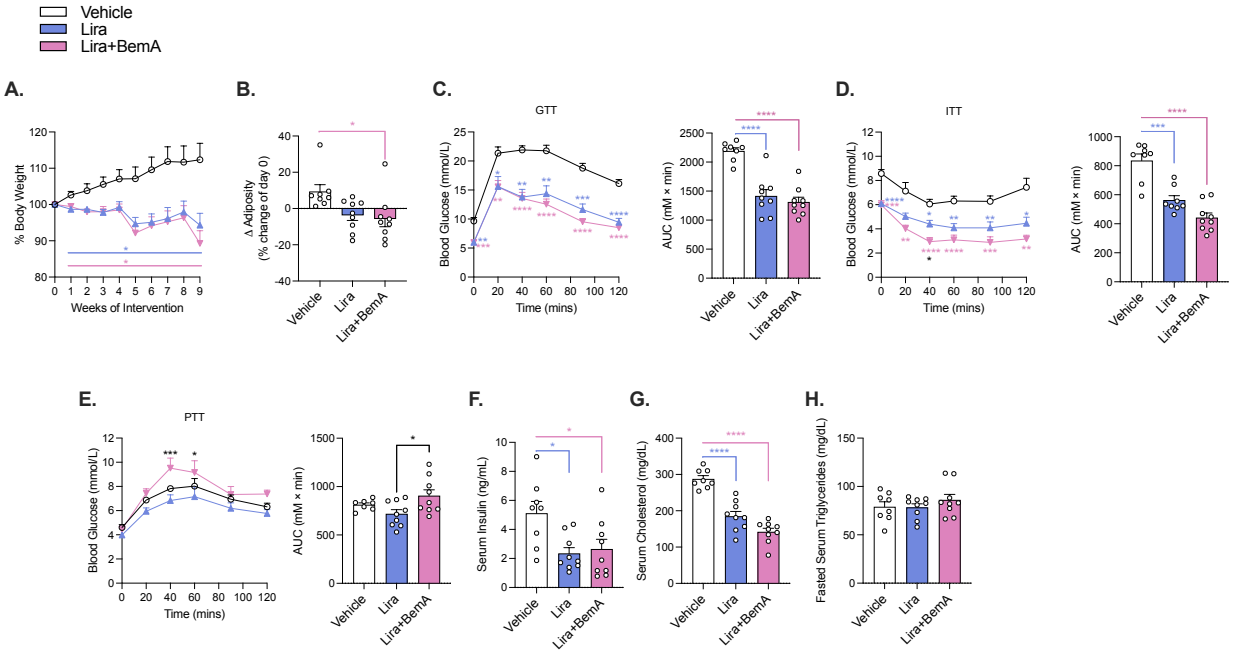

Figure 1. Liraglutide and bempedoic acid lower body mass, adiposity, insulin sensitivity and serum cholesterol without increasing serum triglycerides. Percent change in body weight (A) and change in adiposity (post-pre) (B) throughout intervention. Intraperitoneal glucose tolerance test (GTT) (1.25 g/kg) (C) at 4 weeks intervention, ip insulin tolerance test (ITT) (1.3 U/kg) (D) at 4 weeks intervention and ip pyruvate tolerance test (PTT) (1.5 g/kg) (E) at 5 weeks intervention with time plots and area under the curve (AUC). Fasted serum insulin (F) collected via tail-knick near-end of intervention (9 weeks). Fed serum cholesterol (G) from blood collected by cardiac puncture at sacrifice, and fasted serum triglycerides (H). Data are means ± S.E.M. Colored bars signify comparisons between groups and Vehicle. Significance was accepted at $p < 0.05$ and determined via one-way ANOVA or repeated-measures two-way ANOVA with Tukey posthoc, where appropriate. White circles are individual mice per group (n=8-9 mice/group). *P<0.05, **p<0.01, ***p<0.001, ****p<0.0001. Vehicle (saline treatments subcutaneously every 2 days), Lira (70 µg/kg liraglutide subcutaneously every 2 days before lights out), Lira+BemA (bempdeoic acid 10 mg/kg in diet and 70 µg/kg liraglutide subcutaneously every 2 days before lights out).

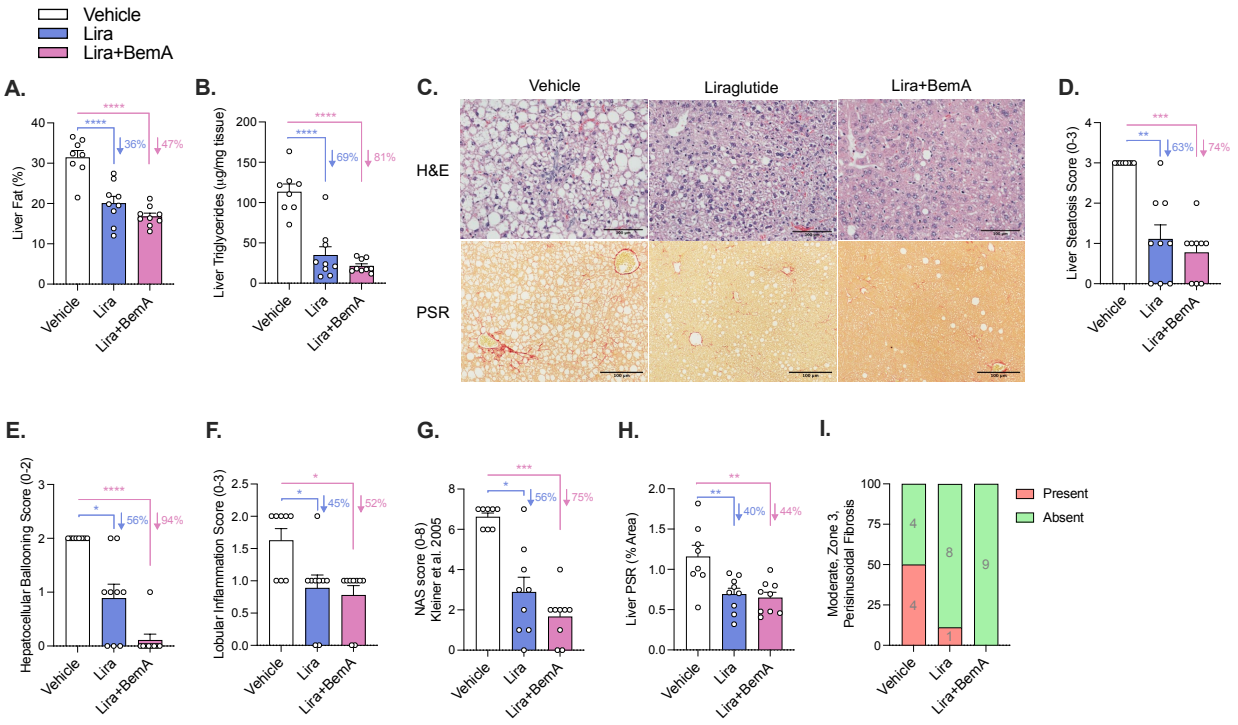

Figure 2. Liraglutide and bempedoic acid reduce liver steatosis, ballooning, inflammation and fibrosis. (A) Liver fat percentage as measured by time-domain NMR. (B) Liver triglycerides. (C) Representative micrographs of H&E (top) and picrosirius red (PSR; bottom) stained sections (10x) along with histograms of histological grades of liver steatosis (D), hepatocellular ballooning (E), lobular inflammation (F), and composite NAFLD activity score (NAS) (G), Percent positive PSR area (H) and parts of whole indicating presence of moderate, zone 3 perisinusoidal fibrosis (I). Data are means ± S.E.M. Colored bars signify comparisons between groups and Vehicle with percentages listed next to them. Significance was accepted at $p < 0.05$ and determined via one-way ANOVA with Tukey posthoc or, for histological score analysis, a Kruskal-Wallis test was used with Dunn's posthoc test to correct for multiple comparisons, where appropriate. White circles are individual mice per group (n=8-9 mice/group). *P<0.05, **p<0.01, ***p<0.001, ****p<0.0001. Vehicle (saline treatments subcutaneously every 2 days), Lira (70 µg/kg liraglutide subcutaneously every 2 days before lights out), Lira+BemA (bempdeoic acid 10 mg/kg in diet and 70 µg/kg liraglutide subcutaneously every 2 days before lights out).

Table 1. Serum markers of inflammation and liver damage.

	Group (Mean±SEM)						Group (Mean±SEM)		
	Vehicle		Lira		Lira+BemA		Control	BemA	
Measure	N=8	P value	N=9	P value	N=9	P value	N=9	N=9	P value
ALT (U/mL)	13.9±1.9	0.4017	20.3±5.4	0.5967	21.5±5.2	0.4936	16.9±2.8	2.0±1.2	**0.0002**
AST (U/mL)	3.8±0.4	0.0598	7.7±1.8	0.1891	8.7±1.7	0.0846	5.6±0.72	1.7±0.3	**0.0001**
SAA (ng/mL)	2743±60	0.8786	1092±248	**0.0004**	1154±331	**0.0005**	2730±49	1064±176	**<0.0001**
CXCL10 (pg/mL)	11.6±1.4	0.6811	10.0±0.6	0.4470	8.4±0.9	0.0689	12.7±1.9	7.3±0.5	**0.0211**
CRP (pg/mL)	29169±5539	0.7668	18033±2133	0.0634	12227±983	**0.0038**	31873±6845	15664±3074	**0.0463**
sPLA2 (nmol/min/mL)	26.9±1.1	0.6052	20.5±0.5	**0.0003**	16.3±1.1	**<0.0001***	28.0±1.7	19.3±0.8	**0.0003**

ALT=Alanine transaminase, AST=Aspartate aminotransferase (AST), SAA=Serum amyloid A

CXCL10=C-X-C motif chemokine ligand 10, also known as interferon gamma-induced protein 10 (IP-10), CRP=C-reactive protein, sPLA2=secretory phospholipase A2. P values reported are based on comparisons used throughout the remainder of manuscript – unpaired t-test between Control and BemA, One-Way ANOVA with Tukey posthoc between Vehicle, Lira, Lira+BemA. Significance was accepted at $p<0.05$. * indicates a significant difference $p<0.05$ between Lira and Lira+BemA

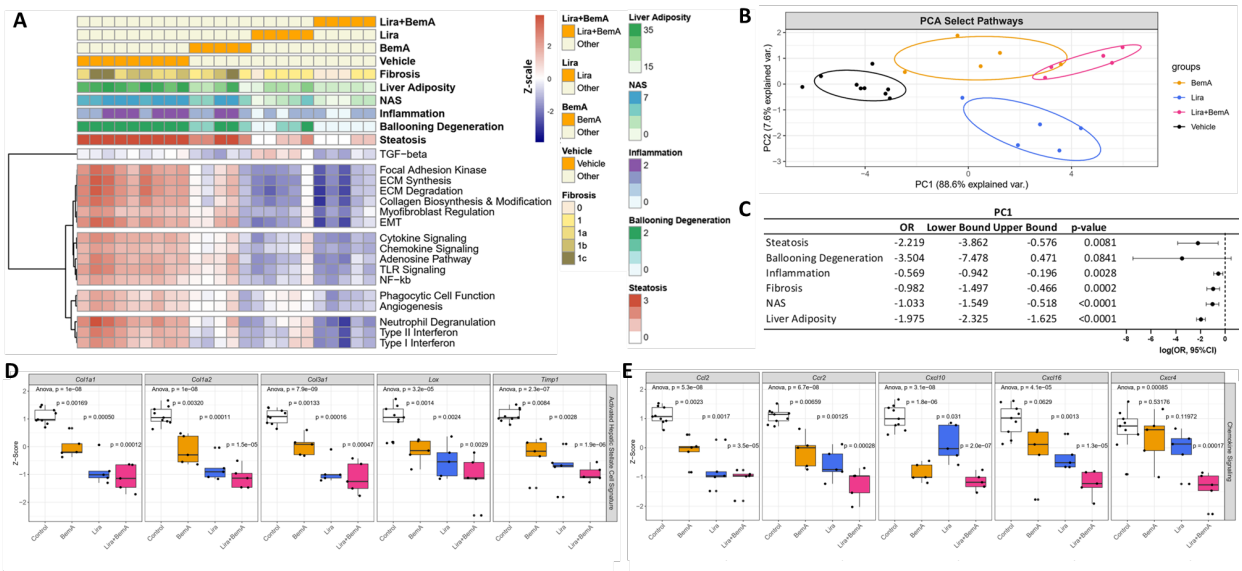

Figure 3. Pathway level gene expression analysis reveals additive downregulation of fibrosis-related pathways that are predictive of NASH resolution. (A) Signature scores of transcriptional pathways most affected by combination treatment. Each heatmap column represents an individual sample, along with rows annotated according to treatment cohort, histology, and pathway scores. (B) PCA of control, monotherapy and combination treatment based on pathway signature scores. (C) Odds ratio and 95% confidence interval associated with hepatic steatosis, ballooning degeneration, inflammation, fibrosis, NAS, and liver adiposity measurements based on PC1 of pathway signature scores. (D) Gene expression of hepatic stellate cell markers and (E) chemokines associated with NASH progression.

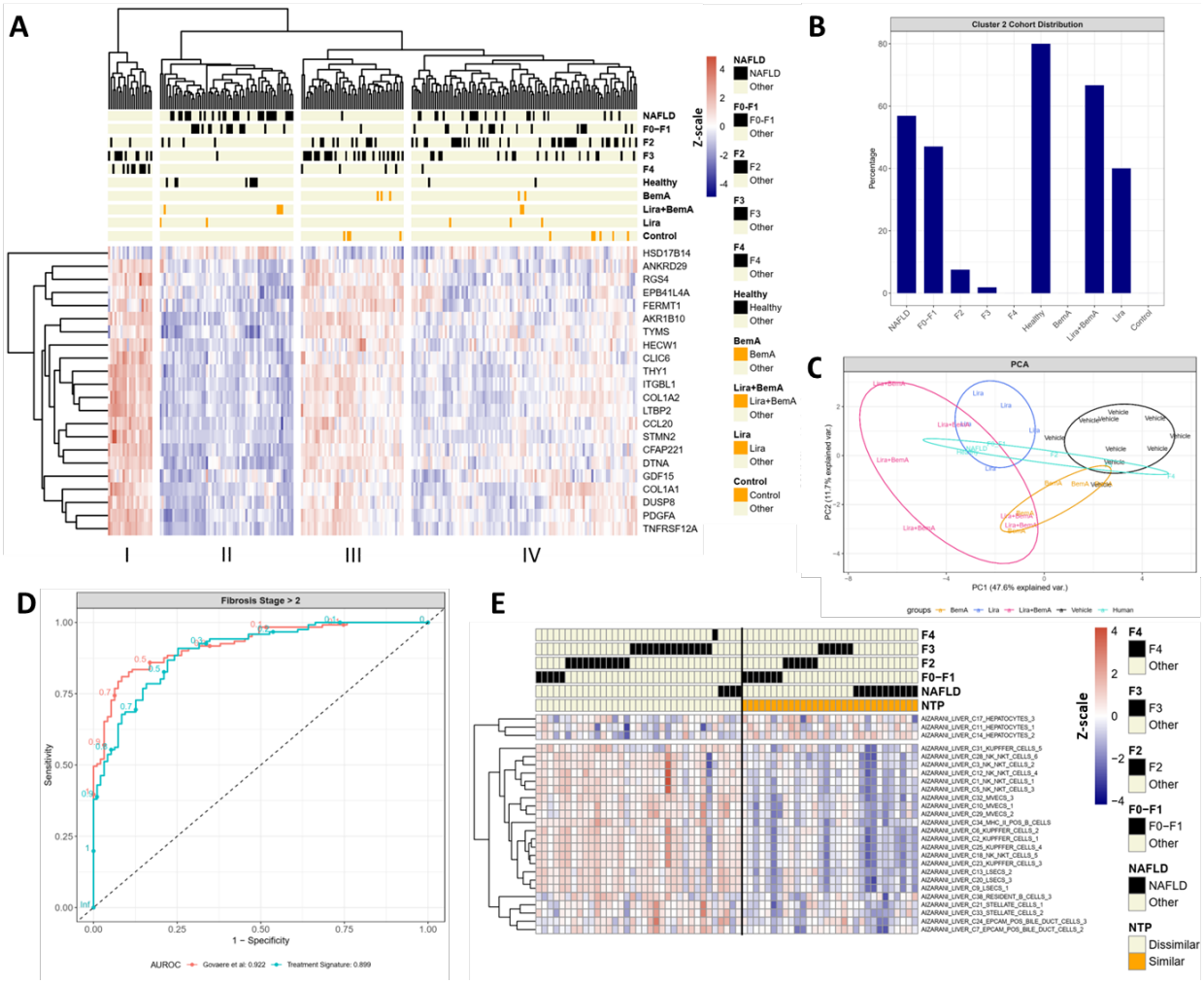

Figure 4. Combination treatment reverses the expression of prognostically significant genes involved in NASH progression and predicts improved fibrosis outcome. (A) Scaled expression of prognostically significant orthologous genes involved in NASH progression in healthy, NASH/NAFLD patients and experimental cohorts. (B) Distribution of disease stages and treatment types in cluster III. (C) PCA of human NASH/NAFLD patients and experimental cohorts based on scaled gene expression. (D) ROC of multivariate logistic regression models using a combination specific gene signature, a smaller subset derived using elastic net regularization, and the 25-gene signature previously reported by Govaere et al. for the prediction of fibrosis stage > 2 among human NASH/NAFLD patients. (E) Classification based on similarity of gene signature expression identifies liver cell types that are differentially expressed between patients classified into the similar or dissimilar classes.

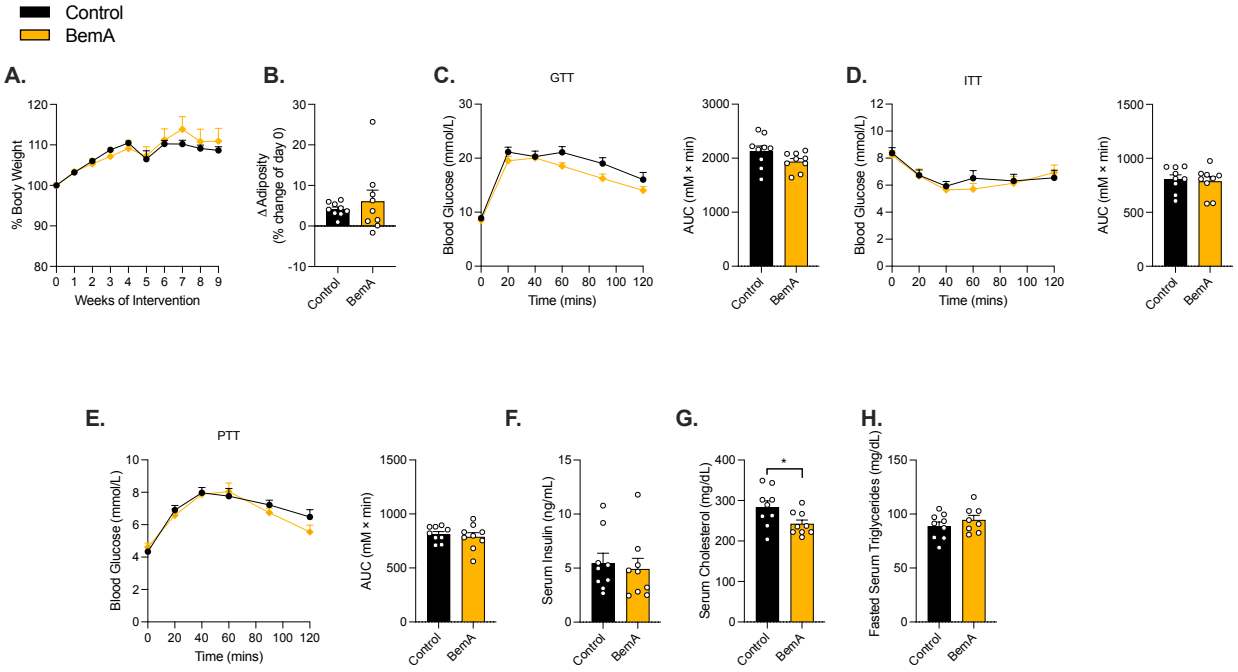

Supplementary 1. Bempedoic acid reduces serum cholesterol, liver steatosis, hepatocellular ballooning and NAFLD activity composite score independently from body weight, adiposity, and insulin sensitivity in a mouse model of diet-induced NASH. Percent change in body weight (A) and change in adiposity (post-pre) (B) throughout intervention. Intraperitoneal glucose tolerance test (GTT) (1.25 g/kg) (C) at 4 weeks intervention, ip insulin tolerance test (ITT) (1.3 U/kg) (D) at 4 weeks intervention and ip pyruvate tolerance test (PTT) (1.5 g/kg) (E) at 5 weeks intervention with time plots and area under the curve (AUC). Fasted serum insulin (F) collected via tail-knick near-end of intervention (9 weeks). Fed serum cholesterol (G) from blood collected by cardiac puncture at sacrifice, and fasted serum triglycerides (H). Data are means ± S.E.M. Black bars signify comparisons between group and control group (ND). Significance was accepted at $p < 0.05$ and determined via unpaired t-test or repeated-measures two-way ANOVA with Sidak posthoc, where appropriate. White circles are individual mice per group (n=8-9 mice/group). *P<0.05. ND (or control), ND+BemA (bempedoic acid 10 mg/kg in diet).

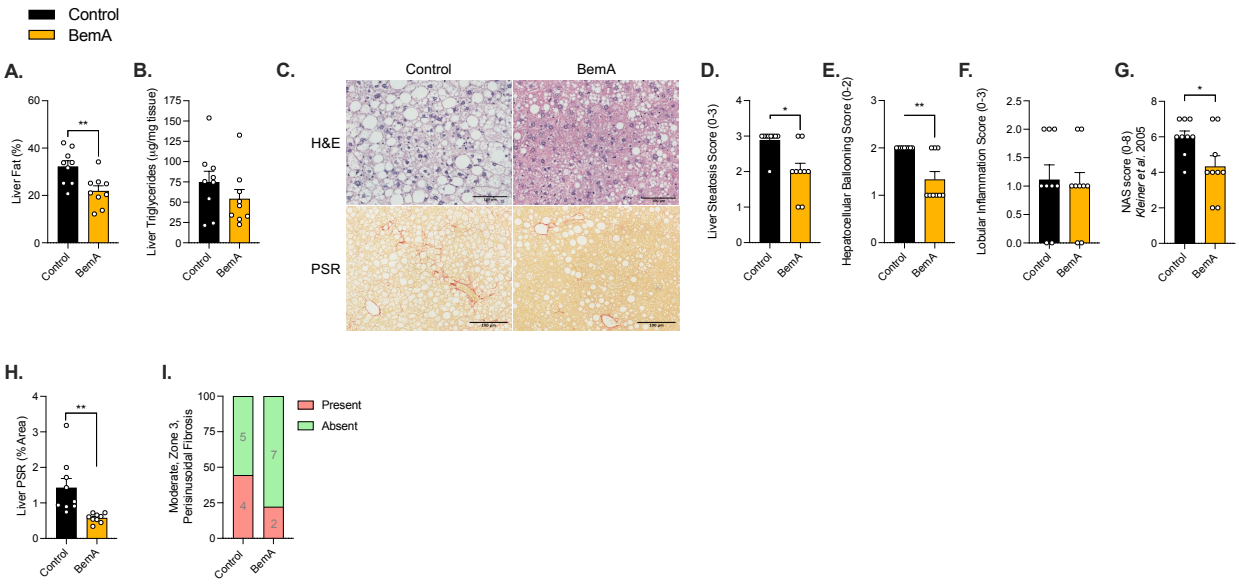

Supplementary 2. Bempedoic acid reduces liver steatosis, hepatocellular ballooning, NAFLD activity composite score, and fibrosis. (A) Liver fat percentage as measured by time-domain NMR. (B) Liver triglycerides. (C) Representative micrographs of H&E (top) and picrosirius red (PSR; bottom) stained sections (10x) along with histograms of histological grades of liver steatosis (D), hepatocellular ballooning (E), lobular inflammation (F), and composite NAFLD activity score (NAS) (G), Percent positive PSR area (H) and parts of whole indicating presence of moderate, zone 3 perisinusoidal fibrosis (I). Data are means ± S.E.M. Black bars signify comparisons between group and control group (ND). Significance was accepted at $p < 0.05$ and determined via unpaired t-test or, for histological score analysis, a Mann-Whitney test was used, where appropriate. *P<0.05, **p<0.01. White circles are individual mice per group (n=8-9 mice/group). ND (or control), ND+BemA (bempedoic acid 10 mg/kg in diet).

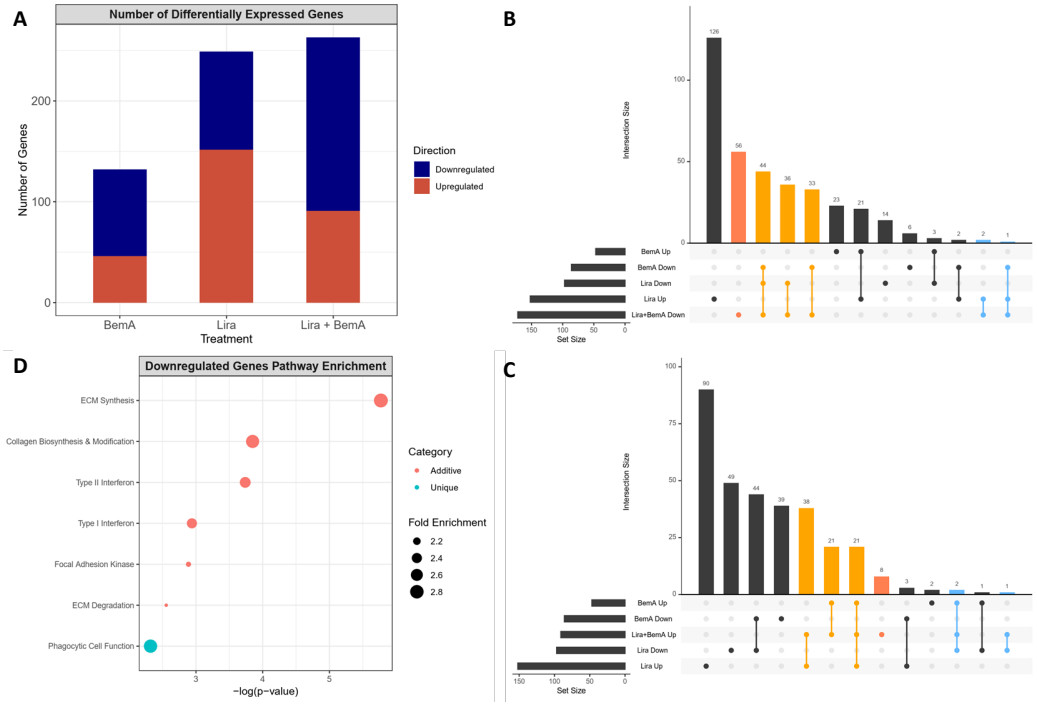

Supplemental Figure 3. Targeted gene expression analysis. (A) Number of differentially expressed genes in each treatment group. (B) Overlap between significantly downregulated and (C) upregulated genes by combination treatment and genes differentially expressed in all other treatment groups. Red indicates genes uniquely regulated by combination treatment. Orange indicates genes up or downregulated in all treatment groups. Blue indicates genes upregulated by monotherapy and downregulated by combination treatment. (D) Over-represented pathway annotations associated with additively and uniquely downregulated genes by combination treatment.

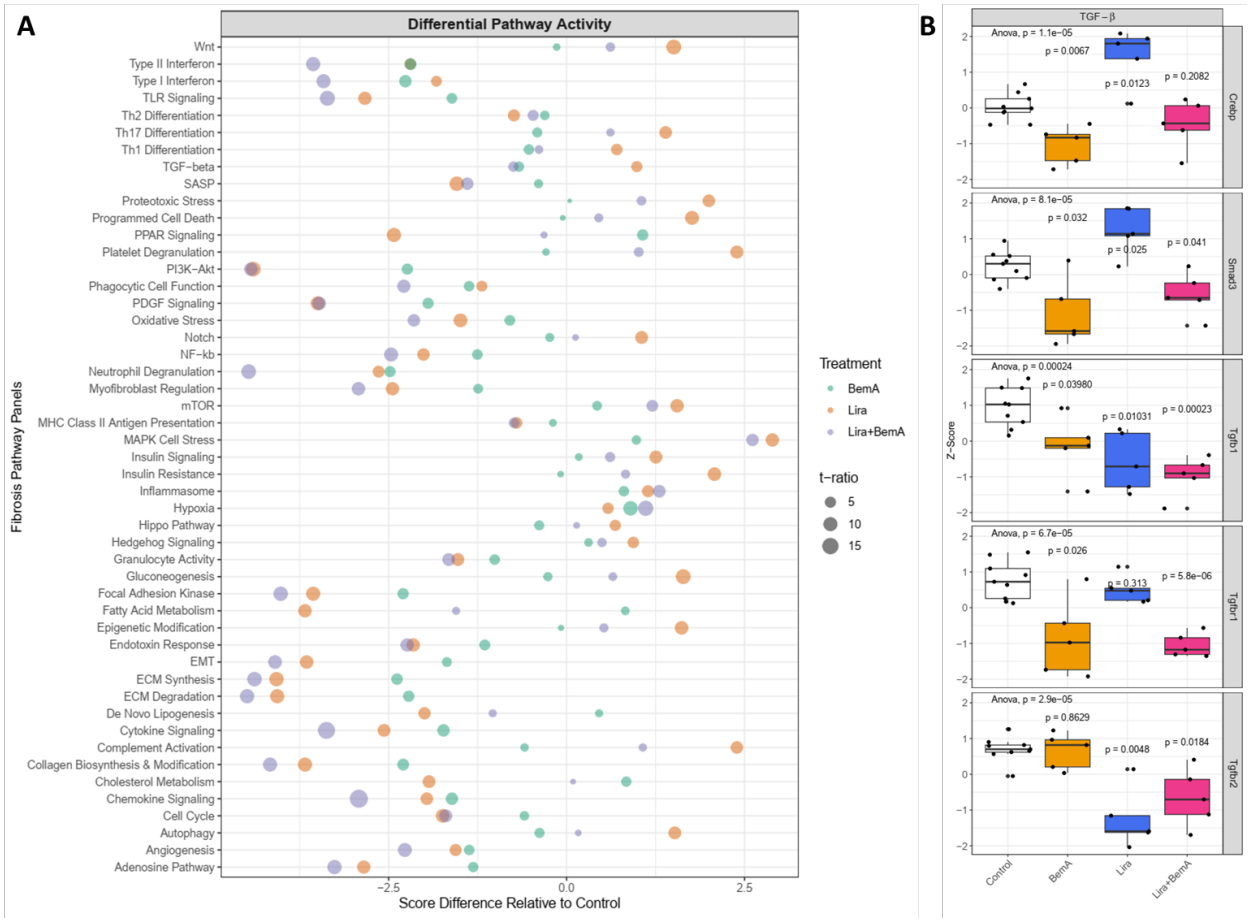

Supplemental Figure 4. Pathway level gene expression analysis and TGFβ-related gene expression. (A) Signature scores of all pathways in the Nanostring nCounter Fibrosis v2 Panel. (B) Gene expression of select genes involved in TGFβ pathway.

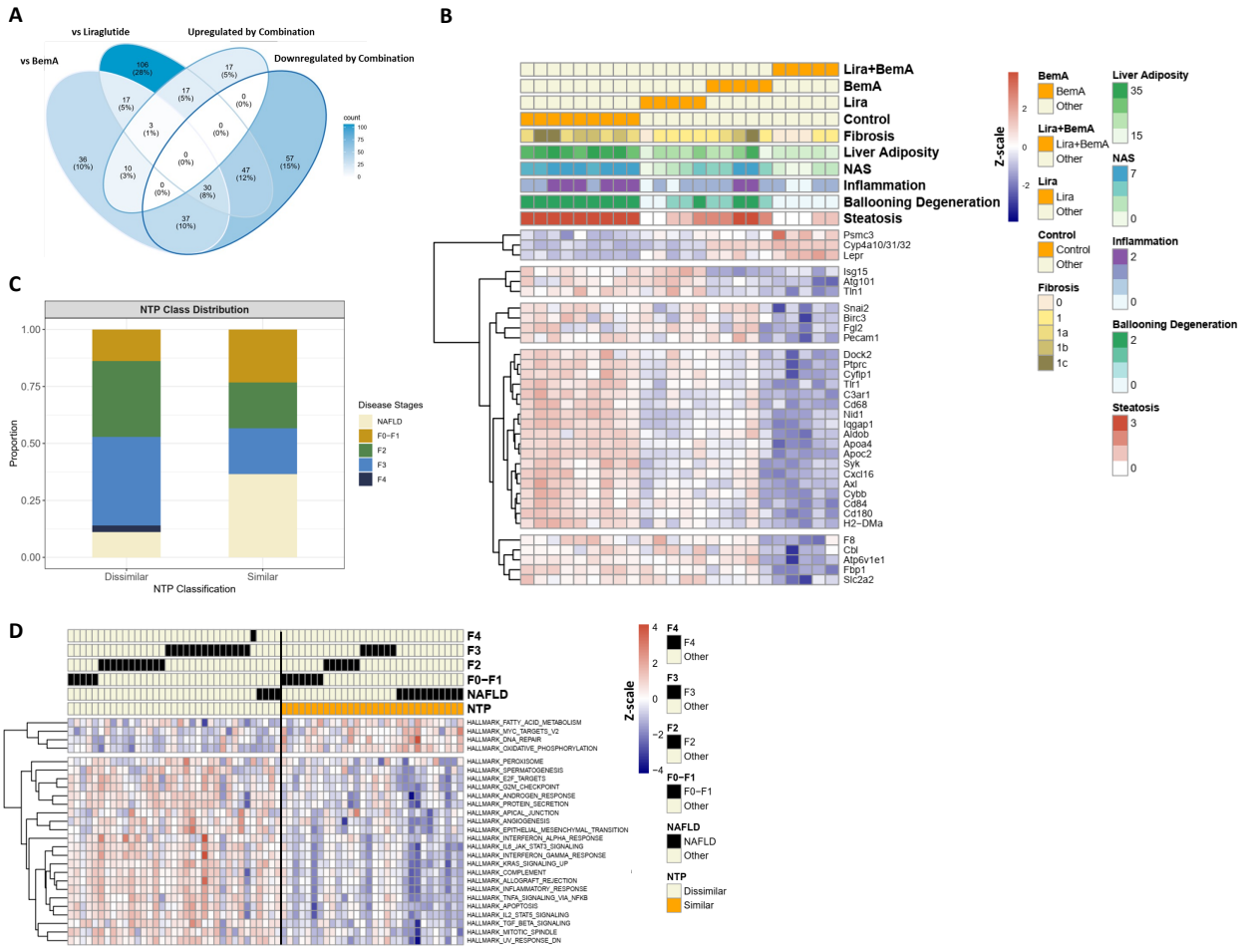

Supplemental Figure 5. Development of a combination treatment specific gene signature for supervised classification. (A) Overlap between genes differentially regulated by combination treatment compared to control as well as monotherapy. (B) Expression of the 33-gene signature. (C) Distribution of disease stages among patients in the similar or dissimilar classes. (D) Classification based on similarity of gene signature expression identifies differential expression of hallmark gene sets between the similar and dissimilar classes.

Table Legends:
Supplemental Table 3: All differentially expressed genes
Supplemental Table 4: Downregulated genes and pathway annotations
Supplemental Table 5: Pathway over-representation analysis of genes uniquely and additively downregulated by combination treatment

CHAPTER FIVE

5. DISCUSSION

5.1 INTRODUCTION

Maintaining cellular homeostasis is crucial to overall health. One key aspect of this is to balance the regulation of nutrient supply with nutrient utilization. This enables cells to optimize their metabolism based on available resources. However, when resources are consistently accessible, as in today's developed world, an imbalance of energy intake and lipid metabolism occurs, leading to the increased prevalence of metabolic diseases such as obesity, diabetes and NAFLD. Mitochondria play an important role in maintaining cellular energy homeostasis by producing ATP through oxidative phosphorylation. Therefore, it is crucial to understand the regulatory mechanisms that control lipid metabolism and mitochondrial function, and how these may be altered within the context of NAFLD and NASH.

An important link communicating nutrient availability with demand is acetyl-CoA, a key intermediate of several metabolic pathways. Its regulation is tightly controlled by two major enzymes, AMPK and ACLY, which are positioned to monitor and adjust their downstream pathways as needed. In the present studies, we aimed to further interrogate the sensing and effector functions of these enzymes in the context of NAFLD, NASH, and hepatic fibrosis.

5.2 ALLOSTERICALLY MODULATING AMPK ACTIVITY TO PROMOTE LIPID HOMEOSTASIS IN THE LIVER

The phosphorylation of AMPK β1 at Ser108 has been extensively studied in structural and cell-based studies. And while these studies established the phosphorylation event to be important in the allosteric activation of AMPK in response to small molecules, natural compounds, and LCFA-CoAs, the *in vivo* physiological importance of this site was not known. In Chapter 2, new insights revealed the importance of AMPK β1 Ser108 phosphorylation in acutely regulating a feedforward pathway of fatty acids promoting their own oxidation, and being a key node to enhance mitochondrial biogenesis and autophagy in response to elevated levels of fatty acids.

We developed and metabolically phenotyped a whole-body knock-in mouse model in which AMPK β1 Ser108 is converted to Ala (S108A-KI), rendering this site unable to be phosphorylated. In this model, we found reductions in AMPK activity in the liver, while AMPK activity in the muscle was unaffected. This is explained because the liver predominantly expresses the AMPK β1 isoform, while the muscle predominately expresses the AMPK β2 isoform. Interestingly, this is the first AMPK mouse model that shows a reduction in AMPK activity without reductions in AMPK subunit expression (i.e. genetic KO of AMPK β1 isoforms).

5.2.1 ROLE FOR AMPK β1 SER108 PHOSPHORYLATION IN LCFA-COA-MEDIATED FATTY ACID OXIDATION

The studies completed in this thesis extend on previous findings in cultured cells, where our lab demonstrated that AMPK β1 Ser108 is important for AMPK to respond to physiologically relevant increases in LCFAs (Pinkosky et al. 2020). Interestingly, there were no detectable differences in AMPK activity in S108A-KI hepatocytes or liver in the basal state. It was only with the challenge of short-term administration of palmitate *in vitro* and intralipid *in vivo* or the long-term exposure to elevated fatty acids via high-fat diet feeding which led to observable changes in ACC phosphorylation by AMPK (Ser79/212) *in vitro*, and an increase in fat oxidation *in vivo*. These data are consistent with previous studies showing that AMPK β1 Ser108 phosphorylation is maintained at low levels in the basal state (Scott et al. 2014).

AMPK increases fatty acid oxidation through inhibitory phosphorylation of ACC1 at Ser79 and ACC2 at Ser212. This reduces the conversion of acetyl-CoA to malonyl-CoA, which in turn reduces the inhibition of CPT1 allowing fatty acyl-CoAs to enter the mitochondria for β-oxidation through the carnitine shuttle. Our studies add a novel step to this model by elucidating the requirement of AMPK β1 Ser108 phosphorylation to interact with LCFA-CoAs to allosterically activate AMPK. This was shown by comparing WT and S108A-KI responses in both primary hepatocytes with the acute palmitate treatment, and in mice with the administration of exogenous fatty acids using intralipid. These data, combined with our previous data showing the similar effects in ACC-DKI mice (Pinkosky et al. 2020), indicate that the acute effects of fatty acids to stimulate fatty acid oxidation are mediated

through an AMPK-ACC-dependent mechanism. Interestingly, LCFA-CoAs are also able to allosterically inhibit ACC activity (Ogiwara et al. 1978). This redundancy bolsters the evidence that the control of fatty acyl-CoA levels and their metabolites are critical to enhance fatty acid oxidation.

Subsequently, although we saw increases in the phosphorylation of AMPK β1 Ser108 in WT mice fed a HFD, we did not observe a reduction of ACC phosphorylation in S108A-KI mice fed a HFD. And although these findings are consistent with the similar rates of fatty acid oxidation found in ACC-DKI mice fed a HFD (Fullerton et al. 2013), this is likely because feeding the HFD reduced the expression of ACC. This finding is consistent with previous findings which found that chronic feeding of a HFD lowers the activity of the transcription factor SREBP1c, which suppresses ACC expression (Duarte et al. 2014; Y. Lee et al. 2002). Repeating the experiments in S108A-KI mice but feeding them a western diet consisting of 40% fat, 20% fructose, 0.02% cholesterol may reveal larger differences in liver steatosis and fibrosis as we have found this maintains the expression of lipogenic enzymes including ACLY and ACC compared to the HFD (Morrow et al. 2022), thereby potentially amplifying the importance of the AMPK-fatty acid sensing mechanism.

We have established a significant role for the Ser108 fatty acid sensing axis in the context of the liver and NAFLD, and these findings complement other preclinical studies illustrating that increases in AMPK activation in the liver results in the attenuation of HFD-induced steatosis (Garcia et al. 2019; Woods et al. 2017;

Neopane et al. 2022; Yang et al. 2008). It would be of interest for future studies to determine the relevance and significance of this pathway in other metabolic pathways such as lipolysis, carbohydrate, and amino acid metabolism, as well as other AMPK β1-expressing cells, tissues, and their associated metabolic diseases. For example, macrophages and kidneys predominantly express AMPK β1, therefore assessing the significance of the AMPK-fatty acid sensing axis in the context of atherosclerosis and autosomal polycystic kidney disease could be of interest. Other metabolic-associated diseases in which this axis in AMPK β1-containing complexes could potentially be relevant could also be acute myocardial infarction, irritable bowel-syndrome, x-linked leukodystrophy, Alzheimer's, pain, and many cancers.

5.2.2 A NOVEL MECHANISM BY WHICH FATTY ACIDS PROMOTE MITOCHONDRIAL BIOGENESIS AND AUTOPHAGY

Considering increased fatty acid exposure leads to increased levels of fatty acid oxidation, it is logical that the machinery for β-oxidation would increase in parallel with chronic exposure. Several studies have shown that HFD feeding and chronic exposure to fatty acids increases mitochondrial biogenesis (Gámez-Pérez et al. 2012; Carabelli et al. 2011; Garcia-Roves et al. 2007). In contrast, several genetic models of AMPK deficiency have reductions in mitochondrial content (Mottillo et al. 2016; H. M. O'Neill et al. 2011; Galic et al. 2011; Hasenour et al. 2014). AMPK plays an important role in multiple pathways regulating mitochondrial

homeostasis, most notably (1) mitochondrial biogenesis, (2) mitochondrial fission, and (3) mitophagy.

Our study found that S108A-KI had similar liver mitochondrial content on a chow-diet, but had reduced content on a HFD. These data, along with experiments showing an attenuated induction of *Cpt1a* and *Ppargc1a* in response to acute palmitate exposure in S108A-KI primary hepatocytes, show that AMPK β1 Ser108 phosphorylation plays an important role in the response of mitochondrial biogenesis to increases in fatty acid levels. One of the most well-reported mechanisms by which AMPK activation can lead to the stimulation of mitochondrial biogenesis is through an effect mediated by the activity of the transcriptional co-activator PGC1α. Though there has been a suggestion of direct phosphorylation of PGC1α Thr177 and Ser538 *in vitro*, there are also other mechanisms by which AMPK can promote the activity of PGC1α, including the activation of sirtuins, p38 MAPK, HDAC5, and TFEB (Jager et al. 2007; Y. Wu et al. 2015; Cantó et al. 2009; Czubryt et al. 2003; Mihaylova et al. 2011; Settembre et al. 2013). Identifying the mechanism by which LCFA-CoA-mediated activation of AMPK stimulates mitochondrial biogenesis was beyond the scope of our current work, however, it would be interesting to determine which of these mechanisms are influenced by this axis and whether there are other novel mechanisms at play.

Mitochondria from livers of S108A-KI mice fed a HFD had altered structures and impaired function compared to their WT counterparts, as measured via transmission electron microscopy (TEM) and oxygen consumption kinetic assays,

respectively. Although we did not assess the contribution of the effects that AMPK has on mitochondrial dynamics, it is possible that S108A-KI mice had a defect in mitochondrial fission, which facilitates the clearance of damaged or dysfunctional mitochondrial sections from their efficient network. AMPK plays a large role in mitochondrial dynamics by phosphorylating dynamin-related protein (DRP1) at Ser637, mitochondrial fission factor (MFF) at Ser155 and Ser172, and mitochondrial fission regulator 1-like protein at Ser103 and Ser238 (Ducommun et al. 2015; Toyama et al. 2016; Xie et al. 2020; Tilokani et al. 2022; C. Zhang and Lin 2016; Herzig and Shaw 2018). And although these processes are intricate and can counteract one another, it has recently been suggested that AMPK can influence the utilization or partitioning of LCFA into lipid droplets via the promotion of mitochondrial fission (J. E. Song et al. 2021). These studies utilized a non-specific activator of AMPK, AICAR, and could be repeated with S108A-KI hepatocytes, as well as specific activators such as A-769662 to determine specificity to allosteric activation of AMPK β1-containing heterotrimers.

Another potential explanation for altered mitochondrial morphology and function in S108A-KI mice fed a HFD was a defect in mitophagy. And although the mechanisms by which AMPK promotes mitophagy are growing more and more complex, we found a reduction in the phosphorylation of the initiating factor ULK1 at Ser555, and in mitochondria-enriched fractions, a reduction in palmitate-induced LC3BII flux in primary hepatocytes from S108A-KI mice. Interestingly, we did not find alterations in the adaptor protein p62, or other markers of mitophagy such as

BNIP3, NIX, and MitoNEET, which have been shown to be under some form of control by the AMPK signalling pathway in other studies (S. Wang et al. 2022). These findings suggest that, at least in part, AMPK's role is to initiate mitophagy through phosphorylation of ULK1 and terminate the process through the promotion of lysosomal biogenesis by promoting TFEB activity. While completing these studies, an interesting report was published indicating a new AMPK-ULK1-Parkin phosphorylation axis (Hung et al. 2021). This analysis was not performed in our studies, however, it would be interesting to see whether LCFA-CoA activation of AMPK results in alterations in the phosphorylation of Parkin at Ser108, and subsequently results in enhanced mitophagy through a PINK1-regulated pathway. Other important concepts that can be explored are the role of the LCFA-CoA-AMPK axis to regulate lipophagy and lipid droplet dispersion (Herms et al. 2015). This highlights the complexity of AMPK and autophagy and is the subject of intense investigation in other labs around the world.

Several questions remain, however one potentially limiting factor which can affect the translatability of our findings to humans is the difference in liver isoform predominance in human versus mouse: human hepatocytes predominantly express AMPK β2-containing heterotrimers (β2-42.7 nTPMs vs. β1-6.4 nTPMS), while mouse hepatocytes predominantly express AMPK β1-containing heterotrimers (Human Protein Atlas). Though the sequence for Ser108 is relatively well-conserved between AMPK β1 and β2, Ser108 is not phosphorylated in AMPK β2-containing isoforms and ADaM site activators do not bind AMPK β2 complexes

(Ford et al. 2015; Dzamko et al. 2010; Stephenne et al. 2011; J. Wu et al. 2013). Furthermore, our previous report showed that AMPK β2-containing heterotrimers were not sensitive to LCFA-CoAs (Pinkosky et al. 2020). Despite this concern, recent studies have illustrated that the activation AMPK β1 in humans is sufficient to increase total liver AMPK activity and may actually be preferred compared to pan-β activators which result in undesired cardiac hypertrophy (Myers et al. 2017; Cokorinos et al. 2017; Esquejo et al. 2018; Cusi et al. 2021; Gluais-Dagorn et al. 2021). To further support this, PXL770, an allosteric activator of AMPK with 20-fold greater propensity to activate AMPK β1-containing heterotrimers, reduced liver steatosis by 13% vs 1% for placebo after 12 weeks in a phase 2a study without any cardiac toxicity (Cusi et al. 2021). Taken together with other studies showing a reduction of NASH and fibrosis in rodents, and reduced DNL, inflammation, and stellate cell activation in primary human cells, these studies support further development of AMPK β1 activators to treat NAFL and NASH (Gluais-Dagorn et al. 2021; Fouqueray et al. 2021).

In summary, the findings in Chapter 2 support the further development of direct AMPK β1 activators for the treatment of NAFLD and NASH by demonstrating that AMPK can promote fatty acid oxidation when challenged with excess fatty acids acutely, while promoting mitochondrial homeostasis in chronic conditions of elevated lipids. Understanding the myriad of molecular mechanisms by which AMPK can improve cellular homeostasis not only increases our confidence in targeting this enzyme for metabolic diseases, but the elucidation of multiple

redundancies within its control of signalling arms emphasizes that, once activated in a physiologically relevant manner, it will regulate itself to overcome potential compensatory mechanisms.

5.3 ALTERNATE MECHANISMS BY WHICH BEMPEDOIC ACID IMPROVES LIVER PATHOLOGY

Previous investigations have shown that the ACLY inhibitor bempedoic acid attenuates the development of, and treats established, hepatic steatosis, inflammation, and glucose intolerance (Pinkosky et al. 2013b; Samsoondar et al. 2017; Morrow et al. 2022). Many of these effects have been attributed to the inhibition of DNL and increases in fatty acid oxidation, resulting in the reduction of lipids including cholesterol and triglycerides. However, as ACLY controls the production of nucleocytosolic acetyl-CoA, it is also positioned to be a regulator of protein acetylation (Pinkosky et al. 2017). In Chapter 3, we have used the STAM mouse model to explore the perhaps less appreciated molecular mechanisms by which bempedoic acid can confer hepatoprotective effects in the context of NASH and fibrosis. This model is not characterized by obesity, or hyperinsulinemia, and is fed a HFD which, as discussed in the previous section, reduces the drive for DNL, yet still rapidly develops NASH and fibrosis with human-like histopathology.

Treatment of STAM mice with bempedoic acid for 4 weeks improved steatosis (albeit it a very small amount due to the already low steatosis grade in this disease model), hepatocellular ballooning, serum triglycerides, and hepatic fibrosis

(Morrow et al. 2022). Using the liver samples collected from these mice, as well as other experiments outlined in Chapter 3, we characterized the changes occurring in bempedoic acid treated STAM mice at the gene, protein, and metabolite levels. Integrating prior knowledge that reduced cytosolic acetyl-CoA levels induce autophagy, and that autophagy is known to be dysregulated in NASH, we measured key markers of the autophagic pathway and found some significant increases with bempedoic acid treatment. This led us to measure autophagic flux, where we found significantly higher flux in cultured rat hepatocytes acutely treated with bempedoic acid compared to vehicle.

The goal of this study was to explore and identify potential alternate mechanisms by which bempedoic acid improved liver histopathology aside from reducing lipids. We identify, that bempedoic acid reduced the acetylation of p300. However, further investigations would be necessary to validate this as a potential mechanism for NASH and fibrosis improvement. For example, an initial study could use cultured hepatocytes in the presence or absence of a p300 inhibitor with or without bempedoic acid to identify whether the increase in autophagic flux from bempedoic acid is altered. As p300 inhibition will induce autophagy on its own, the idea would be to see if there is a further increase in autophagy with bempedoic acid. If there is, it is likely to suggest an alternate mechanism is at play. More sophisticated studies could utilize molecular biology techniques to create mutant forms of lysine residues of p300 identified in our proteomic analyses (k1553,1554,1557) in cultured cells, and shift residues to an arginine to mimic

constitutively acetylated site. However, prior to this, future studies discussed below should be considered.

In 2013 Pinkosky and colleagues described bempedoic acid as an AMPK activator and ACLY inhibitor (Pinkosky et al. 2013b). Ensuing experiments in enzyme preparations showed that AMPK activation by bempedoyl-CoA was AMPK β1-dependent, eluding to an effect which could mimic LCFA-CoA-dependent activation of AMPK (Pinkosky et al. 2016). Though these previous studies concluded that bempedoic acid's positive effects on atherosclerosis were independent from AMPK, it is possible that AMPK activation may be mediating at least some of the favourable effects in NASH and fibrosis. Morrow and colleagues showed an ~25% reduction in hepatocellular ballooning with hepatocyte-specific ACLY knockout mice and an ~50% reduction with bempedoic acid treatment (Morrow et al. 2022). Although the work went on to describe a hepatic stellate cell-mediated mechanism for reduced fibrosis, there remains the possibility of other factors, such as AMPK activation, that may have been important for mediating positive effects. Thus, it would be interesting to repeat experiments performed in either the STAM model or the high-fat high-fructose thermoneutral NASH mouse model with or without bempedoic acid treatment in (1) an inducible hepatocyte-specific knockout of ACLY – to determine whether the effects are ACLY dependent, (2) an inducible hepatic stellate cell knockout of ACLY using an adeno-associated virus with a Cre construct under the lecithin retinol acyltransferase promoter (AAV9-LRAT-Cre) construct administered to an ACLY flox mouse model to

determine whether the effects of reduced hepatic fibrosis are solely due to alterations in hepatic stellate cell activation via ACLY inhibition, and (3) an inducible, liver-specific S108A-KI mouse model – to determine whether effects are partially mediated through AMPK.

The effects of bempedoic acid on acetyl-CoA and autophagy may also be mediated in part through activation of AMPK. First, AMPK phosphorylates acetate-CoA synthetase 2 (ACCS2) at Ser656 causing translocation to the nucleus where it interacts with TFEB, leading to upregulation of the expression of lysosomal and autophagosomal genes (Hao Zhang et al. 2019). Activated ACCS2 also recruits p300 which recaptures acetate from histone deacetylation to reform acetyl-CoA, providing substrates for histone acetyl transferases such as p300. AMPK also directly phosphorylates histone deacetylases (HDACs) including HDAC5 (McGee et al. 2008). Lastly, AMPK regulates p300 through direct phosphorylation and indirectly by inhibiting mTORC1 leading to increases in p300 activity (Vancura et al. 2018; Wan et al. 2017). Taken together, these data indicate there are multiple overlapping pathways by which inhibition of ACLY or activation of AMPK can promote autophagy.

The work in Chapter 3 strengthens evidence suggesting that ACLY-regulated acetylation contributes to changes in mitochondrial function, autophagy, and oxidative stress, specifically in the context of NASH (Su, Wellen, and Rabinowitz 2016; Pinkosky et al. 2017; Wellen et al. 2009). Although speculative, our data support that one of the reasons that ACLY inhibition and AMPK activation by

bempedoic acid may not result in hypertriglyceridemia as observed with ACC inhibitors is because this lowers the acetylation of SREBP1c (Ponugoti et al. 2010).

5.4 CHARACTERIZATION OF A NEW COMBINATION THERAPY TO TREAT NASH, HEPATIC FIBROSIS, AND RELATED COMORBIDITIES

Given the complexity and variability of NASH pathogenesis from patient to patient, it is no surprise that most clinical trials so far do not support a “one size fits all” treatment for NASH. The rationale behind combination therapies is to improve the efficacy of intervention by the development of complementary or synergistic mechanisms of action, while also improving tolerability by the utility of sub-maximal dosing regimens (Dufour, Caussy, and Loomba 2020). In Chapter 4, we characterized a new combination therapy, the GLP-1R agonist liraglutide plus bempedoic acid, utilizing a metabolic-associated NASH mouse model with similar metabolic, histological, and transcriptional characteristics to people with advanced NASH and fibrosis. We chose these two treatments for the following reasons: (1) distinct mechanisms of action likely to affect different portions of NASH pathology, (2) excellent safety profiles, and (3) treat separate comorbidities associated with NASH. We found that, in addition to each drug’s primary approved indications of T2D/obesity and serum cholesterol, the combination of liraglutide and bempedoic acid resulted in greater histopathological reductions in hepatocellular ballooning and hepatic fibrosis compared to either monotherapy alone. These results were

further confirmed with targeted transcriptomics, and with the use of a gene signature predictive of NASH severity, combination therapy resulted in a prognostically favorable profile for fibrosis resolution that closely resembled signatures from healthy human liver.

Both GLP-1R agonists liraglutide and semaglutide have been shown to meet only one of the two histological endpoints that the FDA has set as surrogate endpoint for clinical trials: GLP-1R agonists resolve NASH at a higher percentage than placebo but have not shown a significant effect on improving fibrosis by 1 stage (Armstrong et al. 2016; Newsome et al. 2021). This is significant as liver fibrosis is the key determinant of clinical outcomes in patients with NASH (Angulo et al. 2015). And although some have partially attributed these results to the stages of fibrosis, statistical power, and trial duration, GLP-1R agonists do not act directly on the hepatic stellate cells (HSCs) which drive the process of fibrosis. Recent work from our lab described that bempedoic acid can act directly on HSCs to inhibit DNL and TGFβ-induced proliferation and activation (Morrow et al. 2022). Together with the possibility that data in Chapter 3 showing that bempedoic acid alters acetylation and autophagy as occurs in hepatocytes and possibly HSCs, this combination covers all four aspects of current histopathological scorings.

Although our data provide the first demonstration of a benefit of combining liraglutide and bempedoic acid for the treatment of NASH and hepatic fibrosis, we believe that some of our results were impacted by the strength of improvements seen with liraglutide treatment in mice. We chose our dosing with liraglutide to

mimic the weight loss effects seen in patients (~10%), however, we believe we may be observing a 'basement effect' with the assessment of liver parameters, as liraglutide treatment as a monotherapy results in a comparable liver fat percentage to that of a chow mouse (20.1±2.1 Lira vs. 20.8±1.2 Chow). This likely limited our ability to detect differences between liraglutide monotherapy versus combination therapy as has also been reported in other in other GLP-1R combination studies in mice (Boland et al. 2020). Thus, it would be of interest to repeat these combination experiments with (1) a lower dose of liraglutide or extend to semaglutide since this is the GLP-1R agonist used in clinical trials, and (2) utilize a more severe mouse model of NASH where the intervention begins with severe fibrosis or onset of cirrhosis. The model used in our work has not been validated to reach this critical point in fibrosis development, however, it is likely that increasing the length of time on diet and thermoneutral housing by an additional 20-25 weeks (~45-50 weeks total) might lead to greater fibrosis. It has also been recently reported that utilization of agouti yellow mutant mice with a high-fat high-fructose diet results in further progression of fibrosis compared to wild-type mice (St. Rose et al. 2022). Perhaps using these mice in the setting of thermoneutrality will yield F3 fibrosis and potentially cirrhosis at an earlier timepoint. However, there are currently no reports of metabolic mouse models with liver cirrhosis and this should be an area for future investigation (Gallage et al. 2022).

Our directed transcriptomic analyses revealed a unique counteractive effect on TGFβ effectors when combining bempedoic acid and liraglutide treatments. Interestingly, bempedoic acid reduced Crebp, Smad3, and Tgfbr1, while liraglutide either increased Crebp and Smad3, or had no effect on Tgfbr1. These results are perplexing as it has been previously shown in several studies that liraglutide treatment reduces the expression of Tgfb1 and the phosphorylation of Smad3 (N. Song et al. 2022; Xingchun Wang et al. 2021; Ji et al. 2022; L. H. Zhang et al. 2015; Li et al. 2018). However, we may be unveiling a compensatory mechanism that has not been described previously given previous studies were conducted in mice housed at room temperature. Whether these effects are due to indirect actions of GLP-1R agonism or through direct effect on the liver-localized γδ T cells (B. A. McLean, Wong, Kaur, et al. 2021) could be an interesting investigation, however, repeating these findings in another study to confirm this compensatory response should be performed first. Collectively, it is possible that bempedoic acid negates this compensatory mechanism and could act in synergy with liraglutide to prevent the activation of HSCs and reduce ECM synthesis to prevent hepatic fibrosis progression.

With the very recent CLEAR Outcomes trial results demonstrating that treatment of statin-intolerant patients with bempedoic acid lowers the risk of major adverse CVD events, bempedoic acid is ideally situated to be repurposed for the treatment of NASH (Nissen et al. 2023; Alexander 2023; Keaney 2023). Being approved for the treatment of hyperlipidemia and having an excellent safety profile

further supports its development as a therapy for NASH and hepatic fibrosis, as most patients are at increased risk for death due to CVD complications. In addition, some of the therapies that have been tested in clinical trials, including ACC inhibitors and the FXR agonist obeticholic acid, have resulted in increased measures relating to risk factors for CVD such as hypertriglyceridemia and hypercholesterolaemia, respectively (Pockros et al. 2019; Lawitz et al. 2023). Furthermore, new findings show that the GLP-1R agonist semaglutide does not improve fibrosis in patients with NASH-related cirrhosis (Loomba et al. 2023). Multiple studies have now shown that GLP-1R agonists effectively resolve NASH, but do not improve fibrosis stage. Thus, it has become clear that an additional therapy that reduces fibrosis on its own will be crucial in meeting the surrogate endpoints currently established by the FDA. Collectively, these data support the evaluation of clinical biomarkers of NASH in the bempedoic acid CLEAR outcomes trials. If positive reductions in clinical biomarkers of NASH are observed, subsequent clinical trials could be designed to assess whether bempedoic acid and a GLP-1R agonist can treat biopsy-proven NASH.

5.5 SUMMARY

In this thesis, we gain a greater understanding of the molecular mechanisms by which AMPK and ACLY regulate lipid metabolism within the liver. We identified the physiological role of AMPK β1 Ser108 phosphorylation in sensing LCFA-CoAs to increase fatty acid oxidation, stimulate autophagy, and promote mitochondrial

homeostasis. Under conditions of a chronic HFD, S108A-KI mice had impaired glucose tolerance, greater accumulation of liver lipids, and mitochondrial dysfunction. These data support ongoing clinical efforts in targeting liver AMPK to treat NAFLD and NASH. Subsequently, using a NASH mouse model not characterized by obesity, hyperinsulinemia, and a reduced drive for DNL, we identified that the ACLY inhibitor and AMPK activator bempedoic acid improves liver function in part through changes in acetylation status and the stimulation of autophagy. These hepatoprotective effects likely contribute to the improvements seen in hepatocellular ballooning and fibrosis within multiple NASH mouse models. Lastly, we demonstrated that a combination therapy regime involving bempedoic acid and liraglutide led to greater reductions in NASH and liver fibrosis while reducing common NASH-associated comorbidities including obesity, insulin resistance, hypercholesterolemia, and CVD. Collectively, our data provide further support to develop therapies which target AMPK and ACLY, to help the over 1.8 billion people living with NAFLD and NASH worldwide.

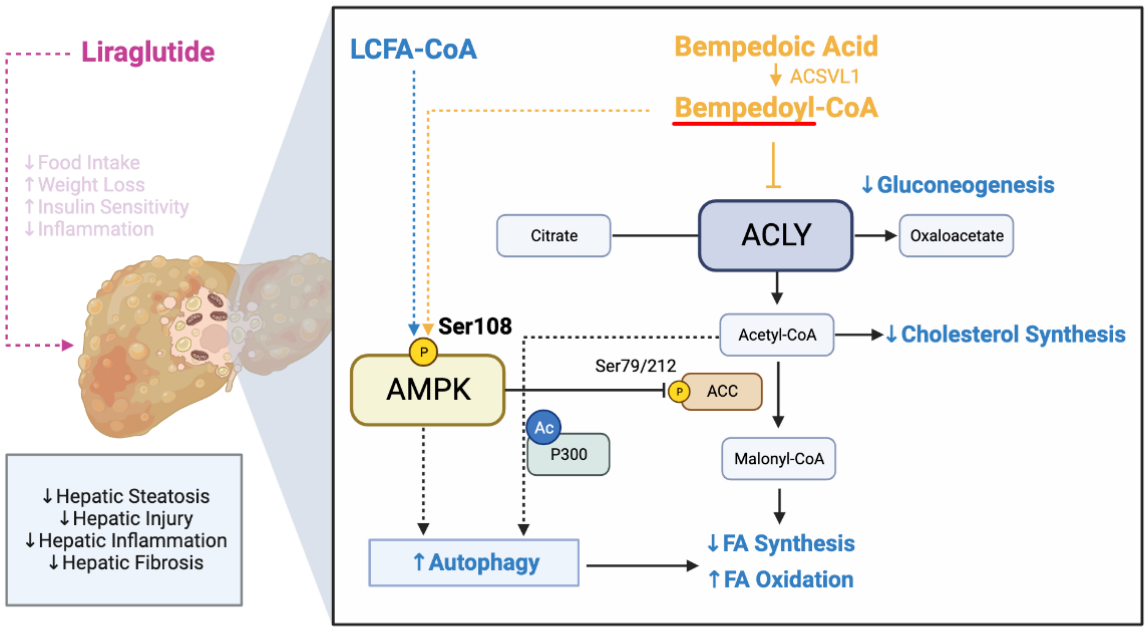

Figure 5.1. New molecular insights and application of AMPK activation and ACLY inhibition to support the development of treatments for NASH and associated comorbidities.

CHAPTER SIX

REFERENCES

Adeva-Andany, María M., Noemi Pérez-Felpete, Carlos Fernández-Fernández, Cristóbal Donapetry-García, and Cristina Pazos-García. 2016. “Liver Glucose Metabolism in Humans.” *Bioscience Reports* 36 (6): 1–15. https://doi.org/10.1042/BSR20160385.

Ahrens, Markus, Ole Ammerpohl, Witigo Von Schönfels, Julia Kolarova, Susanne Bens, Timo Itzel, Andreas Teufel, et al. 2013. “DNA Methylation Analysis in Nonalcoholic Fatty Liver Disease Suggests Distinct Disease-Specific and Remodeling Signatures after Bariatric Surgery.” *Cell Metabolism* 18 (2): 296–302. https://doi.org/10.1016/j.cmet.2013.07.004.

Aizarani, Nadim, Antonio Saviano, Sagar, Laurent Mailly, Sarah Durand, Josip S. Herman, Patrick Pessaux, Thomas F. Baumert, and Dominic Grün. 2019. “A Human Liver Cell Atlas Reveals Heterogeneity and Epithelial Progenitors.” *Nature* 572 (7768): 199–204. https://doi.org/10.1038/s41586-019-1373-2.

Alexander, JH. 2023. “Benefits of Bempedoic Acid - Clearer Now.” *New England Journal of Medicine*, 1–2. https://doi.org/10.1056/NEJMe2301490.

Alkhouri, Naim, Robert Herring, Heidi Kabler, Zeid Kayali, Tarek Hassanein, Anita Kohli, Ryan S. Huss, et al. 2022. “Safety and Efficacy of Combination Therapy with Semaglutide, Cilofexor and Firsocostat in Patients with Non-Alcoholic Steatohepatitis: A Randomised, Open-Label Phase II Trial.” *Journal of Hepatology* 77 (3): 607–18. https://doi.org/10.1016/j.jhep.2022.04.003.

Alves-Bezerra, Michele, and David E. Cohen. 2018. “Triglyceride Metabolism in the Liver.” *Comprehensive Physiology* 8 (1): 1–22. https://doi.org/10.1002/cphy.c170012.

Angulo, Paul, David E. Kleiner, Sanne Dam-Larsen, Leon A. Adams, Einar S. Bjornsson, Phunchai Charatcharoenwitthaya, Peter R. Mills, et al. 2015. “Liver Fibrosis, but No Other Histologic Features, Is Associated with Long-Term Outcomes of Patients with Nonalcoholic Fatty Liver Disease.” *Gastroenterology* 149 (2): 389-397.e10. https://doi.org/10.1053/j.gastro.2015.04.043.

Arab, Juan Pablo, Marco Arrese, and Michael Trauner. 2018. “Recent Insights into the Pathogenesis of Nonalcoholic Fatty Liver Disease.” *Annual Review of Pathology: Mechanisms of Disease* 13: 321–50. https://doi.org/10.1146/annurev-pathol-020117-043617.

Armstrong, Matthew James, Piers Gaunt, Guruprasad P. Aithal, Darren Barton, Diana Hull, Richard Parker, Jonathan M. Hazlehurst, et al. 2016. “Liraglutide Safety and Efficacy in Patients with Non-Alcoholic Steatohepatitis (LEAN): A Multicentre, Double-Blind, Randomised, Placebo-Controlled Phase 2 Study.” *The Lancet* 387 (10019): 679–90. https://doi.org/10.1016/S0140-6736(15)00803-X.

Baggio, Laurie L., and Daniel J. Drucker. 2021. “Glucagon-like Peptide-1

Receptor Co-Agonists for Treating Metabolic Disease." *Molecular Metabolism* 46 (September 2020): 101090. https://doi.org/10.1016/j.molmet.2020.101090.

Ballantyne, Christie M., Maciej Banach, G. B.John Mancini, Norman E. Lepor, Jeffrey C. Hanselman, Xin Zhao, and Lawrence A. Leiter. 2018. "Efficacy and Safety of Bempedoic Acid Added to Ezetimibe in Statin-Intolerant Patients with Hypercholesterolemia: A Randomized, Placebo-Controlled Study." *Atherosclerosis* 277: 195–203. https://doi.org/10.1016/j.atherosclerosis.2018.06.002.

Baselli, Guido A., Oveis Jamialahmadi, Serena Pelusi, Ester Ciociola, Francesco Malvestiti, Marco Saracino, Luigi Santoro, et al. 2022. "Rare ATG7 Genetic Variants Predispose Patients to Severe Fatty Liver Disease." *Journal of Hepatology* 77 (3): 596–606. https://doi.org/10.1016/j.jhep.2022.03.031.

Batchuluun, Battsetseg, Stephen L. Pinkosky, and Gregory R. Steinberg. 2022. "Lipogenesis Inhibitors: Therapeutic Opportunities and Challenges." *Nature Reviews Drug Discovery* 0123456789. https://doi.org/10.1038/s41573-021-00367-2.

Bays, Harold E., Maciej Banach, Alberico L. Catapano, P. Barton Duell, Antonio M. Gotto, Ulrich Laufs, Lawrence A. Leiter, et al. 2020. "Bempedoic Acid Safety Analysis: Pooled Data from Four Phase 3 Clinical Trials." *Journal of Clinical Lipidology* 14 (5): 649-659.e6. https://doi.org/10.1016/j.jacl.2020.08.009.

Beg, Zafarul H., David W. Allmann, and David M. Gibson. 1973. "Modulation of 3-Hydroxy-3-Methylglutaryl Coenzyme A Reductase Activity with CAMP and with Protein Fractions of Rat Liver Cytosol." *Biochemical and Biophysical Research Communications* 54 (4): 1362–69. https://doi.org/10.1016/0006-291X(73)91137-6.

Ben-Moshe, Shani, and Shalev Itzkovitz. 2019. "Spatial Heterogeneity in the Mammalian Liver." *Nature Reviews Gastroenterology and Hepatology* 16 (7): 395–410. https://doi.org/10.1038/s41575-019-0134-x.

Bhattarai, Kashi Raj, Thoufiqul Alam Riaz, Hyung Ryong Kim, and Han Jung Chae. 2021. "The Aftermath of the Interplay between the Endoplasmic Reticulum Stress Response and Redox Signaling." *Experimental and Molecular Medicine* 53 (2): 151–67. https://doi.org/10.1038/s12276-021-00560-8.

Bindesbøll, Christian, Qiong Fan, Rikke C Nørgaard, Laura MacPherson, Hai-Bin Ruan, Jing Wu, Thomas Å Pedersen, et al. 2015. "Liver X Receptor Regulates Hepatic Nuclear O-GlcNAc Signaling and Carbohydrate Responsive Element-Binding Protein Activity." *Journal of Lipid Research* 56 (4): 771–85. https://doi.org/10.1194/jlr.M049130.

Boland, Michelle L., Rhianna C. Laker, Karly Mather, Arkadiusz Nawrocki, Stephanie Oldham, Brandon B. Boland, Hilary Lewis, et al. 2020. "Resolution of NASH and Hepatic Fibrosis by the GLP-1R and GCGR Dual-Agonist Cotadutide via Modulating Mitochondrial Function and Lipogenesis." *Nature*

Metabolism 2 (5): 413–31. https://doi.org/10.1038/s42255-020-0209-6.
Boland, Michelle L, Stephanie Oldham, Brandon B Boland, Sarah Will, Jean-Martin Lapointe, Silvia Guionaud, Christopher J Rhodes, and James L Trevaskis. 2018. "Nonalcoholic Steatohepatitis Severity Is Defined by a Failure in Compensatory Antioxidant Capacity in the Setting of Mitochondrial Dysfunction." *World Journal of Gastroenterology* 24 (16): 1748–65. https://doi.org/DOI: 10.3748/wjg.v24.i16.1748.
Boudaba, Nadia, Allison Marion, Camille Huet, Rémi Pierre, Benoit Viollet, and Marc Foretz. 2018. "AMPK Re-Activation Suppresses Hepatic Steatosis but Its Downregulation Does Not Promote Fatty Liver Development." *EBioMedicine* 28: 194–209. https://doi.org/10.1016/j.ebiom.2018.01.008.
Bouitbir, Jamal, Gerda M Sanvee, Miljenko V Panajatovic, François Singh, and Stephan Krähenbühl. 2020. "Mechanisms of Statin-Associated Skeletal Muscle-Associated Symptoms." *Pharmacological Research* 154 (April): 104201. https://doi.org/10.1016/j.phrs.2019.03.010.
Bratoeva, Kameliya, Silviya Nikolova, Albena Merdzhanova, George St Stoyanov, Eleonora Dimitrova, Javor Kashlov, Nikolay Conev, and Mariya Radanova. 2018. "Association Between Serum CK-18 Levels and the Degree of Liver Damage in Fructose-Induced Metabolic Syndrome." *Metabolic Syndrome and Related Disorders* 16 (7): 350–57. https://doi.org/10.1089/met.2017.0162.
Bricambert, Julien, Jonatan Miranda, Fadila Benhamed, Jean Girard, Catherine Postic, and Renaud Dentin. 2010. "Salt-Inducible Kinase 2 Links Transcriptional Coactivator P300 Phosphorylation to the Prevention of ChREBP-Dependent Hepatic Steatosis in Mice." *Journal of Clinical Investigation* 120 (12): 4316–31. https://doi.org/10.1172/JCI41624.
Byrne, Christopher D, and Giovanni Targher. 2015. "NAFLD: A Multisystem Disease." *Journal of Hepatology* 62 (1 Suppl): S47-64. https://doi.org/10.1016/j.jhep.2014.12.012.
Cantó, Carles, Zachary Gerhart-Hines, Jerome N. Feige, Marie Lagouge, Lilia Noriega, Jill C. Milne, Peter J. Elliott, Pere Puigserver, and Johan Auwerx. 2009. "AMPK Regulates Energy Expenditure by Modulating NAD + Metabolism and SIRT1 Activity." *Nature* 458 (7241): 1056–60. https://doi.org/10.1038/nature07813.
Cao, Jia, Shumei Meng, Evan Chang, Katherine Beckwith-Fickas, Lishou Xiong, Robert N. Cole, Sally Radovick, Fredric E. Wondisford, and Ling He. 2014. "Low Concentrations of Metformin Suppress Glucose Production in Hepatocytes through AMP-Activated Protein Kinase (AMPK)." *Journal of Biological Chemistry* 289 (30): 20435–46. https://doi.org/10.1074/jbc.M114.567271.
Carabelli, Julieta, Adriana L. Burgueño, Maria Soledad Rosselli, Tomas Fernández Gianotti, Nestor R. Lago, Carlos J. Pirola, and Silvia Sookoian. 2011. "High Fat Diet-Induced Liver Steatosis Promotes an Increase in Liver Mitochondrial Biogenesis in Response to Hypoxia." *Journal of Cellular and*

Molecular Medicine 15 (6): 1329–38. https://doi.org/10.1111/j.1582-4934.2010.01128.x.

Carling, David, Victor A. Zammit, and D. Grahame Hardie. 1987. "A Common Bicyclic Protein Kinase Cascade Inactivates the Regulatory Enzymes of Fatty Acid and Cholesterol Biosynthesis." *FEBS Letters* 223 (2): 217–22. https://doi.org/10.1016/0014-5793(87)80292-2.

Carlson, Curtis A, and Ki-Han Kim. 1973. "Regulation of Hepatic Acetyl Coenzyme A Carboxylase by Phosphorylation and Dephosphorylation." *The Journal of Biological Chemistry* 248 (1): 378–80.

Carotti, Simone, Katia Aquilano, Francesca Zalfa, Sergio Ruggiero, Francesco Valentini, Maria Zingariello, Maria Francesconi, et al. 2020. "Lipophagy Impairment Is Associated With Disease Progression in NAFLD." *Frontiers in Physiology* 11 (July): 1–12. https://doi.org/10.3389/fphys.2020.00850.

Chalasani, Naga, Zobair Younossi, Joel E. Lavine, Michael Charlton, Kenneth Cusi, Mary Rinella, Stephen A. Harrison, Elizabeth M. Brunt, and Arun J. Sanyal. 2018. "The Diagnosis and Management of Nonalcoholic Fatty Liver Disease: Practice Guidance from the American Association for the Study of Liver Diseases." *Hepatology* 67 (1): 328–57. https://doi.org/10.1002/hep.29367.

Challa, Tenagne D, Stephan Wueest, Fabrizio C Lucchini, Mara Dedual, Salvatore Modica, Marcela Borsigova, Christian Wolfrum, Matthias Blüher, and Daniel Konrad. 2019. "Liver ASK1 Protects from Non-alcoholic Fatty Liver Disease and Fibrosis." *EMBO Molecular Medicine* 11 (10): 1–17. https://doi.org/10.15252/emmm.201810124.

Chen, Yong Ping, Feng Bin Lu, Yi Bing Hu, Lan Man Xu, Ming Hua Zheng, and En De Hu. 2019. "A Systematic Review and a Dose–Response Meta-Analysis of Coffee Dose and Nonalcoholic Fatty Liver Disease." *Clinical Nutrition* 38 (6): 2552–57. https://doi.org/10.1016/j.clnu.2018.11.030.

Choubey, Vinay, Akbar Zeb, and Allen Kaasik. 2022. "Molecular Mechanisms and Regulation of Mammalian Mitophagy." *Cells* 11 (1). https://doi.org/10.3390/cells11010038.

Clark, Hilary, David Carling, and David Saggerson. 2004. "Covalent Activation of Heart AMP-Activated Protein Kinase in Response to Physiological Concentrations of Long-Chain Fatty Acids." *European Journal of Biochemistry* 271 (11): 2215–24. https://doi.org/10.1111/j.1432-1033.2004.04151.x.

Cohen, Jonathan C., Jay D. Horton, and Helen H. Hobbs. 2011. "Human Fatty Liver Disease: Old Questions and New Insights." *Science* 332 (6037): 1519–23. https://doi.org/10.1126/science.1204265.

Cokorinos, Emily C., Jake Delmore, Allan R. Reyes, Bina Albuquerque, Rasmus Kjøbsted, Nicolas O. Jørgensen, Jean Luc Tran, et al. 2017. "Activation of Skeletal Muscle AMPK Promotes Glucose Disposal and Glucose Lowering in Non-Human Primates and Mice." *Cell Metabolism* 25 (5): 1147-1159.e10. https://doi.org/10.1016/j.cmet.2017.04.010.

Cool, Barbara, Bradley Zinker, William Chiou, Lemma Kifle, Ning Cao, Matthew Perham, Robert Dickinson, et al. 2006. “Identification and Characterization of a Small Molecule AMPK Activator That Treats Key Components of Type 2 Diabetes and the Metabolic Syndrome.” *Cell Metabolism* 3 (6): 403–16. https://doi.org/10.1016/j.cmet.2006.05.005.

Cooper, Allen D. 1997. “Hepatic Uptake of Chylomicron Remnants.” *Journal of Lipid Research* 38 (11): 2173–92. https://doi.org/10.1016/s0022-2275(20)34932-4.

Corte, Claudia Della, Antonella Mosca, Andrea Vania, Arianna Alterio, Salvatore Iasevoli, and Valerio Nobili. 2017. “Good Adherence to the Mediterranean Diet Reduces the Risk for NASH and Diabetes in Pediatric Patients with Obesity: The Results of an Italian Study.” *Nutrition* 39–40: 8–14. https://doi.org/10.1016/j.nut.2017.02.008.

Csak, Timea, Michal Ganz, Justin Pespisa, Karen Kodys, Angela Dolganiuc, and Gyongyi Szabo. 2011. “Fatty Acid and Endotoxin Activate Inflammasomes in Mouse Hepatocytes That Release Danger Signals to Stimulate Immune Cells.” *Hepatology* 54 (1): 133–44. https://doi.org/10.1002/hep.24341.

Cunningham, Rory P., and Natalie Porat-Shliom. 2021. “Liver Zonation – Revisiting Old Questions With New Technologies.” *Frontiers in Physiology* 12 (September): 1–17. https://doi.org/10.3389/fphys.2021.732929.

Cusi, Kenneth, Naim Alkhouri, Stephen A Harrison, Pascale Fouqueray, David E Moller, Sophie Hallakou-Bozec, Sebastien Bolze, et al. 2021. “Efficacy and Safety of PXL770, a Direct AMP Kinase Activator, for the Treatment of Non-Alcoholic Fatty Liver Disease (STAMP-NAFLD): A Randomised, Double-Blind, Placebo-Controlled, Phase 2a Study.” *The Lancet. Gastroenterology & Hepatology* 6 (11): 889–902. https://doi.org/10.1016/S2468-1253(21)00300-9.

Czubryt, Michael P., John McAnally, Glenn I. Fishman, and Eric N. Olson. 2003. “Regulation of Peroxisome Proliferator-Activated Receptor γ Coactivator 1α (PGC-1α) and Mitochondrial Function by MEF2 and HDAC5.” *Proceedings of the National Academy of Sciences of the United States of America* 100 (4): 1711–16. https://doi.org/10.1073/pnas.0337639100.

Dancy, Beverley M., and Philip A. Cole. 2015. “Protein Lysine Acetylation by P300/CBP.” *Chemical Reviews* 115 (6): 2419–52. https://doi.org/10.1021/cr500452k.

Davies, Stephen P., Nicholas R. Helps, Patricia T.W. Cohen, and D. Grahame Hardie. 1995. “5′-AMP Inhibits Dephosphorylation, as Well as Promoting Phosphorylation, of the AMP-Activated Protein Kinase. Studies Using Bacterially Expressed Human Protein Phosphatase-2Cα and Native Bovine Protein Phosphatase-2Ac.” *FEBS Letters* 377 (3): 421–25. https://doi.org/10.1016/0014-5793(95)01368-7.

Day, C. P., and O. F.W. James. 1998. “Steatohepatitis: A Tale of Two ‘Hits’?” *Gastroenterology* 114 (4 I): 842–45. https://doi.org/10.1016/S0016-5085(98)70599-2.

Day, Emily A., Rebecca J. Ford, and Gregory R. Steinberg. 2017. “AMPK as a Therapeutic Target for Treating Metabolic Diseases.” *Trends in Endocrinology and Metabolism* 28 (8): 545–60. https://doi.org/10.1016/j.tem.2017.05.004.

DeBose-Boyd, Russell A., and Jin Ye. 2018. “SREBPs in Lipid Metabolism, Insulin Signaling, and Beyond Russell.” *Trends Biochemical Sciences* 43 (5): 358–68. https://doi.org/10.1016/j.tibs.2018.01.005.SREBPs.

Dikic, Ivan, and Zvulun Elazar. 2018. “Mechanism and Medical Implications of Mammalian Autophagy.” *Nature Reviews Molecular Cell Biology* 19 (6): 349–64. https://doi.org/10.1038/s41580-018-0003-4.

Ding, Hao, Ge Ge, Yujen Tseng, Yanyun Ma, Jun Zhang, and Jie Liu. 2020. “Hepatic Autophagy Fluctuates during the Development of Non-Alcoholic Fatty Liver Disease.” *Annals of Hepatology* 19 (5): 516–22. https://doi.org/10.1016/j.aohep.2020.06.001.

Dite, Toby A., Naomi X.Y. Ling, John W. Scott, Ashfaqul Hoque, Sandra Galic, Benjamin L. Parker, Kevin R.W. Ngoei, et al. 2017. “The Autophagy Initiator ULK1 Sensitizes AMPK to Allosteric Drugs.” *Nature Communications* 8 (1): 1–13. https://doi.org/10.1038/s41467-017-00628-y.

Dongiovanni, P, L Valenti, R Rametta, A K Daly, V Nobili, E Mozzi, J B S Leathart, et al. 2010. “Genetic Variants Regulating Insulin Receptor Signalling Are Associated with the Severity of Liver Damage in Patients with Non-Alcoholic Fatty Liver Disease.” *Gut* 59 (2): 267–73. https://doi.org/10.1136/gut.2009.190801.

Donnelly, Kerry L., Coleman I. Smith, Sarah J. Schwarzenberg, Jose Jessurun, Mark D. Boldt, and Elizabeth J. Parks. 2005. “Sources of Fatty Acids Stored in Liver and Secreted via Lipoproteins in Patients with Nonalcoholic Fatty Liver Disease.” *Journal of Clinical Investigation* 115 (5): 1343–51. https://doi.org/10.1172/JCI23621.

Drucker, Daniel J. 2022. “GLP-1 Physiology Informs the Pharmacotherapy of Obesity.” *Molecular Metabolism* 57 (October 2021): 101351. https://doi.org/10.1016/j.molmet.2021.101351.

Drucker, Daniel J., Joel F. Habener, and Jens Juul Holst. 2017. “Discovery, Characterization, and Clinical Development of the Glucagon-like Peptides.” *Journal of Clinical Investigation* 127 (12): 4217–27. https://doi.org/10.1172/JCI97233.

Duarte, Joao A.G., Filipa Carvalho, Mackenzie Pearson, Jay D. Horton, Jeffrey D. Browning, John G. Jones, and Shawn C. Burgess. 2014. “A High-Fat Diet Suppresses de Novo Lipogenesis and Desaturation but Not Elongation and Triglyceride Synthesis in Mice.” *Journal of Lipid Research* 55 (12): 2541–53. https://doi.org/10.1194/jlr.M052308.

Ducommun, Serge, Maria Deak, David Sumpton, Rebecca J Ford, Antonio Núñez, Martin Kussmann, Benoit Viollet, et al. 2015. “Motif Affinity and Mass Spectrometry Proteomic Approach for the Discovery of Cellular AMPK Targets : Identification of Mitochondrial Fi Ssion Factor as a New AMPK

Substrate." *Cellular Signalling* 27 (5): 978–88. https://doi.org/10.1016/j.cellsig.2015.02.008.

Ducommun, Serge, Maria Deak, Anja Zeigerer, Olga Göransson, Susanne Seitz, Caterina Collodet, Agnete B Madsen, et al. 2019. "Chemical Genetic Screen Identifies Gapex-5/GAPVD1 and STBD1 as Novel AMPK Substrates." *Cellular Signalling* 57 (May): 45–57. https://doi.org/10.1016/j.cellsig.2019.02.001.

Dufour, Jean François, Cyrielle Caussy, and Rohit Loomba. 2020. "Combination Therapy for Non-Alcoholic Steatohepatitis: Rationale, Opportunities and Challenges." *Gut* 69 (10): 1877–84. https://doi.org/10.1136/gutjnl-2019-319104.

Dulai, Parambir S., Siddharth Singh, Janki Patel, Meera Soni, Larry J. Prokop, Zobair Younossi, Giada Sebastiani, et al. 2017. "Increased Risk of Mortality by Fibrosis Stage in Nonalcoholic Fatty Liver Disease: Systematic Review and Meta-Analysis." *Hepatology* 65 (5): 1557–65. https://doi.org/10.1002/hep.29085.

Duve, Christian de. 1963. "The Lysosome." *Scientific American* 208: 64–72. https://doi.org/10.1001/jama.1965.03080170049014.

Dyson, Jessica K, Quentin M Anstee, and Stuart McPherson. 2014. "Non-Alcoholic Fatty Liver Disease: A Practical Approach to Diagnosis and Staging." *Frontline Gastroenterology* 5 (3): 211–18. https://doi.org/10.1136/flgastro-2013-100403.

Dzamko, Nicolas, Bryce J.W. van Denderen, Andrea L. Hevener, Sebastian Beck Jørgensen, Jane Honeyman, Sandra Galic, Zhi Ping Chen, et al. 2010. "AMPK B1 Deletion Reduces Appetite, Preventing Obesity and Hepatic Insulin Resistance." *Journal of Biological Chemistry* 285 (1): 115–22. https://doi.org/10.1074/jbc.M109.056762.

Edmunds, Lia R., Bingxian Xie, Amanda M. Mills, Brydie R. Huckestein, Ramya Undamatla, Anjana Murali, Martha M. Pangburn, et al. 2020. "Liver-Specific Prkn Knockout Mice Are More Susceptible to Diet-Induced Hepatic Steatosis and Insulin Resistance." *Molecular Metabolism* 41 (July): 101051. https://doi.org/10.1016/j.molmet.2020.101051.

Egan, Daniel F, David B Shackelford, Maria M Mihaylova, Sara Gelino, Rebecca A Kohnz, William Mair, Debbie S Vasquez, et al. 2011. "Phosphorylation of ULK1 (HATG1) by AMP-Activated Protein Kinase Connects Energy Sensing to Mitophagy." *Science* 331: 456–62.

Einer, Claudia, Simon Hohenester, Ralf Wimmer, Lena Wottke, Renate Artmann, Sabine Schulz, Christian Gosmann, et al. 2018. "Mitochondrial Adaptation in Steatotic Mice." *Mitochondrion* 40 (April 2017): 1–12. https://doi.org/10.1016/j.mito.2017.08.015.

Esquejo, Ryan M., Christopher T. Salatto, Jake Delmore, Bina Albuquerque, Allan Reyes, Yuji Shi, Rob Moccia, et al. 2018. "Activation of Liver AMPK with PF-06409577 Corrects NAFLD and Lowers Cholesterol in Rodent and Primate Preclinical Models." *EBioMedicine* 31: 122–32.

https://doi.org/10.1016/j.ebiom.2018.04.009.
European Association for the Study of the Liver (EASL), European Association for the Study of Diabetes (EASD) and European Association for the Study of Obesity (EASO). 2016. “EASL–EASD–EASO Clinical Practice Guidelines for the Management of Non-Alcoholic Fatty Liver Disease.” *Journal of Hepatology* 13 (5): 179–86. https://doi.org/10.1016/j.jhep.2015.11.004.
Fan, Nengguang, Lijuan Zhang, Zhenhua Xia, Liang Peng, Yufan Wang, and Yongde Peng. 2016. “Sex-Specific Association between Serum Uric Acid and Nonalcoholic Fatty Liver Disease in Type 2 Diabetic Patients.” *Journal of Diabetes Research* 2016: 3805372. https://doi.org/10.1155/2016/3805372.
Ficht, Xenia, and Matteo Iannacone. 2020. “Immune Surveillance of the Liver by T Cells.” *Science Immunology* 5 (51): 1–11. https://doi.org/10.1126/sciimmunol.aba2351.
Ford, Rebecca J., Morgan D. Fullerton, Stephen L. Pinkosky, Emily A. Day, John W. Scott, Jonathan S. Oakhill, Adam L. Bujak, et al. 2015. “Metformin and Salicylate Synergistically Activate Liver AMPK, Inhibit Lipogenesis and Improve Insulin Sensitivity.” *Biochemical Journal* 468 (1): 125–32. https://doi.org/10.1042/BJ20150125.
Foretz, Marc, Sophie Hébrard, Jocelyne Leclerc, Elham Zarrinpashneh, Maud Soty, Gilles Mithieux, Kei Sakamoto, Fabrizio Andreelli, and Benoit Viollet. 2010. “Metformin Inhibits Hepatic Gluconeogenesis in Mice Independently of the LKB1/AMPK Pathway via a Decrease in Hepatic Energy State.” *Journal of Clinical Investigation* 120 (7): 2355–69. https://doi.org/10.1172/JCI40671.
Fouqueray, Pascale, Sebastien Bolze, Julie Dubourg, Sophie Hallakou-Bozec, Pierre Theurey, Jean Marie Grouin, Clémence Chevalier, Pascale Gluais-Dagorn, David E. Moller, and Kenneth Cusi. 2021. “Pharmacodynamic Effects of Direct AMP Kinase Activation in Humans with Insulin Resistance and Non-Alcoholic Fatty Liver Disease: A Phase 1b Study.” *Cell Reports Medicine* 2 (12). https://doi.org/10.1016/j.xcrm.2021.100474.
Fraile, Julia M., Soumya Palliyil, Caroline Barelle, Andrew J. Porter, and Marina Kovaleva. 2021. “Non-Alcoholic Steatohepatitis (NASH) – A Review of a Crowded Clinical Landscape, Driven by a Complex Disease.” *Drug Design, Development and Therapy* 15: 3997–4009. https://doi.org/10.2147/DDDT.S315724.
Friedman, Scott L., Brent A. Neuschwander-Tetri, Mary Rinella, and Arun J. Sanyal. 2018. “Mechanisms of NAFLD Development and Therapeutic Strategies.” *Nature Medicine* 24 (7): 908–22. https://doi.org/10.1038/s41591-018-0104-9.
Fruci, Barbara, Stefania Giuliano, Angela Mazza, Roberta Malaguarnera, and Antonino Belfiore. 2013. “Nonalcoholic Fatty Liver: A Possible New Target for Type 2 Diabetes Prevention and Treatment.” *International Journal of Molecular Sciences* 14 (11): 22933–66. https://doi.org/10.3390/ijms141122933.
Fukuo, Yuka, Shunhei Yamashina, Hiroshi Sonoue, Atsushi Arakawa, Eisuke

Nakadera, Tomonori Aoyama, Akira Uchiyama, Kazuyoshi Kon, Kenichi Ikejima, and Sumio Watanabe. 2014. “Abnormality of Autophagic Function and Cathepsin Expression in the Liver from Patients with Non-Alcoholic Fatty Liver Disease.” *Hepatology Research* 44 (9): 1026–36. https://doi.org/10.1111/hepr.12282.

Fullerton, Morgan D, Sandra Galic, Katarina Marcinko, Sarah Sikkema, Thomas Pulinilkunnil, Zhi-ping Chen, Hayley M O Neill, et al. 2013. “Single Phosphorylation Sites in Acc1 and Acc2 Regulate Lipid Homeostasis and the Insulin-Sensitizing Effects of Metformin.” *Nature Medicine* 19 (12): 1649–54. https://doi.org/10.1038/nm.3372.

Galic, Sandra, Morgan D. Fullerton, Jonathan D. Schertzer, Sarah Sikkema, Katarina Marcinko, Carl R. Walkley, David Izon, et al. 2011. “Hematopoietic AMPK B1 Reduces Mouse Adipose Tissue Macrophage Inflammation and Insulin Resistance in Obesity.” *Journal of Clinical Investigation* 121 (12): 4903–15. https://doi.org/10.1172/JCI58577.

Gallage, Suchira, Jose Efren Barragan Avila, Pierluigi Ramadori, Enrico Focaccia, Mohammad Rahbari, Adnan Ali, Nisar P. Malek, Quentin M. Anstee, and Mathias Heikenwalder. 2022. “A Researcher’s Guide to Preclinical Mouse NASH Models.” *Nature Metabolism* 4 (December): 1632–49. https://doi.org/10.1038/s42255-022-00700-y.

Galluzzi, Lorenzo, Federico Pietrocola, José Manuel Bravo-San Pedro, Ravi K Amaravadi, Eric H Baehrecke, Francesco Cecconi, Patrice Codogno, et al. 2015. “Autophagy in Malignant Transformation and Cancer Progression.” *The EMBO Journal* 34 (7): 856–80. https://doi.org/10.15252/embj.201490784.

Gámez-Pérez, Yolanda, Gabriela Capllonch-Amer, Magdalena Gianotti, Isabel Lladá, and Ana M. Proenza. 2012. “Long-Term High-Fat-Diet Feeding Induces Skeletal Muscle Mitochondrial Biogenesis in Rats in a Sex-Dependent and Muscle-Type Specific Manner.” *Nutrition and Metabolism* 9: 1–10. https://doi.org/10.1186/1743-7075-9-15.

Garcia-Roves, Pablo, Janice M. Huss, Dong Ho Han, Chad R. Hancock, Eduardo Iglesias-Gutierrez, May Chen, and John O. Holloszy. 2007. “Raising Plasma Fatty Acid Concentration Induces Increased Biogenesis of Mitochondria in Skeletal Muscle.” *Proceedings of the National Academy of Sciences of the United States of America* 104 (25): 10709–13. https://doi.org/10.1073/pnas.0704024104.

Garcia, Daniel, Kristina Hellberg, Amandine Chaix, Martina Wallace, Sébastien Herzig, Mehmet G. Badur, Terry Lin, et al. 2019. “Genetic Liver-Specific AMPK Activation Protects against Diet-Induced Obesity and NAFLD.” *Cell Reports* 26 (1): 192-208.e6. https://doi.org/10.1016/j.celrep.2018.12.036.

Gawrieh, Samer, Mazen Noureddin, Nicole Loo, Rizwana Mohseni, Vivek Awasty, Kenneth Cusi, Kris V. Kowdley, et al. 2021. “Saroglitazar, a PPAR-α/γ Agonist, for Treatment of NAFLD: A Randomized Controlled Double-Blind Phase 2 Trial.” *Hepatology* 74 (4): 1809–24.

https://doi.org/10.1002/hep.31843.
Gebhardt, Rolf. 1992. “Metabolic Zonation of the Liver: Regulation and Implications for Liver Function.” *Pharmacology and Therapeutics* 53 (3): 275–354. https://doi.org/10.1016/0163-7258(92)90055-5.
Geeleher, Paul, Nancy J. Cox, and R. Stephanie Huang. 2014. “Clinical Drug Response Can Be Predicted Using Baseline Gene Expression Levels and in Vitro Drug Sensitivity in Cell Lines.” *Genome Biology* 15 (3): 1–12. https://doi.org/10.1186/gb-2014-15-3-r47.
Glick, Danielle, Wenshuo Zhang, Michelle Beaton, Glenn Marsboom, Michaela Gruber, M. Celeste Simon, John Hart, Gerald W. Dorn, Matthew J. Brady, and Kay F. Macleod. 2012. “BNip3 Regulates Mitochondrial Function and Lipid Metabolism in the Liver.” *Molecular and Cellular Biology* 32 (13): 2570–84. https://doi.org/10.1128/mcb.00167-12.
Gluais-Dagorn, Pascale, Marc Foretz, Gregory R. Steinberg, Battsetseg Batchuluun, Anna Zawistowska-Deniziak, Joost M. Lambooij, Bruno Guigas, et al. 2021. “Direct AMPK Activation Corrects NASH in Rodents Through Metabolic Effects and Direct Action on Inflammation and Fibrogenesis.” *Hepatology Communications* 0 (0): 1–19. https://doi.org/10.1002/hep4.1799.
Goedeke, Leigh, Jamie Bates, Daniel F. Vatner, Rachel J. Perry, Ting Wang, Ricardo Ramirez, Li Li, et al. 2018. “Acetyl-CoA Carboxylase Inhibition Reverses NAFLD and Hepatic Insulin Resistance but Promotes Hypertriglyceridemia in Rodents.” *Hepatology* 68 (6): 2197–2211. https://doi.org/10.1002/hep.30097.
González-Rodríguez, A., R. Mayoral, N. Agra, M. P. Valdecantos, V. Pardo, M. E. Miquilena-Colina, J. Vargas-Castrillón, et al. 2014. “Impaired Autophagic Flux Is Associated with Increased Endoplasmic Reticulum Stress during the Development of NAFLD.” *Cell Death and Disease* 5 (4). https://doi.org/10.1038/cddis.2014.162.
Govaere, Olivier, Simon Cockell, Dina Tiniakos, Rachel Queen, Ramy Younes, Michele Vacca, Leigh Alexander, et al. 2020. “Transcriptomic Profiling across the Nonalcoholic Fatty Liver Disease Spectrum Reveals Gene Signatures for Steatohepatitis and Fibrosis.” *Science Translational Medicine* 12 (572): 1–18. https://doi.org/10.1126/SCITRANSLMED.ABA4448.
Grefhorst, Aldo, Ivo P. van de Peppel, Lars E. Larsen, Johan W. Jonker, and Adriaan G. Holleboom. 2021. “The Role of Lipophagy in the Development and Treatment of Non-Alcoholic Fatty Liver Disease.” *Frontiers in Endocrinology* 11 (February): 1–12. https://doi.org/10.3389/fendo.2020.601627.
Gu, Xin, Yan Yan, Scott J. Novick, Amanda Kovach, Devrishi Goswami, Jiyuan Ke, M. H.Eileen Tan, et al. 2017. “Deconvoluting AMP-Activated Protein Kinase (AMPK) Adenine Nucleotide Binding and Sensing.” *Journal of Biological Chemistry* 292 (30): 12653–66. https://doi.org/10.1074/jbc.M117.793018.
Gwinn, Dana M, David B Shackelford, Daniel F Egan, Maria M Mihaylova,

Annabelle Mery, Debbie S Vasquez, Benjamin E Turk, and Reuben J Shaw. 2008. “AMPK Phosphorylation of Raptor Mediates a Metabolic Checkpoint.” *Molecular Cell* 30 (2): 214–26. https://doi.org/10.1016/j.molcel.2008.03.003.

Harrison, Stephen A., Alina M. Allen, Julie Dubourg, Mazen Noureddin, and Naim Alkhouri. 2023. “Challenges and Opportunities in NASH Drug Development.” *Nature Medicine*. https://doi.org/10.1038/s41591-023-02242-6.

Harrison, Stephen A., Mustafa R. Bashir, Cynthia D. Guy, Rong Zhou, Cynthia A. Moylan, Juan P. Frias, Naim Alkhouri, et al. 2019. “Resmetirom (MGL-3196) for the Treatment of Non-Alcoholic Steatohepatitis: A Multicentre, Randomised, Double-Blind, Placebo-Controlled, Phase 2 Trial.” *The Lancet* 394 (10213): 2012–24. https://doi.org/10.1016/S0140-6736(19)32517-6.

Hasenour, Clinton M., D. Emerson Ridley, Curtis C. Hughey, Freyja D. James, E. Patrick Donahue, Jane Shearer, Benoit Viollet, Marc Foretz, and David H. Wasserman. 2014. “5-Aminoimidazole-4-Carboxamide-1-β-D-Ribofuranoside (AICAR) Effect on Glucose Production, but Not Energy Metabolism, Is Independent of Hepatic AMPK in Vivo.” *Journal of Biological Chemistry* 289 (9): 5950–59. https://doi.org/10.1074/jbc.M113.528232.

Hasenour, Clinton M., D. Emerson Ridley, Freyja D. James, Curtis C. Hughey, E. Patrick Donahue, Benoit Viollet, Marc Foretz, Jamey D. Young, and David H. Wasserman. 2017. “Liver AMP-Activated Protein Kinase Is Unnecessary for Gluconeogenesis but Protects Energy State during Nutrient Deprivation.” *PLoS ONE* 12 (1): 12–15. https://doi.org/10.1371/journal.pone.0170382.

Hawley, S. A., M. D. Fullerton, F. A. Ross, J. D. Schertzer, C. Chevtzoff, K. J. Walker, M. W. Peggie, et al. 2012. “The Ancient Drug Salicylate Directly Activates AMP-Activated Protein Kinase.” *Science* 336 (6083): 918–22. https://doi.org/10.1126/science.1215327.

Hawley, Simon A., Jérôme Boudeau, Jennifer L. Reid, Kirsty J. Mustard, Lina Udd, Tomi P. Mäkelä, Dario R. Alessi, and D. Grahame Hardie. 2003. “Complexes between the LKB1 Tumor Suppressor, STRADα/β and MO25α/β Are Upstream Kinases in the AMP-Activated Protein Kinase Cascade.” *Journal of Biology* 2 (4): 1–16.

Hawley, Simon A., David A. Pan, Kirsty J. Mustard, Louise Ross, Jenny Bain, Arthur M. Edelman, Bruno G. Frenguelli, and D. Grahame Hardie. 2005. “Calmodulin-Dependent Protein Kinase Kinase-β Is an Alternative Upstream Kinase for AMP-Activated Protein Kinase.” *Cell Metabolism* 2 (1): 9–19. https://doi.org/10.1016/j.cmet.2005.05.009.

Herms, Albert, Marta Bosch, Babu J.N. Reddy, Nicole L. Schieber, Alba Fajardo, Celia Rupérez, Andrea Fernández-Vidal, et al. 2015. “AMPK Activation Promotes Lipid Droplet Dispersion on Detyrosinated Microtubules to Increase Mitochondrial Fatty Acid Oxidation.” *Nature Communications* 6 (May): 7176. https://doi.org/10.1038/ncomms8176.

Herzig, Sébastien, and Reuben J. Shaw. 2018. “AMPK: Guardian of Metabolism and Mitochondrial Homeostasis.” *Nature Reviews Molecular Cell Biology* 19 (2): 121–35. https://doi.org/10.1038/nrm.2017.95.

Hickson-Bick, Diane L.M., Maximilian L. Buja, and Jeanie B. McMillin. 2000. "Palmitate-Mediated Alterations in the Fatty Acid Metabolism of Rat Neonatal Cardiac Myocytes." *Journal of Molecular and Cellular Cardiology* 32 (3): 511–19. https://doi.org/10.1006/jmcc.1999.1098.

Horton, Jay D., Joseph L. Goldstein, and Michael S. Brown. 2002. "SREBPs: Activators of the Complete Program of Cholesterol and Fatty Acid Synthesis in the Liver." *Journal of Clinical Investigation* 109 (9): 1125–31. https://doi.org/10.1172/JCI0215593.

Hoshida, Yujin. 2010. "Nearest Template Prediction: A Single-Sample-Based Flexible Class Prediction with Confidence Assessment." *PLoS ONE* 5 (11): 1–8. https://doi.org/10.1371/journal.pone.0015543.

Houde, Vanessa P., Sara Donzelli, Andrea Sacconi, Sandra Galic, Joanne A. Hammill, Jonathan L. Bramson, Robert A. Foster, et al. 2017. "AMPK B1 Reduces Tumor Progression and Improves Survival in P53 Null Mice." *Molecular Oncology* 11 (9): 1143–55. https://doi.org/10.1002/1878-0261.12079.

Houten, Sander M., Sara Violante, Fatima V. Ventura, and Ronald J.A. Wanders. 2016. "The Biochemistry and Physiology of Mitochondrial Fatty Acid β-Oxidation and Its Genetic Disorders." *Annual Review of Physiology* 78: 23–44. https://doi.org/10.1146/annurev-physiol-021115-105045.

Houttu, Veera, Julia Bouts, Yasaman Vali, Joost Daams, Aldo Grefhorst, Max Nieuwdorp, and Adriaan G. Holleboom. 2022. "Does Aerobic Exercise Reduce NASH and Liver Fibrosis in Patients with Non-Alcoholic Fatty Liver Disease? A Systematic Literature Review and Meta-Analysis." *Frontiers in Endocrinology* 13 (November): 1–21. https://doi.org/10.3389/fendo.2022.1032164.

Hung, Chien Min, Portia S. Lombardo, Nazma Malik, Sonja N. Brun, Kristina Hellberg, Jeanine L. Van Nostrand, Daniel Garcia, et al. 2021. "AMPK/ULK1-Mediated Phosphorylation of Parkin ACT Domain Mediates an Early Step in Mitophagy." *Science Advances* 7 (15): 1–15. https://doi.org/10.1126/SCIADV.ABG4544.

Inoki, Ken, Tianqing Zhu, and Kun-Liang Guan. 2003. "TSC2 Mediates Cellular Energy Response to Control Cell Growth and Survival." *Cell* 115 (5): 577–90. https://doi.org/10.1016/s0092-8674(03)00929-2.

Iseli, Tristan J, Mark Walter, Bryce J W Van Denderen, Frosa Katsis, Lee A Witters, Bruce E Kemp, Belinda J Michell, and David Stapleton. 2005. "AMP-Activated Protein Kinase B Subunit Tethers a and y Subunits via Its C-Terminal Sequence (186 – 270)*." *The Journal of Biological Chemistry* 280 (14): 13395–400. https://doi.org/10.1074/jbc.M412993200.

Ishii, Seiji, Katsumi Iizuka, Bonnie C. Miller, and Kosaku Uyeda. 2004. "Carbohydrate Response Element Binding Protein Directly Promotes Lipogenic Enzyme Gene Transcription." *Proceedings of the National Academy of Sciences of the United States of America* 101 (44): 15597–602. https://doi.org/10.1073/pnas.0405238101.

Iwabu, Masato, Toshimasa Yamauchi, Miki Okada-iwabu, Koji Sato, Tatsuro Nakagawa, Masaaki Funata, Mamiko Yamaguchi, et al. 2010. “Adiponectin and AdipoR1 Regulate PGC-1 a and Mitochondria by Ca and AMPK / SIRT1.” *Nature* 464 (7293): 1313–19. https://doi.org/10.1038/nature08991.

Jager, Sibylle, Christoph Handschin, Julie St-Pierre, and Bruce M Spiegelman. 2007. “AMP-Activated Protein Kinase (AMPK) Action in Skeletal Muscle via Direct Phosphorylation of PGC-1a.” *Proceedings of the National Academy of Sciences* 104 (29): 12017–22.

Jeninga, E H, K Schoonjans, and J Auwerx. 2010. “Reversible Acetylation of PGC-1: Connecting Energy Sensors and Effectors to Guarantee Metabolic Flexibility.” *Oncogene* 29 (33): 4617–24. https://doi.org/10.1038/onc.2010.206.

Ji, Jingquan, Ming Feng, Yan Huang, and Xiaohong Niu. 2022. “Liraglutide Inhibits Receptor for Advanced Glycation End Products (RAGE)/Reduced Form of Nicotinamide-Adenine Dinucleotide Phosphate (NAPDH) Signaling to Ameliorate Non-Alcoholic Fatty Liver Disease (NAFLD) in Vivo and Vitro.” *Bioengineered* 13 (3): 5091–5102. https://doi.org/10.1080/21655979.2022.2036902.

Johanns, Manuel, Cyril Corbet, Roxane Jacobs, Melissa Drappier, Guido T. Bommer, Gaëtan Herinckx, Didier Vertommen, et al. 2022. “Inhibition of Basal and Glucagon-Induced Hepatic Glucose Production by 991 and Other Pharmacological AMPK Activators.” *Biochemical Journal* 479 (12): 1317–36. https://doi.org/10.1042/BCJ20220170.

Jørgensen, Sebastian B., Benoit Viollet, Fabrizio Andreelli, Christian Frøsig, Jesper B. Birk, Peter Schjerling, Sophie Vaulont, Erik A. Richter, and Jørgen F.P. Wojtaszewski. 2004. “Knockout of the A2 but Not A1, 5′-AMP-Activated Protein Kinase Isoform Abolishes 5-Aminoimidazole-4-Carboxamide-1-β-4-Ribofuranoside- but Not Contraction-Induced Glucose Uptake in Skeletal Muscle.” *Journal of Biological Chemistry* 279 (2): 1070–79. https://doi.org/10.1074/jbc.M306205200.

Jung, Seonghee, Hyeonjeong Jeong, and Seong Woon Yu. 2020. “Autophagy as a Decisive Process for Cell Death.” *Experimental and Molecular Medicine* 52 (6): 921–30. https://doi.org/10.1038/s12276-020-0455-4.

Karanam, Balasubramanyam, Lihua Jiang, Ling Wang, Neil L. Kelleher, and Philip A. Cole. 2006. “Kinetic and Mass Spectrometric Analysis of P300 Histone Acetyltransferase Domain Autoacetylation.” *Journal of Biological Chemistry* 281 (52): 40292–301. https://doi.org/10.1074/jbc.M608813200.

Kashima, Jumpei, Kaori Shintani-Ishida, Makoto Nakajima, Hideyuki Maeda, Kana Unuma, Yasuo Uchiyama, and Ken Ichi Yoshida. 2014. “Immunohistochemical Study of the Autophagy Marker Microtubule-Associated Protein 1 Light Chain 3 in Normal and Steatotic Human Livers.” *Hepatology Research* 44 (7): 779–87. https://doi.org/10.1111/hepr.12183.

Kaswala, Dharmesh H, Michelle Lai, and Nezam H Afdhal. 2016. “Fibrosis Assessment in Nonalcoholic Fatty Liver Disease (NAFLD) in 2016.”

Digestive Diseases and Sciences 61 (5): 1356–64. https://doi.org/10.1007/s10620-016-4079-4.

Kaushik, Susmita, and Ana Maria Cuervo. 2015. “Degradation of Lipid Droplet-Associated Proteins by Chaperone-Mediated Autophagy Facilitates Lipolysis.” *Nature Cell Biology* 17 (6): 759–70. https://doi.org/10.1038/ncb3166.

Keaney, JF. 2023. “Bempedoic Acid and the Prevention of Cardiovascular Disease.” *New England Journal of Medicine*, 1–4.

Kim, Chai Wan, Carol Addy, Jun Kusunoki, Norma N. Anderson, Stanislaw Deja, Xiaorong Fu, Shawn C. Burgess, et al. 2017a. “Acetyl CoA Carboxylase Inhibition Reduces Hepatic Steatosis but Elevates Plasma Triglycerides in Mice and Humans: A Bedside to Bench Investigation.” *Cell Metabolism* 26 (2): 394-406.e6. https://doi.org/10.1016/j.cmet.2017.07.009.

———. 2017b. “Acetyl CoA Carboxylase Inhibition Reduces Hepatic Steatosis but Elevates Plasma Triglycerides in Mice and Humans: A Bedside to Bench Investigation.” *Cell Metabolism* 26 (2): 394-406.e6. https://doi.org/10.1016/j.cmet.2017.07.009.

Kim, Joungmok, Mondira Kundu, Benoit Viollet, and Kun-Liang Guan. 2011. “AMPK and MTOR Regulate Autophagy through Direct Phosphorylation of Ulk1.” *Nature Cell Biology* 13 (2): 132–41. https://doi.org/10.1038/ncb2152.

Kleiner, David E., Elizabeth M. Brunt, Mark Van Natta, Cynthia Behling, Melissa J. Contos, Oscar W. Cummings, Linda D. Ferrell, et al. 2005. “Design and Validation of a Histological Scoring System for Nonalcoholic Fatty Liver Disease.” *Hepatology* 41 (6): 1313–21. https://doi.org/10.1002/hep.20701.

Klionsky, Daniel J., Amal Kamal Abdel-Aziz, Sara Abdelfatah, Mahmoud Abdellatif, Asghar Abdoli, Steffen Abel, Hagai Abeliovich, et al. 2021. “Guidelines for the Use and Interpretation of Assays for Monitoring Autophagy (4th Edition)1.” *Autophagy* 17 (1): 1–382. https://doi.org/10.1080/15548627.2020.1797280.

Konerman, Monica A., Jacob C. Jones, and Stephen A. Harrison. 2018. “Pharmacotherapy for NASH: Current and Emerging.” *Journal of Hepatology* 68 (2): 362–75. https://doi.org/10.1016/j.jhep.2017.10.015.

Lambert, Jennifer E., Maria A. Ramos-Roman, Jeffrey D. Browning, and Elizabeth J. Parks. 2014. “Increased de Novo Lipogenesis Is a Distinct Characteristic of Individuals with Nonalcoholic Fatty Liver Disease.” *Gastroenterology* 146 (3): 726–35. https://doi.org/10.1053/j.gastro.2013.11.049.

Lawitz, Eric J., Angie Coste, Fred Poordad, Naim Alkhouri, Nicole Loo, Bryan J. McColgan, Jacqueline M. Tarrant, et al. 2018. “Acetyl-CoA Carboxylase Inhibitor GS-0976 for 12 Weeks Reduces Hepatic De Novo Lipogenesis and Steatosis in Patients With Nonalcoholic Steatohepatitis.” *Clinical Gastroenterology and Hepatology* 16 (12): 1983-1991.e3. https://doi.org/10.1016/j.cgh.2018.04.042.

Lawitz, Eric J, Bal Raj Bhandari, Peter J Ruane, Anita Kohli, Eliza Harting, Dora

Ding, Jen-Chieh Chuang, et al. 2023. “Fenofibrate Mitigates Hypertriglyceridemia in Nonalcoholic Steatohepatitis Patients Treated With Cilofexor/Firsocostat.” *Clinical Gastroenterology and Hepatology : The Official Clinical Practice Journal of the American Gastroenterological Association* 21 (1): 143-152.e3. https://doi.org/10.1016/j.cgh.2021.12.044.

Lazarus, Jeffrey V., Henry E. Mark, Quentin M. Anstee, Juan Pablo Arab, Rachel L. Batterham, Laurent Castera, Helena Cortez-Pinto, et al. 2021. “Advancing the Global Public Health Agenda for NAFLD: A Consensus Statement.” *Nature Reviews Gastroenterology & Hepatology* 0123456789. https://doi.org/10.1038/s41575-021-00523-4.

Lee, In Hye, and Toren Finkel. 2009. “Regulation of Autophagy by the P300 Acetyltransferase.” *Journal of Biological Chemistry* 284 (10): 6322–28. https://doi.org/10.1074/jbc.M807135200.

Lee, Y., X. Yu, F. Gonzales, D. J. Mangelsdorf, May Yun Wang, C. Richardson, L. A. Witters, and R. H. Unger. 2002. “PPARα Is Necessary for the Lipopenic Action of Hyperleptinemia on White Adipose and Liver Tissue.” *Proceedings of the National Academy of Sciences of the United States of America* 99 (18): 11848–53. https://doi.org/10.1073/pnas.182420899.

Leite, Nathalie C, Gil F Salles, Antonio L E Araujo, Cristiane A Villela-Nogueira, and Claudia R L Cardoso. 2009. “Prevalence and Associated Factors of Non-Alcoholic Fatty Liver Disease in Patients with Type-2 Diabetes Mellitus.” *Liver International : Official Journal of the International Association for the Study of the Liver* 29 (1): 113–19. https://doi.org/10.1111/j.1478-3231.2008.01718.x.

Lerin, Carles, Joseph T Rodgers, Dario E Kalume, Seung-hee Kim, Akhilesh Pandey, and Pere Puigserver. 2006. “GCN5 Acetyltransferase Complex Controls Glucose Metabolism through Transcriptional Repression of PGC-1alpha.” *Cell Metabolism* 3 (6): 429–38. https://doi.org/10.1016/j.cmet.2006.04.013.

Li, Ya Kun, Dong Xia Ma, Zhi Min Wang, Xiao Fan Hu, Shang Lin Li, Hong Zhe Tian, Meng Jun Wang, Yan Wen Shu, and Jun Yang. 2018. “The Glucagon-like Peptide-1 (GLP-1) Analog Liraglutide Attenuates Renal Fibrosis.” *Pharmacological Research* 131 (February): 102–11. https://doi.org/10.1016/j.phrs.2018.03.004.

Liang, Danyang, Yisha Zhuo, Zeheng Guo, Lihua He, Xueyi Wang, Yulong He, Lexing Li, and Hanchuan Dai. 2020. “SIRT1/PGC-1 Pathway Activation Triggers Autophagy/Mitophagy and Attenuates Oxidative Damage in Intestinal Epithelial Cells.” *Biochimie* 170 (March): 10–20. https://doi.org/10.1016/j.biochi.2019.12.001.

Liang, Zhenxing, Tian Li, Shuai Jiang, Jing Xu, Wencheng di, Zhi Yang, Wei Hu, and Yang Yang. 2017. “AMPK: A Novel Target for Treating Hepatic Fibrosis.” *Oncotarget* 8 (37): 62780–92. https://doi.org/10.18632/oncotarget.19376.

Lobstein, Tim, Rachel Jackson-leach, Jaynaide Powis, Hannah Brinsden, and Maggie Gray. 2023. “World Obesity Atlas 2023.”

Loomba, Rohit, Manal F Abdelmalek, Matthew J Armstrong, Maximilian Jara, Mette Skalshøi Kjær, Niels Krarup, Eric Lawitz, and Vlad Ratziu. 2023. "Semaglutide 2.4 Mg Once Weekly in Patients with Non-Alcoholic Steatohepatitis-Related Cirrhosis : A Randomised , Placebo-Controlled Phase 2 Trial." *The Lancet. Gastroenterology & Hepatology* 1253 (23): 1–12. https://doi.org/10.1016/S2468-1253(23)00068-7.

Loomba, Rohit, Maria Abraham, Aynur Unalp, Laura Wilson, Joel Lavine, Ed Doo, and Nathan M. Bass. 2012. "Association between Diabetes, Family History of Diabetes, and Risk of Nonalcoholic Steatohepatitis and Fibrosis." *Hepatology* 56 (3): 943–51. https://doi.org/10.1002/hep.25772.

Loomba, Rohit, Scott L. Friedman, and Gerald I. Shulman. 2021. "Mechanisms and Disease Consequences of Nonalcoholic Fatty Liver Disease." *Cell* 184 (10): 2537–64. https://doi.org/10.1016/j.cell.2021.04.015.

Loomba, Rohit, Zeid Kayali, Mazen Noureddin, Peter Ruane, Eric J. Lawitz, Michael Bennett, Lulu Wang, et al. 2018. "GS-0976 Reduces Hepatic Steatosis and Fibrosis Markers in Patients With Nonalcoholic Fatty Liver Disease." *Gastroenterology* 155 (5): 1463-1473.e6. https://doi.org/10.1053/j.gastro.2018.07.027.

Ma, Lin, Luke N. Robinson, and Howard C. Towle. 2006. "ChREBP·Mlx Is the Principal Mediator of Glucose-Induced Gene Expression in the Liver." *Journal of Biological Chemistry* 281 (39): 28721–30. https://doi.org/10.1074/jbc.M601576200.

Machovič, Martin, and Štefan Janeček. 2006. "The Evolution of Putative Starch-Binding Domains." *FEBS Letters* 580 (27): 6349–56. https://doi.org/10.1016/j.febslet.2006.10.041.

Madeo, Frank, Federico Pietrocola, Tobias Eisenberg, and Guido Kroemer. 2014. "Caloric Restriction Mimetics: Towards a Molecular Definition." *Nature Reviews Drug Discovery* 13 (10): 727–40. https://doi.org/10.1038/nrd4391.

Magkos, Faidon, Gemma Fraterrigo, Jun Yoshino, Courtney Luecking, Kyleigh Kirbach, Shannon C. Kelly, Lisa De Las Fuentes, et al. 2016. "Effects of Moderate and Subsequent Progressive Weight Loss on Metabolic Function and Adipose Tissue Biology in Humans with Obesity." *Cell Metabolism* 23 (4): 591–601. https://doi.org/10.1016/j.cmet.2016.02.005.

Mancina, Rosellina Margherita, Paola Dongiovanni, Salvatore Petta, Piero Pingitore, Marica Meroni, Raffaela Rametta, Jan Borén, et al. 2016. "The MBOAT7-TMC4 Variant Rs641738 Increases Risk of Nonalcoholic Fatty Liver Disease in Individuals of European Descent." *Gastroenterology* 150 (5): 1219-1230.e6. https://doi.org/10.1053/j.gastro.2016.01.032.

Mardinoglu, Adil, Hao Wu, Elias Bjornson, Cheng Zhang, Antti Hakkarainen, Sari M. Räsänen, Sunjae Lee, et al. 2018. "An Integrated Understanding of the Rapid Metabolic Benefits of a Carbohydrate-Restricted Diet on Hepatic Steatosis in Humans." *Cell Metabolism* 27 (3): 559-571.e5. https://doi.org/10.1016/j.cmet.2018.01.005.

Mariño, Guillermo, Federico Pietrocola, Tobias Eisenberg, Yongli Kong, Shoaib

Ahmad Malik, Aleksandra Andryushkova, Sabrina Schroeder, et al. 2014. “Regulation of Autophagy by Cytosolic Acetyl-Coenzyme A.” *Molecular Cell* 53 (5): 710–25. https://doi.org/10.1016/j.molcel.2014.01.016.

Matsuzaka, Takashi, Hitoshi Shimano, Naoya Yahagi, Michiyo Amemiya-Kudo, Hiroaki Okazaki, Yoshiaki Tamura, Yoko Iizuka, et al. 2004. “Insulin-Independent Induction of Sterol Regulatory Element-Binding Protein-1c Expression in the Livers of Streptozotocin-Treated Mice.” *Diabetes* 53 (3): 560–69. https://doi.org/10.2337/diabetes.53.3.560.

Mauthe, Mario, Idil Orhon, Cecilia Rocchi, Xingdong Zhou, Morten Luhr, Kerst Jan Hijlkema, Robert P. Coppes, Nikolai Engedal, Muriel Mari, and Fulvio Reggiori. 2018. “Chloroquine Inhibits Autophagic Flux by Decreasing Autophagosome-Lysosome Fusion.” *Autophagy* 14 (8): 1435–55. https://doi.org/10.1080/15548627.2018.1474314.

McGee, Sean L., Bryce J.W. Van Denderen, Kirsten F. Howlett, Janelle Mollica, Jonathan D. Schertzer, Bruce E. Kemp, and Mark Hargreaves. 2008. “AMP-Activated Protein Kinase Regulates GLUT4 Transcription by Phosphorylating Histone Deacetylase 5.” *Diabetes* 57 (4): 860–67. https://doi.org/10.2337/db07-0843.

McLean, Brent A., Chi Kin Wong, M Golam Kabir, and Daniel J. Drucker. 2022. *Glucagon-Like Peptide-1 Receptor Tie2+ Cells Are Essential for the Cardioprotective Actions of Liraglutide in Mice with Experimental Myocardial Infarction*. *Molecular Metabolism*. Elsevier GmbH. https://doi.org/10.1016/j.molmet.2022.101641.

McLean, Brent A., Chi Kin Wong, Kiran Deep Kaur, Randy J. Seeley, and Daniel J. Drucker. 2021. “Differential Importance of Endothelial and Hematopoietic Cell GLP-1Rs for Cardiometabolic versus Hepatic Actions of Semaglutide.” *JCI Insight* 6 (22). https://doi.org/10.1172/jci.insight.153732.

McLean, Brent A, Chi Kin Wong, Jonathan E Campbell, David J Hodson, Stefan Trapp, and Daniel J Drucker. 2021. “Revisiting the Complexity of GLP-1 Action from Sites of Synthesis to Receptor Activation.” *Endocrine Reviews* 42 (2): 101–32. https://doi.org/10.1210/endrev/bnaa032.

McLean, Brent, Chi Kin Wong, Kiran Deep Kaur, Randy J. Seeley, and Daniel J. Drucker. 2021. “Differential Importance of Endothelial and Hematopoietic Cell GLP-1Rs for Cardiometabolic vs. Hepatic Actions of Semaglutide.” *JCI Insight*. https://doi.org/10.1172/jci.insight.153732.

Michalopoulos, George K., and Bharat Bhushan. 2021. “Liver Regeneration: Biological and Pathological Mechanisms and Implications.” *Nature Reviews Gastroenterology and Hepatology* 18 (1): 40–55. https://doi.org/10.1038/s41575-020-0342-4.

Mihaylova, Maria M., Debbie S. Vasquez, Kim Ravnskjaer, Pierre Damien Denechaud, Ruth T. Yu, Jacqueline G. Alvarez, Michael Downes, Ronald M. Evans, Marc Montminy, and Reuben J. Shaw. 2011. “Class IIa Histone Deacetylases Are Hormone-Activated Regulators of FOXO and Mammalian Glucose Homeostasis.” *Cell* 145 (4): 607–21.

https://doi.org/10.1016/j.cell.2011.03.043.
Miller, Russell A, Qingwei Chu, Jianxin Xie, Marc Foretz, Benoit Viollet, and Morris J Birnbaum. 2013. “Biguanides Suppress Hepatic Glucagon Signalling by Decreasing Production of Cyclic AMP.” *Nature* 494 (7436): 256–60. https://doi.org/10.1038/nature11808.
Mitchelhill, Ken I., Belinda J. Michell, Colin M. House, David Stapleton, Jason Dyck, James Gamble, Christina Ullrich, Lee A. Witters, and Bruce E. Kemp. 1997. “Posttranslational Modifications of the 5’-AMP-Activated Protein Kinase B1 Subunit.” *Journal of Biological Chemistry* 272 (39): 24475–79. https://doi.org/10.1074/jbc.272.39.24475.
Miyagawa, Koichiro, Shinji Oe, Yuichi Honma, Hiroto Izumi, Ryoko Baba, and Masaru Harada. 2016. “Lipid-Induced Endoplasmic Reticulum Stress Impairs Selective Autophagy at the Step of Autophagosome-Lysosome Fusion in Hepatocytes.” *American Journal of Pathology* 186 (7): 1861–73. https://doi.org/10.1016/j.ajpath.2016.03.003.
Moore, Mary P., Rory P. Cunningham, Grace M. Meers, Sarah A. Johnson, Andrew A. Wheeler, Rama R. Ganga, Nicole M. Spencer, et al. 2022. “Compromised Hepatic Mitochondrial Fatty Acid Oxidation and Reduced Markers of Mitochondrial Turnover in Human NAFLD.” *Hepatology* 76 (5): 1452–65. https://doi.org/10.1002/hep.32324.
Morrow, Marisa R., Battsetseg Batchuluun, Jianhan Wu, Elham Ahmadi, Julie M. Leroux, Pedrum Mohammadi-Shemirani, Eric M. Desjardins, et al. 2022. “Inhibition of ATP-Citrate Lyase Improves NASH, Liver Fibrosis, and Dyslipidemia.” *Cell Metabolism* 34 (6): 919-936.e8. https://doi.org/10.1016/j.cmet.2022.05.004.
Mottillo, Emilio P., Eric M. Desjardins, Justin D. Crane, Brennan K. Smith, Alex E. Green, Serge Ducommun, Tora I. Henriksen, et al. 2016. “Lack of Adipocyte AMPK Exacerbates Insulin Resistance and Hepatic Steatosis through Brown and Beige Adipose Tissue Function.” *Cell Metabolism* 24 (1): 118–29. https://doi.org/10.1016/j.cmet.2016.06.006.
Munday, M R. 2002. “Regulation of Mammalian Acetyl-CoA Carboxylase.” *Biochemical Society Transactions* 30 (6): 1059–64.
Musso, G, M Cassader, F Rosina, and R Gambino. 2012. “Impact of Current Treatments on Liver Disease, Glucose Metabolism and Cardiovascular Risk in Non-Alcoholic Fatty Liver Disease (NAFLD): A Systematic Review and Meta-Analysis of Randomised Trials.” *Diabetologia* 55 (4): 885–904. https://doi.org/10.1007/s00125-011-2446-4.
Myers, Robert W., Hong Ping Guan, Juliann Ehrhart, Aleksandr Petrov, Srinivasa Prahalada, Effie Tozzo, Xiaodong Yang, et al. 2017. “Systemic Pan-AMPK Activator MK-8722 Improves Glucose Homeostasis but Induces Cardiac Hypertrophy.” *Science* 357 (6350): 507–11. https://doi.org/10.1126/science.aah5582.
Nagai, Yoshio, Shin Yonemitsu, Derek M Erion, Takanori Iwasaki, Romana Stark, Dirk Weismann, Jianying Dong, et al. 2009. “The Role of Peroxisome

Proliferator-Activated Receptor Gamma Coactivator-1 Beta in the Pathogenesis of Fructose-Induced Insulin Resistance." *Cell Metabolism* 9 (3): 252–64. https://doi.org/10.1016/j.cmet.2009.01.011.

Napolitano, Gennaro, and Andrea Ballabio. 2016. "TFEB at a Glance." *Journal of Cell Science* 129 (13): 2475–81. https://doi.org/10.1242/jcs.146365.

Neopane, Katyayanee, Natalie Kozlov, Florentina Negoita, Lisa Murray-Segal, Robert Brink, Ashfaqul Hoque, Ashley J. Ovens, et al. 2022. "Blocking AMPK B1 Myristoylation Enhances AMPK Activity and Protects Mice from High-Fat Diet-Induced Obesity and Hepatic Steatosis." *Cell Reports* 41 (12): 111862. https://doi.org/10.1016/j.celrep.2022.111862.

Neuschwander-Tetri, Brent A. 2017. "Non-Alcoholic Fatty Liver Disease." *BMC Medicine* 15 (1): 1–6. https://doi.org/10.1186/s12916-017-0806-8.

Newsome, Philip N., Kristine Buchholtz, Kenneth Cusi, Martin Linder, Takeshi Okanoue, Vlad Ratziu, Arun J. Sanyal, Anne-Sophie Sejling, and Stephen A. Harrison. 2021. "A Placebo-Controlled Trial of Subcutaneous Semaglutide in Nonalcoholic Steatohepatitis." *New England Journal of Medicine* 384 (12): 1113–24. https://doi.org/10.1056/nejmoa2028395.

Nissen, SE, AM Lincoff, D Brennan, KK Ray, D Mason, JJP Kastelein, P D Thompson, et al. 2023. "Bempedoic Acid and Cardiovascular Outcomes in Statin-Intolerant Patients." *New England Journal of Medicine*, 1–12. https://doi.org/10.1056/NEJMoa2215024.

O'Neill, Hayley M, Stine J Maarbjerg, Justin D Crane, Jacob Jeppesen, Sebastian B Jørgensen, Jonathan D Schertzer, Olga Shyroka, et al. 2011. "AMP-Activated Protein Kinase (AMPK) Beta1beta2 Muscle Null Mice Reveal an Essential Role for AMPK in Maintaining Mitochondrial Content and Glucose Uptake during Exercise." *Proceedings of the National Academy of Sciences of the United States of America* 108 (38): 16092–97. https://doi.org/10.1073/pnas.1105062108.

O'Neill, Hayley M O, James S Lally, Sandra Galic, Melissa Thomas, Paymon D Azizi, Morgan D Fullerton, Brennan K Smith, et al. 2014. "AMPK Phosphorylation of ACC2 Is Required for Skeletal Muscle Fatty Acid Oxidation and Insulin Sensitivity in Mice." *Diabetologia* 57: 1693–1702. https://doi.org/10.1007/s00125-014-3273-1.

Oakhill, Jonathan S., Zhi Ping Chen, John W. Scott, Rohan Steel, Laura A. Castelli, Naomi Linga, S. Lance Macaulay, and Bruce E. Kemp. 2010. "β-Subunit Myristoylation Is the Gatekeeper for Initiating Metabolic Stress Sensing by AMP-Activated Protein Kinase (AMPK)." *Proceedings of the National Academy of Sciences of the United States of America* 107 (45): 19237–41. https://doi.org/10.1073/pnas.1009705107.

Ogiwara, Hideo, Tadashi Tanabe, Jun-ichi Nikawa, and Shosaku Numa. 1978. "Inhibition of Rat-Liver Acetyl-Coenzyme-A Carboxylase by Palmitoyl-Coenzyme A." *European Journal of Biochemistry* 89: 33–41.

Omokaro, Stephanie O., and Julie K. Golden. 2020. "The Regulatory State of Nonalcoholic Steatohepatitis and Metabolism." *Endocrinology, Diabetes and*

Metabolism 3 (4): 1–6. https://doi.org/10.1002/edm2.113.

Pafili, Kalliopi, and Michael Roden. 2021. “Nonalcoholic Fatty Liver Disease (NAFLD) from Pathogenesis to Treatment Concepts in Humans.” *Molecular Metabolism* 50 (November 2020): 1–20. https://doi.org/10.1016/j.molmet.2020.101122.

Paquette, Mathieu, Leeanna El-Houjeiri, Linda C. Zirden, Pietri Puustinen, Paola Blanchette, Hyeonju Jeong, Kurt Dejgaard, Peter M. Siegel, and Arnim Pause. 2021. “AMPK-Dependent Phosphorylation Is Required for Transcriptional Activation of TFEB and TFE3.” *Autophagy* 17 (12): 3957–75. https://doi.org/10.1080/15548627.2021.1898748.

Park, Seokjae, Sungjoon Oh, and Eun Kyoung Kim. 2022. “Glucagon-like Peptide-1 Analog Liraglutide Leads to Multiple Metabolic Alterations in Diet-Induced Obese Mice.” *Journal of Biological Chemistry* 298 (12): 102682. https://doi.org/10.1016/j.jbc.2022.102682.

Pattingre, Sophie, Amina Tassa, Xueping Qu, Rita Garuti, Huan Liang Xiao, Noboru Mizushima, Milton Packer, Michael D. Schneider, and Beth Levine. 2005. “Bcl-2 Antiapoptotic Proteins Inhibit Beclin 1-Dependent Autophagy.” *Cell* 122 (6): 927–39. https://doi.org/10.1016/j.cell.2005.07.002.

Payen, Valéry L., Arnaud Lavergne, Niki Alevra Sarika, Megan Colonval, Latifa Karim, Manon Deckers, Mustapha Najimi, et al. 2021. “Single-Cell RNA Sequencing of Human Liver Reveals Hepatic Stellate Cell Heterogeneity.” *JHEP Reports* 3 (3): 100278. https://doi.org/10.1016/j.jhepr.2021.100278.

Perry, Rachel J, João-paulo G Camporez, Romy Kursawe, Paul M Titchenell, Dongyan Zhang, Curtis J Perry, Michael J Jurczak, et al. 2015. “Hepatic Acetyl CoA Links Adipose Tissue Inflammation to Hepatic Insulin Resistance and Type 2 Diabetes.” *Cell* 160 (4): 745–58. https://doi.org/10.1016/j.cell.2015.01.012.Hepatic.

Petersen, Max C., and Gerald I. Shulman. 2018. “Mechanisms of Insulin Action and Insulin Resistance.” *Physiological Reviews* 98 (4): 2133–2223. https://doi.org/10.1152/physrev.00063.2017.

Petit, Jean Michel, Jean Pierre Cercueil, Romaric Loffroy, Damien Denimal, Benjamin Bouillet, Coralie Fourmont, Olivier Chevallier, Laurence Duvillard, and Bruno Vergès. 2017. “Effect of Liraglutide Therapy on Liver Fat Content in Patients with Inadequately Controlled Type 2 Diabetes: The Lira-NAFLD Study.” *Journal of Clinical Endocrinology and Metabolism* 102 (2): 407–15. https://doi.org/10.1210/jc.2016-2775.

Petta, Salvatore, Luca Miele, Elisabetta Bugianesi, Calogero Cammà, Chiara Rosso, Stefania Boccia, Daniela Cabibi, et al. 2014. “Glucokinase Regulatory Protein Gene Polymorphism Affects Liver Fibrosis in Non-Alcoholic Fatty Liver Disease.” *PLoS ONE* 9 (2): 1–7. https://doi.org/10.1371/journal.pone.0087523.

Pietrocola, Federico, Francesca Castoldi, Maria Markaki, Sylvie Lachkar, Guo Chen, David P. Enot, Sylvere Durand, et al. 2018. “Aspirin Recapitulates Features of Caloric Restriction.” *Cell Reports* 22 (9): 2395–2407.

https://doi.org/10.1016/j.celrep.2018.02.024.
Pietrocola, Federico, Lorenzo Galluzzi, José Manuel Bravo-San Pedro, Frank Madeo, and Guido Kroemer. 2015. “Acetyl Coenzyme A: A Central Metabolite and Second Messenger.” *Cell Metabolism* 21 (6): 805–21. https://doi.org/10.1016/j.cmet.2015.05.014.
Pinkosky, Stephen L., Sergey Filippov, Rai Ajit K. Srivastava, Jeffrey C. Hanselman, Cheryl D. Bradshaw, Timothy R. Hurley, Clay T. Cramer, et al. 2013a. “AMP-Activated Protein Kinase and ATP-Citrate Lyase Are Two Distinct Molecular Targets for ETC-1002, a Novel Small Molecule Regulator of Lipid and Carbohydrate Metabolism.” *Journal of Lipid Research* 54 (1): 134–51. https://doi.org/10.1194/jlr.M030528.
———. 2013b. “AMP-Activated Protein Kinase and ATP-Citrate Lyase Are Two Distinct Molecular Targets for ETC-1002, a Novel Small Molecule Regulator of Lipid and Carbohydrate Metabolism.” *Journal of Lipid Research* 54 (1): 134–51. https://doi.org/10.1194/jlr.M030528.
Pinkosky, Stephen L., Pieter H.E. Groot, Narendra D. Lalwani, and Gregory R. Steinberg. 2017. “Targeting ATP-Citrate Lyase in Hyperlipidemia and Metabolic Disorders.” *Trends in Molecular Medicine* 23 (11): 1047–63. https://doi.org/10.1016/j.molmed.2017.09.001.
Pinkosky, Stephen L., Roger S. Newton, Emily A. Day, Rebecca J. Ford, Sarka Lhotak, Richard C. Austin, Carolyn M. Birch, et al. 2016. “Liver-Specific ATP-Citrate Lyase Inhibition by Bempedoic Acid Decreases LDL-C and Attenuates Atherosclerosis.” *Nature Communications* 7 (May). https://doi.org/10.1038/ncomms13457.
Pinkosky, Stephen L., John W. Scott, Eric M. Desjardins, Brennan K. Smith, Emily A. Day, Rebecca J. Ford, Christopher G. Langendorf, et al. 2020. “Long-Chain Fatty Acyl-CoA Esters Regulate Metabolism via Allosteric Control of AMPK B1 Isoforms.” *Nature Metabolism*. https://doi.org/10.1038/s42255-020-0245-2.
Pockros, Paul J, Michael Fuchs, Bradley Freilich, Eugene Schiff, Anita Kohli, Eric J Lawitz, Paul A Hellstern, et al. 2019. “CONTROL: A Randomized Phase 2 Study of Obeticholic Acid and Atorvastatin on Lipoproteins in Nonalcoholic Steatohepatitis Patients.” *Liver International : Official Journal of the International Association for the Study of the Liver* 39 (11): 2082–93. https://doi.org/10.1111/liv.14209.
Ponugoti, Bhaskar, Dong Hyun Kim, Zhen Xiao, Zachary Smith, Ji Miao, Mengwei Zang, Shwu Yuan Wu, Cheng Ming Chiang, Timothy D. Veenstra, and Jongsook Kim Kemper. 2010. “SIRT1 Deacetylates and Inhibits SREBP-1C Activity in Regulation of Hepatic Lipid Metabolism.” *Journal of Biological Chemistry* 285 (44): 33959–70. https://doi.org/10.1074/jbc.M110.122978.
Prashanth, M, H K Ganesh, M V Vima, M John, T Bandgar, Shashank R Joshi, S R Shah, et al. 2009. “Prevalence of Nonalcoholic Fatty Liver Disease in Patients with Type 2 Diabetes Mellitus.” *The Journal of the Association of Physicians of India* 57 (March): 205–10.

Quintana-Cabrera, Rubén, and Luca Scorrano. 2023. “Determinants and Outcomes of Mitochondrial Dynamics.” *Molecular Cell* 1: 857–76. https://doi.org/10.1016/j.molcel.2023.02.012.

Ramos, Vitor de Miranda, Alicia J. Kowaltowski, and Pamela A. Kakimoto. 2021. “Autophagy in Hepatic Steatosis: A Structured Review.” *Frontiers in Cell and Developmental Biology* 9 (April). https://doi.org/10.3389/fcell.2021.657389.

Ray, Kausik K., Harold E. Bays, Alberico L. Catapano, Narendra D. Lalwani, LeAnne T. Bloedon, Lulu R. Sterling, Paula L. Robinson, and Christie M. Ballantyne. 2019. “Safety and Efficacy of Bempedoic Acid to Reduce LDL Cholesterol.” *New England Journal of Medicine* 380 (11): 1022–32. https://doi.org/10.1056/nejmoa1803917.

Ridker, Paul M, Lei Lei, Kausik K Ray, Christie M Ballantyne, Gary Bradwin, and Nader Rifai. 2023. “Effects of Bempedoic Acid on CRP , IL-6 , Fibrinogen and Lipoprotein (a) in Patients with Residual Inflammatory Risk : A Secondary Analysis of the CLEAR Harmony Trial.” *Journal of Clinical Lipidology*, 1–6. https://doi.org/10.1016/j.jacl.2023.02.002.

Rinella, Mary E, Brent A Neuschwander-Tetri, Mohammad Shadab Siddiqui, Manal F Abdelmalek, Stephen Caldwell, Diana Barb, David E Kleiner, and Rohit Loomba. 2023. *AASLD Practice Guidance on the Clinical Assessment and Management of Nonalcoholic Fatty Liver Disease. Hepatology (Baltimore, Md.)*. https://doi.org/10.1097/HEP.0000000000000323.

Romero-Gómez, Manuel, Shira Zelber-Sagi, and Michael Trenell. 2017. “Treatment of NAFLD with Diet, Physical Activity and Exercise.” *Journal of Hepatology* 67 (4): 829–46. https://doi.org/10.1016/j.jhep.2017.05.016.

Rose, Kristy St., Jun Yan, Fangxi Xu, Jasmine Williams, Virginia Dweck, Deepak Saxena, Robert F. Schwabe, and Jorge Matias Caviglia. 2022. “Mouse Model of NASH That Replicates Key Features of the Human Disease and Progresses to Fibrosis Stage 3.” *Hepatology Communications* 6 (10): 2676–88. https://doi.org/10.1002/hep4.2035.

Rui, Liangyou. 2017. “Energy Metabolism in the Liver Liangyou Rui.” *Physiology & Behavior* 176 (5): 139–48. https://doi.org/10.1002/cphy.c130024.Energy.

Ryaboshapkina, Maria, and Mårten Hammar. 2017. “Human Hepatic Gene Expression Signature of Non-Alcoholic Fatty Liver Disease Progression, a Meta-Analysis.” *Scientific Reports* 7 (1): 1–12. https://doi.org/10.1038/s41598-017-10930-w.

Ryan, Marno C., Catherine Itsiopoulos, Tania Thodis, Glenn Ward, Nicholas Trost, Sophie Hofferberth, Kerin O’Dea, Paul V. Desmond, Nathan A. Johnson, and Andrew M. Wilson. 2013. “The Mediterranean Diet Improves Hepatic Steatosis and Insulin Sensitivity in Individuals with Non-Alcoholic Fatty Liver Disease.” *Journal of Hepatology* 59 (1): 138–43. https://doi.org/10.1016/j.jhep.2013.02.012.

Samsoondar, Joshua P., Amy C. Burke, Brian G. Sutherland, Dawn E. Telford, Cynthia G. Sawyez, Jane Y. Edwards, Stephen L. Pinkosky, Roger S. Newton, and Murray W. Huff. 2017. “Prevention of Diet-Induced Metabolic

Dysregulation, Inflammation, and Atherosclerosis in Ldlr-/- Mice by Treatment with the ATP-Citrate Lyase Inhibitor Bempedoic Acid." *Arteriosclerosis, Thrombosis, and Vascular Biology* 37 (4): 647–56. https://doi.org/10.1161/ATVBAHA.116.308963.

Samuel, Varman T., Zhen Xiang Liu, Amy Wang, Sara A. Beddow, John G. Geisler, Mario Kahn, Xian Man Zhang, Brett P. Monia, Sanjay Bhanot, and Gerald I. Shulman. 2007. "Inhibition of Protein Kinase Cε Prevents Hepatic Insulin Resistance in Nonalcoholic Fatty Liver Disease." *Journal of Clinical Investigation* 117 (3): 739–45. https://doi.org/10.1172/JCI30400.

Samuel, Varman T., and Gerald I. Shulman. 2016. "The Pathogenesis of Insulin Resistance: Integrating Signaling Pathways and Substrate Flux." *Journal of Clinical Investigation* 126 (1): 12–22. https://doi.org/10.1172/JCI77812.

Sanchez, Anthony M.J., Alfredo Csibi, Audrey Raibon, Karen Cornille, Stéphanie Gay, Henri Bernardi, and Robin Candau. 2012. "AMPK Promotes Skeletal Muscle Autophagy through Activation of Forkhead FoxO3a and Interaction with Ulk1." *Journal of Cellular Biochemistry* 113 (2): 695–710. https://doi.org/10.1002/jcb.23399.

Schneider, Jaime L., Yousin Suh, and Ana Maria Cuervo. 2014. "Deficient Chaperone-Mediated Autophagy in Liver Leads to Metabolic Dysregulation." *Cell Metabolism* 20 (3): 417–32. https://doi.org/10.1016/j.cmet.2014.06.009.

Schwabe, Robert F., Ira Tabas, and Utpal B. Pajvani. 2020. "Mechanisms of Fibrosis Development in Nonalcoholic Steatohepatitis." *Gastroenterology* 158 (7): 1913–28. https://doi.org/10.1053/j.gastro.2019.11.311.

Schwerbel, Kristin, Anne Kamitz, Natalie Krahmer, Nicole Hallahan, Markus Jähnert, Pascal Gottmann, Sandra Lebek, et al. 2020. "Immunity-Related GTPase Induces Lipophagy to Prevent Excess Hepatic Lipid Accumulation." *Journal of Hepatology* 73 (4): 771–82. https://doi.org/10.1016/j.jhep.2020.04.031.

Scott, John W., Naomi Ling, Samah M.A. Issa, Toby A. Dite, Matthew T. O'Brien, Zhi Ping Chen, Sandra Galic, et al. 2014. "Small Molecule Drug A-769662 and AMP Synergistically Activate Naive AMPK Independent of Upstream Kinase Signaling." *Chemistry and Biology* 21 (5): 619–27. https://doi.org/10.1016/j.chembiol.2014.03.006.

Seitz, Susanne, Yun Kwon, Götz Hartleben, Julia Jülg, Revathi Sekar, Natalie Krahmer, Bahar Najafi, et al. 2019. "Hepatic Rab24 Controls Blood Glucose Homeostasis via Improving Mitochondrial Plasticity." *Nature Metabolism* 1 (10): 1009–26. https://doi.org/10.1038/s42255-019-0124-x.

Settembre, Carmine, Rossella De Cegli, Gelsomina Mansueto, Pradip K. Saha, Francesco Vetrini, Orane Visvikis, Tuong Huynh, et al. 2013. "TFEB Controls Cellular Lipid Metabolism through a Starvation-Induced Autoregulatory Loop." *Nature Cell Biology* 15 (6): 647–58. https://doi.org/10.1038/ncb2718.

Shaw, Reuben J., Monica Kosmatka, Nabeel Bardeesy, Rebecca L. Hurley, Lee A. Witters, Ronald A. DePinho, and Lewis C. Cantley. 2004. "The Tumor Suppressor LKB1 Kinase Directly Activates AMP-Activated Kinase and

Regulates Apoptosis in Response to Energy Stress." *Proceedings of the National Academy of Sciences of the United States of America* 101 (10): 3329–35. https://doi.org/10.1073/pnas.0308061100.

Shaw, Reuben J, Katja A Lamia, Debbie Vasquez, Seung-Hoi Koo, Nabeel Bardeesy, Ronald A Depinho, Marc Montminy, and Lewis C Cantley. 2005. "The Kinase LKB1 Mediates Glucose Homeostasis in Liver and Therapeutic Effects of Metformin." *Science (New York, N.Y.)* 310 (5754): 1642–46. https://doi.org/10.1126/science.1120781.

Singh, M., E. G. Richards, A. Mukherjee, and P. A. Srere. 1976. "Structure of ATP Citrate Lyase from Rat Liver. Physicochemical Studies and Proteolytic Modification." *Journal of Biological Chemistry* 251 (17): 5242–50. https://doi.org/10.1016/s0021-9258(17)33153-8.

Singh, Rajat, Susmita Kaushik, Yongjun Wang, Youqing Xiang, Inna Novak, Masaaki Komatsu, Keiji Tanaka, Ana Maria Cuervo, and Mark J. Czaja. 2009. "Autophagy Regulates Lipid Metabolism." *Nature* 458 (7242): 1131–35. https://doi.org/10.1038/nature07976.

Singh, Siddharth, Alina M. Allen, Zhen Wang, Larry J. Prokop, Mohammad H. Murad, and Rohit Loomba. 2015. "Fibrosis Progression in Nonalcoholic Fatty Liver vs Nonalcoholic Steatohepatitis: A Systematic Review and Meta-Analysis of Paired-Biopsy Studies." *Clinical Gastroenterology and Hepatology* 13 (4): 643-654.e9. https://doi.org/10.1016/j.cgh.2014.04.014.

Smith, Brennan K., Katarina Marcinko, Eric M. Desjardins, James S. Lally, Rebecca J. Ford, and Gregory R. Steinberg. 2016. "Treatment of Nonalcoholic Fatty Liver Disease: Role of AMPK." *American Journal of Physiology - Endocrinology And Metabolism* 311 (4): E730–40. https://doi.org/10.1152/ajpendo.00225.2016.

Smith, Gordon I., Mahalakshmi Shankaran, Mihoko Yoshino, George G. Schweitzer, Maria Chondronikola, Joseph W. Beals, Adewole L. Okunade, et al. 2020. "Insulin Resistance Drives Hepatic de Novo Lipogenesis in Nonalcoholic Fatty Liver Disease." *Journal of Clinical Investigation* 130 (3): 1453–60. https://doi.org/10.1172/JCI134165.

Softic, Samir, David E. Cohen, and C. Ronald Kahn. 2016. "Role of Dietary Fructose and Hepatic De Novo Lipogenesis in Fatty Liver Disease." *Digestive Diseases and Sciences* 61 (5): 1282–93. https://doi.org/10.1007/s10620-016-4054-0.

Song, Jae Eun, Tiago C. Alves, Bernardo Stutz, Matija Šestan-Peša, Nicole Kilian, Sungho Jin, Sabrina Diano, Richard G. Kibbey, and Tamas L. Horvath. 2021. "Mitochondrial Fission Governed by Drp1 Regulates Exogenous Fatty Acid Usage and Storage in Hela Cells." *Metabolites* 11 (5). https://doi.org/10.3390/metabo11050322.

Song, Nazi, Hongjiao Xu, Jiahua Liu, Qian Zhao, Hui Chen, Zhibin Yan, Runling Yang, et al. 2022. "Design of a Highly Potent GLP-1R and GCGR Dual-Agonist for Recovering Hepatic Fibrosis." *Acta Pharmaceutica Sinica B* 12 (5): 2443–61. https://doi.org/10.1016/j.apsb.2021.12.016.

Springer, Maya Z., Logan P. Poole, Lauren E. Drake, Althea Bock-Hughes, Michelle L. Boland, Alexandra G. Smith, John Hart, et al. 2021. “BNIP3-Dependent Mitophagy Promotes Cytosolic Localization of LC3B and Metabolic Homeostasis in the Liver.” *Autophagy* 17 (11): 3530–46. https://doi.org/10.1080/15548627.2021.1877469.

Srere, Paul A. 1959. “The Citrate Cleavage Enzyme.” *Journal of Biological Chemistry* 234 (10): 2544–47. https://doi.org/10.1016/s0021-9258(18)69735-2.

Steinberg, Gregory R., and David Carling. 2019. “AMP-Activated Protein Kinase: The Current Landscape for Drug Development.” *Nature Reviews Drug Discovery* 18: 527–51. https://doi.org/10.1038/s41573-019-0019-2.

Steinberg, Gregory R., and D. Grahame Hardie. 2022. “New Insights into Activation and Function of the AMPK.” *Nature Reviews Molecular Cell Biology*. https://doi.org/10.1038/s41580-022-00547-x.

Steinberg, Gregory R., Hayley M. O’Neill, Nicolas L. Dzamko, Sandra Galic, Tim Naim, René Koopman, Sebastian B. Jørgensen, et al. 2010. “Whole Body Deletion of AMP-Activated Protein Kinase B2 Reduces Muscle AMPK Activity and Exercise Capacity.” *Journal of Biological Chemistry* 285 (48): 37198–209. https://doi.org/10.1074/jbc.M110.102434.

Stephenne, X., M. Foretz, N. Taleux, G. C. Van Der Zon, E. Sokal, L. Hue, B. Viollet, and B. Guigas. 2011. “Metformin Activates AMP-Activated Protein Kinase in Primary Human Hepatocytes by Decreasing Cellular Energy Status.” *Diabetologia* 54 (12): 3101–10. https://doi.org/10.1007/s00125-011-2311-5.

Stiede, Kathryn, Wenyan Miao, Heather S. Blanchette, Carine Beysen, Geraldine Harriman, H. James Harwood, Heather Kelley, Rosana Kapeller, Tess Schmalbach, and William F. Westlin. 2017. “Acetyl-Coenzyme A Carboxylase Inhibition Reduces de Novo Lipogenesis in Overweight Male Subjects: A Randomized, Double-Blind, Crossover Study.” *Hepatology* 66 (2): 324–34. https://doi.org/10.1002/hep.29246.

Straus, Werner. 1964a. “Cytochemical Observations on the Relationship between Lysosomes and Phagosomes in Kidney and Liver by Combined Staining for Acid Phosphatase and Intravenously Injected Horsradish Peroxidase.” *Journal of Cell Biology* 20 (3): 497–507.

———. 1964b. “Occurence of Phagosomes and Phago-Lysosomes in Different Segments of the Nephron in Relation to the Reabsorption, Transport, Digestion, and Extrusion of Intravenously Injected Horseradish Peroxidase.” *Journal of Cell Biology* 21 (3): 295–308.

Su, Xiaoyang, Kathryn E. Wellen, and Joshua D. Rabinowitz. 2016. “Metabolic Control of Methylation and Acetylation.” *Current Opinion in Chemical Biology* 30: 52–60. https://doi.org/10.1016/j.cbpa.2015.10.030.

Sullivan, A N N C, Joseph Triscari, James G Hamilton, and O Neal Miller. 1974. “Effect of (-)-Hydroxycitrate upon the Accumulation Of.” *Lipids* 9 (2): 121–28.

Tanida, Isei, Takashi Ueno, and Yasuo Uchiyama. 2014. “A Super-Ecliptic,

Phluorin-Mkate2, Tandem Fluorescent Protein-Tagged Human LC3 for the Monitoring of Mammalian Autophagy." *PLoS ONE* 9 (10): 3–10. https://doi.org/10.1371/journal.pone.0110600.

Than, Aung, Hui Ling He, Si Hui Chua, Dan Xu, Lei Sun, Melvin Khee Shing Leow, and Peng Chen. 2015. "Apelin Enhances Brown Adipogenesis and Browning of White Adipocytes." *Journal of Biological Chemistry* 290 (23): 14679–91. https://doi.org/10.1074/jbc.M115.643817.

Tilokani, Lisa, Fiona M. Russell, Stevie Hamilton, Daniel M. Virga, Mayuko Segawa, Vincent Paupe, Anja V. Gruszczyk, et al. 2022. "AMPK-Dependent Phosphorylation of MTFR1L Regulates Mitochondrial Morphology." *Science Advances* 8 (45): 1–20. https://doi.org/10.1126/sciadv.abo7956.

Tomfohr, John, Jun Lu, and Thomas B. Kepler. 2005. "Pathway Level Analysis of Gene Expression Using Singular Value Decomposition." *BMC Bioinformatics* 6: 1–11. https://doi.org/10.1186/1471-2105-6-225.

Torrens, Laura, Carla Montironi, Marc Puigvehí, Agavni Mesropian, Jack Leslie, Philipp K. Haber, Miho Maeda, et al. 2021. "Immunomodulatory Effects of Lenvatinib Plus Anti–Programmed Cell Death Protein 1 in Mice and Rationale for Patient Enrichment in Hepatocellular Carcinoma." *Hepatology* 74 (5): 2652–69. https://doi.org/10.1002/hep.32023.

Toyama, Erin Quan, Sébastien Herzig, Julien Courchet, Tommy L Lewis Jr, C Oliver, Kristina Hellberg, Nathan P Young, et al. 2016. "AMP-Activated Protein Kinase Mediates Mitochondrial Fission in Response to Energy Stress." *Science* 351 (6270): 275–81. https://doi.org/10.1126/science.aab4138.AMP-activated.

Trefts, Elijah, Maureen Gannon, and David H. Wasserman. 2017. "The Liver." *Current Biology* 27 (21): R1147–51. https://doi.org/10.1016/j.cub.2017.09.019.

Tsuchida, Takuma, and Scott L. Friedman. 2017. "Mechanisms of Hepatic Stellate Cell Activation." *Nature Reviews Gastroenterology and Hepatology* 14 (7): 397–411. https://doi.org/10.1038/nrgastro.2017.38.

Undamatla, Ramya, Jeffrey Chen, Lia R Edmunds, Amanda Mills, and Gregory Gibson. 2023. "Reduced Hepatocyte Mitophagy Is an Early Feature of NAFLD Pathogenesis and Hastens the Onset of Steatosis , Inflammation and Fibrosis." *Preprint*.

Uyeda, Kosaku, and Joyce J Repa. 2006. "Carbohydrate Response Element Binding Protein, ChREBP, a Transcription Factor Coupling Hepatic Glucose Utilization and Lipid Synthesis." *Cell Metabolism* 4 (2): 107–10. https://doi.org/10.1016/j.cmet.2006.06.008.

Vancura, Ales, Shreya Nagar, Pritpal Kaur, Pengli Bu, Madhura Bhagwat, and Ivana Vancurova. 2018. "Reciprocal Regulation of Ampk/Snf1 and Protein Acetylation." *International Journal of Molecular Sciences* 19 (11): 1–13. https://doi.org/10.3390/ijms19113314.

Verschueren, Koen H.G., Clement Blanchet, Jan Felix, Ann Dansercoer, Dirk De Vos, Yehudi Bloch, Jozef Van Beeumen, et al. 2019. "Structure of ATP

Citrate Lyase and the Origin of Citrate Synthase in the Krebs Cycle." *Nature* 568 (7753): 571–75. https://doi.org/10.1038/s41586-019-1095-5.

Vilar-Gomez, Eduardo, Yadina Martinez-Perez, Luis Calzadilla-Bertot, Ana Torres-Gonzalez, Bienvenido Gra-Oramas, Licet Gonzalez-Fabian, Scott L Friedman, Moises Diago, and Manuel Romero-Gomez. 2015. "Weight Loss Through Lifestyle Modification Significantly Reduces Features of Nonalcoholic Steatohepatitis." *Gastroenterology* 149 (2): 365–67. https://doi.org/10.1053/j.gastro.2015.04.005.

Viollet, Benoit, F Andreelli, S B Jørgensen, C Perrin, D Flamez, J Mu, J F P Wojtaszewski, et al. 2003. "Physiological Role of AMP-Activated Protein Kinase (AMPK): Insights from Knockout Mouse Models." *Biochemical Society Transactions* 31 (Pt 1): 216–19. https://doi.org/10.1042/.

Viollet, Benoit, Fabrizio Andreelli, Sebastian B. Jørgensen, Christophe Perrin, Alain Geloen, Daisy Flamez, James Mu, et al. 2003. "The AMP-Activated Protein Kinase A2 Catalytic Subunit Controls Whole-Body Insulin Sensitivity." *Journal of Clinical Investigation* 111 (1): 91–98. https://doi.org/10.1172/JCI16567.

Viollet, Benoit, Sandrine Horman, Jocelyne Leclerc, Louise Lantier, Marc Foretz, Marc Billaud, Shailendra Giri, and Fabrizio Andreelli. 2010. "AMPK Inhibition in Health and Disease." *Critical Reviews in Biochemistry and Molecular Biology* 45 (4): 276–95. https://doi.org/10.3109/10409238.2010.488215.

Vuppalanchi, Raj, Mohammad S. Siddiqui, Mark L. Van Natta, Erin Hallinan, Danielle Brandman, Kris Kowdley, Brent A. Neuschwander-Tetri, et al. 2018. "Performance Characteristics of Vibration-Controlled Transient Elastography for Evaluation of Nonalcoholic Fatty Liver Disease." *Hepatology* 67 (1): 134–44. https://doi.org/10.1002/hep.29489.

Vuppalanchi, Raj, Aynur Ünalp, Mark L. Van Natta, Oscar W. Cummings, Kumar E. Sandrasegaran, Tariq Hameed, James Tonascia, and Naga Chalasani. 2009. "Effects of Liver Biopsy Sample Length and Number of Readings on Sampling Variability in Nonalcoholic Fatty Liver Disease." *Clinical Gastroenterology and Hepatology* 7 (4): 481–86. https://doi.org/10.1016/j.cgh.2008.12.015.

Wan, Wei, Zhiyuan You, Yinfeng Xu, Li Zhou, Zhunlv Guan, Chao Peng, Catherine C.L. Wong, et al. 2017. "MTORC1 Phosphorylates Acetyltransferase P300 to Regulate Autophagy and Lipogenesis." *Molecular Cell* 68 (2): 323-335.e6. https://doi.org/10.1016/j.molcel.2017.09.020.

Wang, Qiong, Lei Jiang, Jue Wang, Shoufeng Li, Yue Yu, Jia You, Rong Zeng, et al. 2009. "Abrogation of Hepatic ATP-Citrate Lyase Protects Against Fatty Liver and Ameliorates Hyperglycemia in Leptin Receptor-Deficient Mice." *Hepatology* 49 (4): 1166–75. https://doi.org/10.1002/hep.22773.

Wang, Shengyuan, Hongyan Li, Minghao Yuan, Haixia Fan, and Zhiyou Cai. 2022. "Role of AMPK in Autophagy." *Frontiers in Physiology* 13 (November): 1–11. https://doi.org/10.3389/fphys.2022.1015500.

Wang, Xiaojing, Marcelle de Carvalho Ribeiro, Arvin Iracheta-Vellve, Patrick

Lowe, Aditya Ambade, Abhishek Satishchandran, Terence Bukong, Donna Catalano, Karen Kodys, and Gyongyi Szabo. 2019. “Macrophage-Specific Hypoxia-Inducible Factor-1α Contributes to Impaired Autophagic Flux in Nonalcoholic Steatohepatitis.” *Hepatology* 69 (2): 545–63. https://doi.org/10.1002/hep.30215.

Wang, Xiaojuan, Xiang Zhang, Eagle S.H. Chu, Xiaoting Chen, Wei Kang, Feng Wu, Ka Fai To, et al. 2018. “Defective Lysosomal Clearance of Autophagosomes and Its Clinical Implications in Nonalcoholic Steatohepatitis.” *FASEB Journal* 32 (1): 37–51. https://doi.org/10.1096/fj.201601393R.

Wang, Xingchun, Bingwei Ma, Jiaqi Chen, Hui You, Chunjun Sheng, Peng Yang, and Shen Qu. 2021. “Glucagon-like Peptide-1 Improves Fatty Liver and Enhances Thermogenesis in Brown Adipose Tissue via Inhibiting BMP4-Related Signaling Pathway in High-Fat-Diet-Induced Obese Mice.” *International Journal of Endocrinology* 2021. https://doi.org/10.1155/2021/6620289.

Wang, Yuhui, Jose Viscarra, Sun Joong Kim, and Hei Sook Sul. 2015. “Transcriptional Regulation of Hepatic Lipogenesis.” *Nature Reviews Molecular Cell Biology* 16 (11): 678–89. https://doi.org/10.1038/nrm4074.

Watt, Matthew J, Gregory R Steinberg, Zhi-ping Chen, Bruce E Kemp, and Mark A Febbraio. 2006. “Fatty Acids Stimulate AMP-Activated Protein Kinase and Enhance Fatty Acid Oxidation in L6 Myotubes.” *Journal of Physiology* 1: 139–47. https://doi.org/10.1113/jphysiol.2006.107318.

Wei, Xuepeng, Kollin Schultz, Gleb A. Bazilevsky, Austin Vogt, and Ronen Marmorstein. 2020. “Molecular Basis for Acetyl-CoA Production by ATP-Citrate Lyase.” *Nature Structural and Molecular Biology* 27 (1): 33–41. https://doi.org/10.1038/s41594-019-0351-6.

Wellen, Kathryn E., Georgia Hatzivassiliou, Uma M. Sachedeva, Thi V. Bui, Justin R. Cross, and Craig B. Thompson. 2009. “ATP-Citrate Lyase Links Cellular Metabolism to Histone Acetylation.” *Science* 324 (5930): 1–7. https://doi.org/10.1126/science.1164097.ATP-citrate.

Wellen, Kathryn E., and Craig B. Thompson. 2012. “A Two-Way Street: Reciprocal Regulation of Metabolism and Signalling.” *Nature Reviews Molecular Cell Biology* 13 (4): 270–76. https://doi.org/10.1038/nrm3305.

Wieckowska, Anna, Nizar N. Zein, Lisa M. Yerian, A. Rocio Lopez, Arthur J. McCullough, and Ariel E. Feldstein. 2006. “In Vivo Assessment of Liver Cell Apoptosis as a Novel Biomarker of Disease Severity in Nonalcoholic Fatty Liver Disease.” *Hepatology* 44 (1): 27–33. https://doi.org/10.1002/hep.21223.

Willows, Robin, Matthew J. Sanders, Bing Xiao, Bhakti R. Patel, Stephen R. Martin, Jon Read, Jon R. Wilson, Julia Hubbard, Steven J. Gamblin, and David Carling. 2017. “Phosphorylation of AMPK by Upstream Kinases Is Required for Activity in Mammalian Cells.” *Biochemical Journal* 474 (17): 3059–73. https://doi.org/10.1042/BCJ20170458.

Woods, Angela, Kristina Dickerson, Richard Heath, Seung Pyo Hong, Milica

Momcilovic, Stephen R. Johnstone, Marian Carlson, and David Carling. 2005. “Ca2+/Calmodulin-Dependent Protein Kinase Kinase-β Acts Upstream of AMP-Activated Protein Kinase in Mammalian Cells.” *Cell Metabolism* 2 (1): 21–33. https://doi.org/10.1016/j.cmet.2005.06.005.

Woods, Angela, Stephen R. Johnstone, Kristina Dickerson, Fiona C. Leiper, Lee G.D. Fryer, Dietbert Neumann, Uwe Schlattner, Theo Wallimann, Marian Carlson, and David Carling. 2003. “LKB1 Is the Upstream Kinase in the AMP-Activated Protein Kinase Cascade.” *Current Biology* 13 (22): 2004–8. https://doi.org/10.1016/j.cub.2003.10.031.

Woods, Angela, Jennet R. Williams, Phillip J. Muckett, Faith V. Mayer, Maria Liljevald, Mohammad Bohlooly-Y, and David Carling. 2017. “Liver-Specific Activation of AMPK Prevents Steatosis on a High-Fructose Diet.” *Cell Reports* 18 (13): 3043–51. https://doi.org/10.1016/j.celrep.2017.03.011.

Wu, Jiang, Dinesh Puppala, Xidong Feng, Mara Monetti, Amanda Lee Lapworth, and Kieran F. Geoghegan. 2013. “Chemoproteomic Analysis of Intertissue and Interspecies Isoform Diversity of AMP-Activated Protein Kinase (AMPK).” *Journal of Biological Chemistry* 288 (50): 35904–12. https://doi.org/10.1074/jbc.M113.508747.

Wu, Ning, Bin Zheng, Adam Shaywitz, Yossi Dagon, Christine Tower, Gary Bellinger, Che-Hung Shen, et al. 2013. “AMPK-Dependent Degradation of TXNIP upon Energy Stress Leads to Enhanced Glucose Uptake via GLUT1.” *Molecular Cell* 49 (6): 1167–75. https://doi.org/10.1016/j.molcel.2013.01.035.

Wu, Yue, Ping Song, Wencheng Zhang, Junhui Liu, Xiaoyan Dai, Zhaoyu Liu, Qiulun Lu, et al. 2015. “Activation of AMPKα2 in Adipocytes Is Essential for Nicotine-Induced Insulin Resistance in Vivo.” *Nature Medicine* 21 (4): 373–82. https://doi.org/10.1038/nm.3826.

Wu, Zhidan, Pere Puigserver, Ulf Andersson, Chenyu Zhang, Guillaume Adelmant, Vamsi Mootha, Amy Troy, et al. 1999. “Mechanisms Controlling Mitochondrial Biogenesis and Respiration through the Thermogenic Coactivator PGC-1.” *Cell* 98: 115–24.

Xiao, Bing, Richard Heath, Peter Saiu, Fiona C. Leiper, Philippe Leone, Chun Jing, Philip A. Walker, et al. 2007. “Structural Basis for AMP Binding to Mammalian AMP-Activated Protein Kinase.” *Nature* 449 (7161): 496–500. https://doi.org/10.1038/nature06161.

Xiao, Bing, Matthew J. Sanders, David Carmena, Nicola J. Bright, Lesley F. Haire, Elizabeth Underwood, Bhakti R. Patel, et al. 2013a. “Structural Basis of AMPK Regulation by Small Molecule Activators.” *Nature Communications* 4: 1–10. https://doi.org/10.1038/ncomms4017.

———. 2013b. “Structural Basis of AMPK Regulation by Small Molecule Activators.” *Nature Communications* 4: 1–10. https://doi.org/10.1038/ncomms4017.

Xie, Longlong, Feng Shi, Yueshuo Li, We Li, Xinfang Yu, Lin Zhao, Min Zhou, et al. 2020. “Drp1-Dependent Remodeling of Mitochondrial Morphology

Triggered by EBV-LMP1 Increases Cisplatin Resistance." *Signal Transduction and Targeted Therapy* 5 (1): 1–12. https://doi.org/10.1038/s41392-020-0151-9.

Xin, Feng Jiao, Jue Wang, Rong Qing Zhao, Zhi Xin Wang, and Jia Wei Wu. 2013. "Coordinated Regulation of AMPK Activity by Multiple Elements in the α-Subunit." *Cell Research* 23 (10): 1237–40. https://doi.org/10.1038/cr.2013.121.

Xiong, Xiwen, Rongya Tao, Ronald A. DePinho, and X. Charlie Dong. 2012. "The Autophagy-Related Gene 14 (Atg14) Is Regulated by Forkhead Box O Transcription Factors and Circadian Rhythms and Plays a Critical Role in Hepatic Autophagy and Lipid Metabolism." *Journal of Biological Chemistry* 287 (46): 39107–14. https://doi.org/10.1074/jbc.M112.412569.

Xiong, Xuelian, Qiuyu Wang, Shuai Wang, Jinglong Zhang, Tongyu Liu, Liang Guo, Yonghao Yu, and Jiandie D. Lin. 2019. "Mapping the Molecular Signatures of Diet-Induced NASH and Its Regulation by the Hepatokine Tsukushi." *Molecular Metabolism* 20 (December 2018): 128–37. https://doi.org/10.1016/j.molmet.2018.12.004.

Xu, Xiaohan, Kyle L. Poulsen, Lijuan Wu, Shan Liu, Tatsunori Miyata, Qiaoling Song, Qingda Wei, Chenyang Zhao, Chunhua Lin, and Jinbo Yang. 2022. "Targeted Therapeutics and Novel Signaling Pathways in Non-Alcohol-Associated Fatty Liver/Steatohepatitis (NAFL/NASH)." *Signal Transduction and Targeted Therapy* 7 (1). https://doi.org/10.1038/s41392-022-01119-3.

Xu, Yinfeng, and Wei Wan. 2022. "Acetylation in the Regulation of Autophagy." *Autophagy* 19 (2): 379–87. https://doi.org/10.1080/15548627.2022.2062112.

Yabut, Julian M, and Daniel J Drucker. 2022. "Glucagon-like Peptide-1 Receptor-Based Therapeutics for Metabolic Liver Disease." *Endocrine Reviews*, no. July: 1–19. https://doi.org/10.1210/endrev/bnac018.

Yan, Yan, Somnath Mukherjee, Kaleeckal G. Harikumar, Timothy S. Strutzenberg, X. Edward Zhou, Kelly Suino-Powell, Ting Hai Xu, et al. 2021. "Structure of an AMPK Complex in an Inactive, ATP-Bound State." *Science* 373 (6553): 413–19. https://doi.org/10.1126/science.abe7565.

Yan, Yan, X. Edward Zhou, H. Eric Xu, and Karsten Melcher. 2018. "Structure and Physiological Regulation of AMPK." *International Journal of Molecular Sciences* 19 (11). https://doi.org/10.3390/ijms19113534.

Yang, Jian, Shanna Maika, Lauren Craddock, Judy A. King, and Zhi Mei Liu. 2008. "Chronic Activation of AMP-Activated Protein Kinase-Alpha1 in Liver Leads to Decreased Adiposity in Mice." *Biochemical and Biophysical Research Communications* 370 (2): 248–53. https://doi.org/10.1016/j.bbrc.2008.03.094.

Yim, Willa Wen You, and Noboru Mizushima. 2020. "Lysosome Biology in Autophagy." *Cell Discovery* 6 (1). https://doi.org/10.1038/s41421-020-0141-7.

Younossi, Zobair, Quentin M. Anstee, Milena Marietti, Timothy Hardy, Linda Henry, Mohammed Eslam, Jacob George, and Elisabetta Bugianesi. 2018.

"Global Burden of NAFLD and NASH: Trends, Predictions, Risk Factors and Prevention." *Nature Reviews Gastroenterology and Hepatology* 15 (1): 11–20. https://doi.org/10.1038/nrgastro.2017.109.

Younossi, Zobair M. 2019. "Non-Alcoholic Fatty Liver Disease – A Global Public Health Perspective." *Journal of Hepatology* 70 (3): 531–44. https://doi.org/10.1016/j.jhep.2018.10.033.

Younossi, Zobair M., Deirdre Blissett, Robert Blissett, Linda Henry, Maria Stepanova, Youssef Younossi, Andrei Racila, Sharon Hunt, and Rachel Beckerman. 2016. "The Economic and Clinical Burden of Nonalcoholic Fatty Liver Disease in the United States and Europe." *Hepatology* 64 (5): 1577–86. https://doi.org/10.1002/hep.28785.

Younossi, Zobair M., Aaron B. Koenig, Dinan Abdelatif, Yousef Fazel, Linda Henry, and Mark Wymer. 2016. "Global Epidemiology of Nonalcoholic Fatty Liver Disease—Meta-Analytic Assessment of Prevalence, Incidence, and Outcomes." *Hepatology* 64 (1): 73–84. https://doi.org/10.1002/hep.28431.

Younossi, Zobair M., Vlad Ratziu, Rohit Loomba, Mary Rinella, Quentin M. Anstee, Zachary Goodman, Pierre Bedossa, et al. 2019. "Obeticholic Acid for the Treatment of Non-Alcoholic Steatohepatitis: Interim Analysis from a Multicentre, Randomised, Placebo-Controlled Phase 3 Trial." *The Lancet* 394 (10215): 2184–96. https://doi.org/10.1016/S0140-6736(19)33041-7.

Younossi, Zobair, Frank Tacke, Marco Arrese, Barjesh Chander Sharma, Ibrahim Mostafa, Elisabetta Bugianesi, Vincent Wai-Sun Wong, et al. 2019. "Global Perspectives on Nonalcoholic Fatty Liver Disease and Nonalcoholic Steatohepatitis." *Hepatology* 69 (6): 2672–82. https://doi.org/10.1002/hep.30251.

Yousefi, Shida, Remo Perozzo, Inès Schmid, Andrew Ziemiecki, Thomas Schaffner, Leonardo Scapozza, Thomas Brunner, and Hans Uwe Simon. 2006. "Calpain-Mediated Cleavage of Atg5 Switches Autophagy to Apoptosis." *Nature Cell Biology* 8 (10): 1124–32. https://doi.org/10.1038/ncb1482.

Yu, Li, Yang Chen, and Sharon A. Tooze. 2018. "Autophagy Pathway: Cellular and Molecular Mechanisms." *Autophagy* 14 (2): 207–15. https://doi.org/10.1080/15548627.2017.1378838.

Yu, Siyu, Chunlin Li, Guang Ji, and Li Zhang. 2021. "The Contribution of Dietary Fructose to Non-Alcoholic Fatty Liver Disease." *Frontiers in Pharmacology* 12 (November): 1–11. https://doi.org/10.3389/fphar.2021.783393.

Zhang, Chen-song, and Sheng-cai Lin. 2016. "AMPK Promotes Autophagy by Facilitating Mitochondrial Fission." *Cell Metabolism* 23 (3): 399–401. https://doi.org/10.1016/j.cmet.2016.02.017.

Zhang, Hao, Zujian Xiong, Qin He, and Fan Fan. 2019. "ACSS2-Related Autophagy Has a Dual Impact on Memory." *Chinese Neurosurgical Journal* 5: 14. https://doi.org/10.1186/s41016-019-0162-y.

Zhang, Hongbin, Meiping Guan, Kristy L Townsend, Tian Lian Huang, Ding An, Xu Yan, Tim J Schulz, et al. 2015. "MicroRNA- 455 Regulates Brown

Adipogenesis via a Novel HIF 1 an-AMPK-PGC 1 a Signaling Network." *EMBO Reports* 16 (10): 1378–93.

Zhang, Li Hui, Xue Fen Pang, Feng Bai, Ning Ping Wang, Ahmed Ijaz Shah, Robert J. McKallip, Xue Wen Li, Xiong Wang, and Zhi Qing Zhao. 2015. "Preservation of Glucagon-Like Peptide-1 Level Attenuates Angiotensin II-Induced Tissue Fibrosis by Altering AT1/AT2 Receptor Expression and Angiotensin-Converting Enzyme 2 Activity in Rat Heart." *Cardiovascular Drugs and Therapy* 29 (3): 243–55. https://doi.org/10.1007/s10557-015-6592-7.

Zhang, Ning Ping, Xue Jing Liu, Li Xie, Xi Zhong Shen, and Jian Wu. 2019. "Impaired Mitophagy Triggers NLRP3 Inflammasome Activation during the Progression from Nonalcoholic Fatty Liver to Nonalcoholic Steatohepatitis." *Laboratory Investigation* 99 (6): 749–63. https://doi.org/10.1038/s41374-018-0177-6.

Zhang, Xinrong, Grace Lai Hung Wong, and Vincent Wai Sun Wong. 2020. "Application of Transient Elastography in Nonalcoholic Fatty Liver Disease." *Clinical and Molecular Hepatology* 26 (2): 128–41. https://doi.org/10.3350/cmh.2019.0001n.

Zhang, Zeyuan, Qingwen Qian, Mark Li, Fan Shao, Wen Xing Ding, Vitor A. Lira, Sophia X. Chen, et al. 2020. "The Unfolded Protein Response Regulates Hepatic Autophagy by SXBP1-Mediated Activation of TFEB." *Autophagy* 17 (8): 1–15. https://doi.org/10.1080/15548627.2020.1788889.

Zhao, Peng, Xiaoli Sun, Cynthia Chaggan, Zhongji Liao, Kai in Wong, Feng He, Seema Singh, et al. 2020. "An AMPK–Caspase-6 Axis Controls Liver Damage in Nonalcoholic Steatohepatitis." *Science* 367 (6478): 652–60. https://doi.org/10.1126/science.aay0542.

Zhao, Yan G., and Hong Zhang. 2019. "Autophagosome Maturation: An Epic Journey from the ER to Lysosomes." *Journal of Cell Biology* 218 (3): 757–70. https://doi.org/10.1083/jcb.201810099.

Zhou, Cuihong, Wu Zhong, Jun Zhou, Fugeng Sheng, Ziyuan Fang, Yue Wei, Yingyu Chen, Xiaoyan Deng, Bin Xia, and Jian Lin. 2012. "Monitoring Autophagic Flux by an Improved Tandem Fluorescent-Tagged LC3 (MTagRFP-MWasabi-LC3) Reveals That High-Dose Rapamycin Impairs Autophagic Flux in Cancer Cells." *Autophagy* 8 (8): 1215–26. https://doi.org/10.4161/auto.20284.

Zhou, G., R. Myers, Y. Li, Y. Chen, X. Shen, J. Fenyk-Melody, M. Wu, et al. 2001. "Role of AMP-Activated Protein Kinase in Mechanism of Metformin Action." *Journal of Clinical Investigation* 108 (8): 1167–74. https://doi.org/10.1172/JCI13505.

Zhu, Lihui, Xiao Wu, and Rongrong Liao. 2023. "Mechanism and Regulation of Mitophagy in Nonalcoholic Fatty Liver Disease (NAFLD): A Mini-Review." *Life Sciences* 312 (November 2022). https://doi.org/10.1016/j.lfs.2022.121162.